2006-12

# Assessing the ability of hyperspectral data to detect Lyngbya SPP a potential biological indicator for presence of metal objects in the littoral environment

Blankenship, James R.

Monterey California. Naval Postgraduate School


# NAVAL POSTGRADUATE SCHOOL

**MONTEREY, CALIFORNIA**

# THESIS

**ASSESSING THE ABILITY OF HYPERSPECTRAL DATA TO DETECT *LYNGBYA* SPP.: A POTENTIAL BIOLOGICAL INDICATOR FOR PRESENCE OF METAL OBJECTS IN THE LITTORAL ENVIRONMENT**

by

James R. Blankenship

December 2006

Thesis Advisor: Daria Siciliano
Co-Advisor: R. C. Olsen

**Approved for public release; distribution is unlimited**

THIS PAGE INTENTIONALLY LEFT BLANK

| REPORT DOCUMENTATION PAGE | | Form Approved OMB No. 0704-0188 |
|---|---|---|



| 1. AGENCY USE ONLY *(Leave blank)* | 2. REPORT DATE | 3. REPORT TYPE AND DATES COVERED |
|---|---|---|
| | December 2006 | Master's Thesis |

**4. TITLE AND SUBTITLE**
Assessing the Ability of Hyperspectral Data to Detect and Map *Lyngbya* Spp.: A Potential Biological Indicator for Presence of Metal Objects in the Littoral Environment.

**5. FUNDING NUMBERS**

**6. AUTHOR** James R. Blankenship

**7. PERFORMING ORGANIZATION NAME(S) AND ADDRESS(ES)**
Naval Postgraduate School
Monterey, CA 93943-5000

**8. PERFORMING ORGANIZATION REPORT NUMBER**

**9. SPONSORING /MONITORING AGENCY NAME(S) AND ADDRESS(ES)**
N/A

**10. SPONSORING/MONITORING AGENCY REPORT NUMBER**

**11. SUPPLEMENTARY NOTES:** The views expressed in this thesis are those of the author and do not reflect the official policy or position of the Department of Defense or the U.S. Government.

| 12a. DISTRIBUTION / AVAILABILITY STATEMENT | 12b. DISTRIBUTION CODE |
|---|---|
| Approved for public release; distribution is unlimited | A |

**13. ABSTRACT**

The aquatic filamentous bacteria (Cyanobacterium) *Lyngbya majuscula* is a nitrogen-fixer found in coastal waters often attached or adjacent to sea grass, algae and coral. It is characterized by phycobiliproteins, unique pigments found only in cyanobacteria. To sustain photosynthesis and nitrogen fixation, *L. majuscula* requires iron proteins and is therefore sensitive to the availability of this metal. The hypothesis tested in this study concerns the potential use of hyperspectral imaging in detecting *L. majuscula* in coastal regions as biological indicators for the presence of iron debris or metal objects in the littoral environment. This concept would have potential benefits and applications in mine detection and countermeasure techniques. Using a USB2000 field spectroradiometer, a spectral library was developed for the benthic substrates of Midway Atoll, Northwest Hawaiian Islands, spectrally characterizing *L. majuscula* and the surrounding coral reef substrates. The data was analyzed to determine unique spectral characteristics of the benthic cyanobacteria in a mixed coral environment and evaluated against the resampled spectral resolution of a number of hyperspectral sensors: Airborne Visible/Infrared Imaging Spectrometer (AVIRIS), Hyperspectral Mapper (HyMap) and Compact Airborne Spectrographic Imager (CASI). The results of the *in situ* spectroscopy suggest a strong potential for all three sensors to detect these cyanobacteria in a mixed coral reef environment at four distinct wavelengths attributable to phycobiliprotein pigment absorptions unique to cyanobacteria. Of these four discriminative absorption ranges, the phycoerythrin absorption of 565-576 nm shows the greatest potential for segregating cyanobacteria from a mixed algal/ coral / sand environment so long as the coral *Montipora* spp. is not present within the scene, since it has an overlapping absorption in those wavelengths. In the presence of *Montipora* corals, these cyanobacteria are more difficult to detect. However, in a mixed environment composed of *L. majuscula* and *Montipora* corals, the cyanobacteria can be distinguished by a different phycocyanin absorption, at 615-632 nm.

| 14. SUBJECT TERMS | 15. NUMBER OF PAGES |
|---|---|
| Hyperspectral, cyanobacteria, littoral, metal object detection | 261 |
| | 16. PRICE CODE |

| 17. SECURITY CLASSIFICATION OF REPORT | 18. SECURITY CLASSIFICATION OF THIS PAGE | 19. SECURITY CLASSIFICATION OF ABSTRACT | 20. LIMITATION OF ABSTRACT |
|---|---|---|---|
| Unclassified | Unclassified | Unclassified | UL |

NSN 7540-01-280-5500

Standard Form 298 (Rev. 2-89)
Prescribed by ANSI Std. 239-18

THIS PAGE INTENTIONALLY LEFT BLANK

**Approved for public release; distribution is unlimited**

# ASSESSING THE ABILITY OF HYPERSPECTRAL DATA TO DETECT *LYNGBYA* SPP.: A POTENTIAL BIOLOGICAL INDICATOR FOR PRESENCE OF METAL OBJECTS IN THE LITTORAL ENVIRONMENT

James R. Blankenship
Lieutenant Commander, United States Navy
B.A., The Ohio State University, 1994

Submitted in partial fulfillment of the
requirements for the degree of

**MASTER OF SCIENCE IN SPACE SYSTEMS OPERATIONS**

from the

**NAVAL POSTGRADUATE SCHOOL**
**December 2006**

Author: James R. Blankenship

Approved by: Dr. Daria Siciliano
Thesis Advisor

Dr. R. C. Olsen
Co-Advisor

Dr. Rudy Panholzer
Chairman, Department of Space Systems Academic Group

THIS PAGE INTENTIONALLY LEFT BLANK

# ABSTRACT

The aquatic filamentous bacteria (Cyanobacterium) *Lyngbya majuscula* is a nitrogen-fixer found in coastal waters often attached or adjacent to sea grass, algae and coral. It is characterized by phycobiliproteins, unique pigments found only in cyanobacteria. To sustain photosynthesis and nitrogen fixation, *L. majuscula* requires iron proteins and is therefore sensitive to the availability of this metal. The hypothesis tested in this study concerns the potential use of hyperspectral imaging in detecting *L. majuscula* in coastal regions as biological indicators for the presence of iron debris or metal objects in the littoral environment. This concept would have potential benefits and applications in mine detection and countermeasure techniques. Using a USB2000 field spectroradiometer, a spectral library was developed for the benthic substrates of Midway Atoll, Northwest Hawaiian Islands, spectrally characterizing *L. majuscula* and the surrounding coral reef substrates. The data was analyzed to determine unique spectral characteristics of the benthic cyanobacteria in a mixed coral environment and evaluated against the resampled spectral resolution of a number of hyperspectral sensors: Airborne Visible/Infrared Imaging Spectrometer (AVIRIS), Hyperspectral Mapper (HyMap) and Compact Airborne Spectrographic Imager (CASI). The results of the *in situ* spectroscopy suggest a strong potential for all three sensors to detect these cyanobacteria in a mixed coral reef environment at four distinct wavelengths attributable to phycobiliprotein pigment absorptions unique to cyanobacteria. Of these four discriminative absorption ranges, the phycoerythrin absorption of 565-576 nm shows the greatest potential for segregating cyanobacteria from a mixed algal/ coral / sand environment so long as the coral *Montipora* spp. is not present within the scene, since it has an overlapping absorption in those wavelengths. In the presence of *Montipora* corals, these cyanobacteria are more difficult to detect. However, in a mixed environment composed of *L. majuscula* and *Montipora* corals, the cyanobacteria can be distinguished by a different phycocyanin absorption, at 615-632 nm.

THIS PAGE INTENTIONALLY LEFT BLANK

# TABLE OF CONTENTS

THIS PAGE INTENTIONALLY LEFT BLANK

# LIST OF FIGURES

THIS PAGE INTENTIONALLY LEFT BLANK

# LIST OF TABLES

THIS PAGE INTENTIONALLY LEFT BLANK

# ACKNOWLEDGMENTS

I wish to thank all of the professors at the Naval Postgraduate School (NPS) for all of their professional instruction throughout my twenty-seven month tour. I have honestly learned more under their tutelage than I ever thought possible. Several people are due special thanks for assisting me in putting this thesis together. The first person is Dr. Daria Siciliano of the Remote Sensing Lab within the Physics Department at NPS. Without Dr. Siciliano's this thesis would have never been possible. Her love for the marine environment and passion for diving fully inspired me to pursue this work. Dr. Siciliano spent many extra hours teaching, motivating and counseling me, not only as a professor, but also as a friend; something I will always cherish.

Dr. Chris Olsen of the Physics Department sponsored this research and provided all of the financial support required for me to become a certified Advanced Open water SCUBA diver. His remote sensing class and physics of the space environment classes were my favorite classes during my time at NPS. Additionally, Dr. Olsen provided the funding to support two independent trips to Midway Atoll in order to gain all of the research data.

Two other people contributed directly to this thesis, Lieutenant Mark Camacho and Angie Puetz. Mark and I learned SCUBA together and worked together to support each other's thesis. Mark is a great dive buddy and became a close personal friend who helped keep me focused throughout a difficult personal crisis. Without his council, I am not sure I could have done this on time. Angie Puetz, a research assistant in the Remote Sensing Lab at NPS helped me tremendously by teaching me to use ENVI software necessary for analyzing my data and assisted determining the best way to workout some of the noise issues found in my data.

I would also like to thank the U.S. Fish and Wildlife Service for their support in the execution of my research in Midway Atoll. First is Dr. Jim Maragos, the diving safety officer for the Hawaiian Islands, who certified me to conduct diving in the atoll and for taking me on my deepest underwater dive experience. Mr. Barry Christenson and

his staff at Midway Atoll's National Wildlife Refuge provided me a great amount of support and a rich experience I will never forget. I am especially grateful to Dr. John Klavitter for answering all of my questions while at Midway, helping with all of the paperwork to bring back samples, and providing me the experience of swimming with grey reef sharks. Lastly, I must thank Mr. John Miller whose "just have fun" mentality is absolutely contagious.

Finally, I have to thank my son Steven. He has had a rough year and missed a great deal of fun time with Dad while I worked on this thesis. Although he is only seven, I truly appreciate his patience and love!

# I. INTRODUCTION

Current naval doctrine requires a thorough knowledge of the water column and the objects (man-made or natural) located along the coastline, especially in the case of a potentially hostile nation. With the proliferation of inexpensive, yet effective, coastal mining technologies this issue has become an increasing challenge for the Unites States Navy. Traditionally, mine countermeasures have required the use of ships and aircraft equipped with specialized sonar sensors to detect coastal mines and neutralize them, an activity that can place ships and sailors at risk. Depending on the constitution of the ocean floor, bottom mines for example can become buried under silt, sand or marine vegetation, making them nearly impossible to detect even with the most sophisticated sonar equipment. The United States in its de-mining operations would therefore greatly benefit from new technologies, like optical remote sensing, facilitating detection of coastal mines. One appealing remote sensing method for detecting coastal mines is hyperspectral imagery from airborne or space-borne assets. Hyperspectral data offers a more detailed view of the spectral properties of the Earth's surface and can provide specific clues as to the materials that constitute it. Previous work using hyperspectral imaging in mine detection has been carried out on terrestrial environments either with little success (McFee, 1996), or relying on proxies that exploited the Near Infrared (NIR) range of the spectrum (Maathuis and Van Genderen, 2004), which cannot be used in marine environments, since IR radiation is quickly absorbed in water. Very limited work has been carried out in littoral environments, with the exception perhaps of promising ongoing efforts pairing hyperspectral imaging and LIDAR data in mine detection exercises, which have yet to be published.

The types of mines found in littoral environments (bottom, moored and surface mines) all have common materials used in their construction: explosives, electronics, metal and plastics. If any of these constituents can be reliably detected, then perhaps hyperspectral imaging could be employed to detect mines more effectively than *in situ* methods from ships. The metal constituents of the mine structure could be a promising start, but unfortunately, metal is a generic term, comprising a variety of different metals and alloys that are often spectrally non-unique. However, it may be possible to identify

submerged metal objects, such as mines, using biological indicators, i.e. organisms that may reflect the presence of metallic materials on or near the bottom of the ocean, so long as light penetration is sufficient to facilitate the photosynthetic process. It has been hypothesized (Siciliano, 2002) that one such biological indicator in tropical and subtropical marine environments could be represented by benthic cyanobacteria such as *Lyngbya majuscula*, microorganisms that use iron proteins as a catalyst in the biological process of fixing nitrogen, and that bloom in the presence of an iron-leaking submerged object.

The objective of this research was to spectrally characterize the cyanobacteria *Lyngbya majuscula* and identify potential differences between its reflectance spectra and those of the surrounding substrates. Midway Atoll, in the Northwest Hawaiian Islands, was examined for presence and distribution of *Lyngbya majuscula* and a spectral library was built using both *L. majuscula* and the surrounding coral reef substrates. This data was then analyzed and compared with the ultimate goal of 1) determining if unique spectral characters existed to identify benthic cyanobacteria in the mixed coral reef environment investigated, and 2) address the feasibility of currently available hyperspectral sensors such as Airborne Visible/Infrared Imaging Spectrometer (AVIRIS), Hyperspectral Mapper (HyMap) and Compact Airborne Spectrographic Imager (CASI) to detect this biological indicator, hence the presence of iron objects in the littoral environment.

# II. BACKGROUND

## A. HISTORY OF REMOTE SENSING FOR INTELLIGENCE PURPOSES

Remote Sensing is the process of acquiring information about an object by a recording device that is not physically connected to the object itself (Lillesand and Kiefer, 1994). This concept has been militarily significant since the Civil War. Thaddeus Lowe, an entrepreneur and balloonist, in 1861 flew more than 1,000 feet above Arlington, Virginia, telegraphing intelligence information about the Confederate Army positions to the Union Army. Using that information a successful firing was carried out against the Confederate troops, who were more than three miles away in Falls Church, Virginia, Figure 1. The first aerial surveillance success had actually come in July 1861 above Fort Monroe by John LaMountain, who was later dismissed from Union Service by General McClellan for the favored Lowe (U.S. Centennial of Flight Commission, 2006, ¶13).

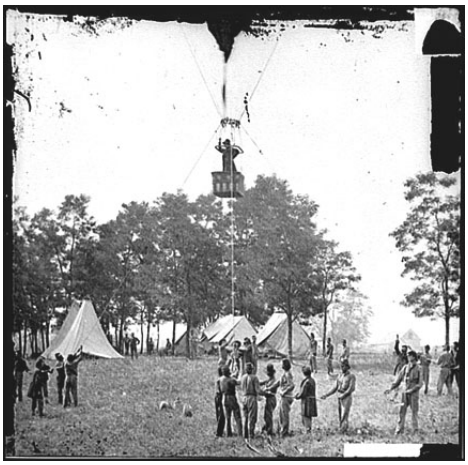

Figure 1. Thaddeus Lowe flying *Intrepid* for Union Army during a Civil War battle. From Library of Congress.

After the civil war, and prior to the Wright brothers' aircraft inventions, remote sensing in the form of aerial photography was actually carried out by pigeons, in 1903, Figure 2. These birds were more difficult to shoot down and were equipped with cameras designed to take photographs every thirty seconds between their launching base and their home shelter (Jensen, 2000). Despite their increased stealthy profile, they were a tasty treat for a few hungry skilled sharpshooters.

Figure 2. Bavarian Pigeon Corp of 1903. From NASA's Observatorium.

The first "human" aerial photography experiment was carried out in 1908 by Wilbur Wright's passenger, L. P. Bonvillain, during a demonstration flight in France. By the time of the Great War, 1914–1918, the military implications of aerial photography were fully recognized by Germany, who took as many as 4,000 photographs a day, and the U.S. Army, who produced more than a million pictures over a four-month period (NASA's Observatorium, 2006).

October 14, 1957, marked the launch of the Soviet satellite Sputnik which was shortly followed by the U.S.'s launch of its first satellite, Van Allen's Explorer spacecraft, on January 31, 1958, marking the beginning of the space race. Recognizing the strategic and tactical capabilities of this new technology, President Eisenhower signed the approval for the Corona program in February 1958 (Olsen, 2006). Although Corona had many failed missions early in its existence, it soon became the gold standard for remote sensing as it provided safe unprecedented intelligence access to otherwise inaccessible territories (Olsen, 2006), see Figure 3. Today, several nations employ satellite remote sensing for intelligence purposes as well as for commercial and environmental monitoring.

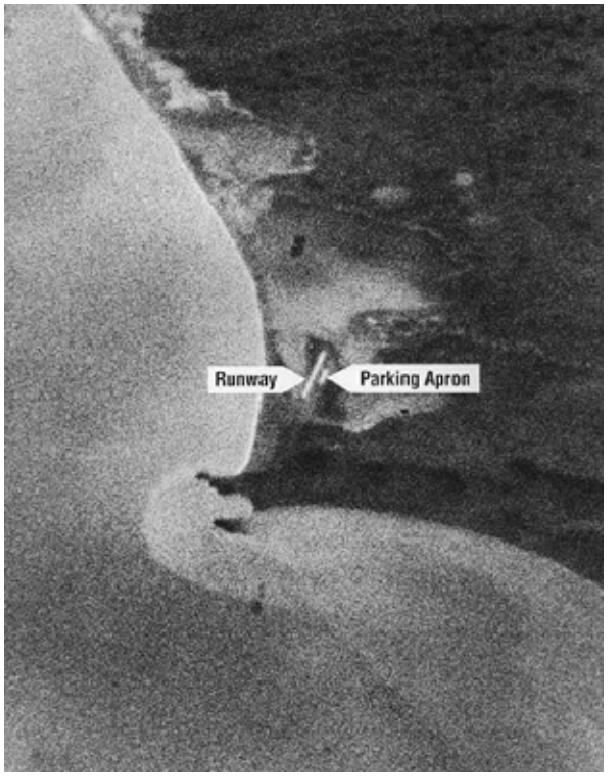


Figure 3. First Imagery Taken By CORONA - Mys Shmidta Air Field, USSR 18 Aug 1960. Retrieved from http://www.nro.gov/corona/imagery.html

## B. OPTICAL REMOTE SENSING

Remote sensing can be passive or active. Passive remote sensing makes use of sensors that detect the reflected or emitted electro-magnetic radiation from natural sources, while active remote sensing uses sensors that detect reflected responses from objects that are irradiated from artificially-generated energy sources, such as radar (Lillesand and Kiefer, 1994). This thesis focuses on hyperspectral imaging, a type of passive, optical remote sensing.

Optical remote sensing exploits visible, near infrared and short-wave infrared sensors to fashion images of the earth's surface by detecting the solar radiation reflected from targets on the ground (Olsen, 2006). Since different materials reflect and absorb differently at different wavelengths, targets can be differentiated by their spectral reflectance signatures in the remotely sensed images. Optical remote sensing systems are classified into the following types, depending on the number of spectral bands used in the imaging process: panchromatic, multispectral, and hyperspectral imaging (Olsen, 2006).

Panchromatic imaging systems are comprised of a single channel detector sensitive to radiation within a broad wavelength range. When the wavelength range coincides with the visible range, the resulting image appears to be a "black-and-white" photograph taken from space (Olsen, 2006). The physical quantity being measured is the apparent brightness of the targets; however, the spectral information of color is lost.

Multispectral imaging systems employ a multi-channel detector with a few spectral bands. Each of the channels is responsive to radiation from a narrow wavelength band. The resulting image is a multilayer image that has both the brightness and spectral (color) information of the targets being imaged (Olsen, 2006).

Hyperspectral Imaging Systems acquire images in about a hundred or more contiguous spectral bands (Olsen, 2006). Because of this high spectral resolution, precise spectral information contained in a hyperspectral image provides an improved characterization and identification of targets. Hyperspectral images have potential applications in fields such as precision agriculture (e.g. monitoring the types, health, moisture status and maturity of crops), and coastal management (e.g. monitoring of phytoplankton, pollution, bathymetry changes) (Barnes et al, 1994), in addition to a range of others.

## C. SPECTRAL REMOTE SENSING

### 1. Spectral Recognition

While experimenting with light in 1666, Sir Isaac Newton used a prism to split light into a spectrum of red, orange, yellow, green, blue, indigo and violet, Figure 4. Through utilization of a second prism, he was able to recombine the colors into white light (Estes, 1999).

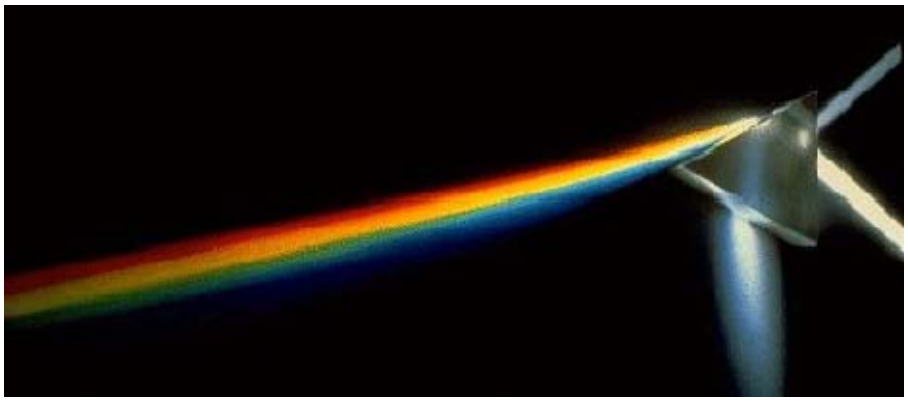

Figure 4. Example of a prism splitting light into a multi-color spectrum.

In 1802, English chemist William Hyde Wollaston became the first to observe dark lines in the solar spectrum, and in 1814 German physicists Joseph Fraunhofer rediscovered these dark absorption lines (Olsen, 2006). However, Fraunhofer discovered that different stars in the solar system had different dark lines when compared to each other and the sun; see Figure 5. It is now understood by scientists that these absorption lines are critical clues to the composition of a solar body's atmosphere. Goetz et al. (1985) first demonstrated the ability to use these unique spectral features to determine the Earth's surface materials composition through spectral imaging; specifically hyperspectral imaging. Additionally, Goetz et al. (1985) pointed out the ability of this technique in a variety of applications, such as in determining the mineral composition of a site as a way to extract important geological information; as well as determining vegetation's health to obtain ecological information about a particular site.

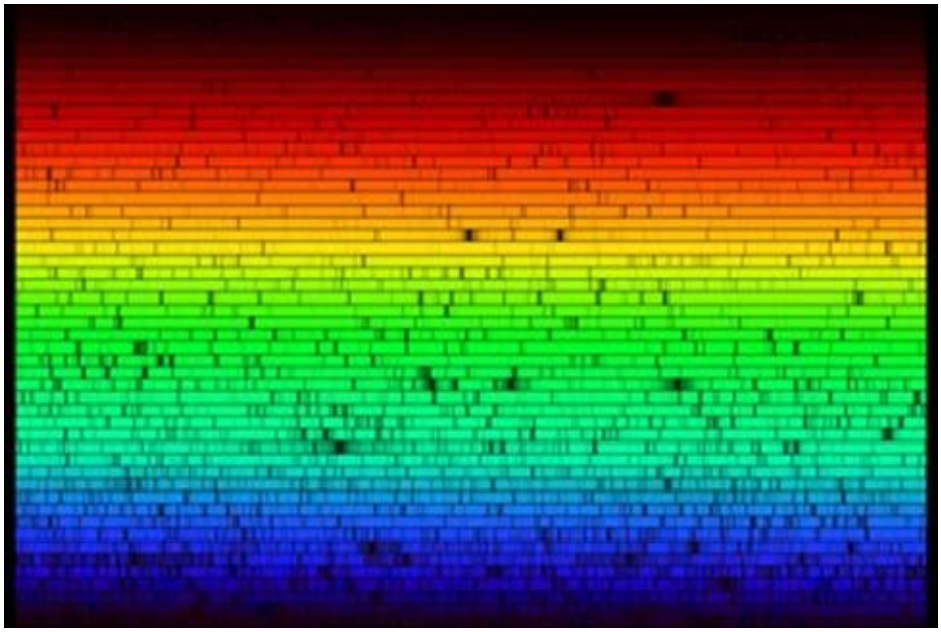

Figure 5. A high resolution version of the spectrum of our Sun. Copyright N.A.Sharp, NOAO/NSO/Kitt Peak FTS/AURA/NSF.

## 2. Hyperspectral Imaging

The importance of hyperspectral imaging has grown in the past two decades as a method for classifying material types on the Earth's surface. It is especially beneficial for agricultural studies, forestry management, mineral exploration, environmental monitoring and national security. These sensors scan an image and measure the spectrum of electromagnetic radiation reflected by the Earth's surface in each of the image "picture element" (pixel). The spectra from each pixel can be analyzed to determine its components and scaled up to determine the earth's surface materials present in the entire image, as illustrated in Figure 6.

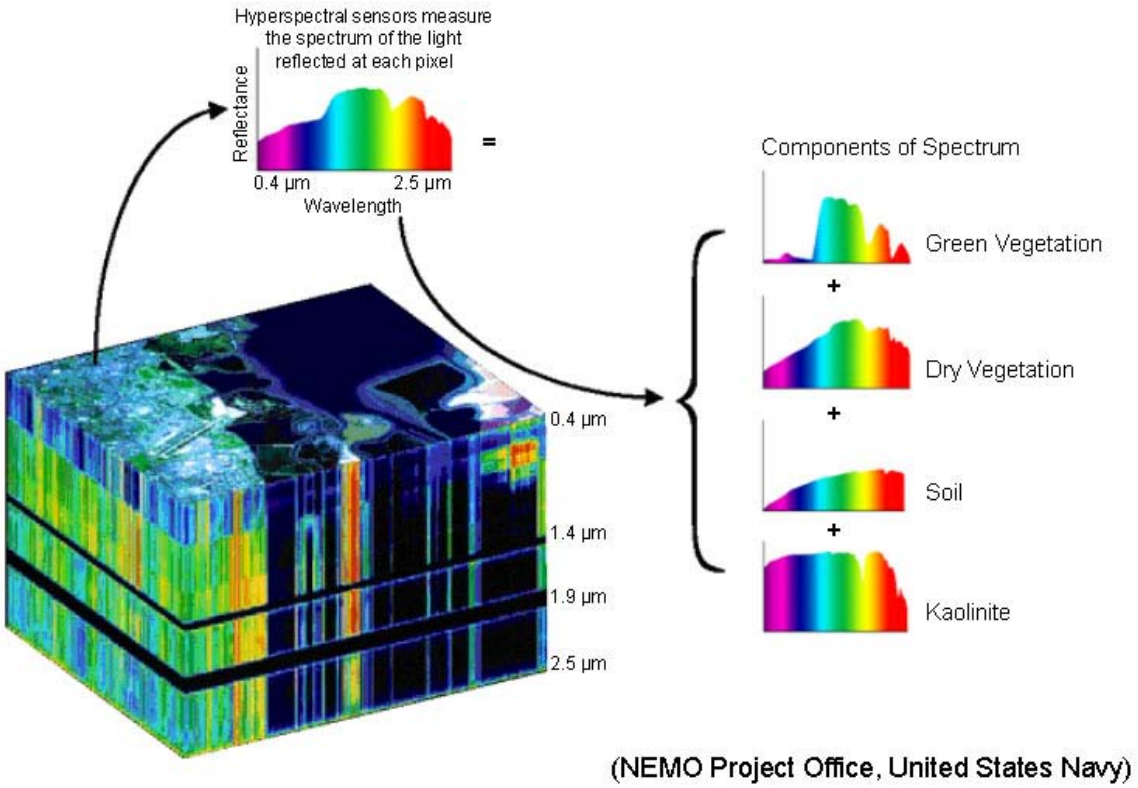


Figure 6. Hyperspectral image cube, taken from NEMO Project Office, United States Navy, 2006

## D. REMOTE SENSING SYSTEMS FOR OCEAN APPLICATIONS

There are a number of remotes sensing system available today, many of which are used in ocean monitoring. This thesis seeks to provide information on a selected few: the Airborne Visible/Infrared Imaging Spectrometer (AVIRIS), Ocean Portable Hyperspectral Imager for Low-Light Spectroscopy (Ocean PHILLS), Compact Airborne Spectrographic Imager (CASI), and Hyperspectral Mapper (HyMap). The selection was made based on sensors that could be used in a future deployment at Midway Atoll or other similar littoral environments.

### 1. AVIRIS

In 1983, the Jet Propulsion Labs (JPL) proposed a design for a hyperspectral imager that would capture 224 contiguous spectral channels (Goetz et al., 1985). Later in 1987, JPL flew the Airborne Visible/Infrared Imaging Spectrometer (AVIRIS), which became the benchmark for spectral imagers (Short, 2006). AVIRIS has a unique optical sensor that provides calibrated images of spectral radiance from 400 to 2500 nanometers (nm). It has been flown on the National Aeronautics and Space Administration's

(NASA) ER-2 jet, Twin Otter International's turboprop, Scaled Composites' Proteus and NASA's WB-57 (www.aviris.nasa.jpl.gov). Each spectral band has a nominal width of 10 nm with a spatial resolution that is dependent on the altitude of the sensor Figure 7. When flying on the ER-2 at 20 km altitude, each pixel is approximately 20 meters, providing a ground swath on the order of 11km. Conversely, when operated from the Twin Otter at 4 km altitude, each ground pixel is 4-m square with a 2-km wide ground swath. AVIRIS is a "whiskbroom" scanner that it utilizes a mirror to sweep back and forth to produce 677 pixels for the 224 detectors. The detectors are made of Silicon (Si) for the visible spectrum while indium gallium arsenide (InGaAs) is used for the near infrared (NIR) and indium-antimonide (InSb) is used for the short-wave infrared (SWIR) detectors. Given AVIRIS's high spectral resolution, it has proven to be a good choice imager for remote sensing projects focusing on the marine environment (e.g., Gross et al., 1988; Richardson and Kruse, 1999; Siciliano et al., 2001.

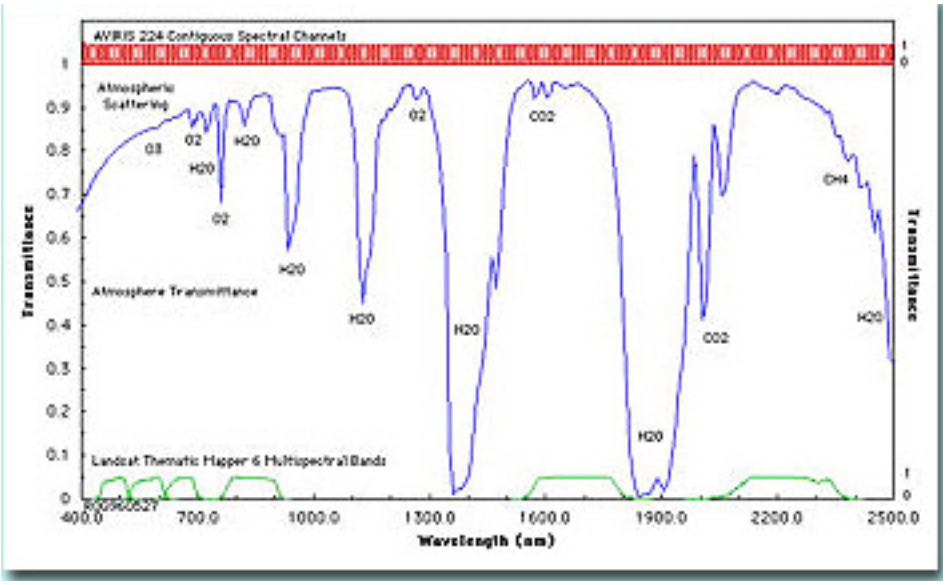


Figure 7. AVIRIS spectral coverage. Taken from aviris.nasa.jpl.gov August 14, 2006.

## 2. Ocean PHILLS

The Ocean Portable Hyperspectral Imager for Low-Light Spectroscopy (Ocean PHILLS) was specifically designed for hyperspectral imaging of the coastal ocean. It actually consists of a series of imagers that were initially designed and fielded in 1994 by the Naval Research Laboratory (NRL). The sensor is a "push-broom" scanning instrument designed for obtaining good returns around the 400-450nm (blue) range,

critical for most ocean applications, with 128 spectral channels of approximately 4.6 nm resolution. Two key elements of Ocean PHILLS are its VS-15 Offner spectrograph and the thinned backside-illuminated CCD cameras. Uniquely, all of the components used to build Ocean PHILLS were commercially available (Davis et al, 2002). A sample image is provided in Figure 8.

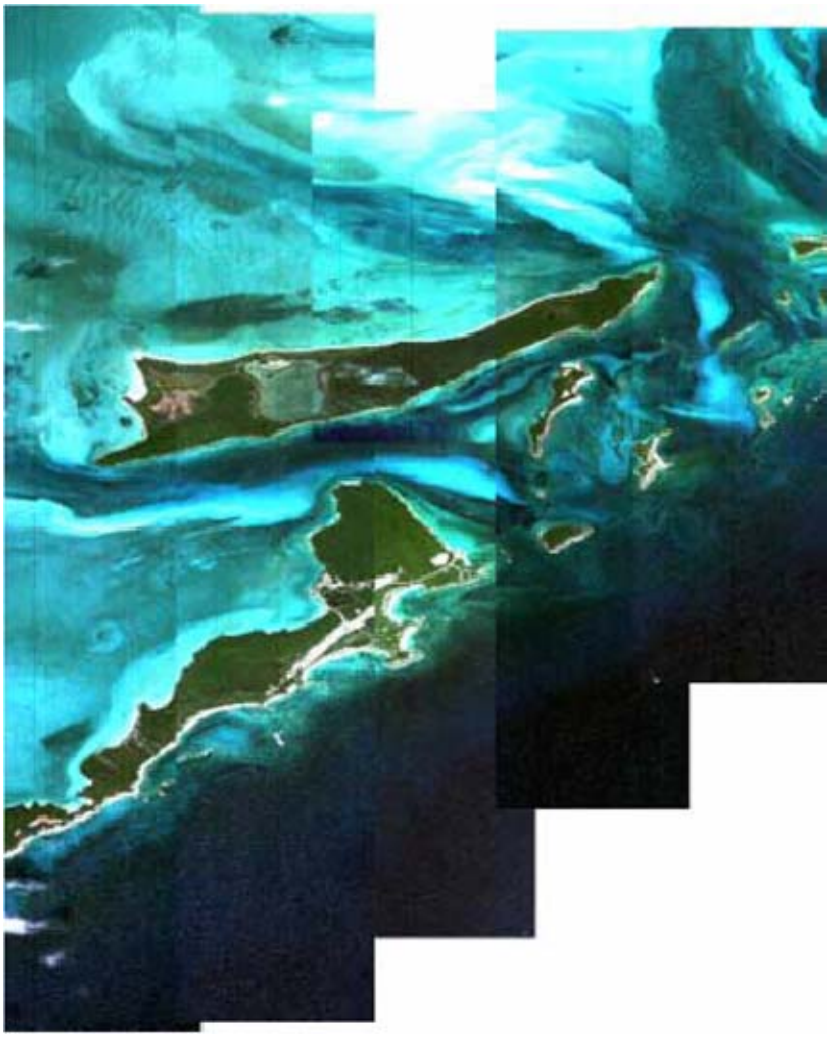

Figure 8. Lee Stocking Island and Norman's Pond Cay 1 June, 1999, 9:00 - 10:00 am NRL Ocean PHILLS hyperspectral data shown as true Color RGB image. From Davis (2002).

## 3. CASI

The Compact Airborne Spectrographic Imager (CASI) was designed by Itres Research Limited of Calgary, Canada (McFee and Ripley, 1997). It is a push-broom imaging spectrograph capable of acquiring visible and near infrared hyperspectral imagery over 288 bands anywhere between 400-1,000 nanometers by using a diffraction grating to spread the slit image across a two dimensional charge-coupled-device (CCD) (McFee and Ripley, 1997). There are two modes of operation available for CASI: spatial and spectral, each maximizing either the spatial or the spectral resolution in the tradeoff. Particularly important to the application discussed in this thesis is that the wavelengths and bandwidths of CASI can be specified by the customer hiring the sensor, with their configuration depending on the areas being surveyed and the target features to be detected (Green et al., 2000). Spatial resolution is variable based upon the altitude from which the imager is flown, airspeed, and sensor integration or exposure time (Smith et al., 2000). Spectrally, CASI has an average resolution of 3 nm (Lewotsky, 1994). The number of CASI bands available is limited by the scanning speed of the instrument and depends on the spatial resolution. For example, Green et al., (2000) report that at a pixel size of 1m, a maximum of 8 bands can be specified; at 3m this increases to 15 . CASI has been used in several marine projects involving the determination of bottom types and marine habitats. One such study was by Borstad et al. (1997) for the Ministry of Fisheries and Marine Resources of the Republic of Mauritious. The study showed an example of the technology for classification of coastal bottom types for hydrographic purposes; see mapping example in Figure 9. A notable and often cited application of CASI to marine environments is the work by Mumby et al. (1998) in the Turks and Caicos Islands in the Caribbean Sea.

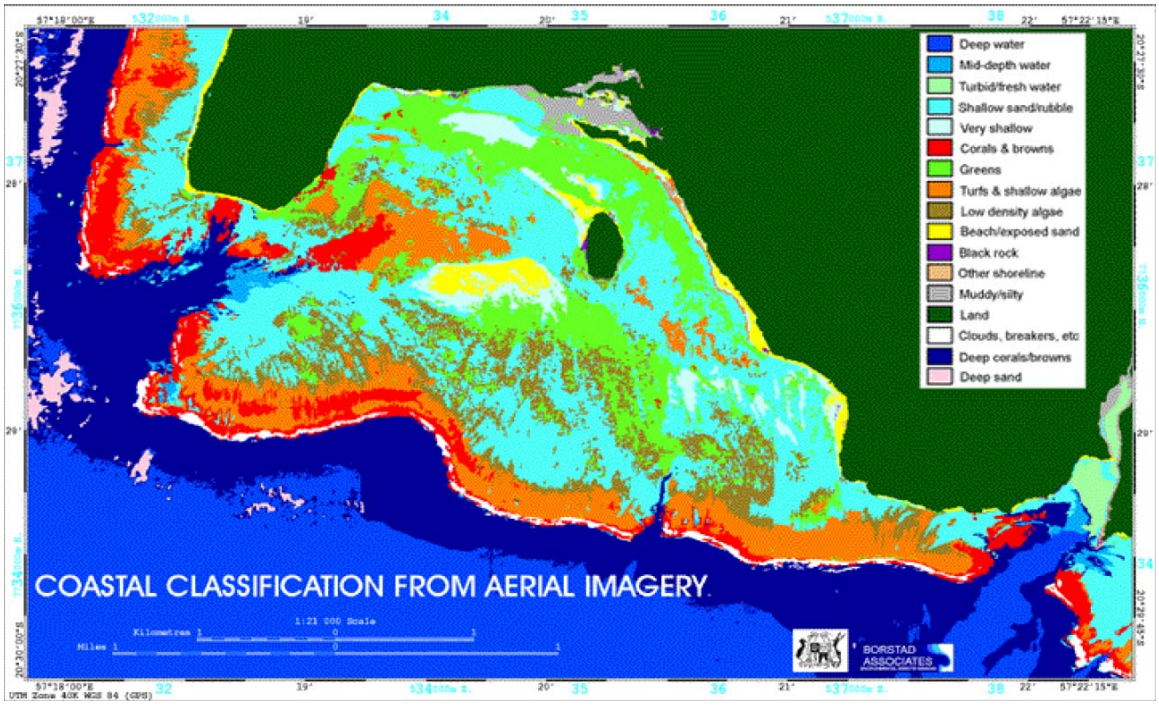


Figure 9. Coastal classification example. Taken from Borstad Industries.

## 4. HYMAP

The Hyperspectral Mapper (HyMap) was developed in Australia (Cocks et al., 1998) and operated by HyVista Corporation around the world, including extensive sites in the U.S. (Kruse et al, 2000). Although originally designed with 96 channels operating over a wavelength range of 550 – 2500 nm, it was later improved to 128 bands covering 450 – 2500 nm. This improvement saw the addition of two thermal bands (one in the 3-5 µm atmospheric window and another in the 8 – 10 µm spectral regions). HyMap has a spectral resolution of 15 nm in the UV/VIS spectrum and approximately 20nm in the SWIR (Cocks et al., 1998). The sensor is typically flown on a Cessna style aircraft at altitudes ranging from 2 – 5 km. This yields a spatial resolution of 2 – 10 m over a swath ranging 2.3 – 4.6 km along track based on a 60-degree field of view (Kruse et al., 2000). Like AVIRIS, HyMap is a "whiskbroom" scanner that uses diffraction gratings and four 32-element detector arrays (one silicon and three liquid-cooled Indium Antimonide) to produce a 512-pixel swath (Kruse et al, 2000). Originally, HyMap had been used primarily to determine mineral composition over terrestrial targets, but later has also been used in environmental and marine research. Jupiter et al., 2002, and Siciliano, 2005, for example used it to study the salt marsh plant *Salicornia virginica* in Elkhorn Slough,

California. These studies highlighted the potential of using HyMap hyperspectral imagery in mapping the coastal environment. One of the advantages of HyMap over AVIRIS is its small, compact size and portability (Figure 10).


Figure 10. HyMap sensor mounted in Cessna style aircraft. From http://www.intspec.com on October 13, 2006.

# III. OPTICAL REMOTE SENSING IN MARINE ENVIRONMENT

## A. DEFINING OPTICAL MEASUREMENTS

Collecting optical measurements in the marine environment involves understanding light interactions in both the atmosphere and water. Radiometry measures electromagnetic, or radiant, energy (Mobley, 1994). It is the foundation for studies of radiative transfer in natural waters, as light is merely electromagnetic energy consisting of photons moving at a speed of $2.998 \times 10^8$ m $s^{-1}$ (also known as the constant *c*).

### 1. Irradiance

As light energy travels from the sun, the energy (photons in all wavelengths, P) per unit time per unit area of the sphere decreases as a matter of $R^{-2}$ (distance from the sun), Equation (1). This light energy is called irradiance ($E_s$) and is measured in watts per square meter ($W\ m^{-2}$).

$$E_s \equiv \frac{P}{4\pi R^2} \qquad \left(W\ m^{-2}\right) \tag{1}$$

At the Earth's atmosphere, irradiance has been measured to be 1367 W $m^{-2}$ (± 50) and is commonly referred to as the solar constant (Mobley, 1994). Upon interaction with the atmosphere, this energy becomes extremely variable based upon solar angle and atmospheric conditions (e.g. cloud cover, aerosols, pollutants) (Halliday et al, 2001). Typical irradiances at sea level are outlined in Table 1.

| Environment | Irradiance (W $m^{-2}$) |
|---|---|
| Solar constant (for comparison) | 522 |
| Clear atmosphere, sun near the zenith | 500 |
| Clear atmosphere, sun at 60˚ from the zenith | 450 |
| Hazy atmosphere, sun at 60˚ from the zenith | 300 |
| Hazy atmosphere, sun near the horizon | 100 |
| Heavy overcast, sun near the horizon | 10 |
| Clear atmosphere, full moon near the zenith | $1 \times 10^{-3}$ |
| Clear atmosphere, starlight only | $3 \times 10^{-6}$ |
| Cloudy night | $3 \times 10^{-7}$ |
| Clear atmosphere, light from a single bright star ($1^{st}$ magnitude) star | $3 \times 10^{-9}$ |
| Clear atmosphere, light from a single, barely visible ($6^{th}$ magnitude) star | $3 \times 10^{-11}$ |

Table 1. Typical total (direct plus diffuse) irradiances at sea level in the visible wavelength ban (400-700 nm). From Mobley (1994).

To detect the "downward" photons emitted by the sun, or downward irradiance, one simply needs to place a photon collector in the plane for viewing the source of emission. Equation (2) describes the measurement of spectral downward plane irradiance ($E_d$) with respect to the wavelength structure of the light field.

$$E_d(\vec{x};t;\lambda) \equiv \frac{\Delta Q}{\Delta t\,\Delta A\,\Delta\lambda} \qquad (W\,m^{-2}\,nm^{-1}) \tag{2}$$

$\Delta Q$ is the radiant energy from an energy source over time ($\Delta t$) which is incident upon the detector element of area $\Delta A$ within a given wavelength band ($\Delta\lambda$). Irradiance is the radiant energy per unit time, per unit area, per unit wavelength measured in watts per square meter per nanometer ($W\,m^{-2}\,n^{-1}$). (Mobley, 1994).

## 2. Radiance

### *a. Radiance Defined*

Radiance describes the measure of light that passes through or is given off by an object and falls within a given solid angle in a particular direction (Robinson, 2004). The term depicts emissions from diffuse sources and reflection-diffuse surfaces. As defined in Equation (3), radiance is dependent on direction and characterizes the measurements received by an imaging instrument (Mobley, 1994).

$$L(\vec{x};t;\vec{\xi};\lambda) \equiv \frac{\Delta Q}{\Delta t\,\Delta\,A\,\Delta\,\Omega\,\Delta\lambda} \qquad (W\,m^{-2}\,sr^{-1}\,nm^{-1}) \tag{3}$$

Measured in watts per square meter per steradian per nanometer (W $m^{-2}$ $sr^{-1}$ $nm^{-1}$), radiance tells us the amount of power emitted by an emitting or reflecting object that can be received by an optical system looking from an angle of view. The solid angle ($\Delta\Omega$) is subtended by the optical system's opening or aperture from the direction $\xi$ (Mobley, 1994), as seen in Figure 11.

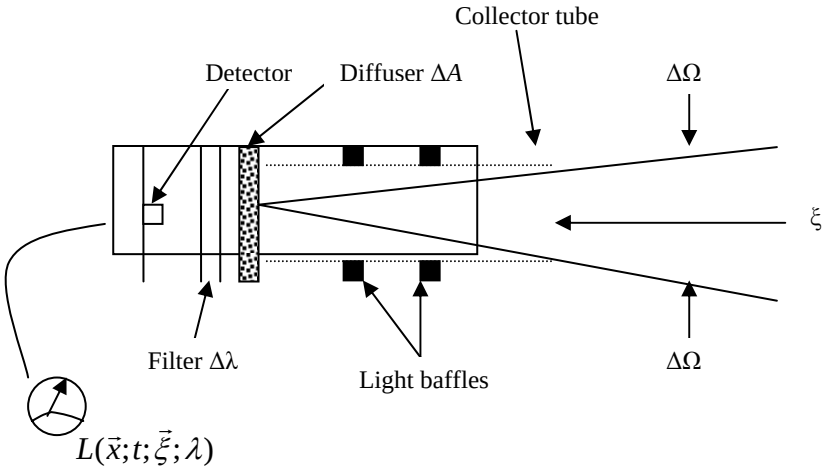


Figure 11. Schematic design of an instrument for measuring unpolarized spectral radiance. From Mobley (1994).

***b. Radiance Invariance Law***

One fundamental property of radiance is that it does not vary along the path of the photon when in a vacuum. As a result, the amount of radiation arriving to the detector has no dependence on the distance the detector is from the emission source because the source radiance ($L_s = \Phi_o / A_r\Omega_r$) is equal to the received radiance ($L_r = \Phi_o / A_s\Omega_s$). By definition of the solid angle, Equation (4), yields Equations (5) through (7) (Mobley, 1994).

$$\frac{A_s A_r}{r^2} = \Omega_r A_r = A_s \Omega_s \tag{4}$$

$$L_r = \frac{\Phi_r}{A_s \Omega_s} \tag{5}$$

$$L_s = \frac{\Phi_s}{A_r \Omega_r} \tag{6}$$

$$L_r = L_s \tag{7}$$

A geometric representation of the radiance inversion law is illustrated in Figure 12.

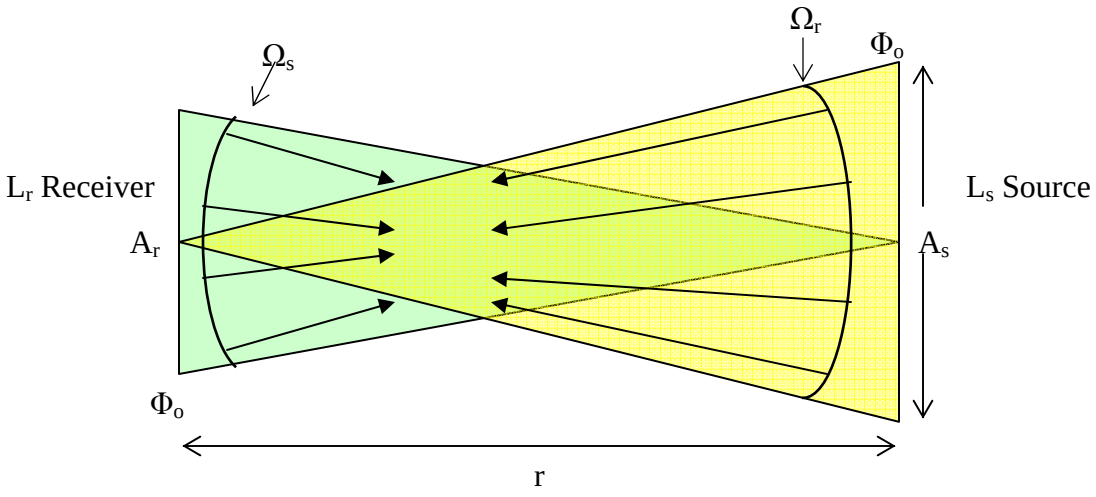


Figure 12. Geometric proof of the radiance invariance law. Redrawn from Cornell (2004)

The above associations are only valid in a vacuum. In the real world, there are multitudes of objects that exist within our atmosphere that causes the radiance from the surface of the Earth to be diffused, reflected or diffracted prior to be received by our detector. Several models exist to rectify the phenomenon (Robinson, 2004).

## B. INTERACTIONS BETWEEN LIGHT AND WATER

Light traveling from the sun to the surface of the Earth interacts with the atmosphere and its particle constituents, affecting the photons path in their journey to the Earth's surface. Radiative transfer scientists have been able to reasonably model the atmosphere in order to interpret remotely sensed images more accurately and allow spectral classification and identification of the earth's surface. On the other hand, while the earth's atmosphere is generally assumed to be relatively homogeneous in these models, the interactions between light and water are more complex due to the spatial and temporal variability of the properties of the liquid medium (Robinson, 2004), so that the same assumption cannot be reasonably applied to the water column. Modeling radiative transfer in the water column in therefore a more uncertain science than atmospheric modeling. Water can be categorized into three broad classes: pure water, pure seawater and natural waters. Pure water contains only water molecules and is difficult to produce

even in a laboratory. Pure seawater is similar to pure water with the added content of various dissolved salts; again not found in nature and difficult to produce. Natural waters (the category to which the water bodies found on the earth's surface belong) have a variety of dissolved and particulate substances that vary greatly because of their biologic, physical and chemical influences (Mobley, 1994), and greatly affect radiative transfer in this medium. The optical properties of water have been broken into two broad optical categories: Inherent Optical Properties (IOP) and Apparent Optical Properties (AOP).

### 1. Inherent Optical Properties (IOP)

As light propagates through water it will either become absorbed, scattered or transmitted depending upon the type and amount of molecular or particulate matter present in the water column. The properties that describe these interactions are known as **inherent optical properties** (IOP) (Robinson, 2004). IOPs are defined as those properties that depend solely upon the medium and are independent of the light field within the medium (Mobley, 1994). An illustration of incident radiant light from a narrow collimated beam of monochromatic light with a power $\Phi_i(\lambda)$, W nm$^{-1}$ passing through a volume of water is represented in Figure 13 and will help visualize the different IOPs.

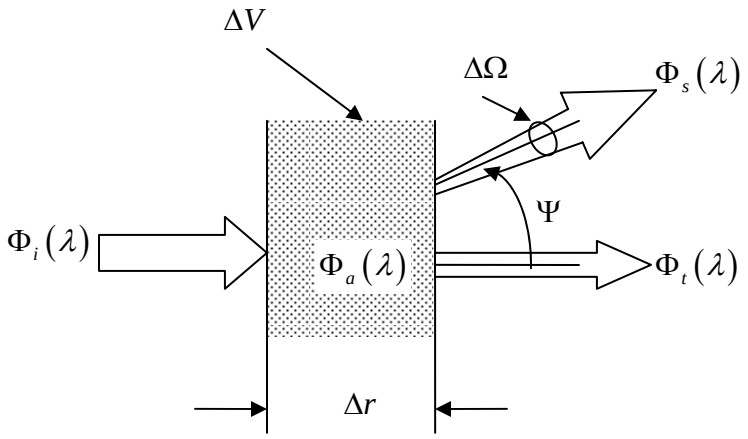


Figure 13. Geometry used to define inherent optical properties. From Mobley (1994).

As light passes through this medium, three things occur. A portion of $\Phi_i(\lambda)$ is being absorbed by the molecules within the volume ($\Phi_a(\lambda)$) while yet another portion of the radiant power is being scattered ($\Phi_s(\lambda)$) away from the transmitted path leaving only the

transmitted radiant power $\Phi_t(\lambda)$ (Mobley, 1994). Through simple geometry, conservation of energy yields the following relationship found in Equation (8):

$$\Phi_i(\lambda) = \Phi_a(\lambda) + \Phi_s(\lambda) + \Phi_t(\lambda) \tag{8}$$

***a. Spectral Absorption Coefficient***

The fraction of incident power absorbed within the volume, $A(\lambda)$, is known as *spectral absorptance* and is a function of the wavelength as defined in Equation (9).

$$A(\lambda) \equiv \frac{\Phi_a(\lambda)}{\Phi_i(\lambda)} \tag{9}$$

Using our geometrical representation from Figure 13, we now take the limit of $A(\lambda)$ and divide the length of the water column $\Delta r$. Equation (10) is now realized as it defines the **spectral absorption coefficient,** $a(\lambda)$ in units of $m^{-1}$, which is the fraction of the incident light flux absorbed per unit width of a sample volume (Chang and Dickey, 1999).

$$a(\lambda) \equiv \lim_{\Delta r \to 0} \frac{A(\lambda)}{\Delta r} \qquad (m^{-1}) \tag{10}$$

***b. Spectral Scattering Coefficient***

Similarly, *spectral scatterence* $B(\lambda)$ is defined as the fraction of incident power scattered out of the beam by the volume of water, as shown in Equation (11), and is used to define the **spectral scattering coefficient** $b(\lambda)$, which is the fraction of incident light flux scattered per unit thickness of a sample volume, Equation (12) (Mobley, 1994).

$$B(\lambda) \equiv \frac{\Phi_s(\lambda)}{\Phi_i(\lambda)} \tag{11}$$

$$b(\lambda) \equiv \lim_{\Delta r \to 0} \frac{B(\lambda)}{\Delta r} \qquad (m^{-1}) \tag{12}$$

***c. Spectral Beam Attenuation Coefficient***

The result of these associations leads to an understanding of the *spectral transmittance*, $T(\lambda)$, which is defined as the portion of incident power transmitted through the volume of water yielding Equation (13).

$$T(\lambda) \equiv \frac{\Phi_t(\lambda)}{\Phi_i(\lambda)} \tag{13}$$

Reviewing Equations (9), (11) and (13), it is quickly recognized that the sum of these ratios equals 1, [Equation (14)] (Gordon, 1994).

$$A(\lambda) + B(\lambda) + T(\lambda) = 1 \tag{14}$$

Additionally, the **spectral beam attenuation coefficient**, $c(\lambda)$ measured in $m^{-1}$, can be determined by simply summing the spectral absorption coefficient with the spectral scattering coefficient as reflected in Equation (15) (Mobley, 1994).

$$c(\lambda) \equiv a(\lambda) + b(\lambda) \quad (m^{-1}) \tag{15}$$

***d. Volume Scattering Function***

Careful examination of Figure 13 reveals two remaining angles that must be addressed, the solid angle ($\Delta\Omega$) and the scattering angle ($\psi$). The scattering angle is defined to exist within the interval $0 \leq \psi \leq \pi$. The angular dispersal of $\Phi_s(\lambda)$ has a fractional element of incident power that is scattered out of the beam through the scattering angle $\psi$ into the solid angle $\Delta\Omega$ which is focused on $\psi$. This element is identified as the angular scatterence per unit distance and unit solid angle, $\beta(\psi;\lambda)$ (Kirk, 1994). When the incident power $\Phi_i(\lambda)$ illuminates an area $\Delta A$, the resultant incident irradiance is $E_i(\lambda) = \Phi_i(\lambda)/\Delta A$ with $\Delta V = \Delta r \Delta A$. Combining this with the definition of $\beta(\psi;\lambda)$:

$$\beta(\psi;\lambda) \equiv \lim_{\Delta r \to 0} \lim_{\Delta\Omega \to 0} \frac{\beta(\psi;\lambda)}{\Delta r \Delta\Omega} = \lim_{\Delta r \to 0} \lim_{\Delta\Omega \to 0} \frac{\Phi_s(\psi;\lambda)}{\Phi_i(\lambda)\Delta r \Delta\Omega} \qquad (m^{-1}\, sr^{-1})$$

We can now define the ***spectral volume scattering function*** with Equation (16):

$$\beta(\psi;\lambda) = \lim_{\Delta V \to 0} \frac{I_s(\psi;\lambda)}{E_i(\lambda)\Delta V} \tag{16}$$

By integrating $\beta(\psi;\lambda)$ over all solid angles, we can now determine a new form of the spectral scattering coefficient $b(\lambda)$ as presented in Equation (17) (Mobley, 1994).

$$b(\lambda) = 2\pi \int_0^{\pi} \beta(\psi;\lambda) \sin\psi \, d\psi \tag{17}$$

The spectral scattering coefficient can be subdivided into the forward scattering coefficient ($b_f$) and backscattering coefficients ($b_b$), Equations (18) and (19).

$$b_f(\lambda) \equiv 2\pi \int_0^{\pi/2} \beta(\psi;\lambda) \sin\psi \, d\psi \tag{18}$$

$$b_b(\lambda) \equiv 2\pi \int_{\pi/2}^{\pi} \beta(\psi;\lambda) \sin\psi \, d\psi \tag{19}$$

Of these two equations, backscattering is the most significant to remote sensing as these are the photons detected by a remote spectral sensor (Robinson, 2004).

IOPs provide the framework for better understanding the constituents of a particular volume of water. However, knowledge of the contributions made by Apparent Optical Properties (AOPs) is also required to understand a particular body of water.

## 2. Apparent Optical Properties (AOP)

AOPs have a dependence on IOPs, but their value varies based on surface illumination. Sun angle, ratio of sky light to direct sunlight, wind and cloud cover all create this variability and establish the dependence of AOPs not only on the medium alone, but also on the directional structure of the ambient light field (Gordon, 1994). Thus, in order to measure AOPs, the ambient radiance distribution of the water column must be determined. To quantify AOPs the diffuse (or "uncollimated") attenuation coefficients for down-welling and upwelling irradiances must be examined, along with spectral irradiance and spectral remote-sensing reflectances.

### *a. Diffuse Attenuation Coefficient of Down-welling Irradiance*

Previous studies have shown that radiances and irradiances decrease nearly exponentially with depth in oceanic conditions (Mobley, 1994). One of the parameters controlling light propagation through water is the **diffuse attenuation coefficient of downward irradiance**, $K_d(z,\lambda)$ in $m^{-1}$ (Mishra *et al.*, 2005). It is

comprised of down-welling irradiance, $E_d(\lambda)$ (W $m^{-2}$), and the thickness, or depth, (*dz* (m)), of the medium through which the light is passing. It is defined in Equation (20).

$$K_d(z,\lambda) = -\frac{1}{E_d(\lambda)}\frac{dE_d}{dz} \qquad m^{-1} \tag{20}$$

The mixture of constituents in the water column, along with the directional components of the ambient light field in the medium determine the value of $K_d(z,\lambda)$. Therefore, elements such as time of day (which is related to sun angle), wind, and cloud cover, must be assessed when determining $K_d(z,\lambda)$. However, as pointed out by Kirk (1994), IOPs remain the primary driver for the value of $K_d(z,\lambda)$ vice the incident radiation field (Kirk, 1994).

***b. Diffuse Attenuation Coefficient of Upwelling Irradiance***

Upwelling irradiance describes the upward path of a photon. Therefore, the **diffuse attenuation coefficient of upwelling irradiance** is defined by Equation (21) (Mobley, 1994).

$$K_u(z,\lambda) = -\frac{1}{E_u(\lambda)}\frac{dE_u}{dz} \qquad m^{-1} \tag{21}$$

***c. Spectral Irradiance Reflectance***

**Spectral irradiance reflectance** is simply the ratio between spectral upwelling and down-welling irradiances, Equation (22), and is usually measured just below the surface of the water (Mobley, 1994).

$$R(z;\lambda) \equiv \frac{E_u(z;\lambda)}{E_d(z;\lambda)} \tag{22}$$

***d. Spectral Remote-Sensing Reflectance***

**Spectral remote-sensing reflectance** describes the ratio of down-welling light (down-welling irradiance, $E_d$) incident upon the water surface that is returned through the surface in the direction of a remote sensor oriented in the opposite direction, Equation (23).

$$R_{rs}\left(\theta,\phi;\lambda\right)\equiv\frac{L_u\left(z=a;\theta,\phi;\lambda\right)}{E_d\left(z=a;\lambda\right)}\qquad\left(sr^{-1}\right)\qquad(23)$$

With depth $z = a$, $R_{rs}$ is measured as a function of $L$ and $E_d$ in the air. $L$ is "water-leaving" radiance and is defined as radiance backscattered out of the water back towards the sensor (Gordon, 1994). This quantity can be measured by a spectrometer and is the basis for the study carried out in this thesis.

## 3. Modeling Absorption in Water

To model absorption in water, an understanding is required of how the particulate and dissolved matter found in the water column absorbs light. Water, whether fresh or oceanic, is comprised of many constituents, including organic and inorganic particles. Seawater has the additional component of varying amounts of dissolved salts, resulting in a 30% greater amount of scattering than fresh water (Mobley, 1994). Natural water constituents are categorized into dissolved and particulate matter. Dissolved matter is defined as matter that is less than 0.4 μm in diameter, while particulate matter is anything larger than 0.4 μm. This is significant because 0.4 μm (= 400 nm) is the shortest wavelength of visible light, which limits the ability to optically examine the dissolved matter (Mobley, 1994). It is important to note that particulate matter is divided into organic (of biological source) and inorganic sources, based on origin. Some common organic and inorganic constituents of water, along with their size and a brief description of how they affect light propagation in water, are listed in Table 2.

| Type of Particle | Size of Particle | Contribution to Light Propagation in Water |
|---|---|---|
| **Organic Particles** | | |
| Viruses | 20-250 nm | Due to their size, viruses tend to be inefficient absorbers and scatters. However, there is the possibility of a significant contribution to the backscatter coefficient $b_b$ in the blue wavelengths. |
| Colloids | 0.4-1.0 μm | Significantly contribute to backscattering |
| Bacteria | 0.2-1.0 μm | Significant scatters and absorbers especially at blue wavelengths and in clear oceanic waters. |
| Phytoplankton | <1 - >200 μm | Primarily responsible for determining the optical properties of most oceanic waters and contribute very little to backscatter. |
| Detritus | <1 - >20 μm | Residues of decomposed cells of phytoplankton and are major backscatters in the ocean. |
| **Inorganic Particles** | | |
| Quartz Sand | 0.1 - >100 μm | Very finely ground sand that results from erosion. |
| Clay Minerals | 0.1 - >100 μm | Wind blown dust usually from coastal waters. |

Table 2. Types of Water Constituents. Modified from Mobley (1994).

### *a. Pure Water*

Pure water, defined as containing only water molecules (Mobley, 1994), is a medium in which particulate backscattering, particulate absorption, and the absorption due to dissolved organic materials is considered to be zero. As a result, we can model the absorption and scattering of light in pure water through an understanding solely of electromagnetic wave propagation. Since the speed of light is dependent upon the medium in which it propagates, all materials have both a real and a complex index of refraction. The complex index of refraction $k(\lambda)$ dominates the absorption properties of pure water.

Equation (24) describes the relationship between the absorption coefficient $a(\lambda)$ and the complex index of refraction $k(\lambda)$ where $\lambda$ is the *in vacuo* wavelength.

$$a(\lambda) = \frac{4\pi k(\lambda)}{\lambda} \tag{24}$$

When plotted together as a function of wavelength, one can graphically represent the optical constants of pure water as seen in Figure 14.

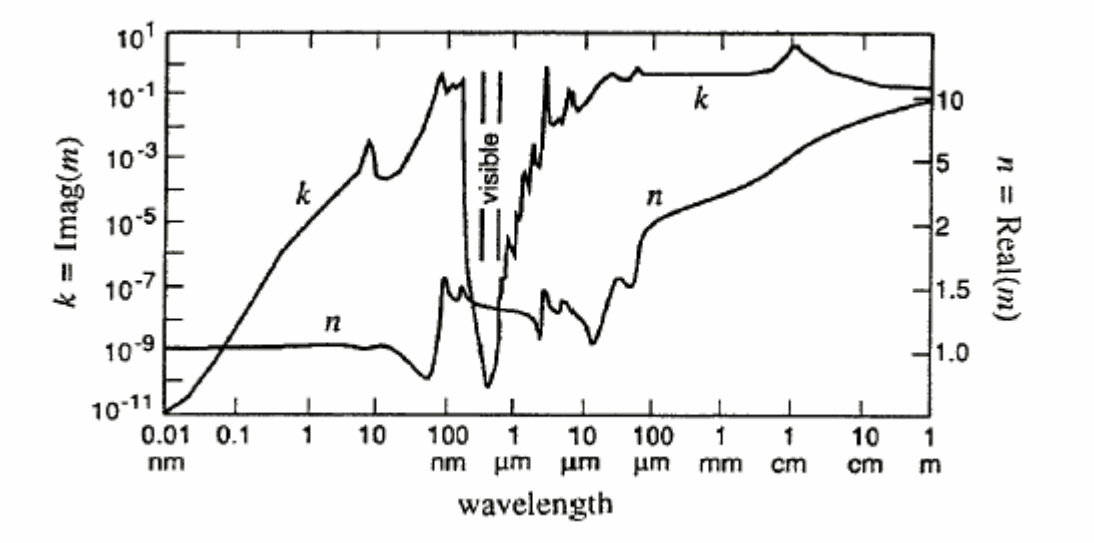


Figure 14. The optical constants of pure water. From Mobley (1994).

The narrow window between the near ultraviolet and visible light, seen as the nine orders of magnitude decrease in $k(\lambda)$, provides a corresponding window in the spectral absorption coefficient $a(\lambda)$; see Figure 15. It is this unique characteristic of water that allows photosynthesis to occur, a process necessary to sustain life in the marine environment.

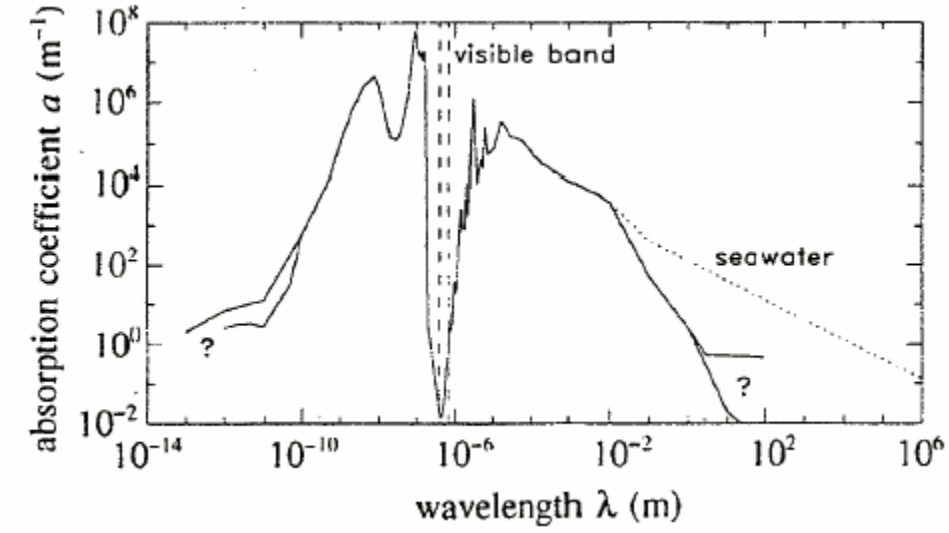


Figure 15. Spectral absorption coefficient of pure water (solid line) and of pure seawater (dotted line) as a function of wavelength. From Mobley (1994).

### *b. Pure Sea Water*

Smith and Baker in 1981 reported a set of absorption values for pure seawater, widely accepted in marine optics since its publication (Mobley, 1994). Their numbers were based upon the assumptions that in the clearest natural waters 1) salt and other dissolved substances had an insignificant absorption factor, 2) the sole source of scattering was by water molecules and salt ions, and 3) no inelastic scattering occurred (Smith and Baker, 1981). Gordon (1994) further refined their submission by dividing the diffuse attenuation function $K_d(\lambda)$ by $D_o(\lambda)$, the measurable distribution function which corrects sun angle and sea state effects. Mobley (1994) caveats the use of the aforementioned absorption properties of pure seawater because they were derived from "clearest natural waters," which are known to hold some amount of dissolved and particulate matter.

### *c. Dissolved Organic Matter*

Dissolved organic compounds exist in both fresh and sea water at varying concentrations. These compounds are produced through the decaying process of plants and are generally brown in color. When sufficient quantities exist, the color of the water can appear a brownish yellow; hence, it is commonly called "yellow matter" or more formally Colored Dissolved Organic Matter (CDOM). CDOM can be modeled by Equation (25) (Mobley, 1994).

$$a_y(\lambda) = a_y(\lambda_o) e^{-0.014(\lambda-\lambda_o)} \tag{25}$$

where $\lambda_o$ is the reference wavelength, usually 440 nm, and $a_y(\lambda_o)$ is the absorption as a result of the yellow matter at $\lambda_o$. Therefore the value of $a_y(\lambda_o)$ is heavily dependent upon the amount of CDOM present in the water. The exponential decay describes the dependence on the proportion of specific types of yellow matter (Mobley, 1994).

### *d. Phytoplankton*

Phytoplankton is a term describing unicellular and multicellular microscopic plant organisms that drift in the water column (Mobley, 1994). They are strong absorbers in the blue (due to chlorophylls and carotenoids) and red (due to chlorophyll *a*) regions of the EM spectrum with minimum absorption in the green region

(Shifrin, 1988). The chlorophyll-specific spectral absorption coefficient for eight species of phytoplankton showing their maxima in the blue and red regions of the visible spectrum is illustrated in Figure 16.

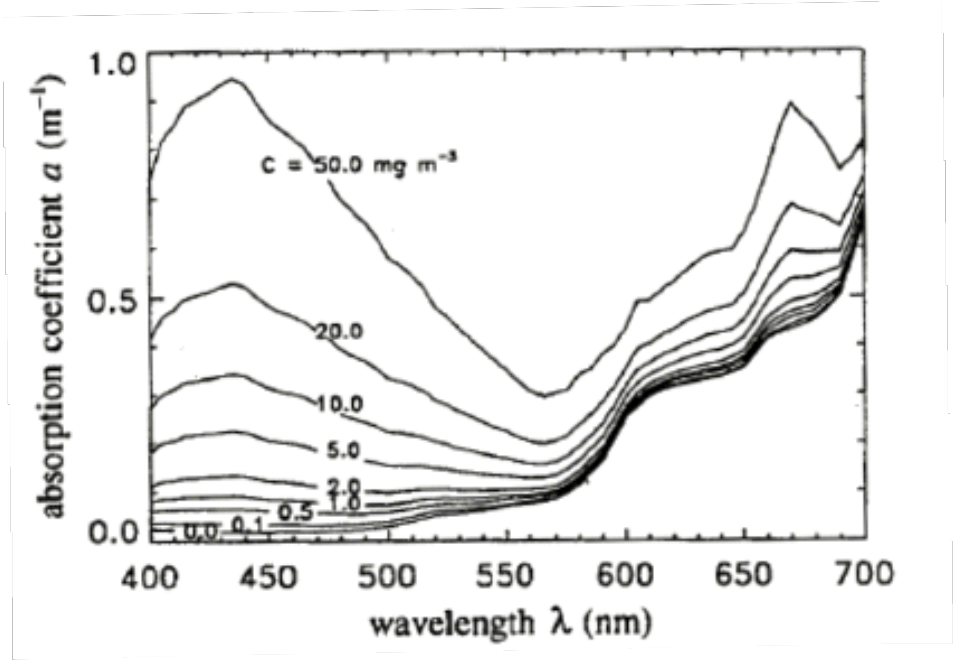


Figure 16. Chlorophyll-specific spectral absorption coefficients for eight species of phytoplankton. From Mobley (1994).

### *e. Organic Detritus*

Organic detritus is non-living organic particles produced by the biologic breakdown of phytoplankton. These particles are major backscatters and differ from the absorption characteristics of phytoplankton because they only absorb in the blue region of the spectrum. They are modeled by Equation (26) (Mobley, 1994).

$$a_{\text{det}}(\lambda) = a_{\text{det}}(400)e^{-0.011(\lambda-400)} \tag{26}$$

### *f. Total Absorption Model*

Variant upon concentration levels of dissolved substances, phytoplankton, and detritus, the total spectral absorption coefficient for any water sample will range from that of pure water to ones that show orders of magnitude greater than pure water. Morel (2001) proposed a bio-optical model that reflects the spectral absorption coefficient for case I waters. The absorption coefficient is heavily parameterized in terms of the chlorophyll concentration C (mg $m^{-3}$) as shown in Equation (27) (Kirk, 1994).

$$a(\lambda) = \left(a_w(\lambda) + 0.06 a_c^*(\lambda) C^{0.65}\right)\left(1 + 0.2e - 0.014(\lambda - 440)\right) \quad (27)$$

$a_w(\lambda)$ is the absorption coefficient of pure water ($m^{-1}$) and $a_c^*(\lambda)$ is the non-dimensional chlorophyll-specific absorption coefficient while $\lambda$ is the wavelength expressed in nm resulting $a(\lambda)$ in $m^{-1}$. Chlorophyll concentrations have been tested in a variety of waters. They can range from 0.01 mg $m^{-3}$ in clear open ocean waters to 10 mg $m^{-3}$ in coastal upwelling regions, to 100 mg $m^{-3}$ in estuaries or lakes (Vince and Earnshaw, 2002). A summary example of spectral absorption coefficients $a(\lambda)$ for various waters is shown in Figure 17. Panel (a) shows a(λ) for waters dominated by phytoplankton, panel (b) is for waters with a high concentration of non-pigmented particles, and panel (c) is for waters rich in yellow matter. From Mobley (1994).

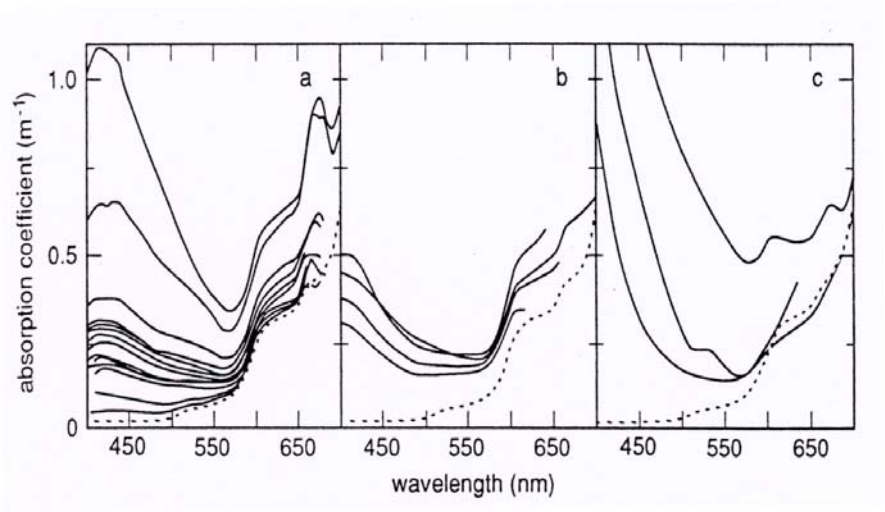


Figure 17. Examples of spectral absorption coefficients for various waters.

### 4. Modeling Scattering in Water

Scattering occurs when incident photons get redirected in their path, and there is a subsequent energy exchange. Given the extreme variability of water constituents, the size of the constituents and the random molecular motions between the constituents and the photons, it is extremely difficult to measure *in situ* scattering in natural waters. The phenomenon of scattering was carefully studied by Lord Rayleigh in the late 19th century.

Unfortunately, studies led him to the false conclusion the oceans color was due to reflection of the sky, a fact refuted by the work of Raman (1922).

### *a. Scattering by Particles*

Particles wreak havoc on the volume scattering function causing it to peak in the forward direction with more than an order-of-magnitude increase in the scattering coefficient including a four-order-of magnitude increase in scattering for $90° \leq \psi \leq 0°$ (Mobley, 1994). Equation (28) represents the effect of particulate matter on the total volume scattering function $\beta(\psi;\lambda)$.

$$\beta_p(\psi;\lambda) \equiv \beta(\psi;\lambda) - \beta_w(\psi;\lambda) \tag{28}$$

The subscript *p* refers to the particles in the water. Examples of particle volume scattering functions from Mobley (1994) determined from in situ measurements in a variety of waters are shown in Figure 18. The graph represents particle volume scattering functions from *in situ* measurements in various waters.

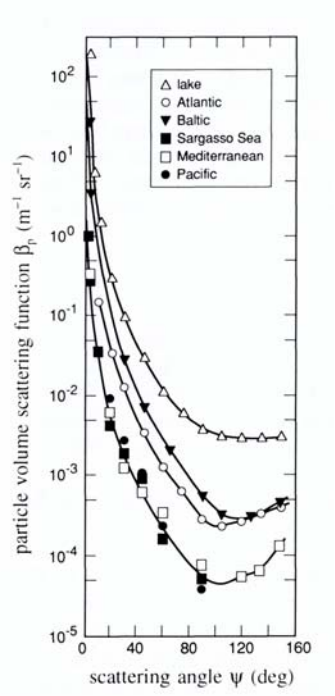


Figure 18. In situ measurements of particle volume scattering. From Mobley (1994)

### *b. Scattering by Turbulence*

Given all the other dynamics of the ocean environment and its effects on scattering, turbulence is very small and almost insignificant contributor, especially for $\psi > 1°$.

### *c. Mie Theory*

Gustav Mie (1908) developed a mathematical model for electromagnetic radiation scattering by spherical particles that is increasingly useful in hydrologic optics. Mie theory is a very complex set of mathematical functions, but the functional elements of the formulas are well modeled by computers. Mobley (1994) presents a single formula that sums up scattering due to the individual inputs by individual particles, represented in Equation (29).

$$b(\lambda) = \int_{all\,m} \int_{all\,d} \sigma_b(D; m_r; \lambda) n(D) dD\, dm_r \tag{29}$$

where $n(D)$ is the particle number size distribution with $m_r$ representing the particle size.

## C. RADIATIVE TRANSFER

Radiative transfer theory illustrates the system of radiation transfer from one point to another regardless of the medium traversed. This theory is the basis for modeling radiation transfers through differing mediums, like the atmosphere and the water column. One simplified example of Radiative Transfer Equation (RTE), is Equation (30), which describes the radiance paths of atmospheric path radiance, $L_p$, water-leaving radiance, $L_w$, and radiance just above the surface due to sea surface reflections, $L_r$, and back to the sensor, $L_s$.

$$L_s = L_p + TL_w + TL_r \tag{30}$$

$T$ is the direct or beam transmittance of the atmosphere and is a multiple to the surface-leaving radiances not scattered out of the field of view to the sensor (Robinson, 2004). *Sky glitter* often is combined with *sun glitter* to form the $L_r$ term.

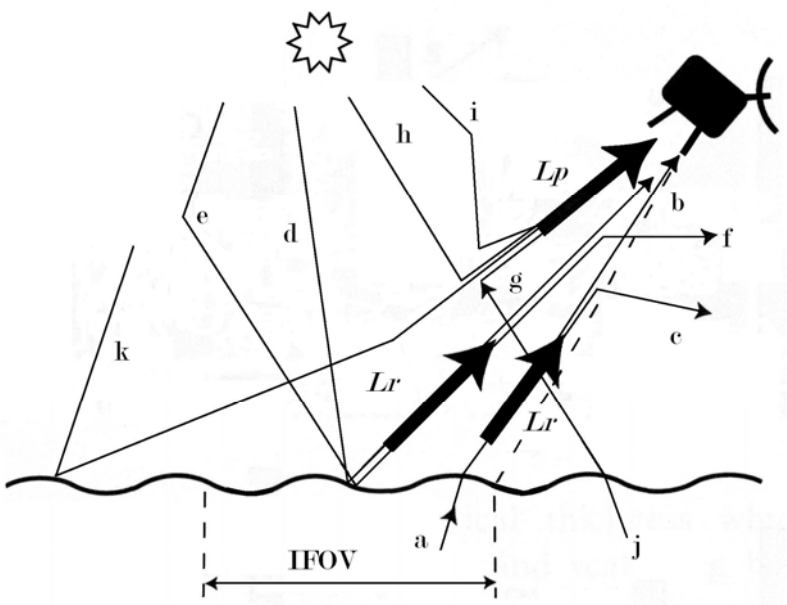


Figure 19. Optical pathways between the sea and the sensor (See text for explanations). Redrawn from Robinson (2004).

Robinson (2004) illustrates these terms in a diagram showing how they each contribute to the radiance received by a sensor, Figure 19. The components in the diagrams are defined as follows: (a) indicates the rays that upwell from below the sea surface and after they are refracted in the direction of the sensor. (b) represents the rays making up $L_w$ that reach the sensor. (c) represents rays either absorbed or reflected in the atmosphere out of the field of view (FOV) of the sensor. Notice (b) and (c) have split from (a). (d) indicates rays from the sun that reflect from the sea surface into the FOV of the sensor (*sun glitter*). (e) Rays scattered by the atmosphere into the FOV of the sensor (*sky glitter*). (f) Rays of $L_r$ scattered away from the FOV of the sensor. (g) $L_r$ rays which reach the sensor. (h) Sun rays scattered into the sensor by the atmosphere as they cross the FOV. (i) Rays scattered in the atmosphere and then subsequently scattered again into the FOV of the sensor. (j) Rays that upwell outside the initial FOV (IFOC) of the sensor and then subsequently scattered by the atmosphere back into the FOV of the sensor. (k) Rays reflected by the surface outside of the IFOV then scattered by the atmosphere into the FOV of the sensor but do not contribute to $L_r$. Therefore in this model (h), (i), (j), and (k) all become part of $L_p$ (Robinson, 2004).

As can be gleaned by the graph above, modeling the atmosphere is a complex problem. Several modeling programs have been developed to address this problem and try to correct for atmospheric and water column effects, none of which is yet considered completely satisfactory.

## D. OPTICAL CLASSIFICATIONS OF NATURAL WATERS

Jerlov (1976) classified marine waters into different categories based on the curve of percentage transmittance of the downward irradiance against wavelength. This resulted in the recognition of three basic oceanic water types: I, II, and III, with nine types of coastal waters in decreasing order of transmittance, or in essence, water clarity as quantified by $K_d(w,\lambda)$ (Mobley, 1994). Another useful classification was developed by Morel & Prieur (1977) which broke these classes into 'Case 1' and 'Case 2' waters. Kirk (1994) points out that this classification was later refined by Gordon & Morel (1983).

### 1. Gordon and Morel (1983)'s Classification

Case 1 is waters are those whose optical properties are mostly characterized by phytoplankton, whose by-products have a dominant role in the optical properties of the ocean (Kirk, 1994). These waters can be very clear to very turbid depending on the concentration level of the phytoplankton and make up approximately 98% of the world's open ocean and coastal waters (Mobley, 1994).

Case 2 waters are defined as waters where particulate matter is not so dependent upon phytoplankton, but rather land-derived CDOM is dominant. These waters are mostly located in areas where river inputs, land drainage, and sludge dumping etc. exist. This typically occurs in coastal waters (Robinson, 2004).

### 2. Jerlov (1976)'s Classification

Jerlov's classification scheme is numbered I, IA, IB, II and III for the open ocean, and 1 through 9 for coastal waters. Type I waters are optically clear while Type III are turbid (Jerlov, 1976). However, Jerlov's types I-III roughly correspond to Case 1 waters in Gordon & Morel (1983)'s scheme. Similarly, types 1-9 align with Case 2 waters.

THIS PAGE INTENTIONALLY LEFT BLANK

# IV. MIDWAY AS AN IDEAL LABORATORY

The field site for this study is Midway Atoll, the second northernmost isle of the Northwest Hawaiian Islands; Figure 20. The atoll lies 2,800 miles west of San Francisco and 2,200 miles east of Japan. Midway is comprised of three small islands, Sand Island (1,200 acres), Eastern Island (529 acres), and Spit Island (6 acres); Sand Island being the only one currently inhabited (Saldino, 1998). In contrast, the circular shaped atoll has more than 85,900 acres of reef area, which hosts a diversity of marine life (Hoover, 2004). As the second most northern coral atoll (Kure Atoll, at 65 miles west northwest, is the northernmost in the world), Midway owes its existence to the coral reefs that built up from an ancient volcano, a process that took millions of years. Throughout this time, coral and algal growth has created a limestone crown that is in places 500 feet thick over the basalt volcanic foundation (Hoover, 2004). The sand and rubble that accumulated along the rim have formed the aforementioned sandy islets that exist today.

Figure 20. 2004 Quickbird image of Midway Atoll.

Midway Atoll was discovered July 5, 1859, by Captain N.C. Middlebrooks. The atoll, known as the "Middlebrook Islands" or the "Brook Islands," was claimed by the United States (U.S.) under the Guano Islands Act of 1856, authorizing the temporary occupation of uninhabited islands to mine guano. However, in August 1867, Captain William Reynolds of the USS LACKAWANNA formally took possession of the atoll for the U.S. At some point after this, the island took on the name "Midway" (Ladd, 1967).

Midway's strategic importance for control of the Pacific became apparent in the early 1900s. Its position along standard naval routes to the Asian continent made it a vital stop for Navy ships during their journeys (Ladd, 1967). Midway was also important for aviation purposes as a convenient refueling stop for transpacific flights (Ladd, 1967). In fact, Midway continues to serve as an emergency landing strip for commercial jetliners today.

Midway has an illustrious place in U.S. history and for the U.S. Navy in particular. In the early 1940s, the military situation in the Pacific was beginning to deteriorate with increased tensions between Japan and the United States. This catalyzed further development of the island (Ladd, 1967), including new gun installations and a seaplane base (one of the long-term environmentally damaging consequences of this new construction was the dredging carried out to widen the south channel, visible in Figure 20 to accommodate larger naval ships and a much larger human population). Six months after the Japanese attack on Pearl Harbor, on June 4, 1942, a naval battle near Midway saw the U.S. Navy deliver a crushing defeat to the Japanese Navy; see Figure 21 which has been argued to have been the turning point of World War II's fate. Despite its glorious past, all of these events on Midway have created severe imbalances on the atoll's natural environment.


Figure 21. Burning oil tanks on Sand Island during the Battle of Midway. From Ladd, 1967.

On April 22, 1988, Midway was designated a National Wildlife Refuge even though it was still under the primary jurisdiction of the United States Navy. As part of the Base Realignment and Closure process, the Navy facility on Midway operationally closed on September 10, 1993, and the last contingent of Navy personnel left on 30 June 1997 (Ladd, 1967). On October 31, 1996, President Bill Clinton signed Executive Order 13022, transferring jurisdiction and control of the atoll to the U.S. Department of the Interior, under the U.S. Fish and Wildlife Service (US FWS). In 2006, President George W. Bush designated the Northwest Hawaiian Islands as a Marine National Monument making it the largest Marine Protected Area in the world (a distinction formerly carried by the Great Barrier Reef in Australia). The U.S. Fish and Wildlife Service continues to manage Midway Atoll National Wildlife Refuge today as part of the National Monument.

The rich biological and historical character of Midway Atoll has made it a great laboratory for scientific study in different disciplines, from geology to biology to oceanography. The naval and wartime actions have introduced a large amount of manmade artifacts throughout the atoll that have upset the ecological balance of the island, which the US FWS continues to try to mitigate. However, for our purposes some of this debris presented an opportunity for testing techniques for detecting man-made materials in littoral environments. Additionally, the Type I waters that characterize coral

reef environments like Midway are the optimal setting for optical remote sensing experiments, an additional reason why this atoll is an ideal location for this study.

# V. BIOLOGICAL INDICATORS

Cyanobacteria is a phylum of Bacteria that obtain their energy through photosynthesis, and are found in many habitats from the oceans to fresh water to dry soil. Originally called blue-green algae, they are among the oldest living organisms on Earth. Estimated to have been in existence for more than three billion years, cyanobacteria are thought to have been considerable contributors to the oxygenation of Earth's ancient atmosphere (Schopf, 1975). Several genera of cyanobacteria exist both in the aquatic and terrestrial environments playing a vital role in the Earth's nitrogen cycle as nitrogen fixers. Biotic nitrogen fixation is a process that converts relatively inert atmospheric nitrogen ($N_2$) into nitrogen compounds such as ammonia, and nitrate, all of which are useful for other biochemical processes. Among nitrogen-fixing organisms, cyanobacteria are the only truly photoautotrophic aerobic nitrogen fixers serving a vital role in nature and the oceans (Apte and Probhavathi, 1994).

The process of biological nitrogen fixation is catalyzed by nitrogenase, a highly conserved enzyme complex consisting of two proteins, an iron protein (Fe-protein) and an iron-molybdenum protein (Mo-Fe-protein) (Berman-Frank et al., 2003). Iron is often a limiting nutrient in oceanic waters (Behrenfeld and Kolber, 1999). Therefore an extraneous iron source in the aquatic environment enhances the growth of cyanobacteria, allowing them to bloom (reproduce rapidly) under these favorable conditions. These blooms are often apparent as thick mats covering the bottom. The hypothesis being tested in this thesis is that detection of a "bloom" of certain benthic cyanobacteria (*Lyngbya* spp., present in the Hawaiian archipelago) would suggest the presence of submerged metal in a littoral environment.

*Lyngbya* spp., is a filamentous, non-heterocystous cyanobacteria (Jones et al., 1987) found in the Tropical Pacific Ocean, and observed to bloom at shipwreck sites in Pearl and Hermes, Midway, and Kure atolls in the Northwest Hawaiian Islands (Maragos and Siciliano, pers. comm.), due to the scattered metal debris found at these sites. Roelfsema et al. (2006) also report it in Moreton Bay, Queensland, Australia. Given the need for iron to support its biological processes, *Lyngbya* spp. is hypothesized to be a

good bio-indicator of ferrous debris in the water or man-made materials leaking iron (Siciliano, 2002) and could therefore be used to detect underwater mines and range residues. Spectral characterization of *Lyngbya* spp. is the first step in this endeavor, with the goal of looking for discriminative absorption features that would enable detection of *Lyngbya* spp. using hyperspectral imagery, and associated metal objects. Despite the need to monitor *L. majuscula* with remote sensing given its often negative ecological impacts in marine environments, until now, there have been no published spectral characterizations of *Lyngbya* spp., beyond the work of Roelfsema et al. (2001), who studied *Lyngbya majuscula* in Moreton Bay, Australia, but failed to report detailed spectral characteristics of the cyanobacteria. On the other hand, multiple works treat reflectance analysis of different genera of cyanobacteria that are planktonic, rather than benthonic, like *Lyngbya* spp.

The pigments and other biochemical constituents found in other benthic organisms in coral reef environments, like coral, algae and inorganic substrates, have been widely documented in the last few decades. Holden and LeDrew (2001), for example, conducted *in situ* measurements of corals in Fiji Islands in the Pacific, and St. Croix in the Caribbean. Considering discrete wavelengths separately and using second derivative analysis, they were able to discriminate between sand, bleached or algae covered surfaces and healthy coral with 77% accuracy (Holden and LeDrew, 2001). Generally, healthy coral spectra displayed a reflectance minimum at 670 nm and a dramatically decreasing slope starting at 650 nm. There are also twin peaks in reflectance at 575 and 605 nm for healthy coral (Holden and LeDrew, 2001); see Figure 22. Coral is generally distinguishable from algae in the region 500-625 nm, while sand gives a very bright reflectance (Hochberg and Atkinson, 2003). In comparison, *Lyngbya* spp. has been reported to be optically dark and absorbing light both in the visible and infrared regions (350 – 1050 nm) (Roelfsema *et al*, 2006). Absorption features in cyanobacteria at 564 and 620 nm were documented by Jupp et al. (1994) suggesting their association with the pigments phycocyanin and phycoerythrin.

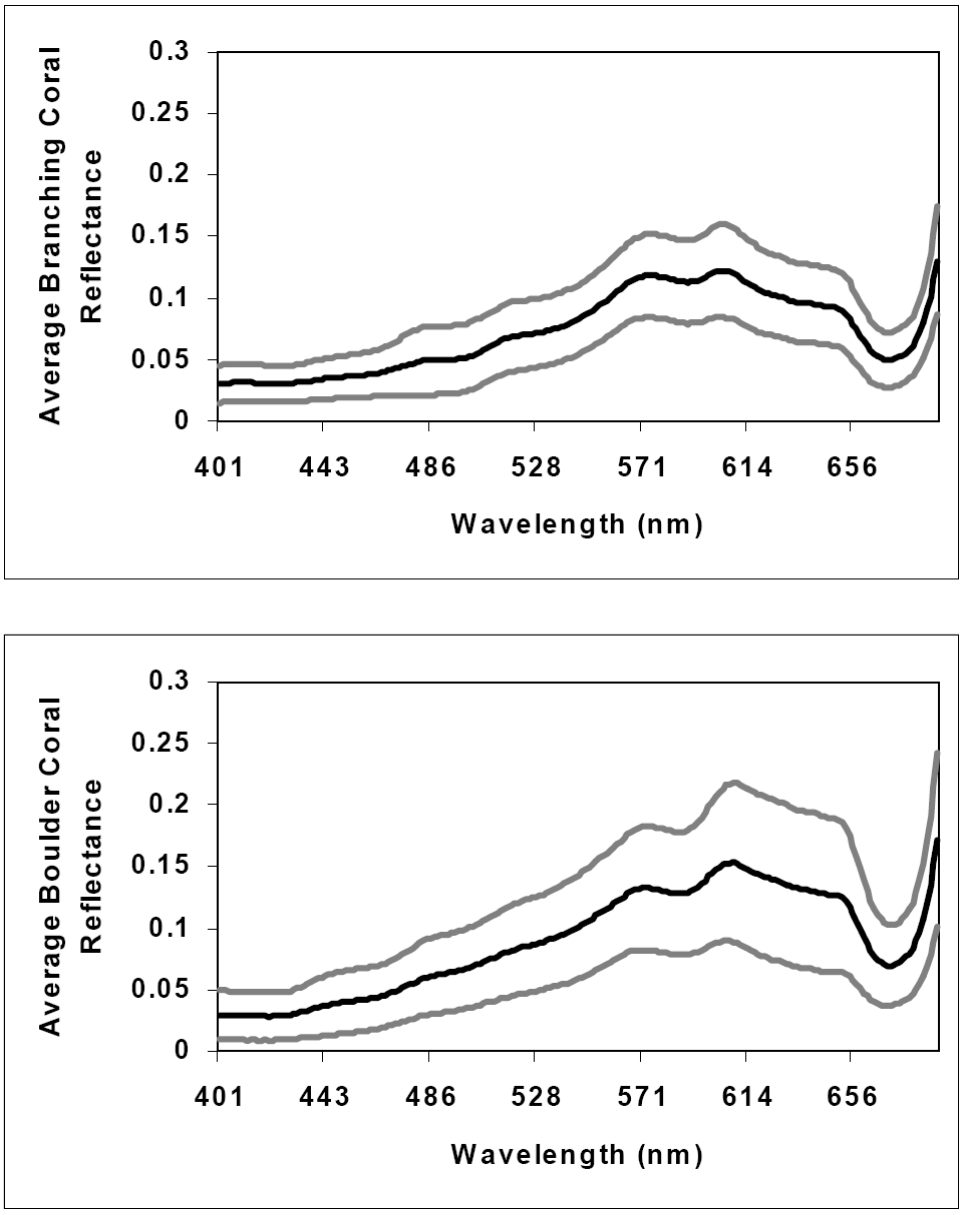


Figure 22. Healthy coral spectra average reflectance (black lines) and standard deviation (gray lines). From Holden and Ledrew, 2001.

All cyanobacteria are in fact characterized by pigments called phycobilins (phycocyanin, phycoerythrin and allophycocyanin), water-soluble fluorescent proteins which are an important part of their photosynthetic apparatus. They harvest light energy in the visible spectrum at those wavelengths poorly exploited by chlorophyll pigments (Lemasson et al, 1973). Through fluorescence energy transfer, they convey the energy to chlorophyll at the photosynthetic reaction center (Boussiba, S. and Richmond, 1980).

Phycoerythrins (absorbing green light) have an absorption maxima that lies between 490 and 570 nm while phycocyanins (absorbing red light) have an absorption maxima found between 610 and 665 nm (Seppala et al, 2005). Allophycocyanins are more restrictive and absorb in the red around 652 nm (Hedley and Mumby, 2002). Additionally, allophycocyanin has been suggested to be most efficient as a light-harvesting pigment in cyanobacteria (Lemasson et al., 1973). A thorough characterization of the absorbance/reflectance spectrum of *Lyngbya* spp. and other aquatic, benthic cyanobacteria has not been attempted to date. As an effort to start filling the vacuum, this thesis therefore aims at spectrally characterizing benthic cyanobacteria and surrounding substrates (coral, sand and algae) present within Midway Atoll, as the first step for testing hyperspectral imaging's capabilities to detect this organism in littoral environments as an indicator of man-made metal objects.

# VI. DATA AND METHODOLOGY (TOOLS AND TECHNIQUES)

## A. OCEAN OPTICS USB2000 FIBER OPTIC SPECTROMETER

Spectral remote sensing reflectance for this study was measured using an Ocean Optics USB2000 Fiber Optic Spectrometer that was controlled and operated by a laptop computer. The spectrometer collected light in the wavelength ($\lambda$) range 200-1100 nm $\left(\frac{650\,nm\,spectral\,range}{2048\,pixels} = .3173\,nm\right)$ with a spectral resolution of 1.33 nm full-width-half-maximum (dispersion × pixel resolution = 0.317 nm pixel$^{-1}$ × 4.2 pixels). A technical illustration of the spectrometer is shown in Figure 23. It provides a technical description of the spectrometer with the components ordered as follows: 1) SubMiniature series A (SMA) connector, 2) 25 µ slit, 3) filter, 4) collimating mirror, 5) Grating #3 650 nm spectral range grating blazed at 500 nm with a maximum efficiency (> 30%) from 350-850 nm, 6) focusing mirror, 7) L2 detector collection lens, and 8) Sony ILX511 linear silicon CCD array. For a listing of predicted ranges and resolutions based on a 600 mm$^{-1}$ grating and 25-µ slit, see Figure 24.

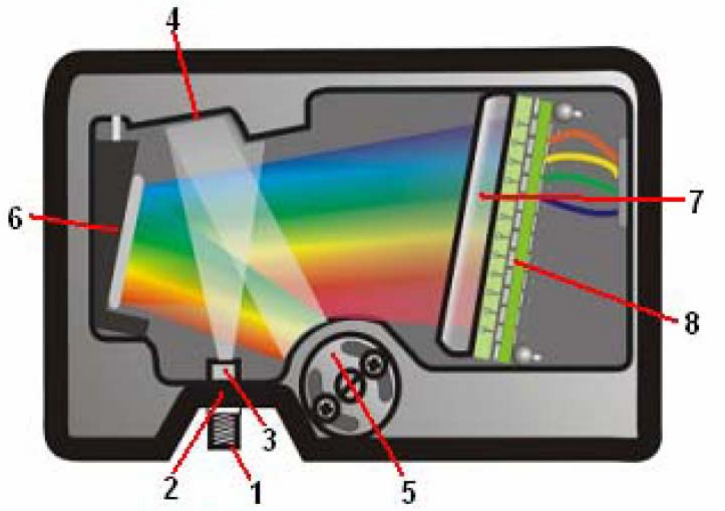


Figure 23. USB2000 Spectometer with components. From USB2000 Fiber Optic Spectrometer Installation and Operation Manual.

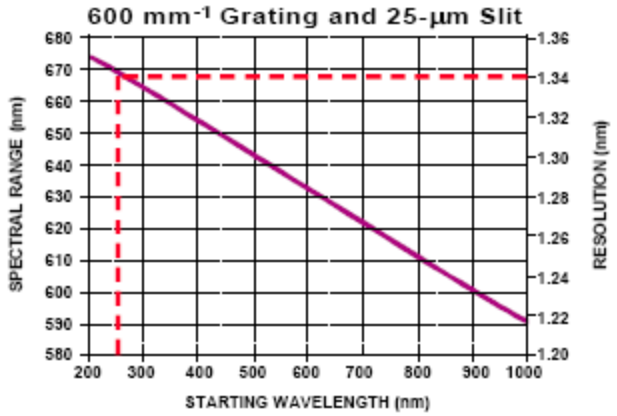


Figure 24. USB2000 predicted ranges and resolutions chart. From http://www.oceanoptics.com/technical/rangeandres.asp

## B. OPTICAL GROUND TRUTH AND SPECTRAL PROCESSING

Optical ground truth measurements were conducted *in situ* at Midway Atoll from an 18-foot Boston Whaler provided to the researchers by the Fish and Wildlife Service during the period July 14-26, 2006. The spectral collection employed the Ocean Optics USB2000 spectrometer with an attached 10.m cable used to transmit light from its collecting tip to the spectrometer. The fiber-optic cable had a maximum efficiency in the visible-near infrared (400-2100 nm) with a field of view (FOV) of 24.8°. The USB2000 was connected to a laptop computer managed by the boat operator. One diver on SCUBA would dive to the target benthic substrate with the collection end of the fiber-optic cable and signal to the boat operator for measurement acquisition (communication occurred through a series of signals issued via a tethered rope, i.e., two tugs on the rope indicated that a reference spectra was to be taken).

In order to relate radiance measurements to irradiance, it is assumed that benthic surfaces act as Lambertian reflectors directing radiance in all directions equally (Hochberg and Atkinson, 2000). Thus, to measure *L*, the collecting tip of the fiber-optic cable was pointed directly at the target and the spectrum saved to the computer. To measure $E_d$, down-welling irradiance, a reference measurement was made using a 32 mm Ocean Optics WS-1 95% diffuse reflectance standard placed at the depth of the target and held parallel to the surface of the water and its spectrum measured; see Figure 25. To correct for light signal when the detector array is closed, a dark current measurement was subtracted from each measurement. If multiple targets were to be measured at an equal

depth, only one reference measurement was made between these targets. However, if depth or cloud cover changed between measurements, a new reference and dark measurement were collected to ensure the highest degree of accuracy.

Figure 25. Ocean Optics WS-1 Diffuse Reflectance Standard. From Operating Instructions for WS-1 Diffuse Reflectance Standard.

All measurements were taken between 09:30 and 16:30 hours local time to ensure a minimum sun angle of 30 degrees above the horizon. The spectrometer was programmed to average five measurements of both down-welling irradiance and upwelling radiance. Each single spectrum acquired is thus the automatically computed average of five spectra. In addition, for each specified target, a minimum of five spectra were collected to account for variability and possible inconsistencies in the collections. As a test for possible effects of light attenuation through the water column at depth, one cyanobacteria spectral collection (subsequently identified as Cyanobacteria 6), was removed from the water, placed into a 30-cm patch on the gunwale of the boat, and five spectra were thus collected above water for this specimen.

Measuring spectral remote sensing reflectance dictates simultaneous measurements of upwelling and down-welling irradiances, as indicated in Equation (23) in Chapter III of this thesis. In a coral reef benthic environment, light travels in all upward directions including light scattered by the surrounding benthos (Mobley, 1994). To minimize this effect, the collection end of the cable was held at a fixed distance above the spectral target. This avoided casting a collector's shadow, while ensuring an adequate collection of the single target and minimizing collection of upwelling radiance from

surrounding substrates. The area of the target being measured is defined by a circle with radius *r*, found using Equation (31) (Holden and LeDrew, 2001), where *d* is the height above the spectral target.

$$r = d \times \tan\left(\frac{FOV}{2}\right) \tag{31}$$

Given a distance between the end of the fiber-optic cable and the target of 5 cm, the radius of the circle measured was approximately 1.1 cm and its area equaled 3.8 $cm^2$. This was chosen as a reasonable distance/area measured since the coral reef substrates being measured have a comparable minimum surface area.

Underwater photographs were taken of most features measured in order to supplement the spectral library collected. Notes were taken on underwater paper on a pre-printed table with the following information: date, time, dive number, GPS location, dive distance and bearing from boat, photograph numbers, depth, spectrum numbers, target type, reef habitat, surrounding substrate, and color as well as any other information deemed important for that particular target acquisition (see Appendix A). The target type would fall into one of five broad categories: sand, algae, coral, metal (galvanized, steel, or iron), and cyanobacteria (filamentous or non-filamentous). Reef organisms were characterized based on size (small = <30-cm, medium = 30-60-cm, and large >60-cm) and morphology (branching, encrusting or massive). Surrounding substrate classifications were assigned based on field observations and review by marine taxonomy experts of the underwater photographs taken at the time of collection. Broad categories were unconsolidated sediments, hard bottom, submerged vegetation, live coral, other invertebrates, and artificial substrate.

## C. CYANOBACTERIA IDENTIFICATION

To verify that the targets of the collected spectra were indeed the cyanobacteria *Lyngbya* spp., multiple sample specimens were collected and placed in Ziploc bags filled with seawater for storage from the dive site to the workshop. All samples were then transferred to 20-mL vials fixed with a 5% formalin solution so they could be transported to a biology lab for microscopic analysis. Dr. Donald Potts, Department of Ecology and

Evolutionary Biology University of California, Santa Cruz, and Dr. Daria Siciliano, Department of Physics at the Naval Postgraduate School, Monterey, California, conducted a microscopic analysis of the samples. Notes from these analyses complemented the notes taken in the field, and allowed positive taxonomic identification.

## D. NOISE AND SPECTRAL SMOOTHING

"Real" spectra contain both the actual signal as well as noise (Talsky, 1994). Noise in spectrometry is created by a multitude of sources including temperature gradients, scattering, light fluctuations, electrical noise inherent to the spectrophotometer, converters etc., and leads to errors in spectral data which must be addressed when conducting spectral analysis (Talsky, 1994). Noise must be characterized by determining the ratio of the true signal amplitude ($A_s$) over the amplitude of the noise signal ($A_{Ds}$) or signal-to-noise ratio (SNR), Equation (32) (Li and Shi, 1986).

$$SNR = \left( \frac{A_s}{A_{Ds}} \right) \tag{32}$$

Upon inspection of the spectra collected at Midway with the USB2000, it was observed that each spectrum had distinctive aperiodic noise that masked reflectance and absorption features of the original signal. To suppress the noise and restore overall structure to the spectra, a triangular smoothing algorithm, Equation (33), was applied to each spectrum individually. $R_j$ represents the new reflectance value after the original reflectance ($R$) has been averaged with the surrounding reflectance of the two adjacent bands (Christian and O'Reilly, 1986).

$$R_j = \frac{R_{j-2} + 2R_{j-1} + 3R_j + 2R_{j+1} + R_{j+2}}{9} \tag{33}$$

This weighted average formula is considered ideal for peak-type signals in that it creates less peak distortion (attenuation and broadening) for a given measure of noise reduction (Christian and O'Reilly, 1986). This mathematical method can be applied multiple times against the same spectra until the desired results are achieved. However, it is important to realize that with excessive iterations, some true features of the original signal are going to degrade.

To make use of this tool, the original spectrum were converted to an ASCII text file and imported into Microsoft Excel ® worksheets, Figure 26. Through application of the circular reference function, a macro was written to allow user input in the number of iterations to apply to a given spectrum. This allowed adjusting the number iterations required to meet the stated objective of suppressing the noise while retaining true features of the original signal, on a case-by-case spectrum. Information regarding the number of iterations applied to each spectrum can be found in Appendix A.

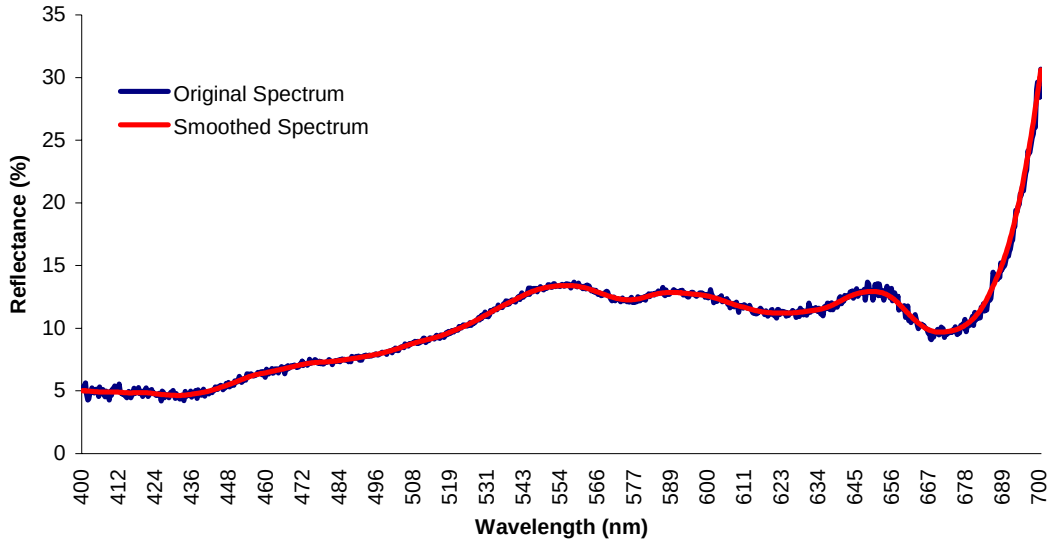


Figure 26. Example of smoothing algorithm plot. Blue curve represents original spectrum and red represents smoothed spectrum.

## E. SPECTRAL AVERAGING

Once each spectrum was smoothed, the spectra associated with an individual target were visually reviewed for their quality and all spectra were compared to published sources for overall structure. The spectra deemed as bad quality were omitted from further analysis. At the completion of this examination, all 'good' spectra associated to a specific target (usually 5, as stated in section B; exact information on this is found in Table 3 of the Results) were averaged together.

## F. DERIVATIVE SPECTROSCOPY

Derivative spectroscopy employs a mathematical method that resolves fine structure in spectra by differentiation (Talsky, 1994). It is mainly employed for ultraviolet and visible spectra to deconvolute poorly defined peaks (Talsky, 1994) due to absorption properties of overlapping biochemical constituents or minerals in spectra of the earth's materials. Derivatives are also used in analytical spectroscopy to spectrally discriminate small structural differences between similar spectra as well as provide a technique to correct for extraneous background absorption in favor of multi-component analysis (Malmstadt et al., 1974). First, second, and higher-order derivatives became an established technique to reduce low frequency background noise and for resolution of overlapping spectra in the 1950's (Butler and Hopkins, 1970).

Derivative analysis has been used in hyperspectral remote sensing for nearly two decades. For example, Demetriades-Shah et al. (1990) used derivative analysis to resolve interference from the Earth's atmosphere in remote sensing. Holden and LeDrew (1999) used first derivatives to test the ability to distinguish coral reef features and later improved on that work (Holden and LeDrew, 2000) using second derivatives to determine coral health in coral reef habitats.

Differentiation in spectroscopy provides higher resolution of overlapping spectra with relative amplitudes becoming greater with increasing derivative orders (Butler and Hopkins, 1970; Fell and Smith, 1982). Derivative spectra (*s*), were obtained using a finite approximation to calculate the change in reflectance over a bandwidth $\Delta\lambda$, defined as $\Delta\lambda = \lambda_j - \lambda_i$, where $\lambda_j > \lambda_i$ (Tsai and Phipot, 1998). Estimation of the first derivative is found using Equation (34). The $n^{th}$ derivative is computed using Equation (35).

$$\frac{ds}{d\lambda}\Big|_i \approx \frac{s(\lambda_i) - s(\lambda_j)}{\Delta\lambda} \tag{34}$$

$$\frac{d^n s}{d\lambda^n}\Big|_j = \frac{d}{d\lambda}\left(\frac{d^{(n-1)}s}{d\lambda^{(n-1)}}\right) \tag{35}$$

In general, first derivatives provide the rate of change of reflectance with wavelength, while second derivatives measure the curvature or rate change of the slope.

Higher order derivatives deliver finer spectral resolution while improving signal to noise ratios (Butler and Hopkins, 1970), but it can be much more difficult to interpret the measured quantity (Hedley and Mumby, 2002). Nonetheless, fourth order derivatives have been routinely used to discern greater information in areas of overlapping absorptions due to pigments and atmospheric absorptions (Richardson et al., 1994; Hochberg and Atkinson, 2000).

In the interpretation of derivative spectra, maxima represent extrema in even derivatives and zero crossing in odd derivatives; inflection points in the original spectra yield zero crossings in even derivatives and extrema in odd derivatives (Talsky, 1994). It is also important to understand that each successive even ordered derivative is 180° opposite of the reflectance spectra. As such, the positive peaks of second derivatives mark absorptions while in fourth order derivatives, absorptions are represented as troughs. Successive derivatives of Gaussian analytical bands are shown in Figure 27 in which a) shows the fundamental curve at the bottom and building to the fourth-order derivative on the top, while b) represents a fundamental curve at the bottom and builds to the fourth-order derivative on the top of two superposed Gaussian bands. This figure shows that with this technique, overlapping peaks become distinct, their magnitude quantifiable, and they can be related to the abundance of the biochemical or mineral constituent of the material being analyzed (Talsky, 1994).

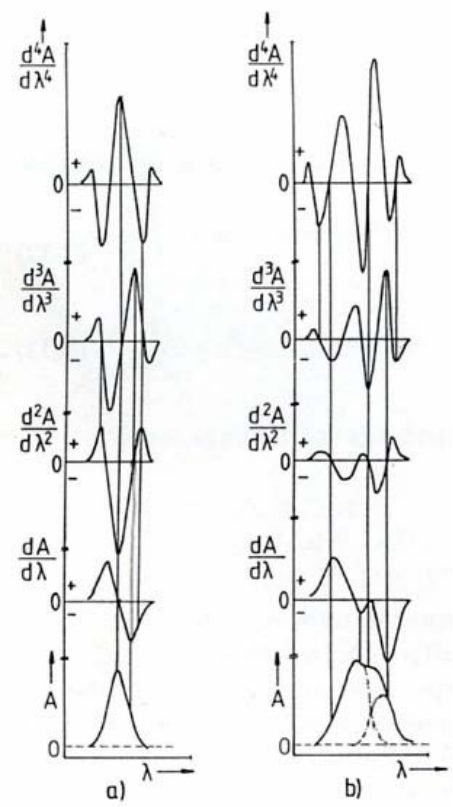


Figure 27. Differentiation of computed Gaussian analytical bands. a) Fundamental curve and its first to fourth-order derivatives; b) Fundamental curve and first to fourth-order derivatives of two superposed Gaussian bands. From Talsky, 1994.

Successive differentiation provides increased definition of peaks and shoulders as seen in Figure 28. However, while peaks and shoulders gain increased sharpness, flat portions of the main signal disappear altogether when higher-order differentiation is performed (Talsky, 1994). There is a limit to the amount of sharpness in that sixth-order differentiation and higher provide minor sharpening to the signal (Talsky, 1994).

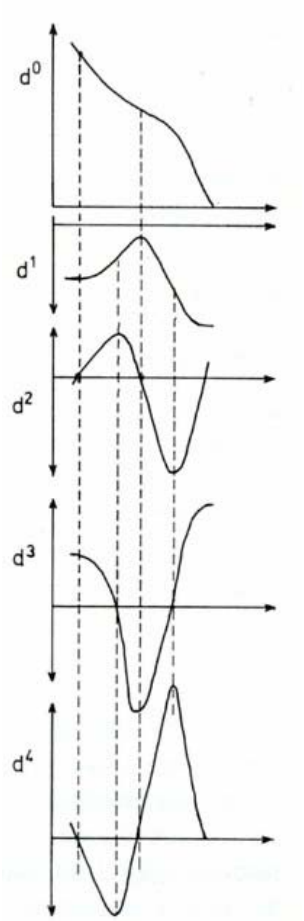


Figure 28. Signal sharpening by differentiation of shoulders. From Talsky, 1994.

# VII. RESULTS

## A. SPECTRAL LIBRARY

Table 3 provides a list of all targets, the number of spectra collected, whether they were considered for further analysis, and naming convention used in subsequent analysis. After inspection of the spectra collected for the twenty-five targets, spectra for five targets were considered invalid. The remaining targets (n=20) were then grouped based on taxonomic classification to compare their spectral character. This resulted in five main groupings: Cyanobacteria, *Montipora* spp., *Porites* spp. and *Pocillopora* spp. corals, and the algae.

| Target | # of valid Spectra | Action Taken | Name convention |
|---|---|---|---|
| Algae (Brown) | 5 of 5 | Analyzed | Brown Algae |
| Algae (*Laurentia* spp., Brown) | 5 of 5 | Analyzed | Algae *Laurentia* spp. |
| Algae (Green) | 5 of 5 | Analyzed | Green Algae |
| Coral (*Montipora* spp.) | 5 of 5 | Analyzed | *Montipora* spp. 1 |
| Coral (*Montipora* spp.) | 5 of 5 | Analyzed | *Montipora* spp. 2 |
| Coral (*Montipora* spp.) | 6 of 6 | Analyzed | *Montipora* spp. 3 |
| Coral (*Montipora* spp.) | 5 of 5 | Analyzed | *Montipora* spp. 4 |
| Coral (*Montipora* spp.) non-pigmented | 6 of 6 | Analyzed | *Montipora* spp. non-pigmented |
| Coral (*Pocillopora damicornis*) | 5 of 5 | Analyzed | *Pocillopora damicornis* |
| Coral (*Pocilliopora ligulata*) | 3 of 5 | Analyzed | *Pocillopora ligulata* |
| Coral (*Porites compressa* (cf.)) | 5 of 5 | Analyzed | *Porites compressa* (cf.) |
| Coral (*Porites lobata*) | 5 of 5 | Analyzed | *Porites lobata* 1 |
| Coral (*Porites lobata*) | 4 of 5 | Analyzed | *Porites lobata* 2 |
| Coral (*Porites lobata*) | 5 of 5 | Analyzed | *Porites lobata* 3 |
| Cyanobacteria spp. (Brown) | 0 of 5 | Discarded | |
| Cyanobacteria spp. (Brown) | 0 of 5 | Discarded | |
| Cyanobacteria spp. (Brown) | 0 of 5 | Discarded | |
| Cyanobacteria spp. (Brown) | 4 of 5 | Analyzed | Cyanobacteria 5 |
| Cyanobacteria spp (Green) | 3 of 5 | Analyzed | Cyanobacteria 1 |
| Cyanobacteria spp (Green) | 3 of 5 | Analyzed | Cyanobacteria 2 |
| Cyanobacteria spp (Green) | 5 of 5 | Analyzed | Cyanobacteria 3 |
| Cyanobacteria spp. (Green) | 0 of 5 | Discarded | |
| Cyanobacteria spp. (Green) | 3 of 5 | Analyzed | Cyanobacteria 4 |
| Cyanobacteria spp. (Green) | 0 of 5 | Discarded | |
| Cyanobacteria spp. (Green) | 4 of 5 | Analyzed | Cyanobacteria 6 (Above water) |

Table 3. Spectral library table of all targets collected.

### 1. Cyanobacteria (n=6)

Eleven targets of cyanobacteria spectra were collected at depths of 1.5 to 5 feet. However, five of the eleven spectra were discarded because of bad collections due to errors with the Ocean Optics spectrometer. Therefore, the six good spectra were re-numbered Cyanobacteria 1-6 for ease of organization Table 3.

Reflectance spectra show absorptions from 410-442 nm followed by increasing reflectance with minor absorptions until approximately 524 nm in samples 1 through 5 Figure 29. At 524 nm, these spectra begin a moderate reflective feature peaking in the green range between 549-560 nm with the exception of cyanobacteria 5 that peaks at 535 nm.

Sample 6 (above water) is more reflective in the blue and green region than the spectra collected below water. There is a deflective trough apparent around 517 nm with the more dominant absorption around 549 nm. This absorption ultimately bottoms out at 687 nm. The remaining five spectra have additional absorption peaks between 570-580 nm following their green reflective feature. Of note, cyanobacteria number 5 has its strongest reflective peak at 605 nm while 1 through 4 shows a lower magnitude peak between 600-610 nm. Further common absorption bands occur in specimen 1 through 5 at 622-634 nm followed by reflective point between 648-654 nm; see Figure 29. The dominant absorption in all spectra remains the ubiquitous chlorophyll absorption 670-690 nm.

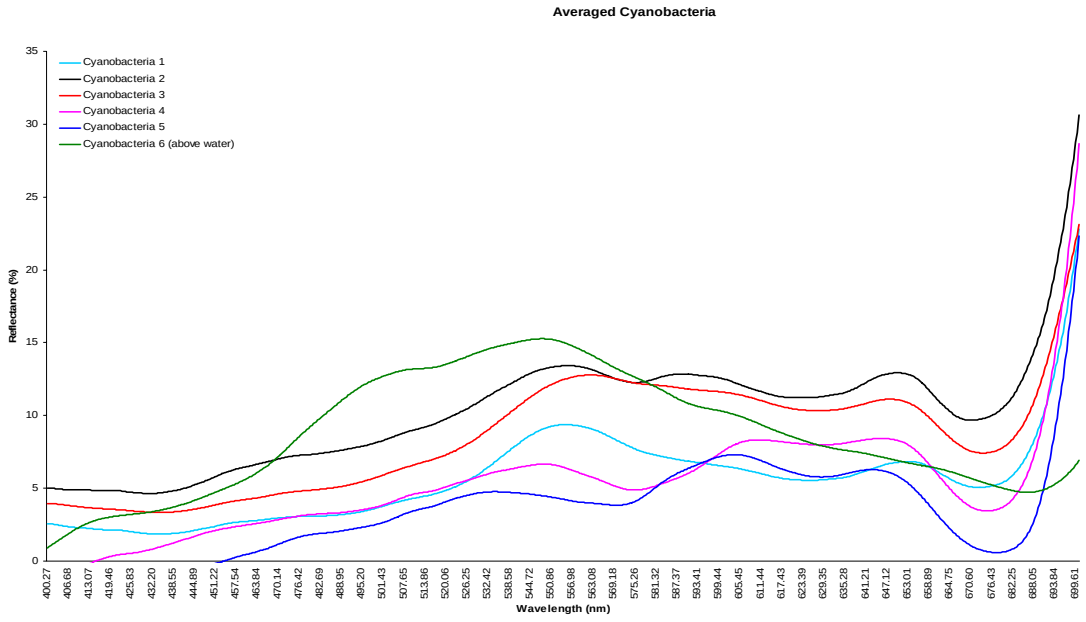


Figure 29. Average reflectance spectra for cyanobacteria samples 1 through 6.

Second derivatives show all six samples share the following absorption bands: 424-452 nm, 460-474 nm, 567-585 nm, 612-641 nm and 660-700 nm; see Figure 30. Although these bands are common to each of the six samples, each has differing details that make them unique. Cyanobacteria 1 through 4 are spectrally most similar to each other. Additionally, second derivative analyses provide the greatest resolution of details for samples 1 through 5. Spectra 1 through 4 have absorption peaks around 407-408 nm, 430-434 nm, 463-465 nm, 525-527 nm, 618-620 nm, 636-638 nm, while cyanobacteria 1 through 5 have peaks at 575-577 nm, 594-596 nm, and 668-671 nm.

The absorption peaks found by second derivative analysis were placed for reference in a table (Appendix E) which lists solely the peaks attributable to cyanobacteria, without regard to their magnitude or width of absorption.

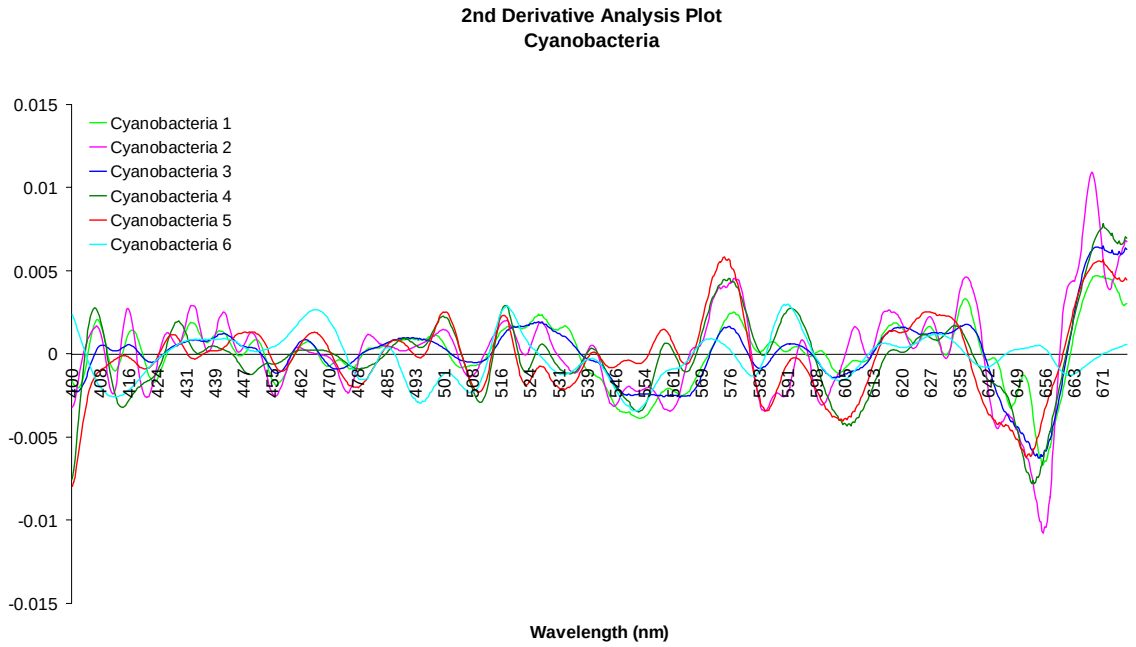


Figure 30. Second derivative spectra for cyanobacteria targets 1-6.

### 2. *Montipora* spp. (n=4)

*Montipora* spp., which in the Hawaiian archipelago is most often characterized by a blue/purple color, is the only target that indeed reflects appreciably in the blue region; see Figure 31. Of the five *Montipora* spp. Spectra collected, one is unique in that it is void of pigments, due to bleaching. Reflectance spectra for the four non-bleached *Montipora* spp. collections illustrate common absorptions between 419-435 nm with moderate reflection throughout the blue region of the spectrum and becoming negative in slope at 500 nm; see Figure 32. Each spectrum has a strong absorption feature prominent at approximately 585 nm with a reflective hump between 615-650 nm followed by the strong chlorophyll absorption feature of 670-690 nm.

Figure 31. Photograph of *Montipora* spp.

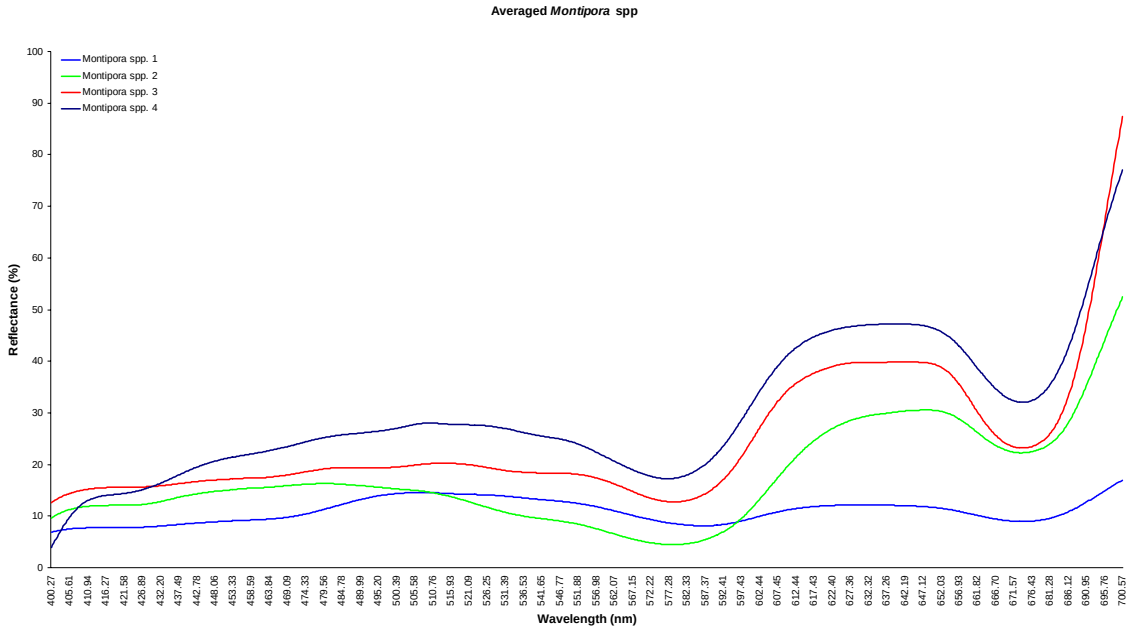


Figure 32. Average reflectance spectra for *Montipora* spp.. 1 through 4.

In the second derivative Figure 33 each of the four spectra reveals strong positive absorption between 661-694 nm with *Montipora* spp. 2 and 3 displaying a small shoulder that peaks between 669-672 nm. *Montipora* spp. 1, 2 and 4 have maximum absorptions

at 684 nm whereas sample 3 has a maximum at 689 nm. Second derivative analyses highlight the spectral similarity between spectra 1 and 4, as well as 2 and 3. Samples 1 and 4 have weak absorption bands from 417-437 nm, 513-522 nm and 536-543 nm. *Montipora* spp. 2 and 3 have small positive absorptions at 423-435 nm, 460-468 nm and 495-501 nm. Finally, all four spectra share a common absorption from 561-602 nm; see Figure 33.

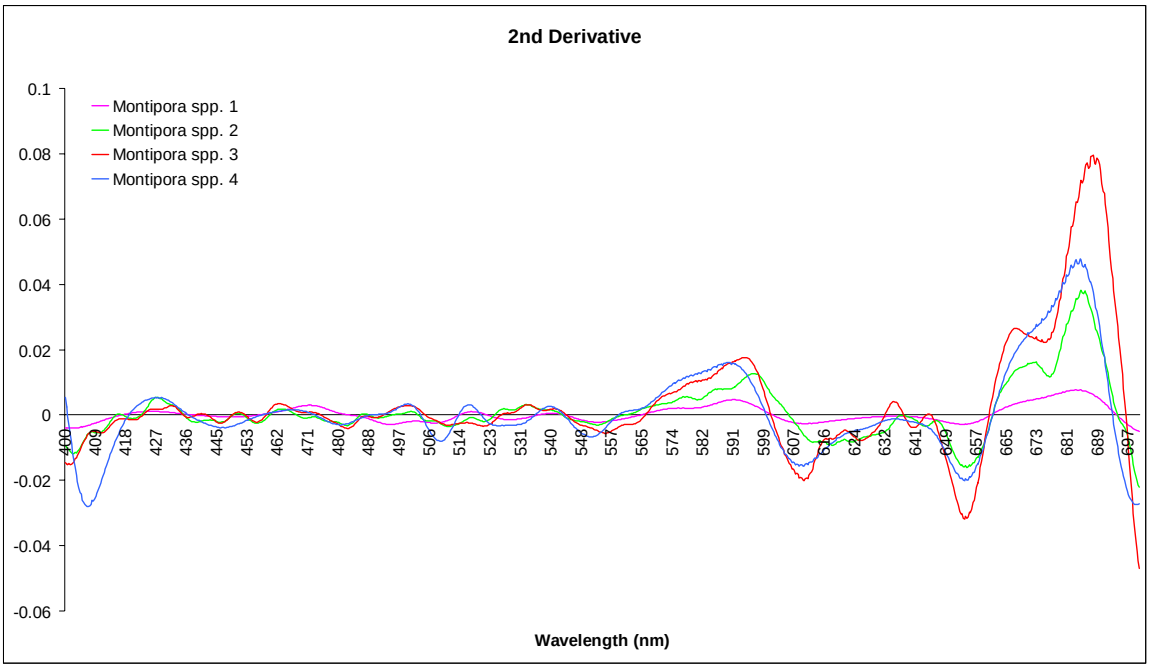


Figure 33. Second derivatives for coral target *Montipora* spp. 1 through 4.

### 3. *Porites lobata* (n=3)

All three *Porites lobata* reflectance spectra are similar with absorptions from 410-427 nm, 584-591 nm, 625-644 nm and 665-680 nm while remaining reflective throughout the green portion of the spectrum peaking at approximately 577 nm. Additional peak reflections exist at 577 nm, 606 nm, and 653 nm; see Figure 34.

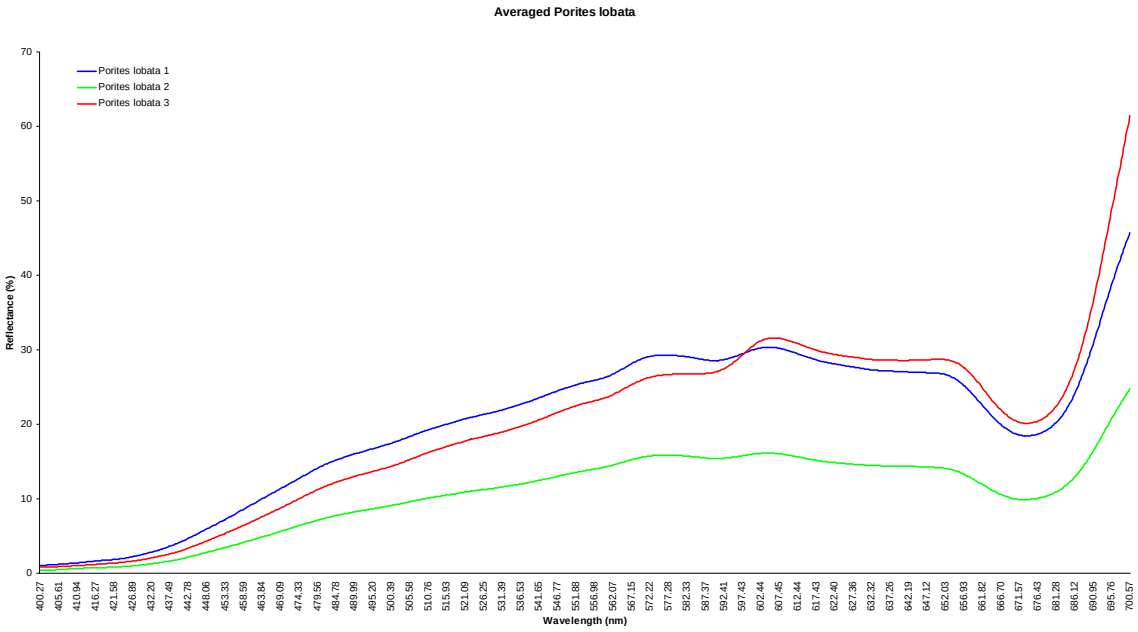


Figure 34. Average reflectance of *Porites lobata* coral targets 1 through 3.

Second derivative analyses characterize only slight differences between the three samples with *P. lobata* 1 and 2 being most similar; see Figure 35. Otherwise, dominant absorption features mirror each other in each of the spectra at 556-566 nm, 585-598 nm, 613-625 nm, 629-637 nm and 662-693 nm.

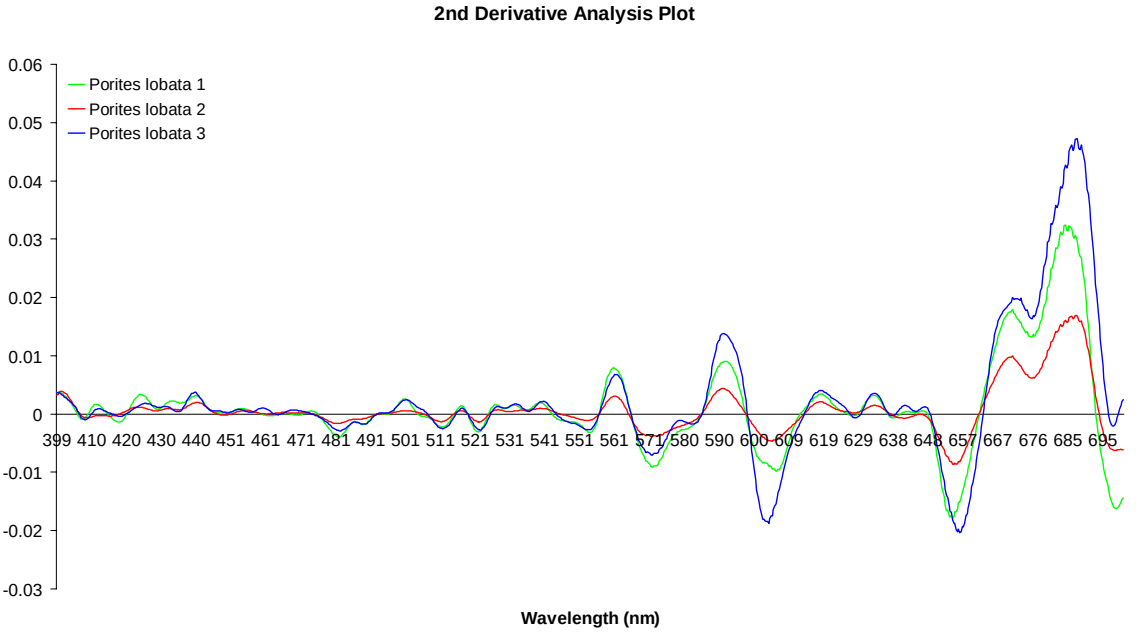


Figure 35. Second derivative spectra for *Porites lobata* coral targets 1-3.

### 4. *Pocillopora* spp. (n=2)

*Pocillopora ligulata* is primarily reflective in the green, peaking at 573 nm, yet absorptions are seen at 409-414 nm, 467 nm, 594 nm, and the strongest at 674 nm; see Figure 36. The second derivative (Figure 36, right graph) shows that multiple absorptions occur throughout the spectrum with the more prominent bands at 400-435 nm, 458-473 nm, 536-551 nm, 586-599 nm, 613-640nm and 660-698 nm. These culminate in peaks around 517 nm, 590 nm and 690 nm respectively.

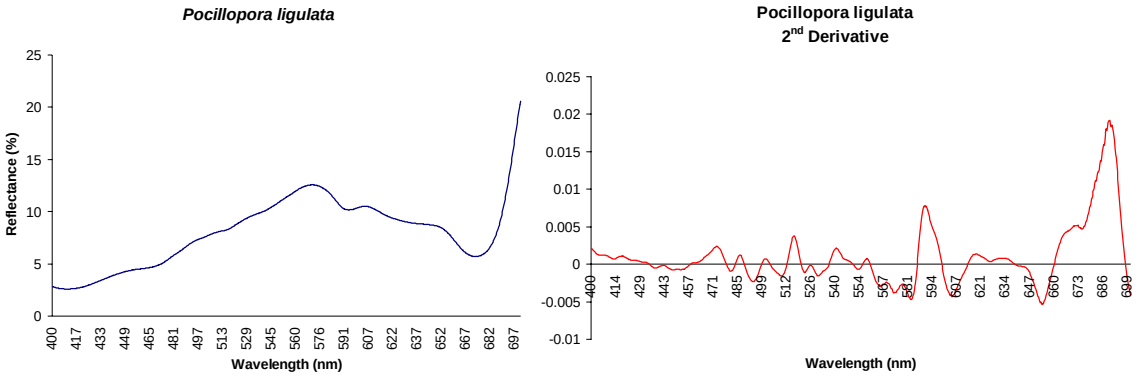


Figure 36. Reflectance spectrum and second derivative of *Pocillopora ligulata*.

*Pocillopora damicornis* has a pyramid shaped reflectance curve that displays absorption at 405-420 nm becoming highly reflective with a peak at 571 nm. This is followed by a deep absorption that maximizes at 679 nm. In the second derivative 9 absorptions become apparent, 417-442 nm, 455-474 nm and 484-489 nm in the blue band, 498-505 nm, 512-522 nm and 536-546 nm in the green band, and 587-598 nm, 611-635 nm and a much broader feature between 656-692 nm at the red end of the spectrum.

### 5. Algae (n=3)

The brown algae target (refer to Table 3) has a reflectance spectrum that highlights absorptions between 410-464 nm, at which point the spectrum becomes increasingly more reflective up through 587 nm, where it peaks; see Figure 37. There is an absorption feature around 557-570 nm, but the more outstanding spectral features occur at 617-638 nm and 677 nm. In the second derivative, multiple weak absorptions are seen between 410-488 nm ranging from 4 nm to 10 nm wide; see Figure 38. 488-508 nm is the first significant absorption albeit with a relatively small magnitude, as is the

535-543 nm absorption. There is a moderately strong absorption between 561-576 nm that becomes maxima at 568 nm. The red end of the spectrum features two small absorptions at 600-621 nm and 623-636 nm, and a large positive absorption around 660-695 nm (displaying duel peaks at 668 nm and 684 nm).

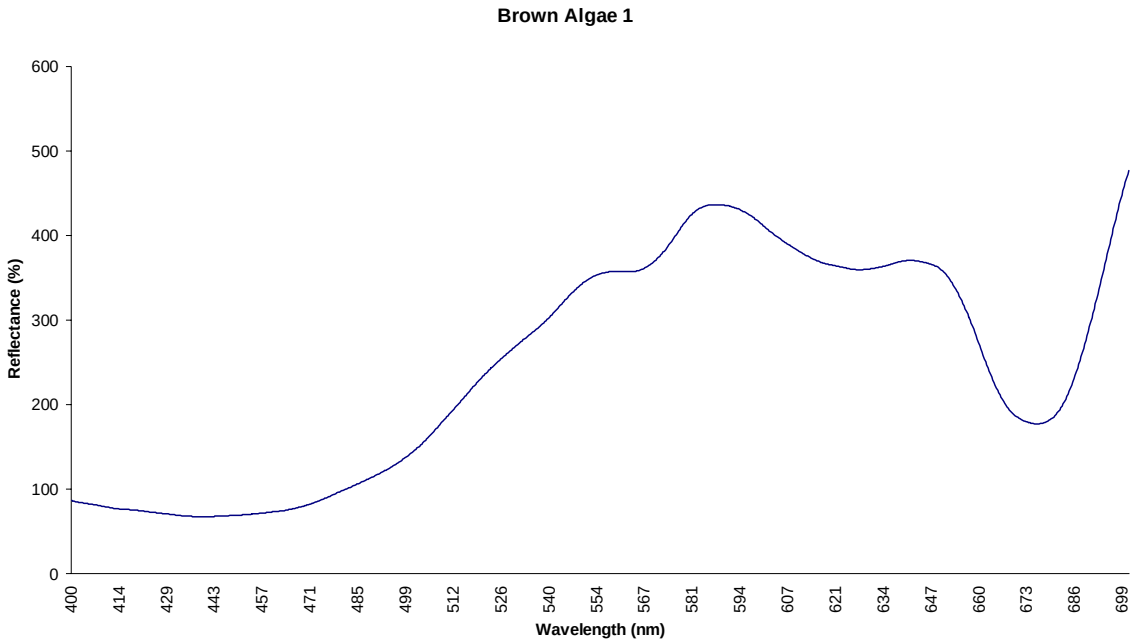


Figure 37. Reflectance spectra for brown algae.

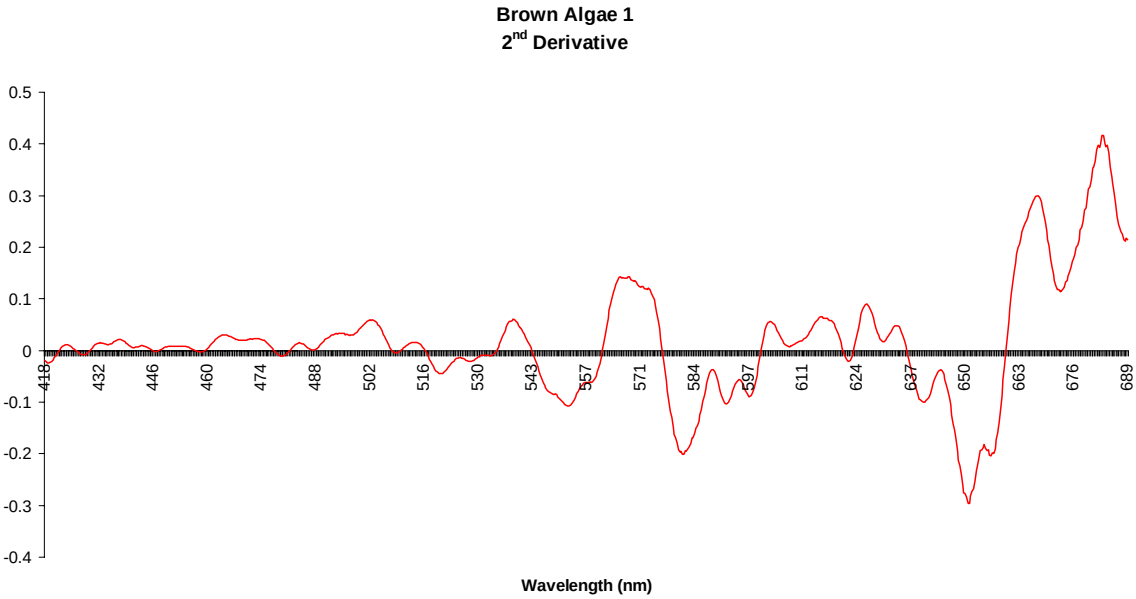


Figure 38. Second derivative spectra for brown algae.

The reflectance spectrum of *Laurentia* spp., also a brown alga, shows two small depressions between 419-429 nm and 437-445 nm. The spectrum then becomes more positively reflective at 500 nm and continues this trend through 602 nm with a prominent absorption between 562-571 nm. There is a 17 nm wide absorption between 618-635 nm followed by a second reflectance peak at 646 nm; see Figure 39. In the second derivative, weak absorptions are shown in the blue at 422-430 nm, 437-444 nm, and 452-458 nm. Broader absorptions exist between 489-511 nm and 552-545 nm. A prominent green absorption is present between 560-578 nm, while a broader absorption is portrayed in the red from 610-636 nm; all of which, as expected, is similar to the Brown algae spectrum reported above. The spectrum also exhibits the ubiquitous 667-695nm Chl *a* absorption present in all algae; see Figure 40.

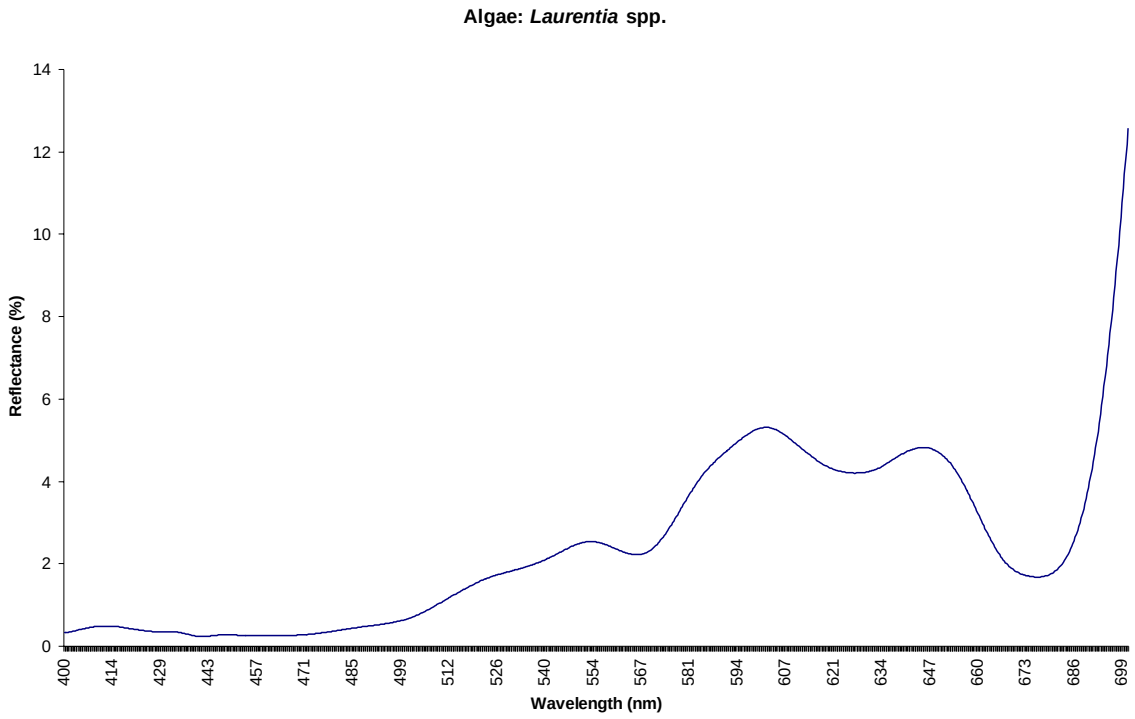


Figure 39. Reflectance spectra for *Laurentia* algae .

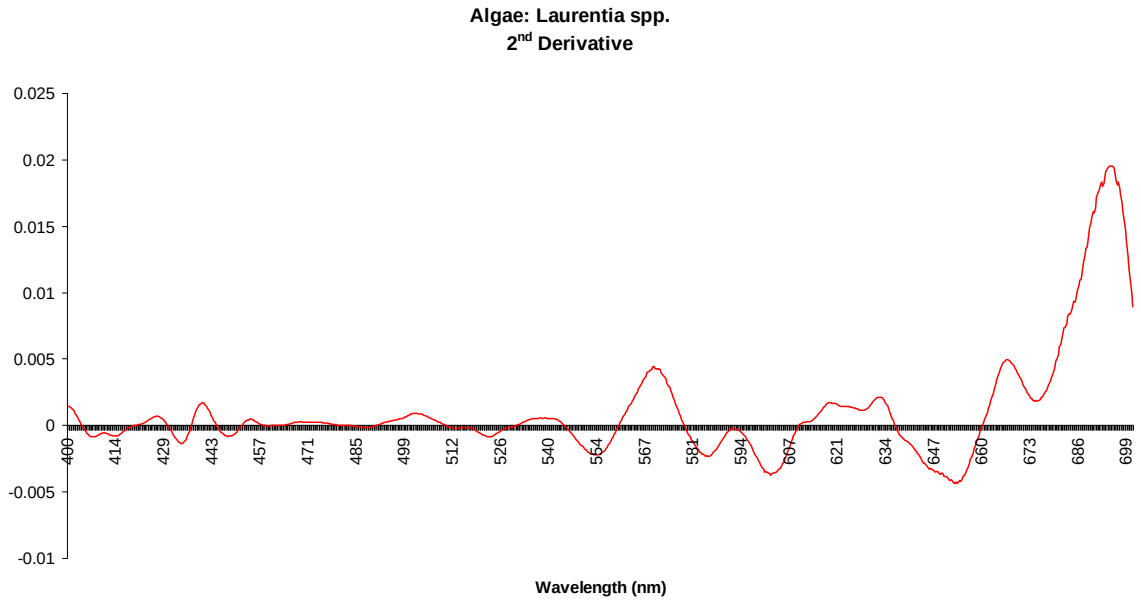


Figure 40. Second derivative spectral for *Laurentia* algae .

Reflectance data for green algae shows an absorption centered around 400-441 nm with the spectrum becoming highly reflective around 495 nm, peaking at 566 nm. The bands 590 nm and 636 nm mark two absorption points, while the strongest absorption, again, is at 674 nm. However, a reflective peak occurs at 648 nm; see Figure 41. In the second derivative, all of the above-mentioned absorptions are highlighted with two additional absorptions becoming apparent at 457-473 nm and 486-520 nm. The larger absorption peaks are located at 590 nm, 670 nm and 682 nm as seen in Figure 42.

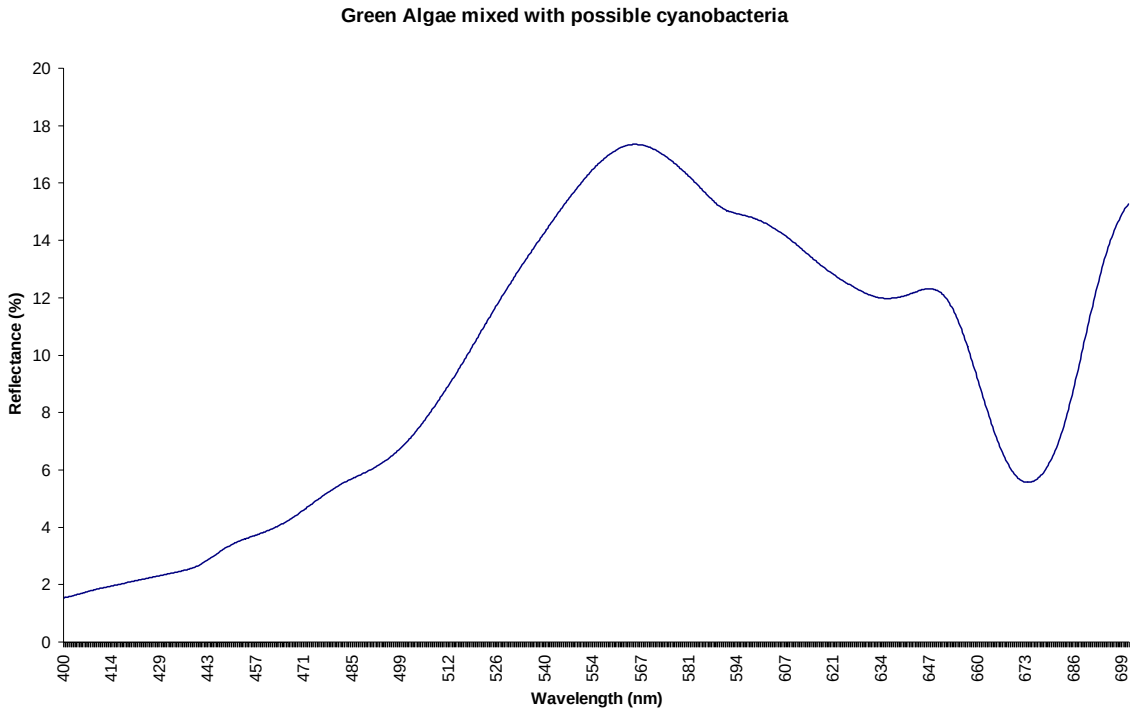


Figure 41. Reflectance spectra for a green algae target.

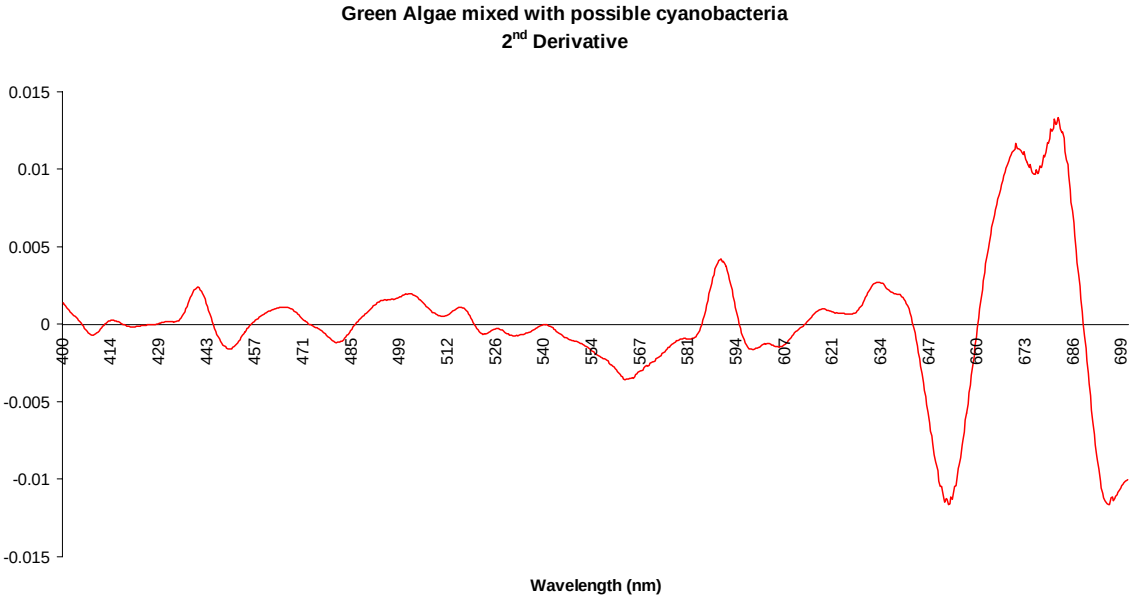


Figure 42. Second derivative spectral for a green algae target.

## B. COMPARATIVE RESULTS

When comparing cyanobacteria spectra to the spectra of the surrounding benthic environment, discriminative characteristics become evident.

### 1. *Porites* spp. versus Cyanobacteria spp.

The reflective range of 645-660 nm is ambiguous for most of the substrates, but becomes an obvious difference between cyanobacteria and *P. lobata*, which is weakly absorbent in the 640-649 range. Spectra of the targets *Porites lobata* and *Porites compressa* (cf.) have several spectral differences between them, but when compared to cyanobacteria spectra a strong discriminatory characteristic becomes evident for both at 565-576 nm (a phycoerythrin absorption) as shown in Figure 43 and Figure 44. Additionally, *P. compressa* (cf.) provides a second potential discriminator at 490-496 nm (also due to phycoerythrin) as can be seen in Figure 44.

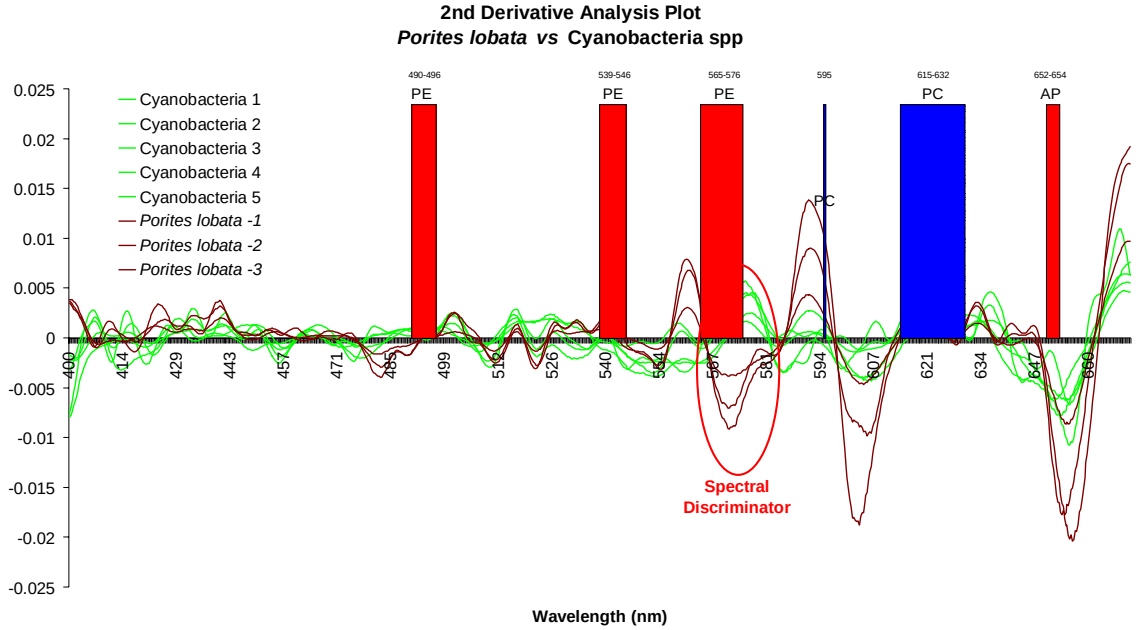


Figure 43. *Porites lobata* versus cyanobacteria spp. comparative analysis.

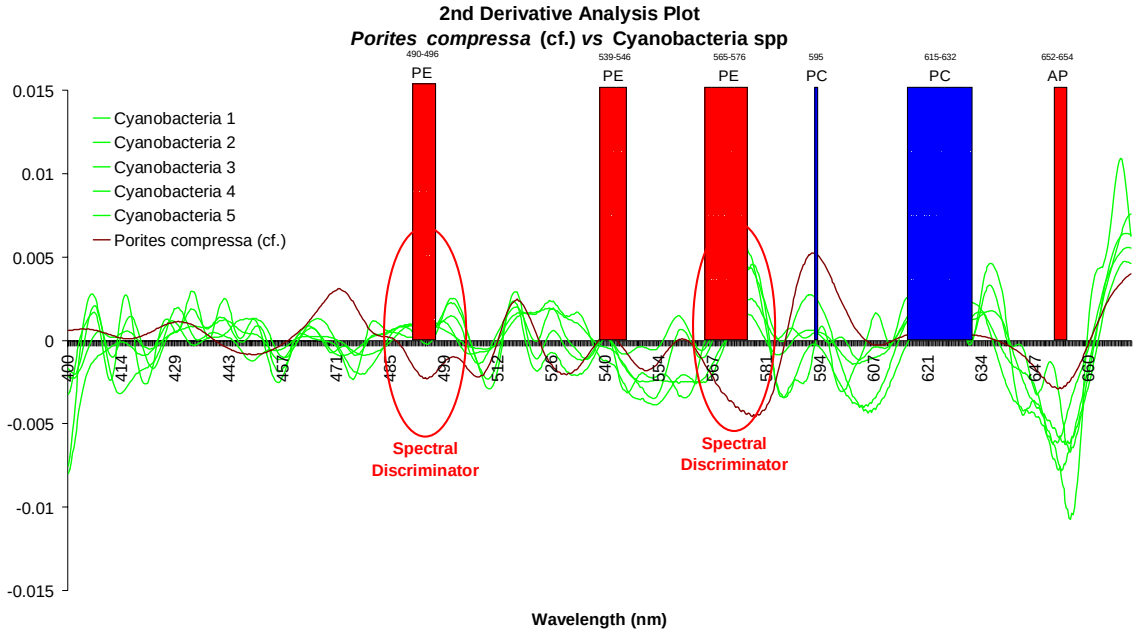


Figure 44. *Porites compressa* (cf.) versus cyanobacteria spp. comparative analysis.

### 2. *Pocillopora* spp. versus Cyanobacteria spp.

*Pocillopora ligulata* and *Pocillopora damicornis* derivative spectra, Figure 45 highlight discrimination bands when compared to cyanobacteria derivative spectra. The stronger of the two exist at the phycoerythrin absorption band of 565-576 nm, as previously seen with the *Porites* spp. spectra, but a second potential feature is seen at the phycoerythrin absorption of 490-496 nm.

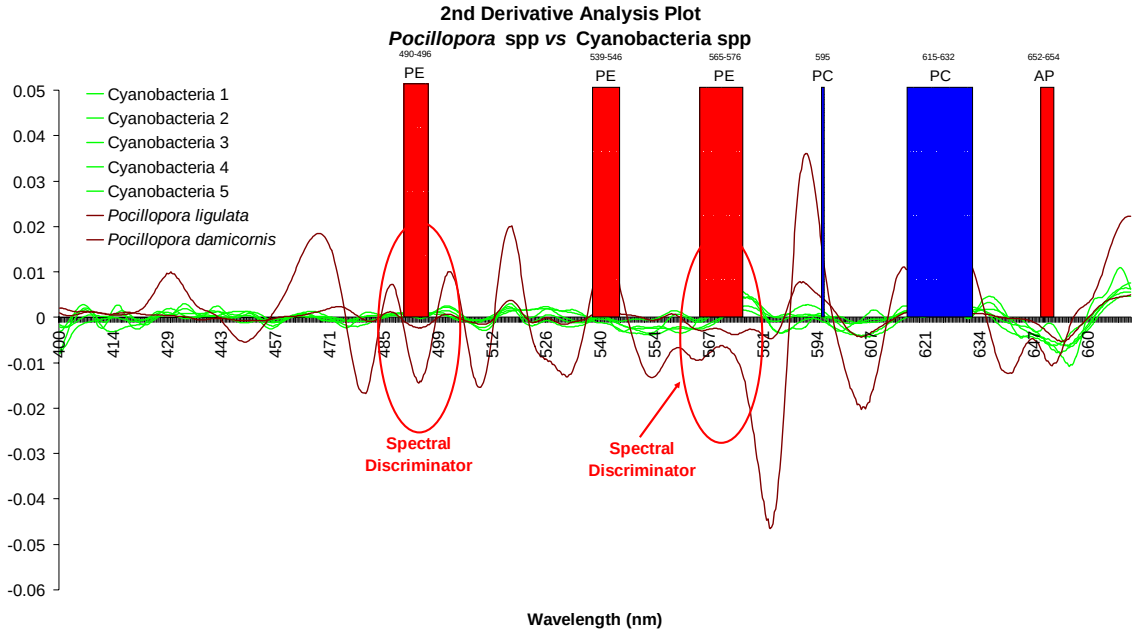


Figure 45. *Pocillopora* spp. versus cyanobacteria spp. comparative analysis.

### 3. *Montipora* spp. versus Cyanobacteria spp.

*Montipora* spp. is unique from the other coral reef substrates in this study in that it has a broad absorption band that overlaps the phycoerythrin absorption at 565-576 nm. Since phycoerythrin is a cyanobacterial pigment and is not present in coral (Hedley and Mumby, 2002) this absorption must be due to an accessory pigment not identified here, possibly typical of this genus or of this endemic Hawaiian species. However, *Montipora* spp. can be spectrally distinguished from cyanobacteria at the phycocyanin absorption band of 615-632 nm, as shown in Figure 46.

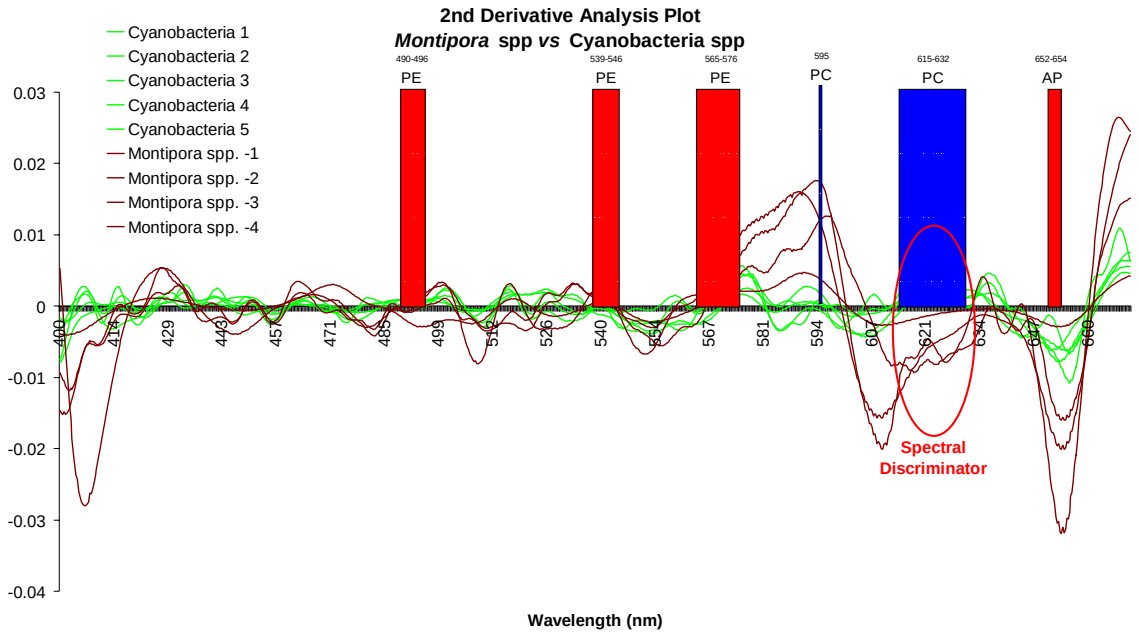


Figure 46. Montipora spp. versus cyanobacteria spp. comparative analysis.

### 4. Algae versus Cyanabacteria spp.

Algae appear to be more challenging to discriminate from cyanobacteria than the rest of the substrates, as they share many of the absorptions attributed to cyanobacteria's pigments. However, green algae are spectrally different at the green wavelengths of 565-576 nm, because, as their color suggests, they are reflective in this region of the spectrum. Although *Laurentia* spp., a brown alga, is more difficult to discriminate from cyanobacteria than green algae, there is a small difference observed between 647-652 nm, which in cyanobacteria spp. has a reflective shoulders that may be attributed to allophycocyanin, which is not present in the *Laurentia* spectrum, see Figure 47. The derivative plot of brown algae compared to cyanobacteria is not shown here because the reflectance spectra of the brown algae targets were so bright that their features overwhelm the less intense spectra of the cyanobacteria, making it difficult to graphically display the spectral differences in a comparative plot.

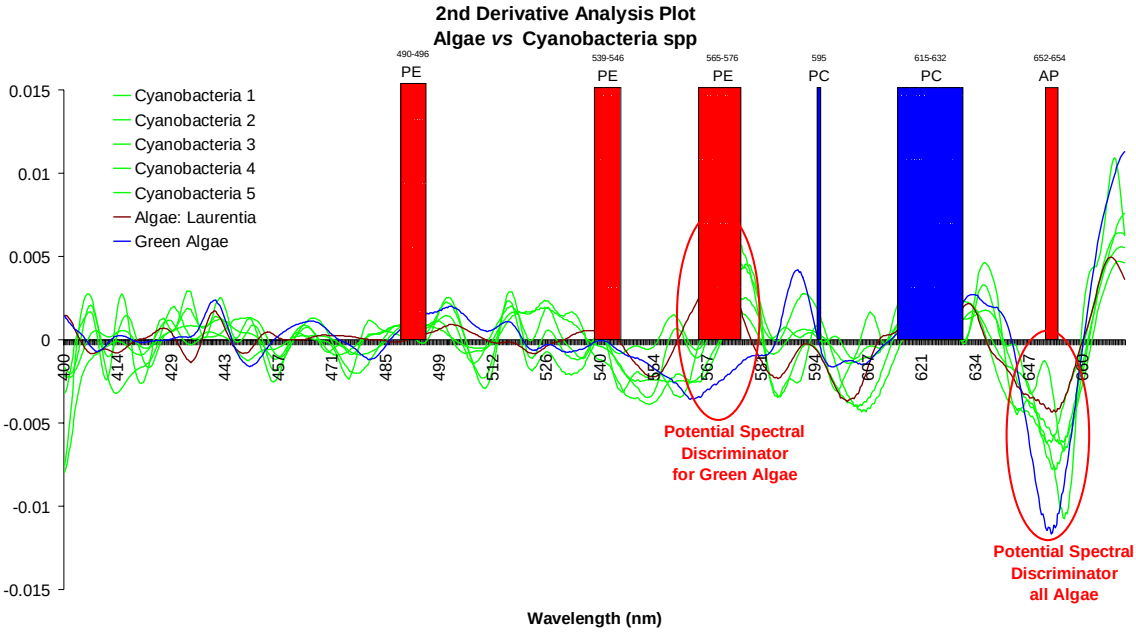


Figure 47. Algae versus cyanobacteria spp. comparative analysis.

### 5. Allophycocyanin Absorption

There is one potential unique spectral discriminator for all of the spectral targets reported in this thesis located in the 647-652 nm wavelengths. Each of the cyanobacteria spectra has a reflective band from 642-660 nm, as does each of the reported coral reef substrates. However, all of the cyanobacteria targets (with the exception of the one collected and measured above water) have an absorption shoulder at the wavelengths 647-652 nm that is attributable to an allophycocyanin absorption.

THIS PAGE INTENTIONALLY LEFT BLANK

# VIII. DISCUSSION AND CONCLUSIONS

## A. UNIQUE ABSORPTIONS OF CYANOBACTERIA

In order to assess and evaluate phycobiliprotein pigment absorptions indicative of cyanobacteria, an extensive literature search was summarized in Table 4, which lists all of the published spectral absorptions of coral reef benthos with the associated pigments responsible for the absorptions. This table, and the studies it references, was used to interpret the spectral features reported in this thesis.

| **Pigments** | **Absorption Bands** | | | **Source** |
|---|---|---|---|---|
| **Chlorophylls** | **Green** | **Blue** | **Red** | |
| chl-a | 435 | | 670-680 | Hedley & Mumby (2002) |
| | 430-435 | | 676 | Richardson et al. (1994) |
| | 418, 437-441 | | 623, 681 | Smith & Alberte (1994) |
| | 425, 445, 450 | | | Louchard et al. (2002) |
| | 422 | | 659 | Andrefouet et al. (2003) |
| | | | 678 | Lemasson et al. (1973) |
| | 439 | | 674 | Beach et al. (1997) |
| | | | 660, 680 | Jupp et al. (1994) |
| | | | 675 | Joyce & Phin (2003) |
| | 418-450 | | 660-680 | Combined from above sources |
| chl-b | 480 | | 650 | Hedley & Mumby (2002) |
| | 470-480 | | | Louchard et al. (2002) |
| | 471, 490 | | 653 | Smith & Alberte (1994) |
| | 470-490 | | 650-653 | Combined from above sources |
| chl-c | | | 645 | Hedley & Mumby (2002) |
| | | 585 | | Louchard et al. (2002) |
| | 465-469 | | 636 | Smith & Alberte (1994) |
| | 460 | | 633 | Beach et al. (1997) |
| | 460-469 | | 644-645 | Combined from above sources |
| **Carotenoids** | | | | |
| α | 423, 444, 473 | | | Hedley & Mumby (2002) |
| | 422, 448 | | | Andrefouet et al (2003) |
| | 422-423, 444-448 | | | Combined from above sources |
| β | 427, 449, 475 | | | Hedley & Mumby (2002) |
| | 495 | | | Louchard et al. (2002) |
| | 492 | | | Smith & Alberte (1994) |
| | 492-495 | | | Combined from above sources |
| Peridinin | 475 | | | Hedley & Mumby (2002) |

| | | | | |
|---|---|---|---|---|
| **Xanthophylls** | | | | |
| Zeaxanthin | 428, 450, 478 | | | Hedley & Mumby (2002) |
| | 495 | | | Louchard et al. (2002) |
| Neoxanthin | 415, 438, 467 | | | Hedley & Mumby (2002) |
| Lutein | 422, 445, 474 | | | Hedley & Mumby (2002) |
| | 495 | | | Louchard et al. (2002) |
| Violaxanthin | 417, 440, 469 | | | Hedley & Mumby (2002) |
| Fucoxanthin | 426, 449, 465 | | | Hedley & Mumby (2002) |
| | 498 | 545, 586 | | Smith & Alberte , 1994 |
| | 491 | 590 | | Beach et al. (1997) |
| Diataxanthin | 425, 449, 475 | | | Hedley & Mumby (2002) |
| Diadionxanthin | 424, 445, 474 | | | Hedley & Mumby (2002) |
| Dinoxanthin | 418,442, 470 | | | Hedley & Mumby (2002) |
| Siphonxanthin | | 540 | | Hedley & Mumby (2002) |
| **Phycobilins** | | | | |
| Phycocyanin | | | 618 | Hedley & Mumby (2002) |
| | | | 620, 630 | Louchard et al. (2002) |
| | | | 620 | Roelfsema et al. (2001) |
| | | | 627-630 | Smith & Alberte (1994) |
| | | 595 | 632 | Andrefouet et al. (2003) |
| | | | 615 | Lemasson et al. (1973) |
| | | | 625, 632 | Beach et al. (1997) |
| | | | 618, 623 | Jupp et al. (1994) |
| | | | 615-632 | Combined from above sources |
| Phycoerythrin | 490 | 546, 576 | | Hedley & Mumby (2002) |
| | | 565 | 620 | Roelfsema et al. (2001.) |
| | 496 | 542, 567 | | Smith & Alberte (1994) |
| | | 539, 569 | | Andrefouet et al. (2003) |
| | | 565 | | Lemasson et al. (1973) |
| | | 565 | | Hoge et al. (1999) |
| | | 535, 540, 568 | | Beach et al. (1997) |
| | | 550 | | Saffo (1987) |
| | | 567 | | Jupp et al. (1994) |
| | 490-496 | 539-546<br>565-576 | | Combined from above sources |
| Allophycocyanin | | | 654 | Hedley & Mumby (2002) |
| | | | 652 | Lemasson et al. (1973) |
| | | | 652-654 | Combined from above sources |

Table 4. Summary of biological pigments common to coral reef environments with corresponding references.

In the following discussion, all spectral targets were grouped according to spectral absorptions unique to cyanobacterial pigments.

**1. Phycoerythrin Absorption (490-496 nm) I**

Let us recall from our discussion in Chapter V that phycoerythrin primarily absorbs in the green band (i.e., where chlorophyll is reflective). However, it does have a small absorption in the blue, in slightly longer wavelength than the blue chlorophyll absorption (see Table 4). This absorption band does distinguish cyanobacteria from *P. lobata* and *Pocillopora* spp. However, when compared with the algae (green and brown) and *Montipora* spp. corals this wavelength is not indicative as these substrates all show absorptions in this range, making this absorption band limited in use for discriminative purposes.

**2. Phycoerythrin Absorption (539-546 nm) II**

None of the cyanobacteria in this sample set show a very strong absorption within these wavelengths. Second and fourth derivative analysis show primarily a reflectance feature within this band, but both derivative orders highlight either a shoulder or a distinct absorption peak (specifically in cyanobacteria 5) suggesting an influence by this pigment. Five of the cyanobacteria targets are green in color, while cyanobacteria 5 is brown; see Figure 48. It can therefore be inferred that the chlorophyll pigment, which confers the green color, has a stronger effect on the reflectance spectra of the green cyanobacteria than the absorption feature expected of Phycoerythrin co-occurring in this region. This feature is in fact visible in the brown colored cyanobacteria, which presumably has a lower amount of chlorophyll that does not overpower the Phycoerythrin absorption.

Figure 48. Left is *in situ* photograph of brown-colored cyanobacteria. Right is *in situ* photograph of green-colored cyanobacteria.

Conversely, all coral targets show an absorption in this region, which may be attributed to the accessory pigment fucoxanthin (a zooxanthellae pigment common to all reef building corals) reported to absorb at 545 nm (Smith and Alberte, 1994; see Table 4). Although it is interesting to see it cause such a large absorption, it not surprising since all reef-building corals contain large amounts of zooxanthellae.

Brown algae (including *Laurentia*) also show an absorption in this bandwidth while the green alga spectrum shows characteristics similar to those found in cyanobacteria. This is somewhat expected for both algae based on color, but further investigation (more spectra to augment the existing library) is necessary in the future to resolve this point.

**3. Phycoerythrin Absorption (565-576 nm) III**

When compared to *P. lobata*, to *Pocillopora* spp., or to green algae, this wavelength is an excellent discriminator for detection of cyanobacteria. This is not the case for *Montipora* spp. or brown algae: *Montipora* spp. spectra have a broad positive absorption that generally begins at 565 nm and ends at 603 nm, as noted in the Results chapter, see Figure 33, brown algae have a narrower absorption band of 560-578 nm. This latter feature in red/brown algae has been reported by Lemasson et al. (1973) and confirmed in Hedley and Mumby (2002), and is specific to rhodophytes; see Figure 49.

Figure 49. Image of Rhodaphyta, “red-algae”. Taken from http://www.ucmp.berkeley.edu/protista/rhodophyta.html 9 September 2006.

**4. Phycocyanin Absorption (595 nm) I**

A secondary absorption of phycocyanin, this band is minimally absorbed in each of the cyanobacteria spectra. All coral targets show high absorptions within a 5 nm range of this feature, probably attributable to the Fucoxanthin pigment or to Chlorophyll c; see Table 4. *Laurentia* spp. and green algae spectra show minor absorptions; hence, this is not a good cyanobacteria discriminator from these substrates either. However, this wavelength is indeed a good discriminator between cyanobacteria and brown algae targets.

**5. Phycocyanin Absorption (615-632 nm) II**

All spectral targets collected except *Montipora* spp. absorb in this region, through overlapping absorptions by other biochemical constituents, most likely due to chlorophyll c (Table 4). Thus, this bandwidth fails to provide a good spectral discriminator in a mixed coral environment.

**6. Allophycocyanin Absorption (652-654 nm)**

The third of the phycobiliprotein pigments, allophycocyanin, uniquely absorbs from 652-654 nm. All coral targets are highly reflective in this region as well as the algae targets, potentially making this a good discriminator wavelength for cyanobacteria detection. However, all but cyanobacteria 6 (the sample collected above water), have reflective properties in the 645-660 nm range. Second derivatives analysis however shows a shoulder that is prominent in all five remaining cyanobacteria spectra between 648-650 nm, possibly suggesting allophycocyanin presence. The green and brown algae targets are reflective in this wavelength while *Laurentia* spp. displays a shoulder near 643 nm, similar to the cyanobacteria spectra. Therefore, this feature serves as a minor discriminator against coral targets and most algae.

**7. 515-522 nm Absorption**

A thorough literature search provided no other reports of this absorption in the marine environment (cf. Table 4), but inspection of spectra shown in Beach et al. (1997), Jupp et al. (1994), Holden and LeDrew (2002), Wettle et al., (2003), and Hochberg et al. (2004) show varying degrees of absorption in this region. However, each fails to report the contributing cause.

### 8. Summary of Comparisons

In summary, the phycoerythrin absorption at 564-576 nm appears to provide the greatest level of discrimination for green algae, *Pocillopora* spp., *P. compressa* (cf.) substrates, but especially *P. lobata.* This absorption range does not provide a distinction for neither brown algae nor *Montipora* spp. Despite this challenge, a distinct classification exists at the phycocyanin absorption at 615-632 nm. However, brown algae, including *Laurentia*, are much more difficult to discern when compared to cyanobacteria. Only small differences were found to exist at 690-694 nm, which coincides with an allophycocyanin absorption. Upon close inspection, most of the cyanobacteria samples show a small absorption shoulder at approximately 690-692 nm, a characteristic not found in any of the algae samples.

### 9. Comparison to Previously Reported Spectra

Several authors such as Hochberg and Atkinson (2000), Holden and LeDrew (1999 and 2001) and Andréfouët (2003) have reported several coral spectra collected in the Pacific Ocean with Hochberg's et al. (2006) work focusing on corals in the Hawaiian Islands. Spectra collected for this study were compared to these papers and seemed to match closely with what was reported. Curiously, *P. lobata* spectra reported in this thesis differed slightly from other papers as all three spectra show a double-peaked absorption between 613-634 nm not readily attributed to any of the pigments reported in Table 4. Hochberg et al. (2006) measured reflectance spectra for *P. lobata* in the main Hawaiian Islands but did not show any second derivative analysis of such absorptions. Holden and LeDrew (2001), who conducted extensive work with second derivative analysis of coral environments, specifically point out a reflective maximum between 610-650 nm in *P. lobata*, which is in contrast to the absorptions reported here, but no further information is provided. This could be attributed to evolutionary differences between the *P. lobata* species found in Midway Atoll and that found in the Fiji Islands, where Holden and LeDrew carried out their spectral work. It would be interesting if these species differences may come across spectrally as suggested here, but further research would be needed to support this. Additionally, a weak absorption feature exists at 537 nm in each of the *P. lobata* spectra, which is also reported in Hochberg et al. (2000), Hochberg et al. (2004), Hochberg et al. (2006) as well as Holden and LeDrew (1999).

## B. APPLICABILITY TO AIRBORNE SENSORS

### 1. AVIRIS

AVIRIS has great potential to detect the narrow bandwidth absorption features of cyanobacteria because of its high spectral resolution. Richardson et al. (1994) conducted a study using AVIRIS to detect photosynthetic accessory pigments in saltwater ponds throughout the San Francisco Bay area. Their research used 20 nm resampled AVIRIS data to generate fourth order derivatives, which were compared to field spectra from a Shimadzu UV/VIS scanning spectrophotometer. This study clearly shows the potential that AVIRIS has in detecting narrow bandwidth absorptions found in the marine environment. Despite the 10 nm nominal spectral resolution, AVIRIS was able to detect two relatively narrow absorption peaks, 508 nm (carotenoid myxoxanthophyll) and 632 nm (phycocyanin). However Richardson et al. (1994)'s study was aimed at detecting phytoplankton pigments in the water column, rather than pigments found in benthic environments, which is a more difficult task as the signal is confounded by the water column.

When considering AVIRIS' ability in detecting the narrow bandwidths reported in this thesis, spatial resolution becomes an equally important factor to identify cyanobacteria within an image. When flown from the ER-2, AVIRIS has a nominal pixel resolution of 17-20 meters. In a mixed substrate of algae, coral, and cyanobacteria, this would make detection of cyanobacteria challenging unless cyanobacterial mats are so extensive that they are the dominant feature of the pixel. However, when flown from the NOAA Twin Otter aircraft, spatial resolutions of 2-4 meters are achievable, making this the preferred platform for imaging Midway Atoll if the AVIRIS sensor is to be used.

To simulate an AVIRIS collection and determine its viability in detecting cyanobacteria in Midway Atoll from a purely spectral resolution standpoint, the original reflectance data was resampled to 10 nm (the resolution of the AVIRIS sensor) and then successive derivative orders were applied. The new second derivatives were then compared as reported in Chapter VII to determine what unique discriminate characteristics were preserved. Although the allophycocyanin "shoulder" absorptions (652-654 nm) unique to the cyanobacteria disappeared, the 565-576 nm (phycoerythrin) spectral discriminator retained prominent differences between *P. lobata, P. compressa*

(cf.), *P. ligulata*, *P. damicornis*, the green algae and the cyanobacteria targets (see Figure 50, Figure 51, Figure 52, and Figure 53). The phycoerythrin absorption 490-496 nm also retained the differences previously reported for *P. compressa* (cf.), *P. ligulata*, and *P. damicornis* and the cyanobacteria spectra; see Figure 50, Figure 51 and Figure 52.

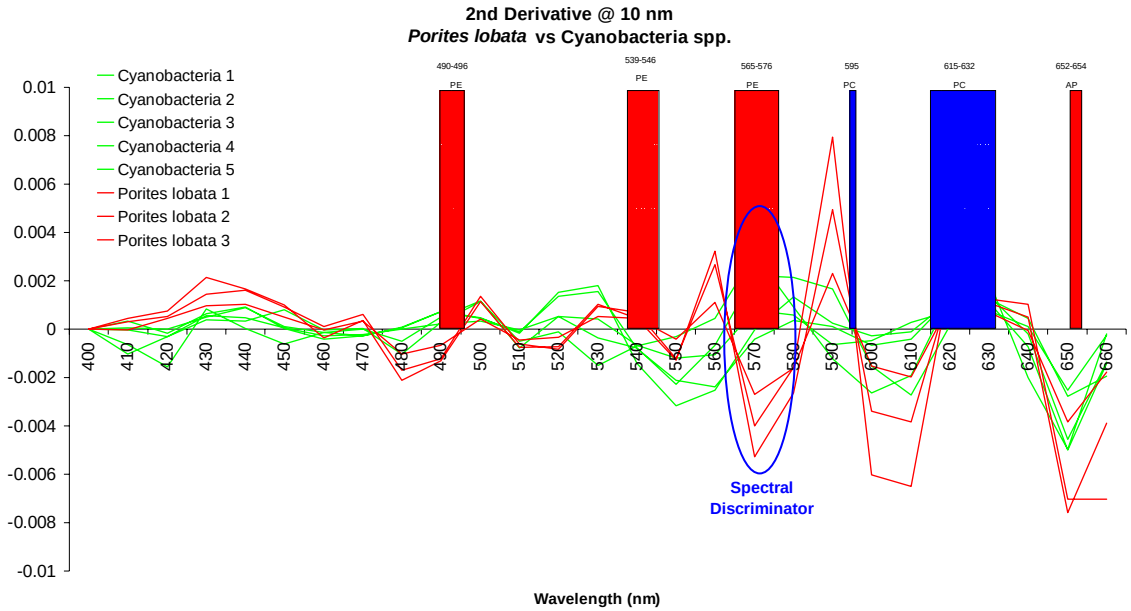


Figure 50. Resampled to 10 nm *Porites lobata* versus cyanobacteria spp. comparative analysis.

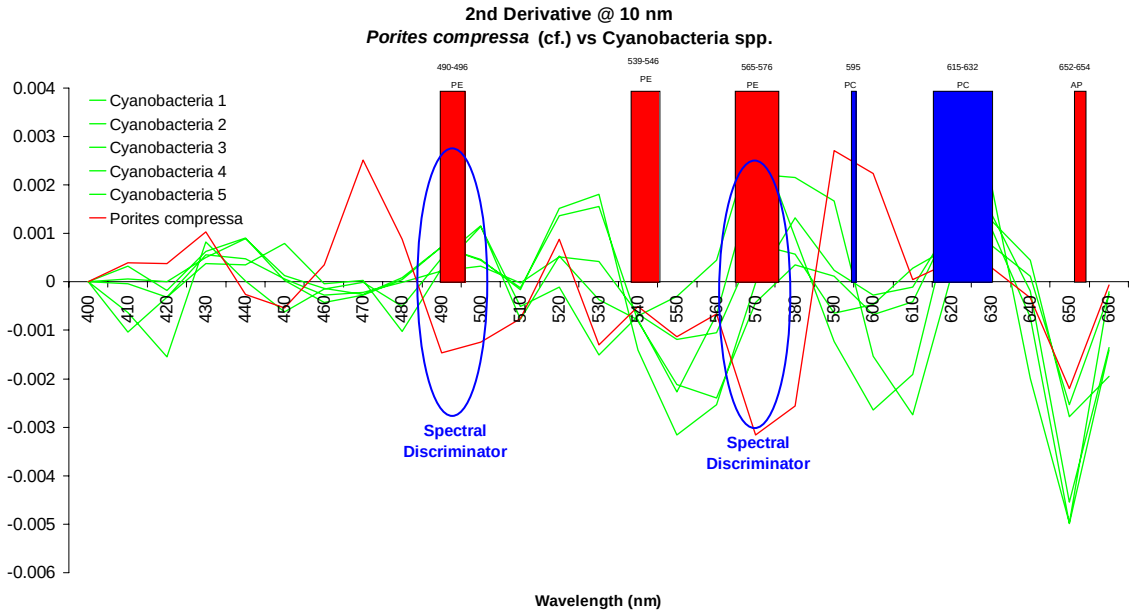


Figure 51. Resampled to 10 nm *Porites compressa* (cf.) versus cyanobacteria spp. comparative analysis.

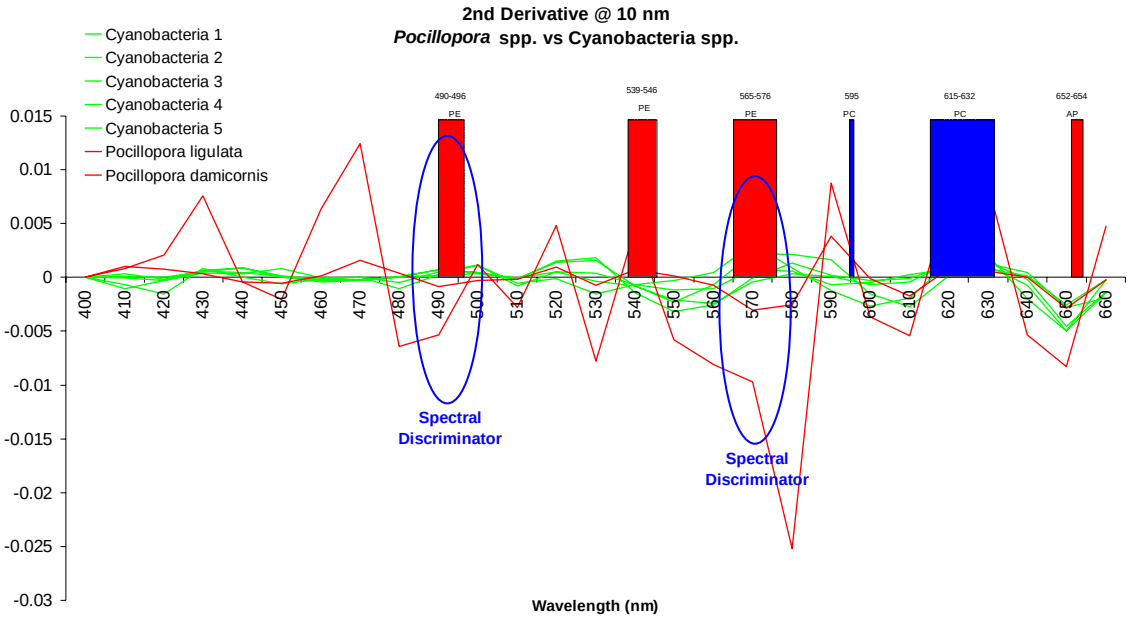


Figure 52. Resampled to 10 nm *Pocillopora* spp. versus cyanobacteria spp. comparative analysis.

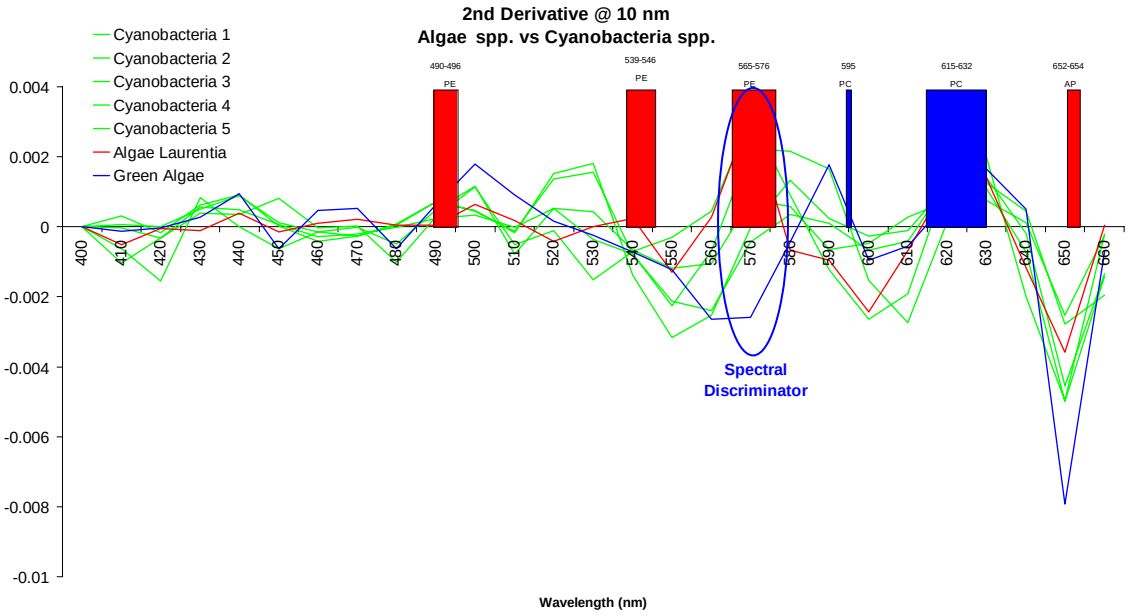


Figure 53. Resampled to 10 nm algae versus cyanobacteria spp. comparative analysis.

Resampled data show spectral differences between *Montipora* spp. and cyanobacteria at the phycocyanin absorption 615-632 nm, as can be seen in Figure 54.

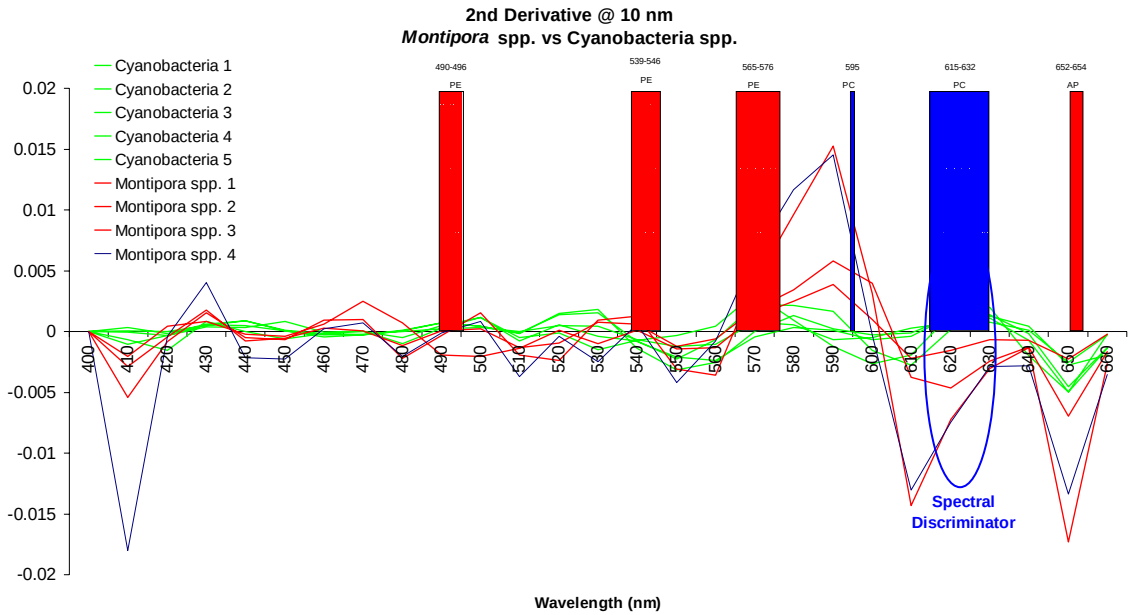


Figure 54. Resampled to 10 nm *Montipora* spp. versus cyanobacteria spp. comparative analysis plot.

## 2. HYMAP

Work by Richardson et al. (1999) applied to AVIRIS data concluded that it is possible to detect narrowband absorptions indicative of cyanobacteria suspended in the water column, exploiting several wavelengths in the visible range of the spectrum. In contrast to AVIRIS, HyMap lacks spectral coverage in the critical range 400-450 nm, a primary absorption by Chlorophyll *a*. However, this thesis did not find significant spectral differences in this region.

Resampling the data from the Results (Chapter VII) to 15 nm, which is HyMap's spectral resolution, again produced promising results for HyMap's ability to detect the 565-576 nm phycoerythrin absorptions that spectrally discriminate *P. lobata*, *P. compressa* (cf.), *P. ligulata* and *P. damicornis* from cyanobacteria. At this coarser resolution, *P. lobata* and cyanobacteria resampled spectra show a second potential spectral discriminator at the 490-496nm phycoerythrin absorption not noticeable before while *P. compressa* (cf.), *P. ligulata*, and *P. damicornis* corroborate findings of the

higher spectral resolution showing 2 important spectral discriminator wavelengths; see Figure 55, Figure 56, and Figure 57. However, as shown in Figure 58, the algae resampled spectra did not show any good discriminative wavelengths when compared to the cyanobacteria.

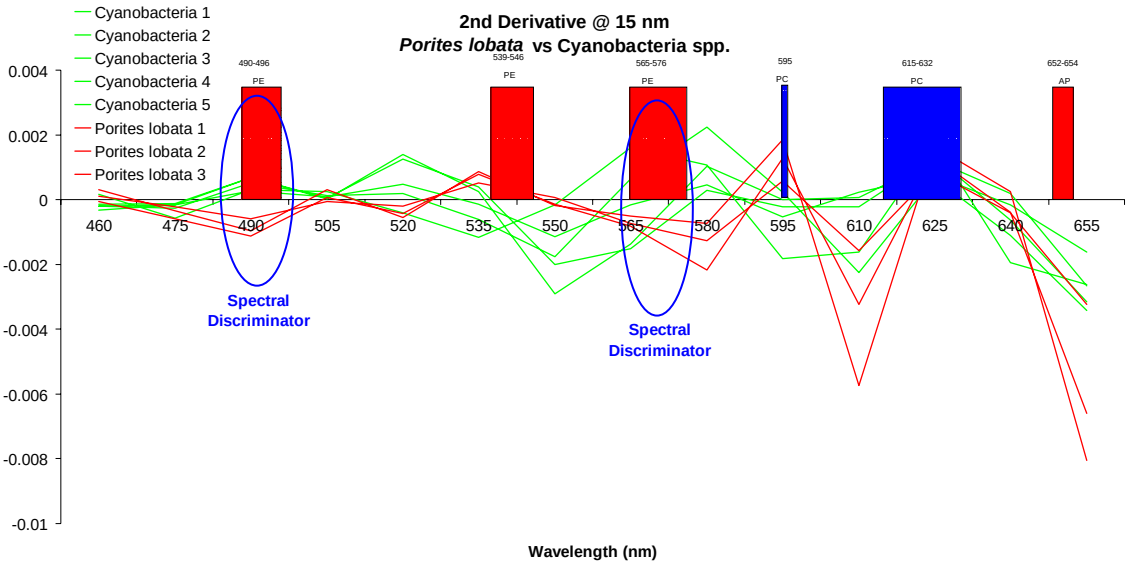


Figure 55. Resampled to 15 nm *Porites lobata* versus cyanobacteria spp. comparative analysis.

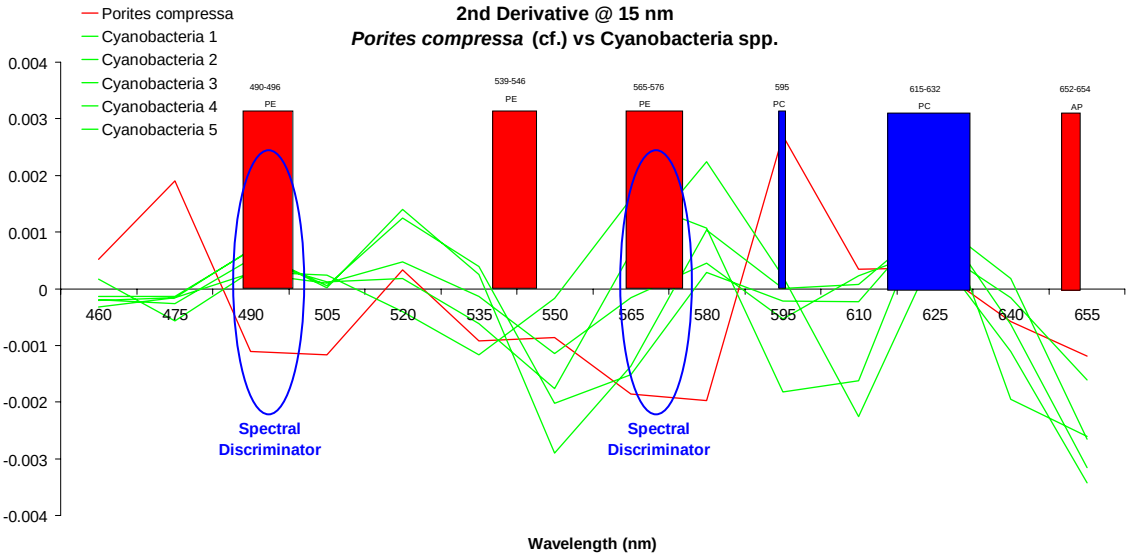


Figure 56. Resampled to 15 nm *Porites compressa* (cf.) versus cyanobacteria spp. comparative analysis.

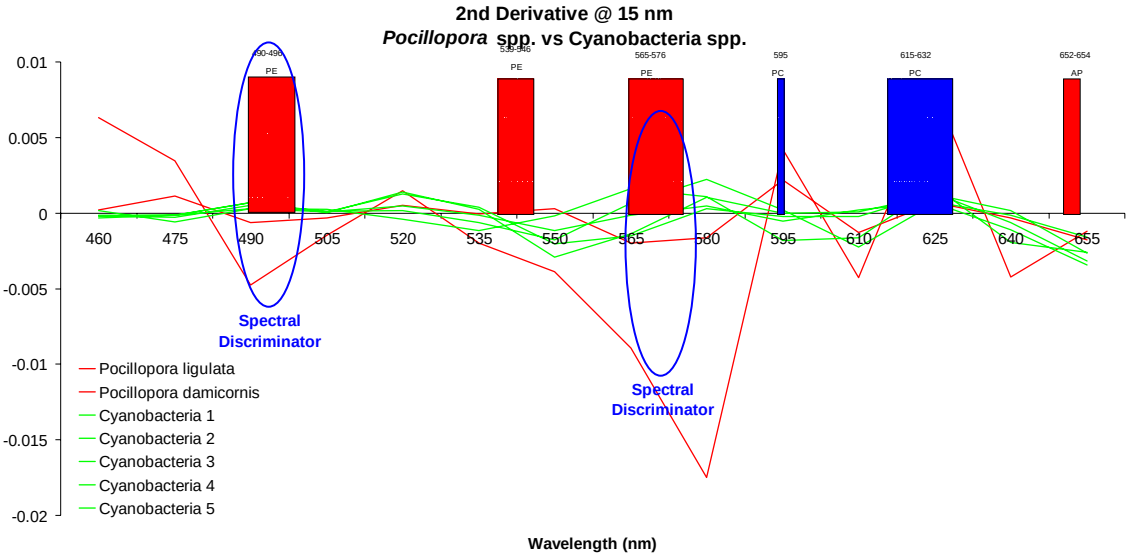


Figure 57. Resampled to 15 nm *Pocillopora* spp. versus cyanobacteria spp. comparative analysisy.

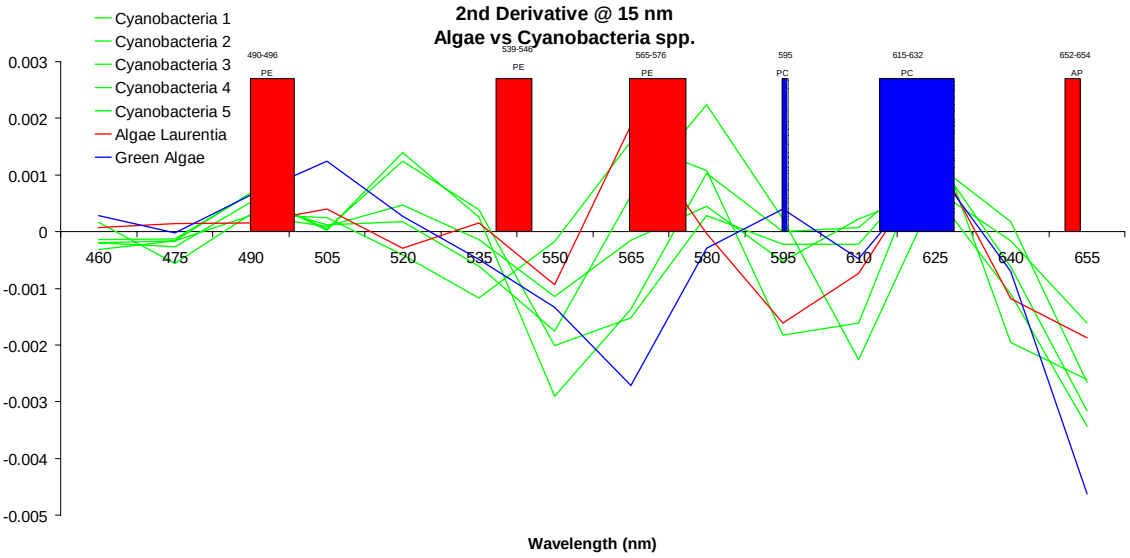


Figure 58. Resampled to 15 nm algae versus cyanobacteria spp. comparative analysis.

After resampling, *Montipora* spp. retains its spectral discriminator at the phycocyanin absorption of 615-632 nm; see Figure 59. However, none of the spectra resampled with HyMap's 15nm resolution detect the allophycocyanin absorption 652-654 nm, which was to be expected since this was a very narrow feature.

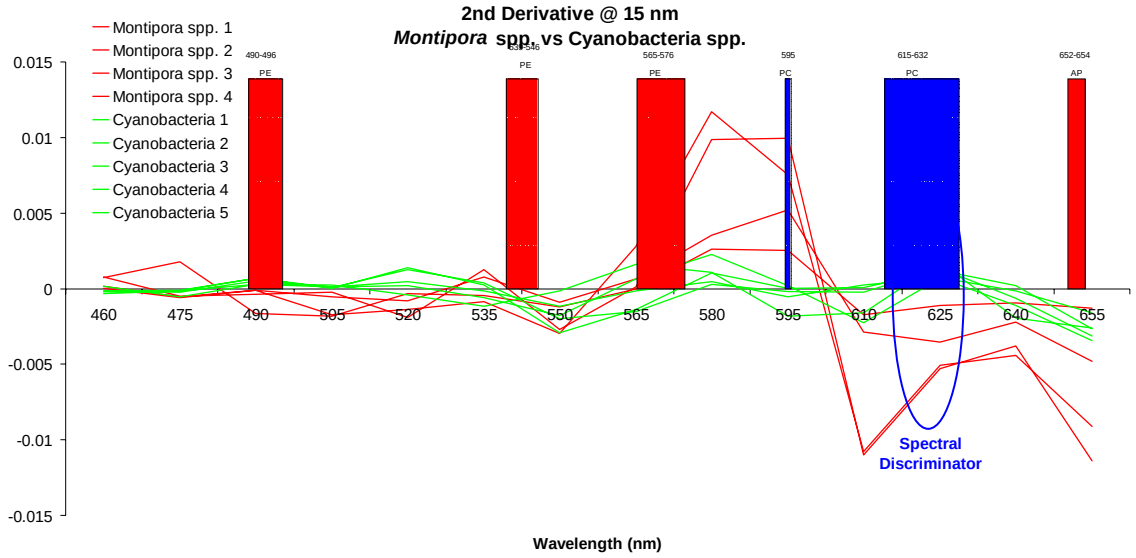


Figure 59. Resampled to 15 nm *Montipora* spp. versus cyanobacteria spp. comparative analysis.

### 3. CASI

CASI has the greatest potential for the ability to detect benthic cyanobacteria in the *Lyngbya* genus at Midway Atoll. Combined with derivative analysis, CASI appears to be the imager of choice for detecting the spectral characteristics indicative of this study. In spatial mode, selected bands can be programmed over the discriminative wavelength pointed out in this study. This will allow spatial resolutions close to 1m, which is highly beneficial for a heterogeneous coral reef environment like the one found at Midway Atoll. Spectral assignments should be designed to center on the phycoerythrin absorption at 565 to 576 nm when operating over a known mixed benthic coral reef environment consisting of *P. lobata* (Figure 60), *P. compressa* (cf.) (Figure 61), *P. ligulata* and *P. damicornis* (Figure 62), and green algae, (Figure 63). If operating over a known substrate that only includes *Montipora* spp., greater emphasis should be placed on the 615-632 nm, as seen in Figure 64.

In hyperspectral mode, as many as 72 spectral bands can be assigned with a spectral resolution of 4.2 to 4.3 nm (McFee and Ripley, 1997). However, Lewotsky (1994) reports an average of 3 nm spectral resolution, which is the one chosen for the resampling purposes in this thesis.

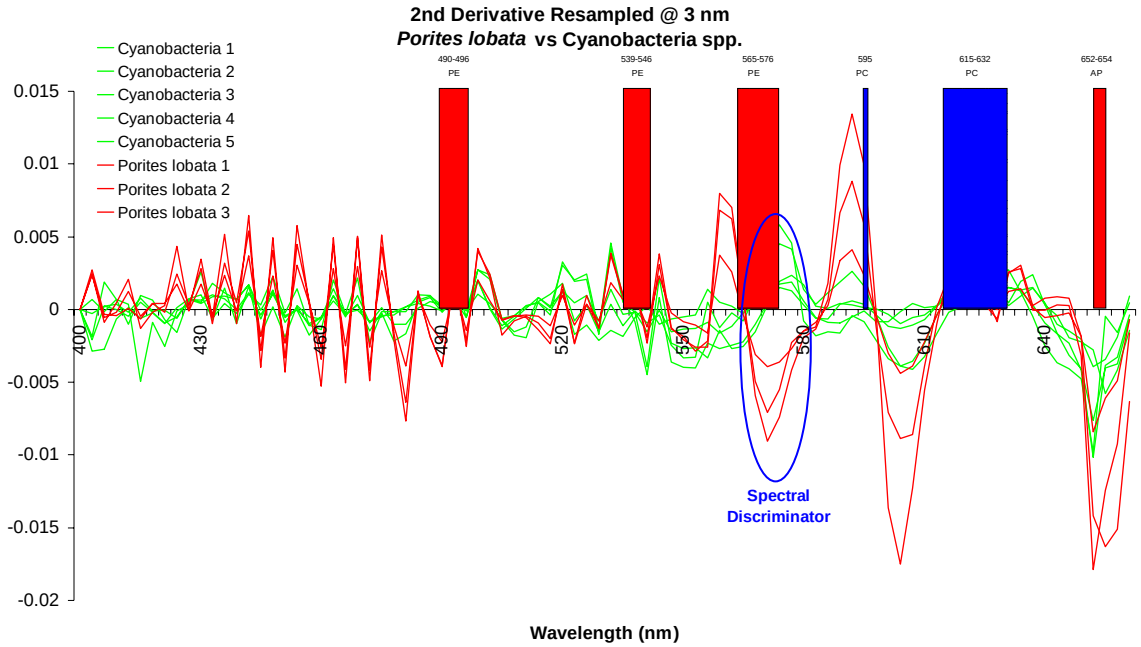


Figure 60. Resampled to 3 nm *Porites lobata* versus cyanobacteria spp. comparative analysis.

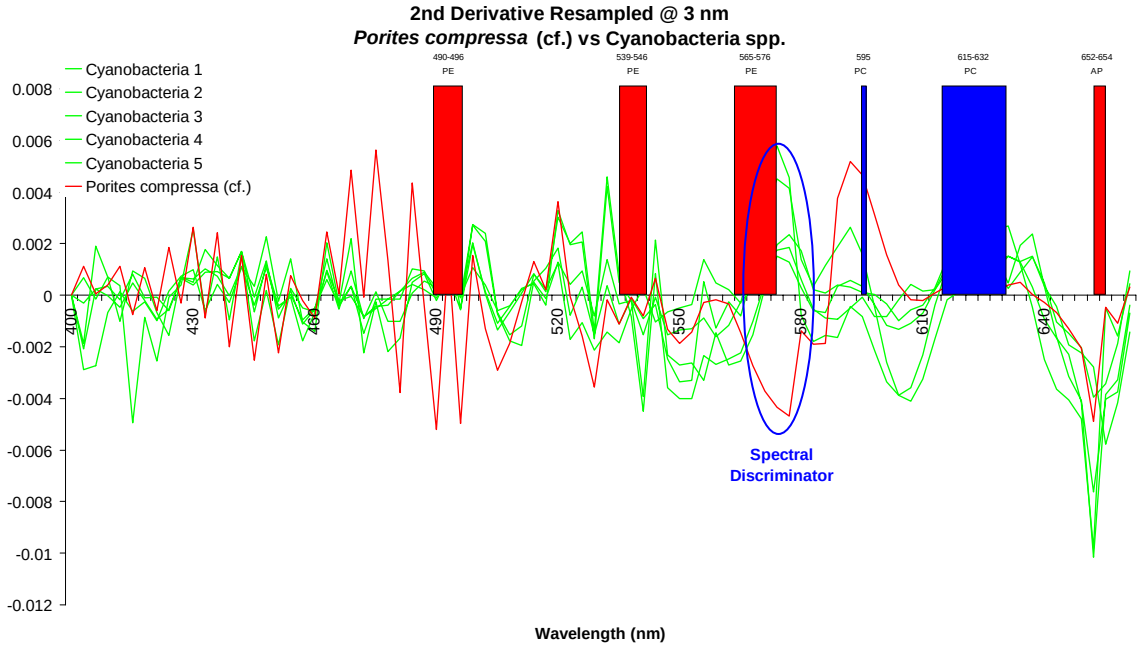


Figure 61. Resampled to 3 nm *Porites compressa* (cf.) versus cyanobacteria spp. comparative analysis.

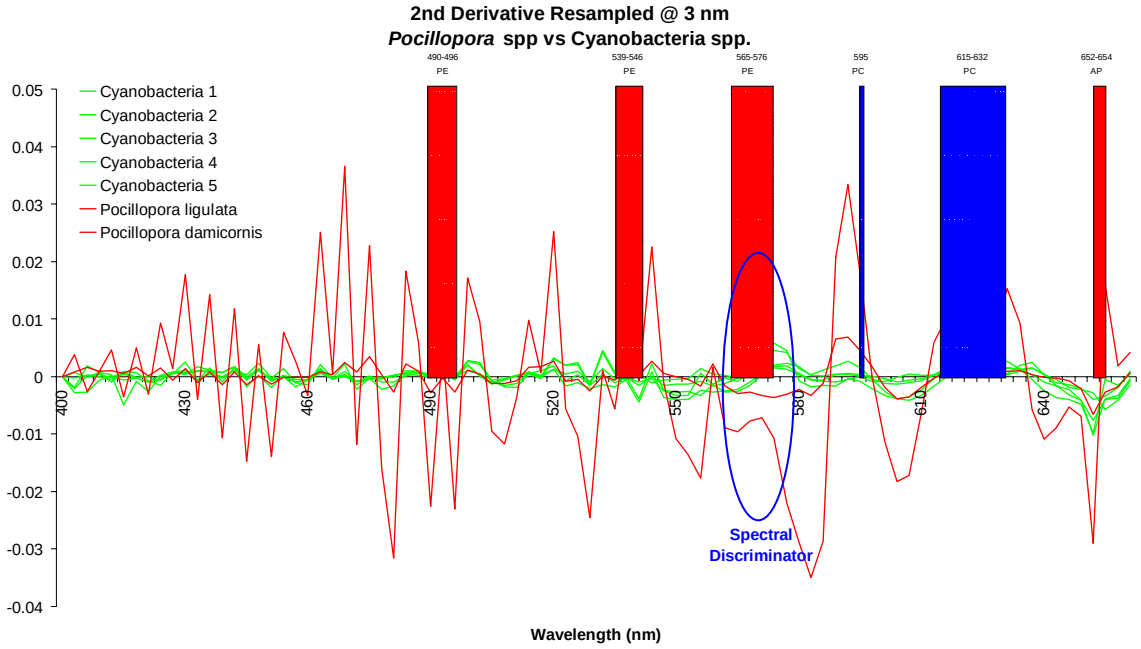


Figure 62. Resampled to 3 nm *Pocillopora* spp. versus cyanobacteria spp. comparative analysis.

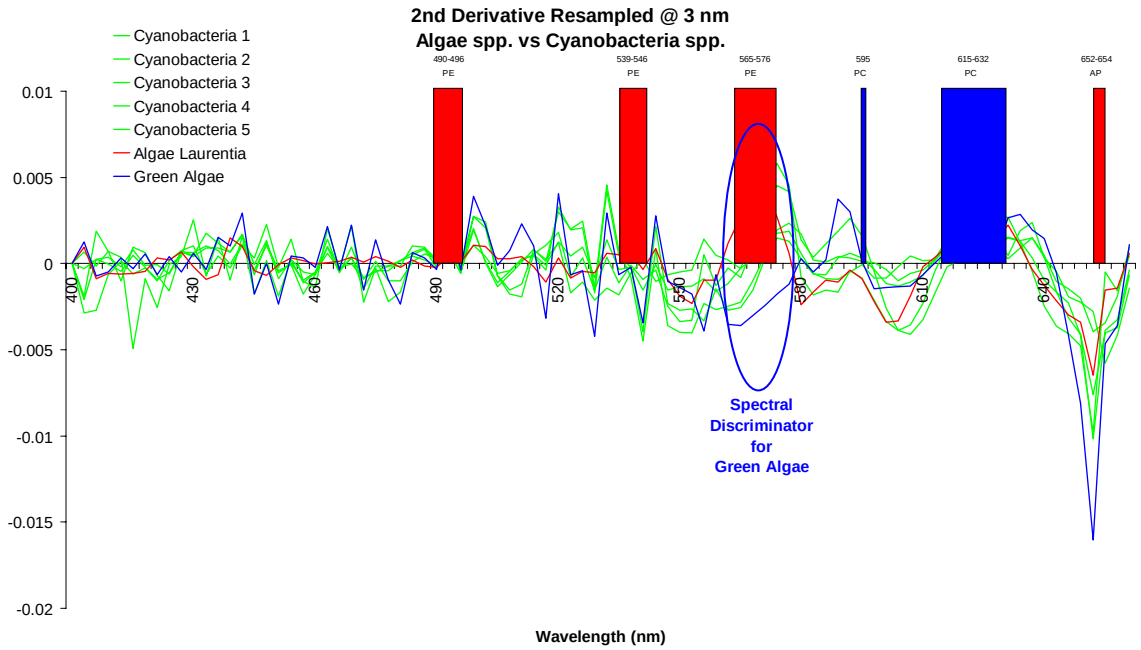


Figure 63. Resampled to 3 nm algae versus cyanobacteria spp. comparative analysis.

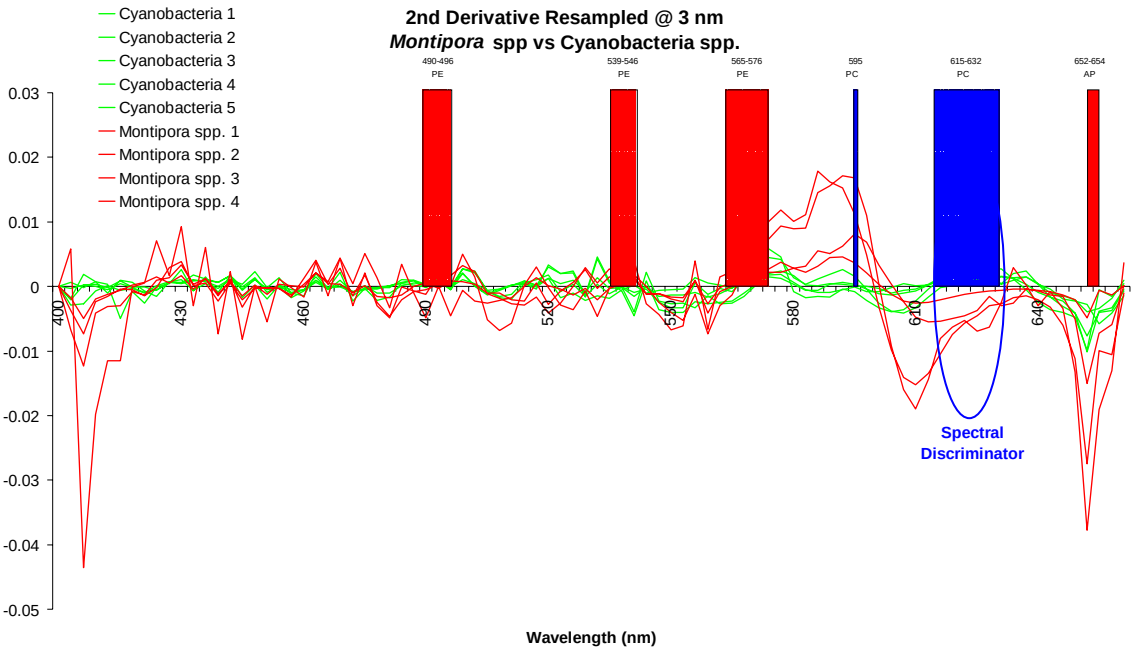


Figure 64. Resampled to 3 nm Montipora spp. versus cyanobacteria spp. comparative analysis.

# IX. FUTURE WORK

## A. LESSONS LEARNED

### 1. Larger Sample Size

Although this study produced good preliminary results, the limited sample size of 20 total targets measured *in situ* with the spectroradiometer cannot yet provide statistically rigorous results that can be used reliably to guide an airborne sensor deployment, and needs therefore to be augmented with additional spectra. Additionally, in this study spectra collections were carried out only in two areas within Midway Atoll (known to Midway staff as "Rusty Bucket" and "Reef Hotel"), which were known for the presence of iron products and of extensive benthic cyanobacteria mats in the *Lyngbya* genus, documented by other researchers shortly before our field trip to Midway Atoll. These locations were convenient for the purpose of conducting ground truth spectral collections, but future spectra collections should gather data throughout Midway Atoll in order to augment the spectral library of organisms existing in this diverse coral reef environment. A more thorough search of the presence of cyanobacterial mats throughout the atoll would also be important, aided by the photographic library of the target cyanobacteria shown in Appendix B, so that a greater number of spectra can be acquired for this critical target species.

### 2. Spectrometer

The USB2000 Fiber Optic Spectrometer is a high quality spectrum collector that has been used in the past by several researchers. Despite conducting numerous tests prior to the fieldwork in Midway Atoll, the USB2000 showed a great deal of noise in each of the spectra collected for this study. Although this challenge was overcome by smoothing the spectra as reported in Chapter VI, future endeavors need to consider carrying a second spectrometer as a backup in the event similar problems are experienced.

## B. FUTURE WORK

### 1. Validate Results

Because of the small sample size collected for this thesis, follow on work is necessary to validate the results reported in Chapter VII. Provided the results of this

study are corroborated, future work in Midway Atoll will serve to increase the sample size and lend greater statistical significance to these results. Ultimately, it would be useful to test the hypothesis outlined in this thesis in benthic environments other than Midway Atoll. Tropical waters tend to be the ideal laboratory for remote sensing studies, since these environments are typically classified as Type I optical waters, i.e., of great clarity and high light penetration.

### 2. Test Hypothesis with Airborne Sensor

Besides augmenting the spectral library acquired for this study and corroborating the results presented here, the next step would be to conduct a collection with an airborne sensor over Midway Atoll, and test airborne imagery's ability to detect *Lyngbya* spp. As reported in Chapter IX, any of the three sensors (AVIRIS, HyMap, or CASI) could be utilized to detect the presence of cyanobacteria in the benthic environment of Midway Atoll, although CASI would be the preferred sensor for the reason outlined in the previous chapter.

# APPENDIX A. FIELD LOGSHEETS

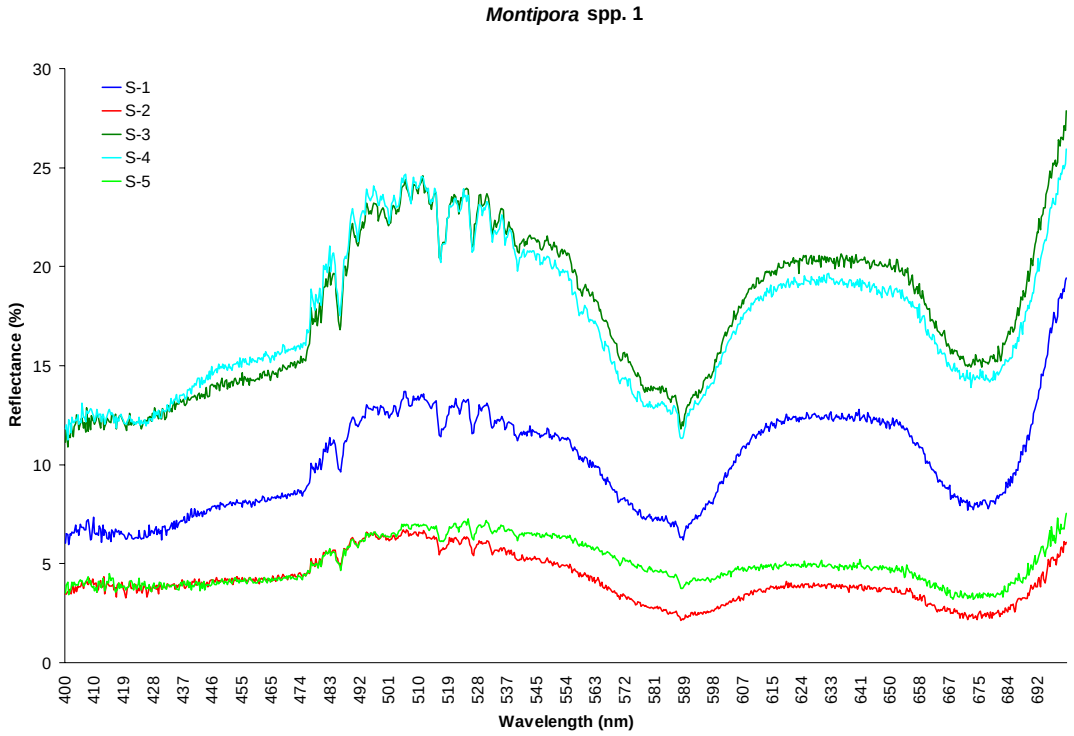


| | | |
|---|---|---|
| **Target:** | *Montipora* spp.. | |
| **Size/Morphology:** | Small, encrusting | |
| **GPS** | 23-14.795 N | |
| | 177-19.537 W | |
| **Depth:** | 2 feet | |
| **Date:** | 23 Jul 2006 @ 13:59 | |
| **Dive dist/bearing from boat:** | 5 meter SE | |
| **Photo #** | Img_0001.jpg | |
| **Spectrum #:** | 0001 – Nadir View @ 1359 | 200 |
| | 0002 – North View @ 1359 | 220 |
| | 0003 – East View @ 1359 | 270 |
| | 0004 – South View @ 1400 | 270 |
| | 0005 – West View @ 1400 | 250 |
| **Surrounding substrate:** | Sand, live/dead coral | |
| **Notes:** Patch reef with north side mostly living coral while the southern and western edges were mostly dead. Reference spectrum was nearly off the charts, but the reflective spectrum was fairly flat. | | |

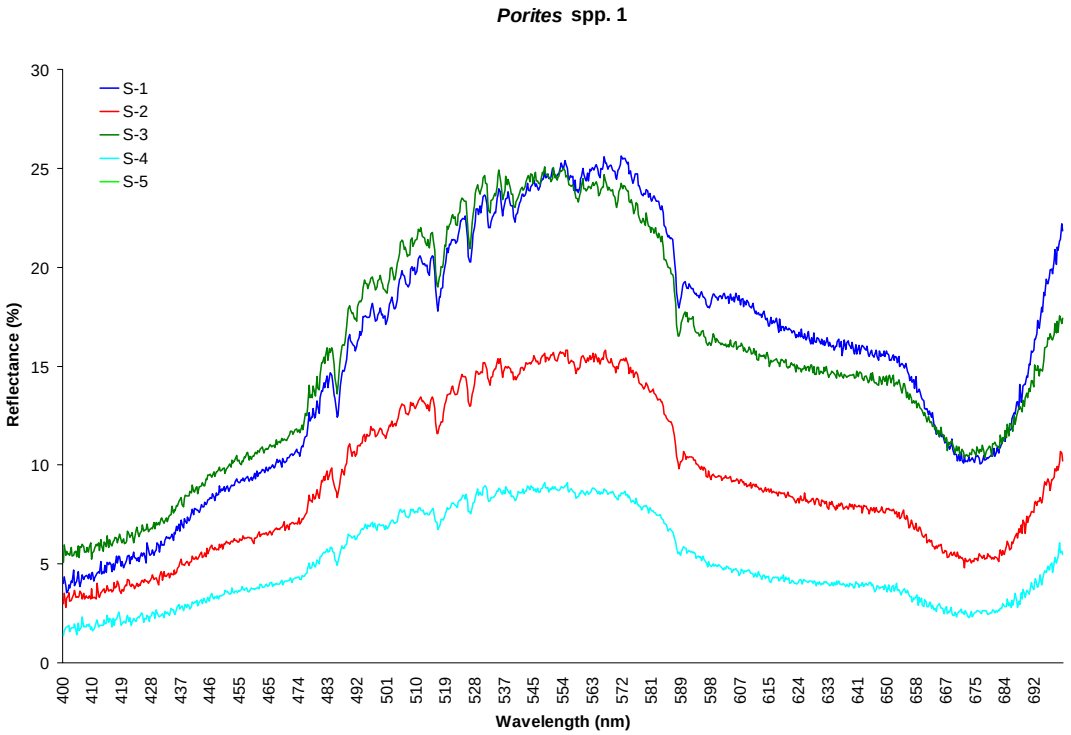


| | | |
|---|---|---|
| **Target:** | *Porite lobata/lutea/ compressa* | |
| **Size/Morphology:** | Small Branching | |
| **GPS** | 28-14.795 N | |
| | 177-19.537 W | |
| **Depth:** | 2.5 Feet | |
| **Date:** | 23 Jul 2006 @ 14:02 | |
| **Dive dist/bearing from boat:** | 5 meter SE | |
| **Photo #** | Img_0002.jpg | |
| **Spectrum #:** | 0006 – Nadir View @ 1402 | 220 |
| | 0007 – North View @ 1402 | 220 |
| | 0008 – East View @ 1402 | 230 |
| | 0009 – South View @ 1403 | 220 |
| | 0010 – West View @ 1403 | |
| **Surrounding substrate:** | Sand, live/dead coral | |
| **Notes:** Patch reef with north side mostly living coral while the southern and western edges were mostly dead. Reference spectrum was nearly off the charts, but the reflective spectrum was fairly flat. | | |

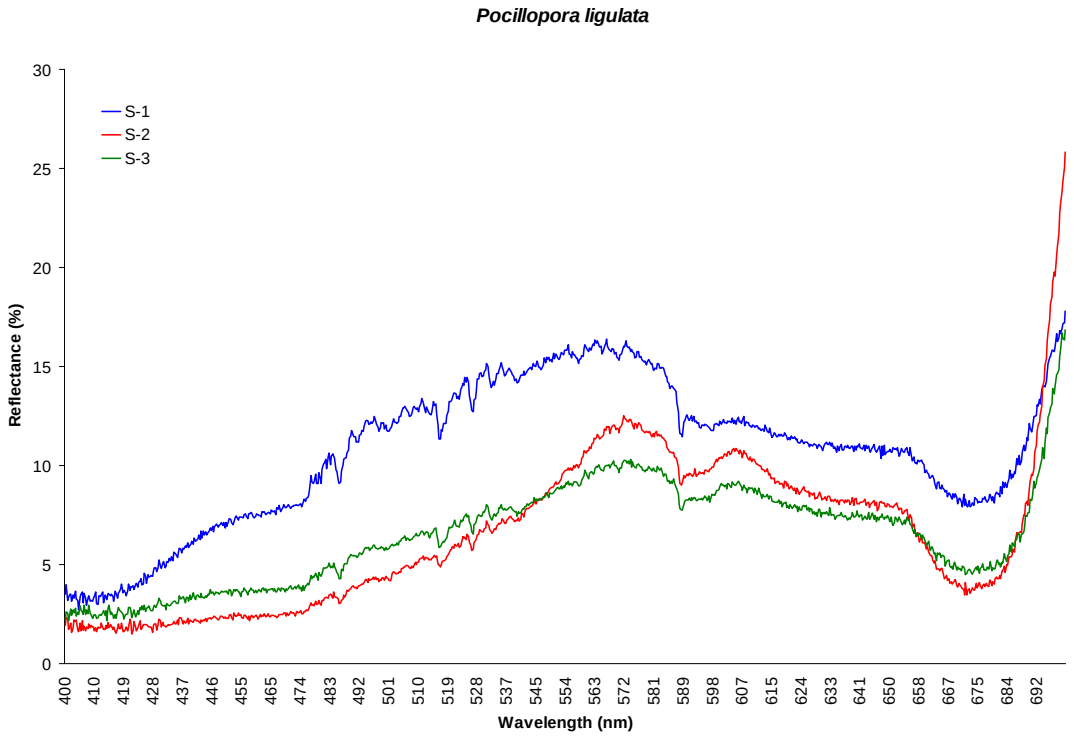


| | | |
|---|---|---|
| **Target:** | *Pocillopora ligulata* | |
| **Size/Morphology:** | Small Branching | |
| **GPS** | 28-14.795 N | |
| | 177-19.537 W | |
| **Depth:** | 2.5 Feet | |
| **Date:** | 23 Jul 2006 @ 14:04 | |
| **Dive dist/bearing from boat:** | 5 meter SE | |
| **Photo #** | Img_0003.jpg | |
| **Spectrum #:** | 0011 – Nadir View @ 1404 | 200 |
| | 0012 – North View @ 1405 | 55 |
| | 0013 – East View @ 1405 | |
| | 0014 – South View @ 1405 | |
| | 0015 – West View @ 1405 | 150 |
| **Surrounding substrate:** | Sand, live/dead coral | |
| **Notes:** Nadir view. Patch reef with north side mostly living coral while the southern and western edges were mostly dead. Reference spectrum was nearly off the charts, but the reflective spectrum was fairly flat. Branching coral. | | |

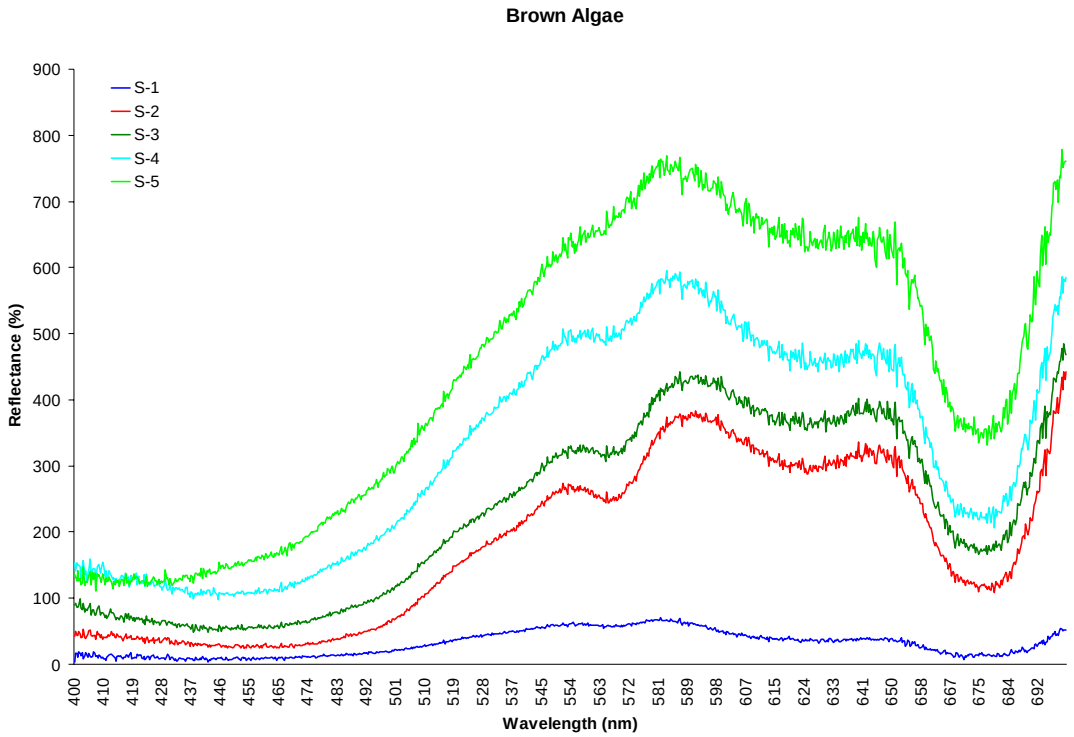


| | | |
|---|---|---|
| **Target:** | Brown Algae | |
| **Size/Morphology:** | Small encrusting | |
| **GPS** | 28-14.795 N | |
| | 177-19.537 W | |
| **Dive dist/bearing from boat:** | 5 meter SE | |
| **Depth:** | 1.5 Feet | |
| **Date:** | 23 Jul 2006 @ 14:11 | |
| **Photo #** | Img_0004.jpg | |
| **Spectrum #:** | 0016 –@ 1411 | 50 |
| | 0017 –@ 1411 | 55 |
| | 0018 –@ 1411 | 60 |
| | 0019 –@ 1411 | 60 |
| | 0020 –@ 1412 | 40 |
| **Surrounding substrate:** | Sand, live/dead coral | |
| **Notes:** Patch reef with north side mostly living coral while the southern and western edges were mostly dead. Reference spectrum was nearly off the charts, but the reflective spectrum was fairly flat. All spectra taken with a nadir view. Brown Algae. | | |

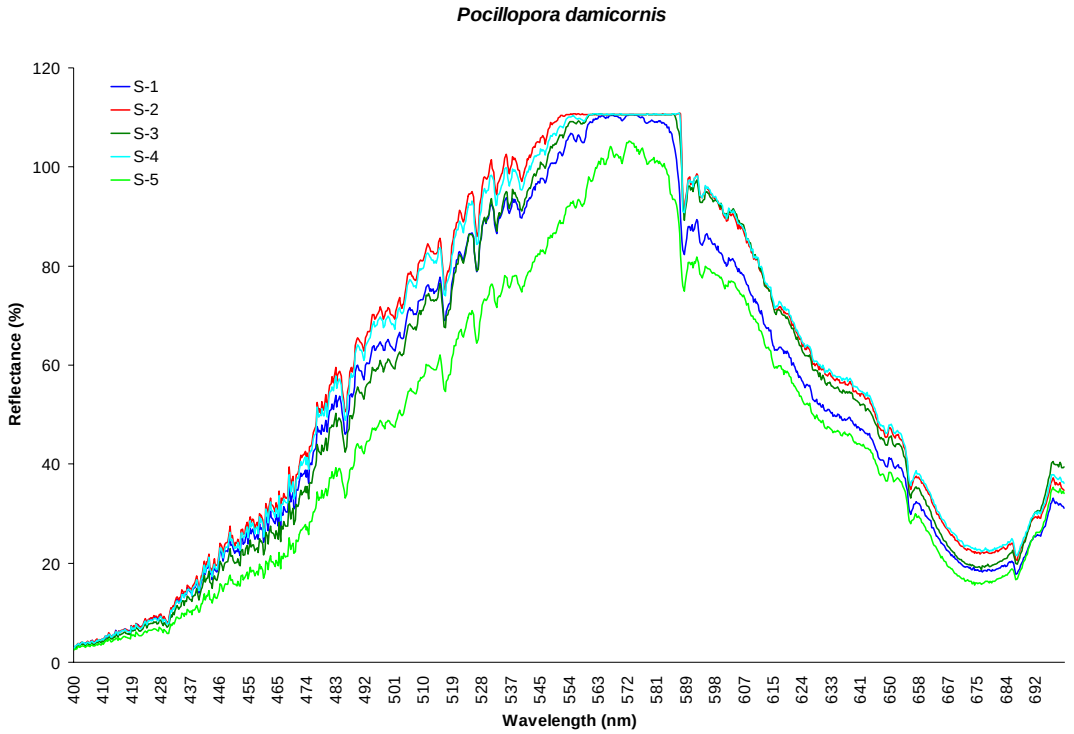


| | | |
|---|---|---|
| **Target:** | *Pocillopora damicornis* | |
| **Size/Morphology:** | Small Branching Coral | |
| **GPS** | 28-12.996 N | |
| | 177-23.434 W | |
| **Depth:** | 2.5 feet | |
| **Date:** | 24 Jul 2006 @ 11:15 | |
| **Dive dist/bearing from boat:** | 4 meter N | |
| **Photo #** | Img_0009.jpg | |
| **Spectrum #:** | 0036 –@ 1115 | 120 |
| | 0037 –@ 1116 | 150 |
| | 0038 –@ 1116 | 165 |
| | 0039 –@ 1117 | 160 |
| | 0040 –@ 1118 | 120 |
| **Surrounding substrate:** | Dead coral (continued in notes) | |
| **Notes:** Sporadic branching coral, mostly dead coral with some rubble and sand. Quite a bit of the brown cyanobacteria throughout along with small green plantlike things. Several urchins in the area.<br>Rusty Bucket | | |

***Montipora* spp. 2**

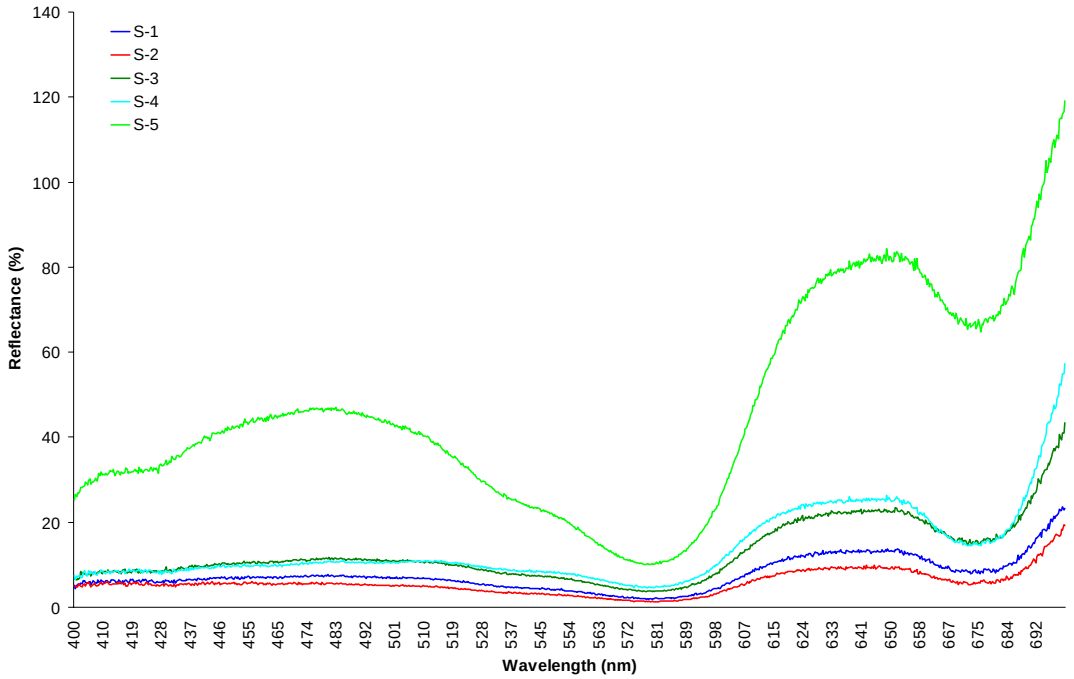


| | | |
|---|---|---|
| **Target:** | *Montipora flabellata/capitata* | |
| **Size/Morphology:** | Medium Encrusting | |
| **GPS** | 28-16.662 N | |
| | 177-22.043 W | |
| **Depth:** | 4.5 Feet | |
| **Date:** | 24 July 2006 @ 15:01 | |
| **Dive dist/bearing from boat:** | 8 meter N | |
| **Photo #** | Img_0010.jpg | |
| **Spectrum #:** | 0041 –@ 1501 | 60 |
| | 0042 –@ 1502 | 75 |
| | 0043 –@ 1502 | 55 |
| | 0044 –@ 1502 | 35 |
| | 0045 –@ 1502 | 40 |
| **Surrounding substrate:** | Metal debris (see notes) | |
| **Notes:** Sand, dead coral, green algae stuff, urchins.<br>Cloudy condition<br>Reef Hotel | | |

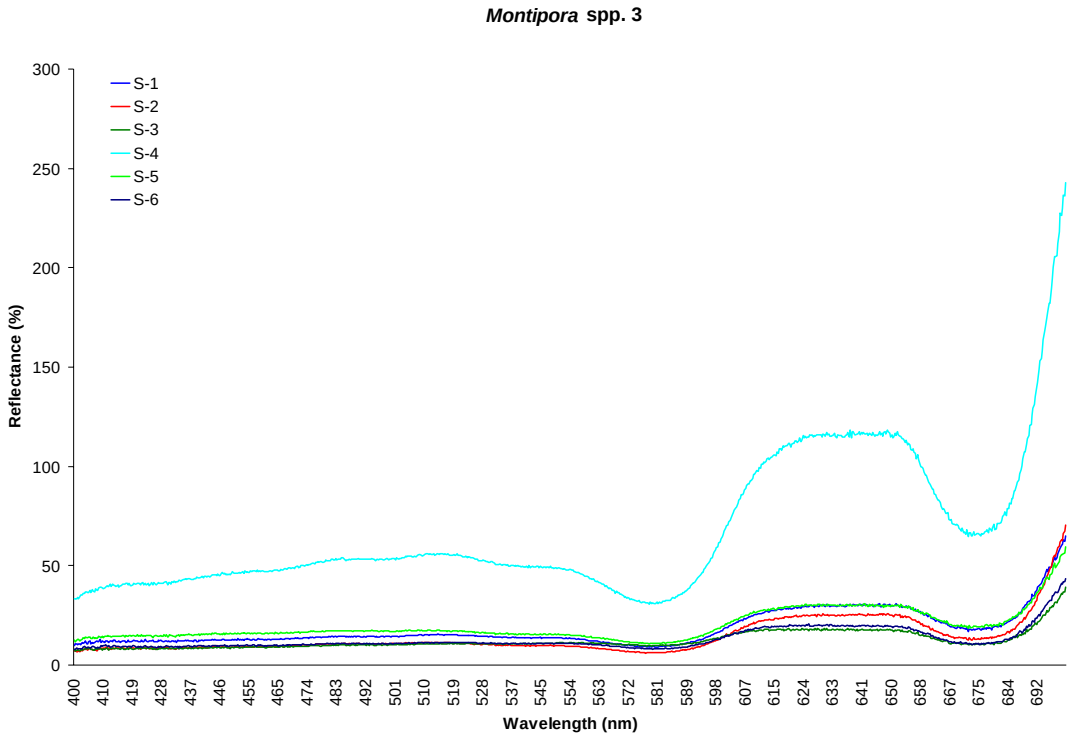


| | | |
|---|---|---|
| **Target:** | *Montipora flabellate* | |
| **Size/Morphology:** | Medium Encrusting | |
| **GPS** | 28-16.662 N | |
| | 177-22.043 W | |
| **Depth:** | 3.5 Feet | |
| **Date:** | 24 July 2006 @ 15:06 | |
| **Dive dist/bearing from boat:** | 9 meter N | |
| **Photo #** | Img_0011.jpg | |
| **Spectrum #:** | 0046 – @ 1506 | 70 |
| | 0047 – @ 1506 | 55 |
| | 0048 – @ 1506 | 80 |
| | 0049 – @ 1506 sun out | 40 |
| | 0050 – @ 1507 | 65 |
| | 0051 – @ 1507 | 60 |
| **Surrounding substrate:** | Metal debris (see notes) | |
| **Notes:** Sand, dead coral, green algae stuff, urchins.<br>Cloudy conditions<br>Reef Hotel | | |

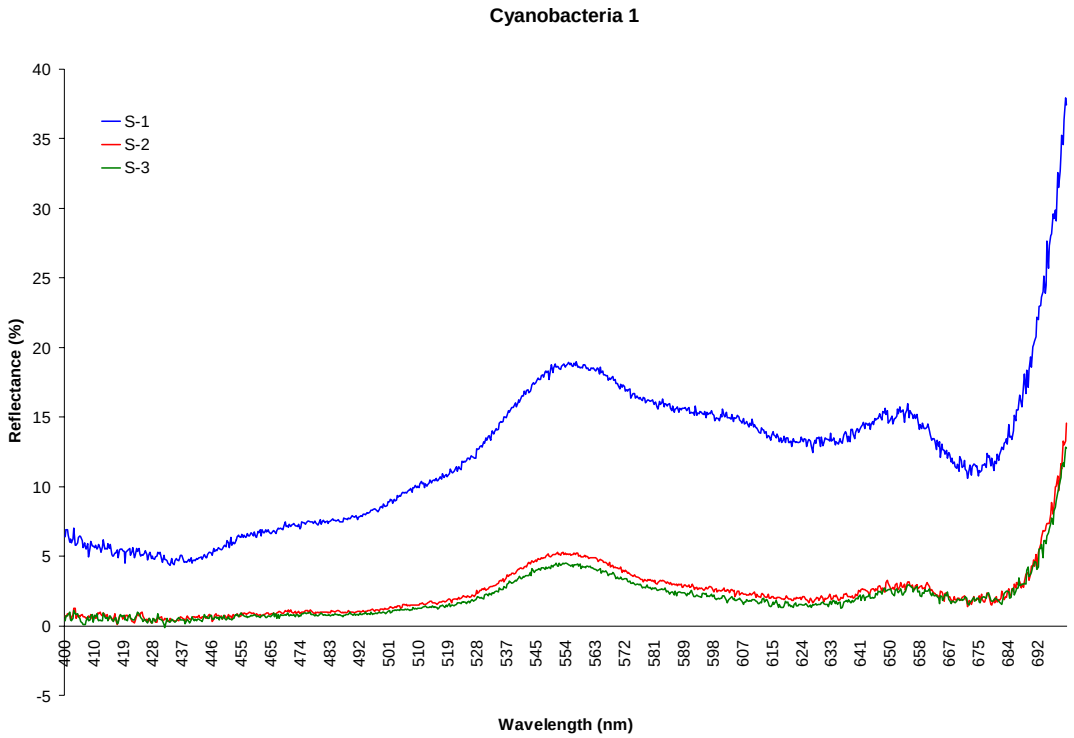


| | | |
|---|---|---|
| **Target:** | Green w/ white stalks Cyanobacteria | |
| **Size/Morphology:** | Medium Encrusting | |
| **GPS** | 28-16.662 N | |
| | 177-22.043 W | |
| **Depth:** | 3.8 Feet | |
| **Date:** | 24 July 2006 @ 15:16 | |
| **Dive dist/bearing from boat:** | 6 meter N | |
| **Photo #** | Img_0012.jpg, Img_0013.jpg, Img_0014.jpg | |
| **Spectrum #:** | 0052 – @ 1516 | 55 |
| | 0053 – @ 1516 | 75 |
| | 0054 – @ 1517 | |
| | 0055 – @ 1518 | 50 |
| | 0056 – @ 1521 | |
| **Surrounding substrate:** | Metal debris (see notes) | |
| **Notes:** Sand, dead coral, green algae stuff, urchins<br>Took samples and placed in vials (52-56) as sample # 004<br>Reef Hotel<br><br>Unclear as for difference between 0052 and the rest. | | |

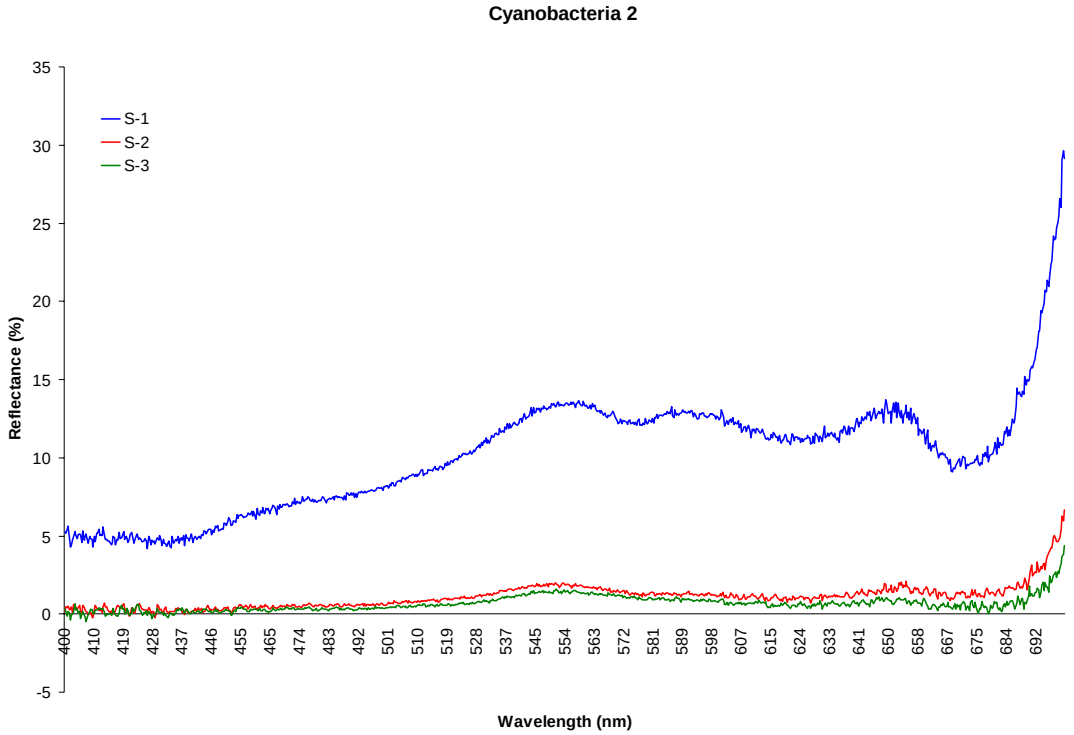


| | | |
|---|---|---|
| **Target:** | Green w/ white stalks Cyanobacteria | |
| **Size/Morphology:** | Medium Encrusting | |
| **GPS** | 28-16.662 N | |
| | 177-22.043 W | |
| **Depth:** | 4.5 Feet | |
| **Date:** | 24 July 2006 @ 15:31 | |
| **Dive dist/bearing from boat:** | 7 meter N | |
| **Photo #** | Img_0015.jpg, Img_0016.jpg, Img_0017.jpg | |
| **Spectrum #:** | **0057 – @ 1531** | **50** |
| | 0058 – @ 1531 | |
| | 0059 – @ 1532 | |
| | 0060 – @ 1532 | 150 |
| | 0061 – @ 1532 | 150 |
| **Surrounding substrate:** | Metal debris (see notes) | |
| **Notes:** Sand, dead coral, green algae stuff, urchins<br><br>Reef Hotel<br>Blurry photos | | |

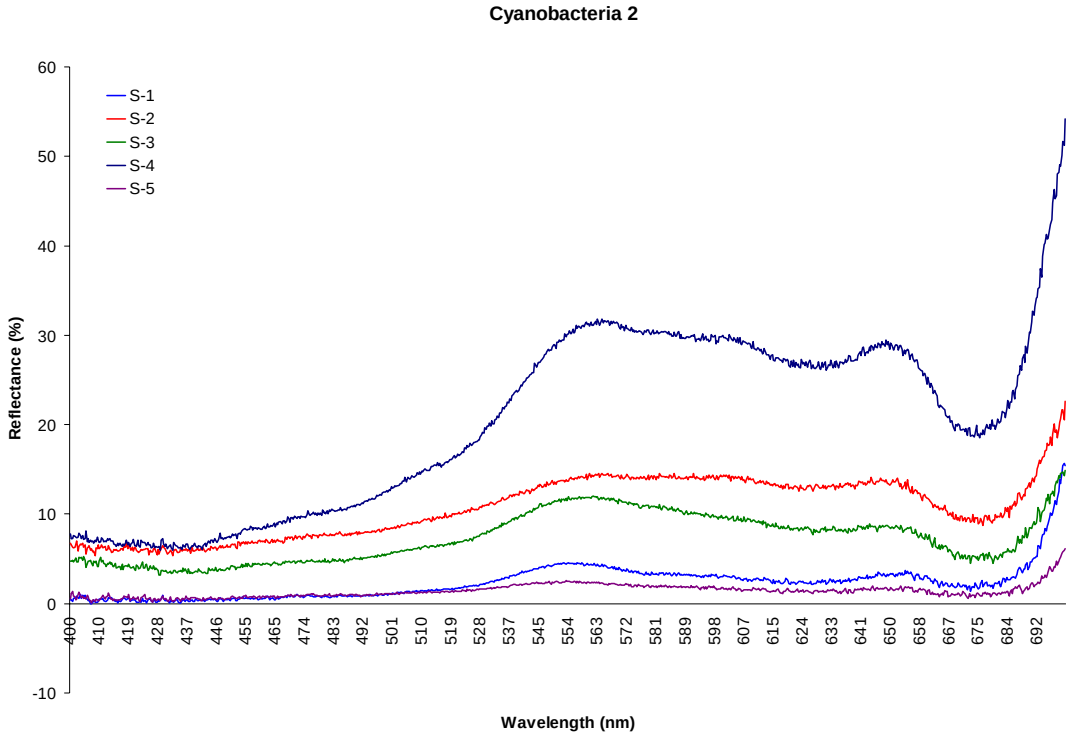


| | | |
|---|---|---|
| **Target:** | Green w/ white stalks Cyanobacteria | |
| **Size/Morphology:** | Medium Encrusting | |
| **GPS** | 28-16.662 N | |
| | 177-22.043 W | |
| **Depth:** | 5 Feet | |
| **Date:** | 24 July 2006 @ 15:39 | |
| **Dive dist/bearing from boat:** | 10 meter N | |
| **Photo #** | N/A | |
| **Spectrum #:** | 0062 – @ 1539 | 100 |
| | 0063 – @ 1541 | 100 |
| | 0064 – @ 1541 | 100 |
| | 0065 – @ 1542 | 70 |
| | 0066 – @ 1542 | 120 |
| **Surrounding substrate:** | Metal debris (see notes) | |

**Notes:** Sand, dead coral, green algae stuff, urchins
Took samples and placed in vial (62-66) as sample # 005

Reef Hotel

Evaluated as cyanobacteria Lyngbya (majuscula or semiplena)
Green cyanobacteria by similar target

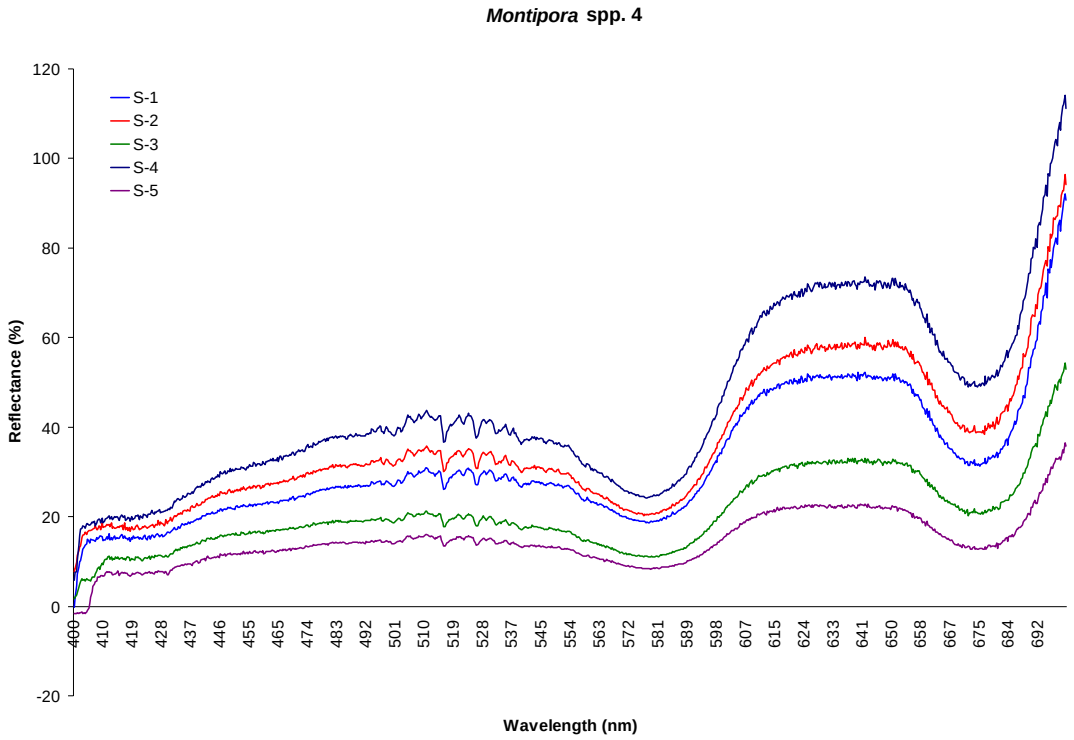


| | | |
|---|---|---|
| **Target:** | *Montipora spp.* - pigmented | |
| **Size/Morphology:** | Medium Encrusting | |
| **GPS** | 28-16.645 N | |
| | 177-22.049 W | |
| **Depth:** | 2.5 Feet | |
| **Date:** | 25 July 2006 @ 10:34 | |
| **Dive dist/bearing from boat:** | 4.5 meter SE | |
| **Photo #** | Img_0022.jpg | |
| **Spectrum #:** | 0072 – @ 1034 | 170 |
| | 0073 – @ 1035 | 150 |
| | 0074 – @ 1035 | 145 |
| | 0075 – @ 1035 | 150 |
| | 0076 – @ 1035 | 220 |
| **Surrounding substrate:** | Iron rafters (see notes) | |
| **Notes:** Iron rafters, live/dead coral, Lyngbya patches, urchins, rock and sand.<br><br>Reef Hotel | | |

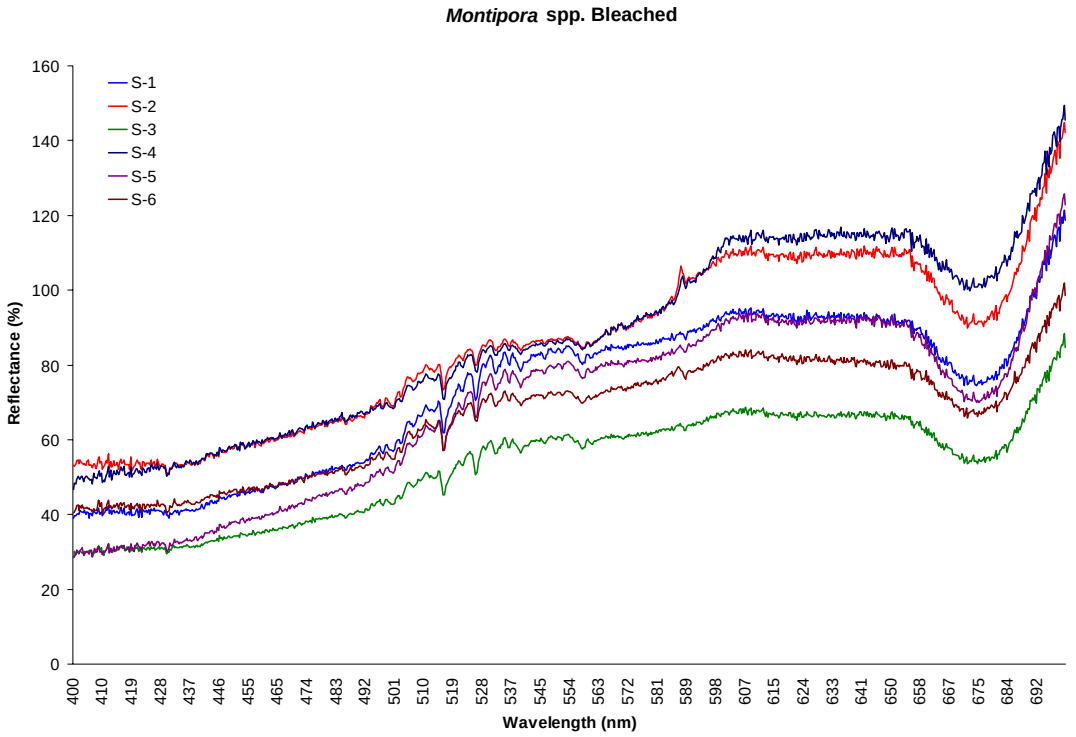


| | | |
|---|---|---|
| **Target:** | *Montipora spp.*. - bleached | |
| **Size/Morphology:** | TBD | |
| **GPS** | 28-16.645 N | |
| | 177-22.049 W | |
| **Depth:** | 3 Feet | |
| **Date:** | 25 July 2006 @ 10:35 | |
| **Dive dist/bearing from boat:** | 4.6 meter SE | |
| **Photo #** | Img_0021.jpg | |
| **Spectrum #:** | 0077 – @ 1035 | 150 |
| | 0078 – @ 1035 | 140 |
| | 0079 – @ 1036 | 150 |
| | 0080 – @ 1036 | 145 |
| | 0081 – @ 1036 | 150 |
| | 0082 – @ 1036 | 170 |
| **Surrounding substrate:** | Iron rafters (see notes) | |
| **Notes:** Iron rafters, live/dead coral, Lyngbya patches, urchins, rock and sand.<br><br>Reef Hotel | | |

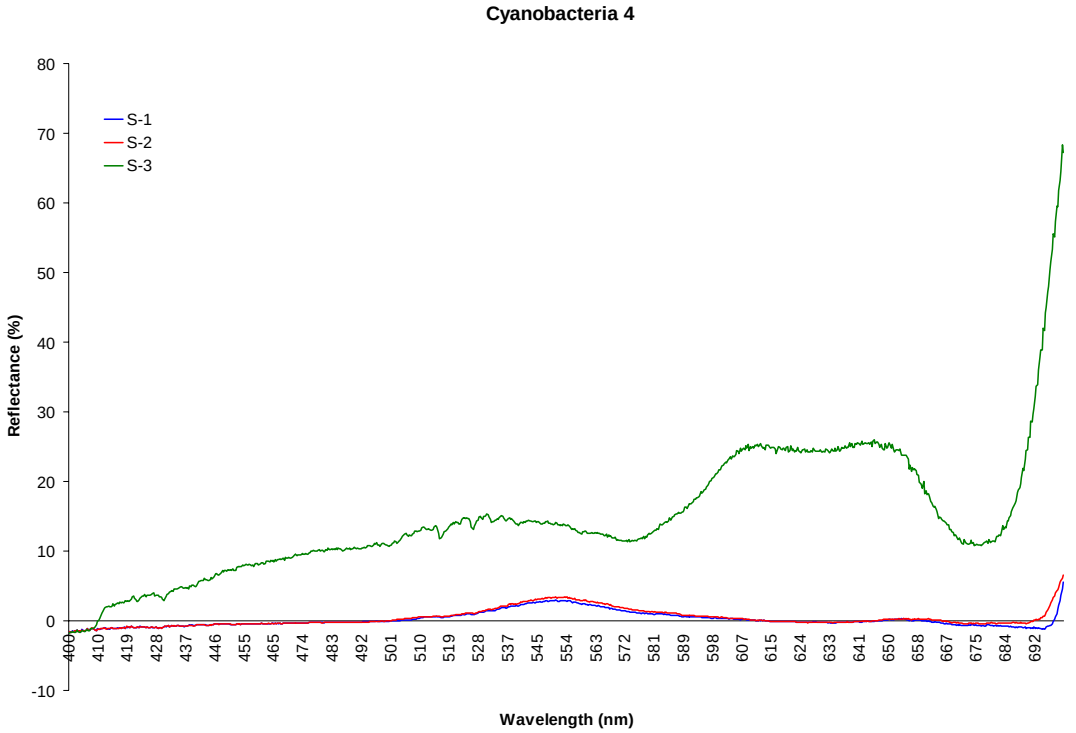


| | | |
|---|---|---|
| **Target:** | Green w/white stalks Cyanobacteria | |
| **Size/Morphology:** | Small encrusting | |
| **GPS** | 28-16.645 N | |
| | 177-22.049 W | |
| **Depth:** | 3.5 Feet | |
| **Date:** | 25 July 2006 @ 10:44 | |
| **Dive dist/bearing from boat:** | 10 meter NW | |
| **Photo #** | Img_0026.jpg, Img_0027.jpg | |
| **Spectrum #:** | 0083 – @ 1044 | |
| | 0084 – @ 1044 | 60 |
| | 0085 – @ 1045 | 75 |
| | 0086 – @ 1045 | |
| | **0087 – @ 1045** | **90** |
| **Surrounding substrate:** | Iron rafters (see notes) | |
| **Notes:** Iron rafters, live/dead coral, Lyngbya patches, urchins, rock and sand.<br><br>Reef Hotel | | |

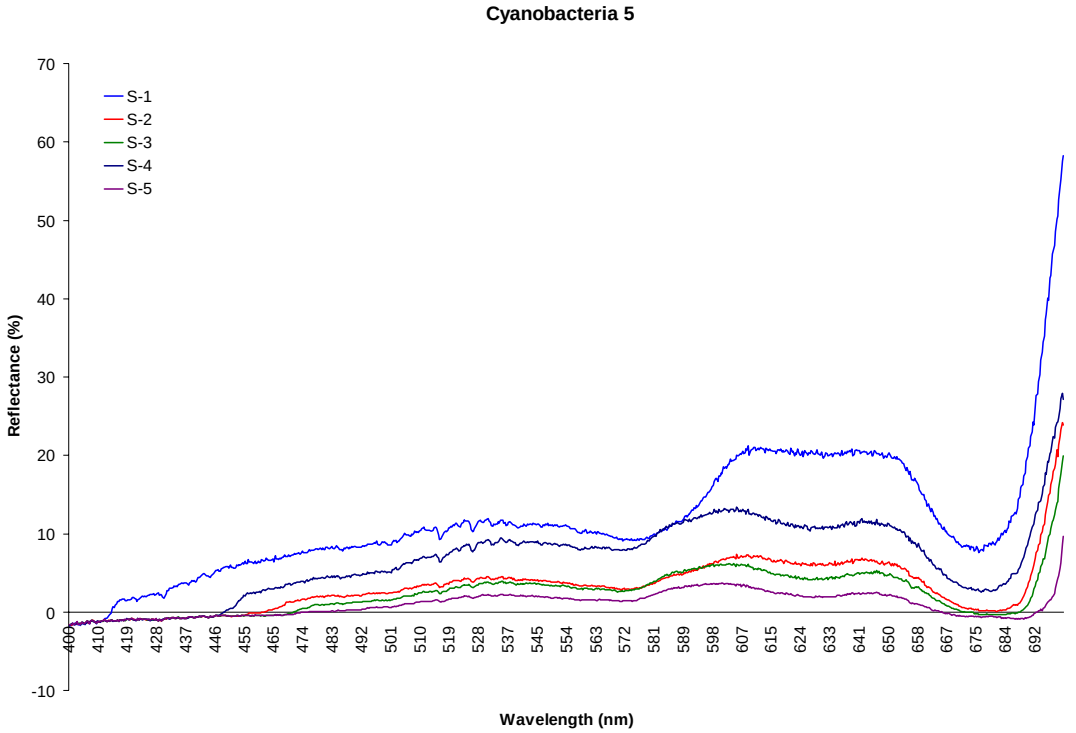


| | | |
|---|---|---|
| **Target:** | Brown Cyanobacteria | |
| **Size/Morphology:** | Small encrusting | |
| **GPS** | 28-16.645 N | |
| | 177-22.049 W | |
| **Depth:** | 3.5 Feet | |
| **Date:** | 25 July 2006 @ 10:45 | |
| **Dive dist/bearing from boat:** | 10 meter NW | |
| **Photo #** | Img_0028.jpg, Img_0029.jpg | |
| **Spectrum #:** | **0088 – @ 1045** | **80** |
| | 0089 – @ 1045 | 70 |
| | 0090 – @ 1046 | 90 |
| | **0091 – @ 1046** | **75** |
| | **0092 – @ 1047** | **75** |
| **Surrounding substrate:** | Iron rafters (see notes) | |

**Notes:** Iron rafters, live/dead coral, Lyngbya patches, urchins, rock and sand.
Took samples and placed them in vials (88-92) as sample # 007.

Reef Hotel

Evaluated samples as Lyngbya Majuscula

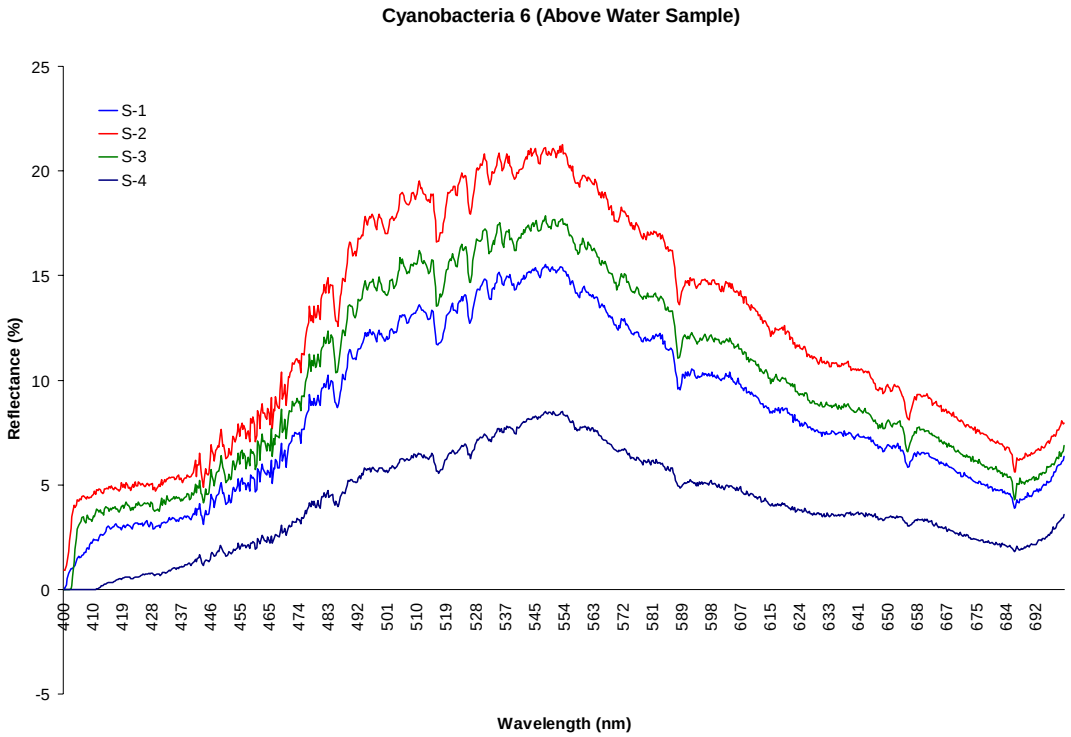


| | | |
|---|---|---|
| **Target:** | Green Cyanobacteria | |
| **Size/Morphology:** | N/A | |
| **GPS** | 28-16.645 N | |
| | 177-22.049 W | |
| **Depth:** | | |
| **Date:** | 25 July 2006 @ 11:47 | |
| **Dive dist/bearing from boat:** | | |
| **Photo #** | Img_0035.jpg, Img_0036.jpg, Img_0037.jpg | |
| **Spectrum #:** | 0098 – @ 1147 | 260 |
| | 0099 – @ 1147 | 280 |
| | 0100 – @ 1147 | |
| | 0101 – @ 1147 | 260 |
| | 0102 – @ 1148 | 90 |
| **Surrounding substrate:** | | |
| **Notes:** Took a large sampling of suspected Lyngbya and placed it on the deck of the boat in a 12 cm radius patch and took spectra.<br><br>From Reef Hotel | | |

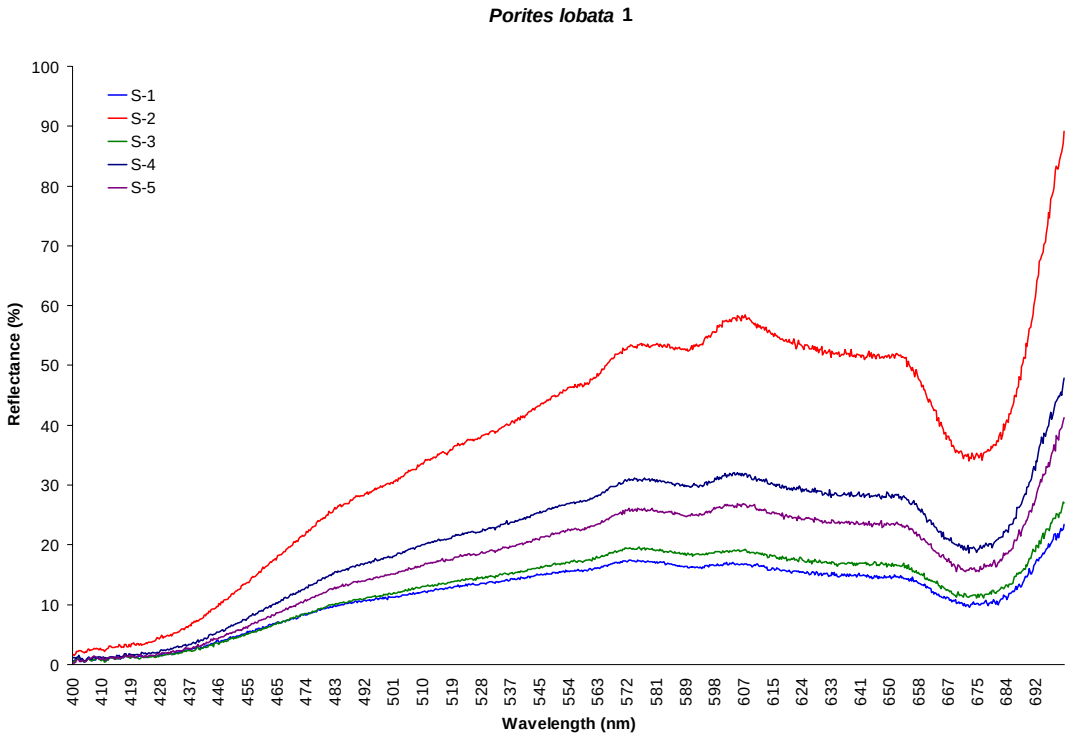


| | | |
|---|---|---|
| **Target:** | *Porites lobata* | |
| **Size/Morphology:** | Medium encrusting | |
| **GPS** | 28-14.318 N | |
| | 177-19.243 W | |
| **Depth:** | 3.5 Feet | |
| **Date:** | 25 July @ 15:24 | |
| **Dive dist/bearing from boat:** | 4 meter NW | |
| **Photo #** | Img_0038.jpg | |
| **Spectrum #:** | 0103 – @ 1524 | 60 |
| | 0104 – @ 1524 | 40 |
| | 0105 – @ 1524 | 45 |
| | 0106 – @ 1524 | 55 |
| | 0107 – @ 1524 | 45 |
| **Surrounding substrate:** | Sand and rubble | |
| **Notes:** Rubble and sand dominate area, but there are other coral of the same type and size within the outer boundary of a 10 meter radius.<br>There are some small spots of the blue encrusting coral on the bottom, but rare. | | |

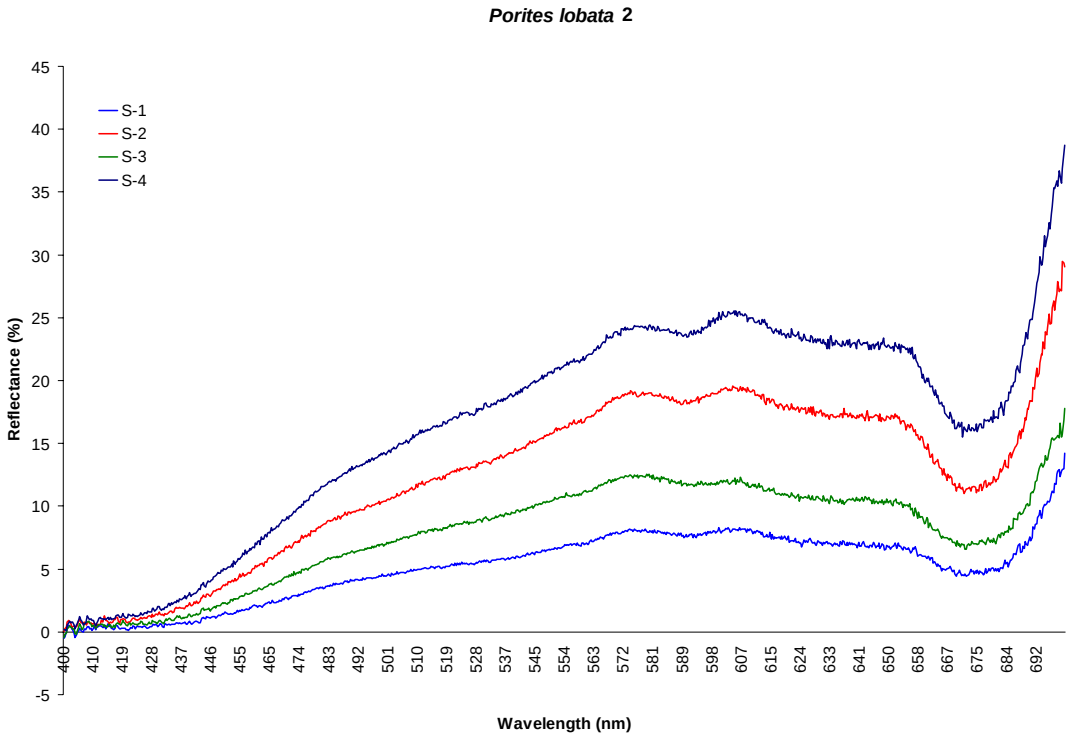


| | | |
|---|---|---|
| **Target:** | *Porites lobata* | |
| **Size/Morphology:** | Medium encrusting | |
| **GPS** | 28-14.318 N | |
| | 177-19.243 W | |
| **Depth:** | 5 Feet | |
| **Date:** | 25 July @ 15:25 | |
| **Dive dist/bearing from boat:** | 7 meter NW | |
| **Photo #** | Img_0039.jpg | |
| **Spectrum #:** | 0108 – @ 1525 | 75 |
| | 0109 – @ 1525 | 60 |
| | 0110 – @ 1525 | 75 |
| | 0111 – @ 1525 | 60 |
| | **0112 – @ 1525 THROW OUT** | |
| **Surrounding substrate:** | Sand and rubble | |
| **Notes:** Rubble and sand dominate area, but there are other coral of the same type and size within the outer boundary of a 10 meter radius.<br>There are some small spots of the blue encrusting coral on the bottom, but rare. | | |

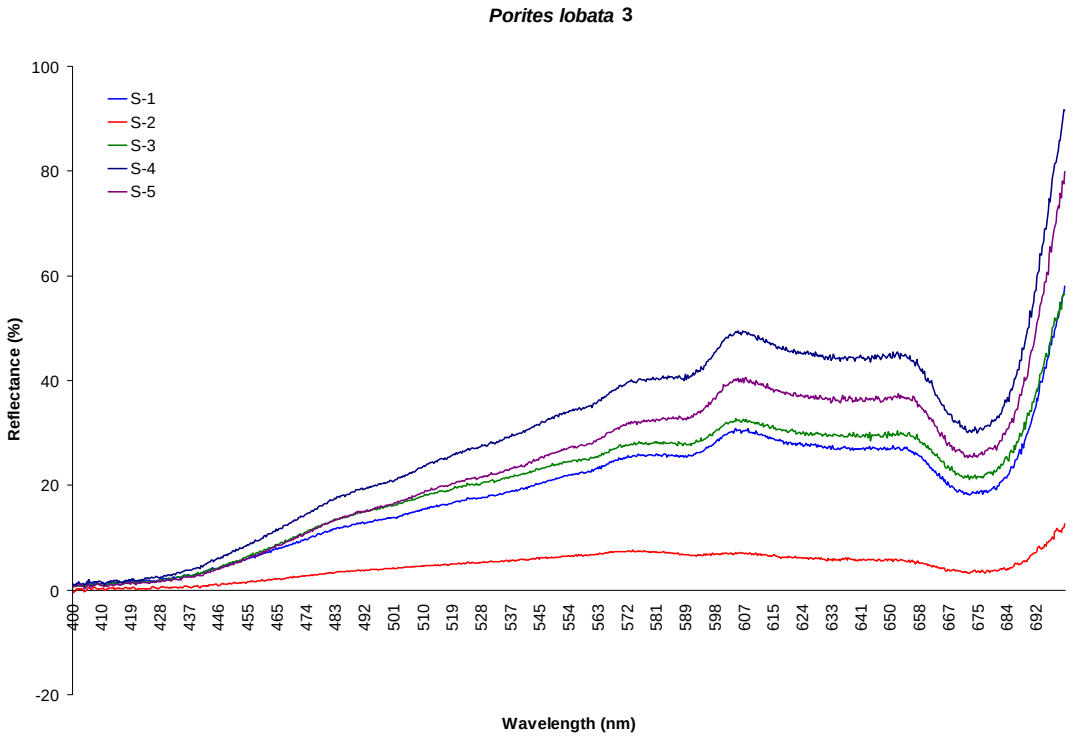


| | | |
|---|---|---|
| **Target:** | *Porites lobata* | |
| **Size/Morphology:** | Medium encrusting | |
| **GPS** | 28-14.318 N | |
| | 177-19.243 W | |
| **Depth:** | 1.5 Feet | |
| **Date:** | 25 July @ 15:29 | |
| **Dive dist/bearing from boat:** | 5 meter N | |
| **Photo #** | Img_0040.jpg | |
| **Spectrum #:** | 0113 – @ 1529 | 50 |
| | 0114 – @ 1529 | 85 |
| | 0115 – @ 1529 | 40 |
| | 0116 – @ 1529 | 60 |
| | 0117 – @ 1530 | 40 |
| **Surrounding substrate:** | Sand and rubble | |
| **Notes:** Rubble and sand dominate area, but there are other coral of the same type and size within the outer boundary of a 10 meter radius.<br>There are some small spots of the blue encrusting coral on the bottom, but rare. | | |

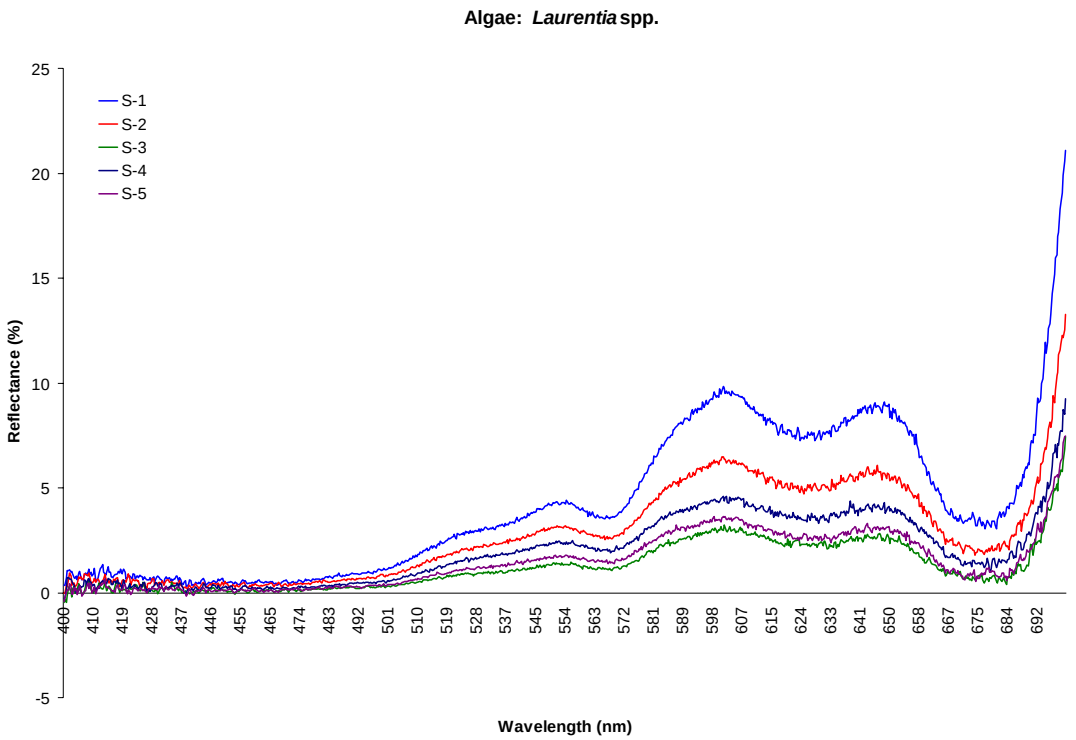


| | | |
|---|---|---|
| **Target:** | Algae, *Laurentia spp.*. | |
| **Size/Morphology:** | N/A | |
| **GPS** | 28-14.315 N | |
| | 177-19.244 W | |
| **Depth:** | 1.5 Feet | |
| **Date:** | 25 July @ 15:44 | |
| **Dive dist/bearing from boat:** | 4.5 meter S | |
| **Photo #** | Img_00041.jpg | |
| **Spectrum #:** | 0118 – @ 1544 | 60 |
| | 0119 – @ 1544 | 60 |
| | 0120 – @ 1544 | 60 |
| | 0121 – @ 1544 | 60 |
| | 0122 – @ 1545 | 80 |
| **Surrounding substrate:** | Sand and rubble | |
| **Notes:** Rubble and sand dominate area, but there are other coral of the same type and size within the outer boundary of a 10 meter radius.<br>Took a sample of the algae just for general purpose and placed in vials (118-122) as sample # 008. | | |

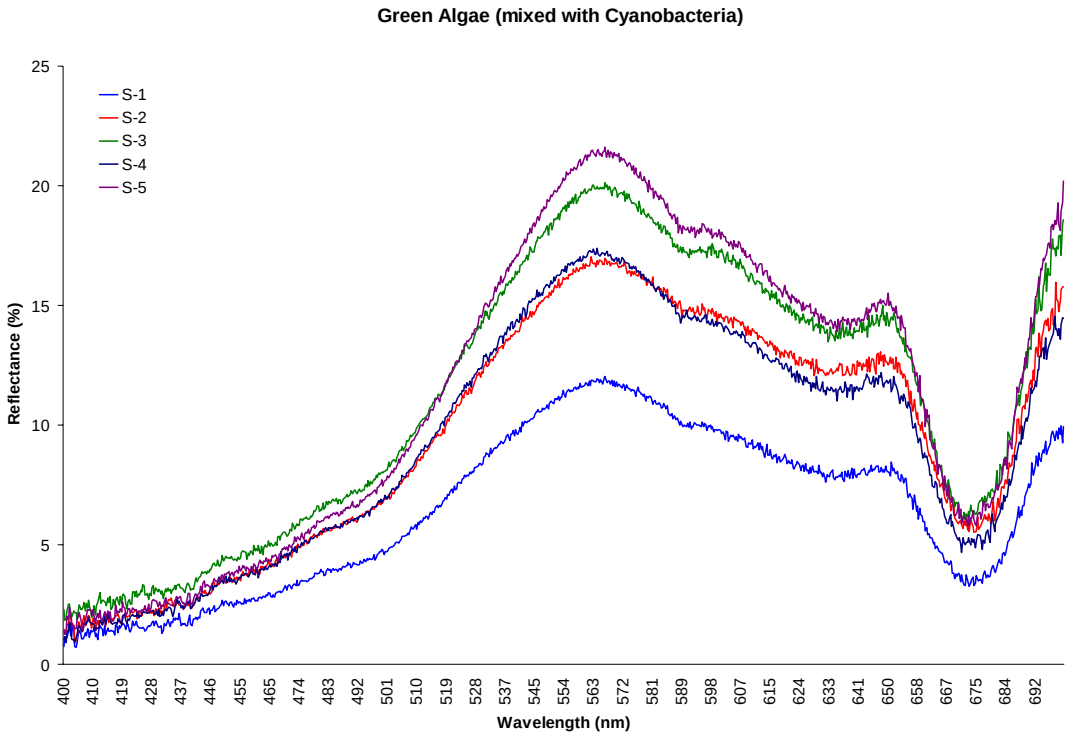


| | | |
|---|---|---|
| **Target:** | Green Algae | |
| **Size/Morphology:** | N/A | |
| **GPS** | 28-14.315 N | |
| | 177-19.244 W | |
| **Depth:** | 6.6 Feet | |
| **Date:** | 25 July @ 15:51 | |
| **Dive dist/bearing from boat:** | 6.6 meter S | |
| **Photo #** | Img_0042.jpg, Img_0043.jpg, Img_0044.jpg, Img_0045.jpg | |
| **Spectrum #:** | 0123 – @ 1551 | 100 |
| | 0124 – @ 1551 | 75 |
| | 0125 – @ 1551 | 90 |
| | 0126 – @ 1551 | 90 |
| | 0127 – @ 1552 | 60 |
| **Surrounding substrate:** | Sand and rubble | |
| **Notes:** Rubble and sand dominate area, but there are other coral of the same type and size within the outer boundary of a 10 meter radius.<br>Took a sample of the algae just for general purpose and placed in vials (122-127) as sample # 009.<br><br>Evaluated as a mix of algae and possible cyanobacteria, but inconclusive on all. | | |

# APPENDIX B. TARGET PHOTOS

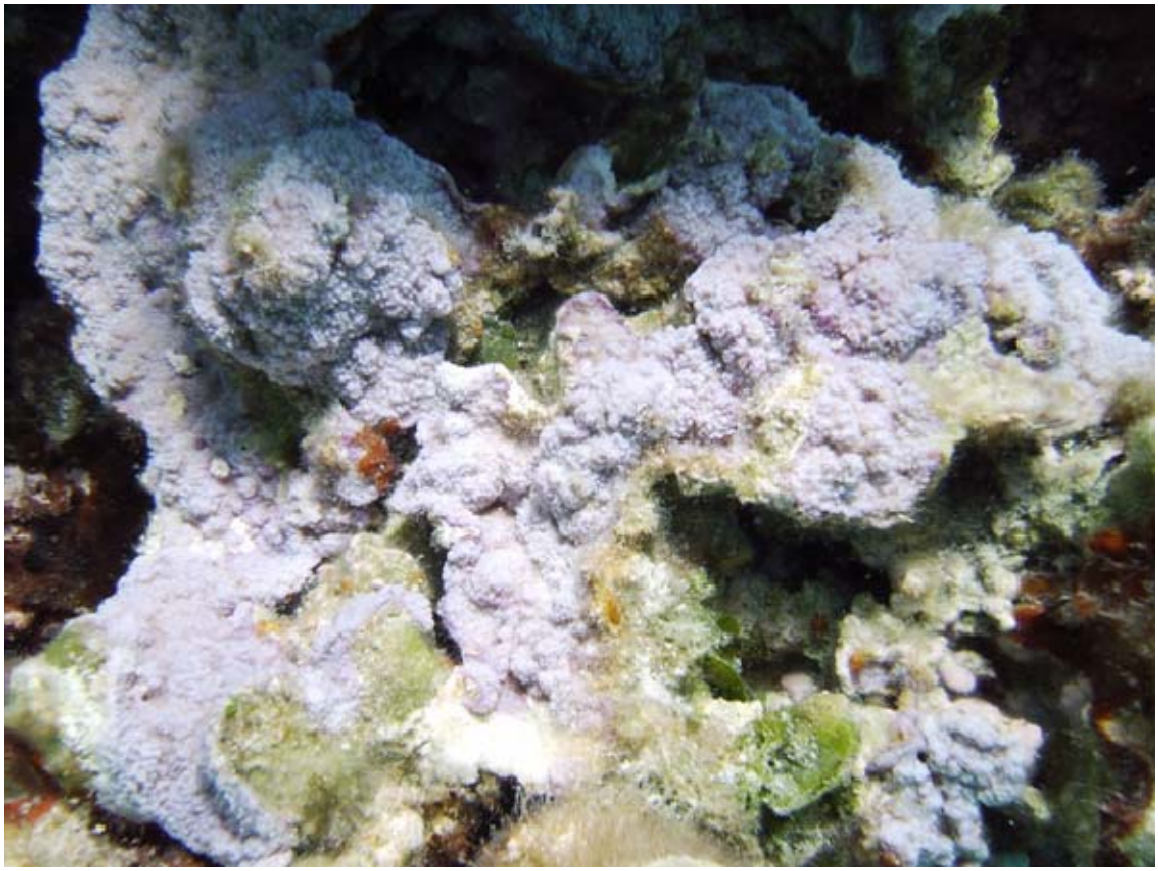

Img_0001.jpg

Img_0002.jpg

Img_0003.jpg

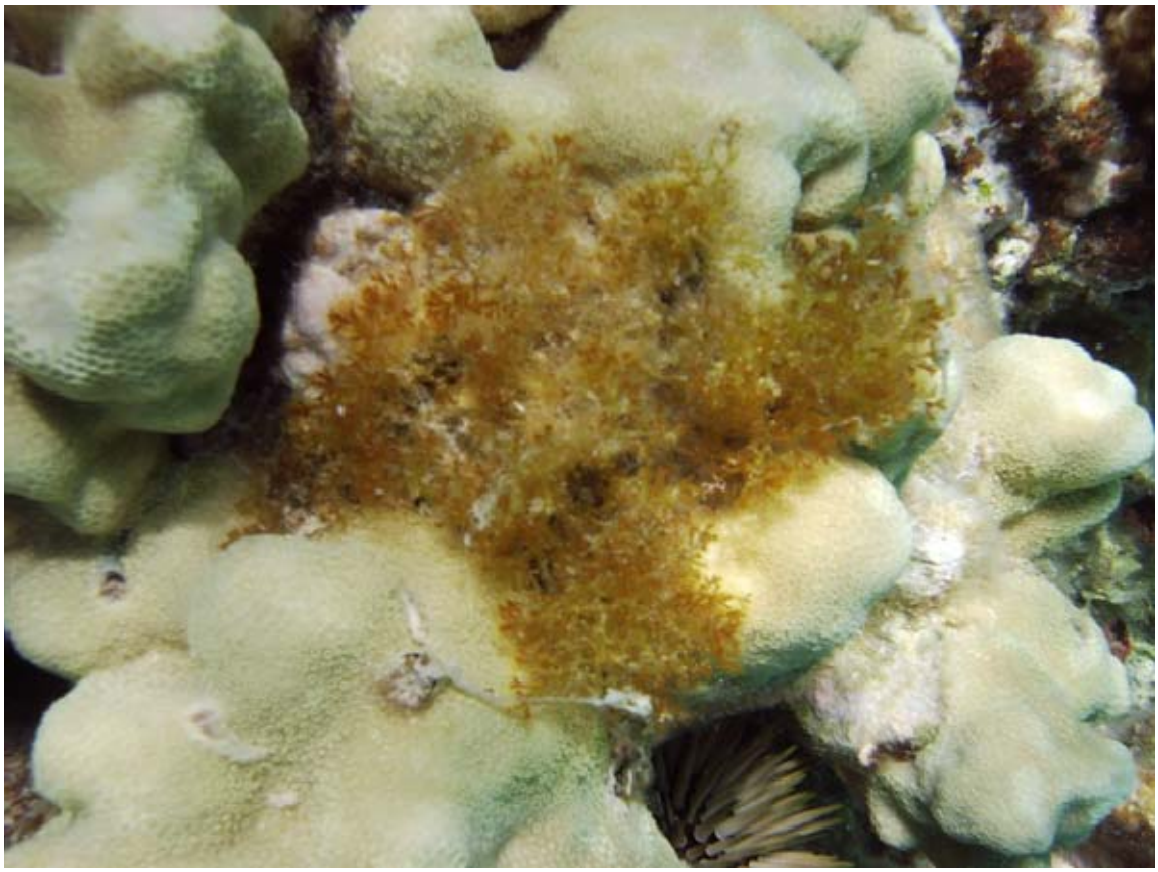

Img_0004.jpg

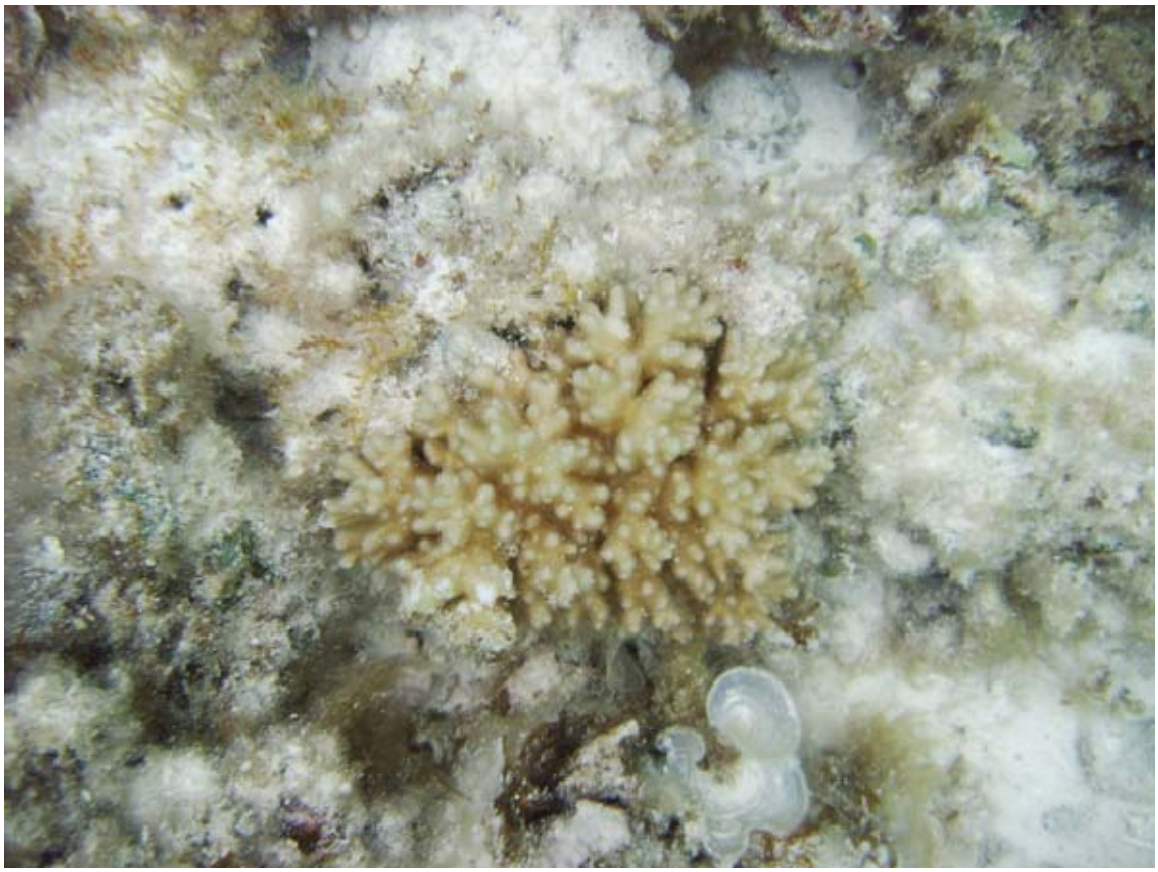

Img_0009.jpg

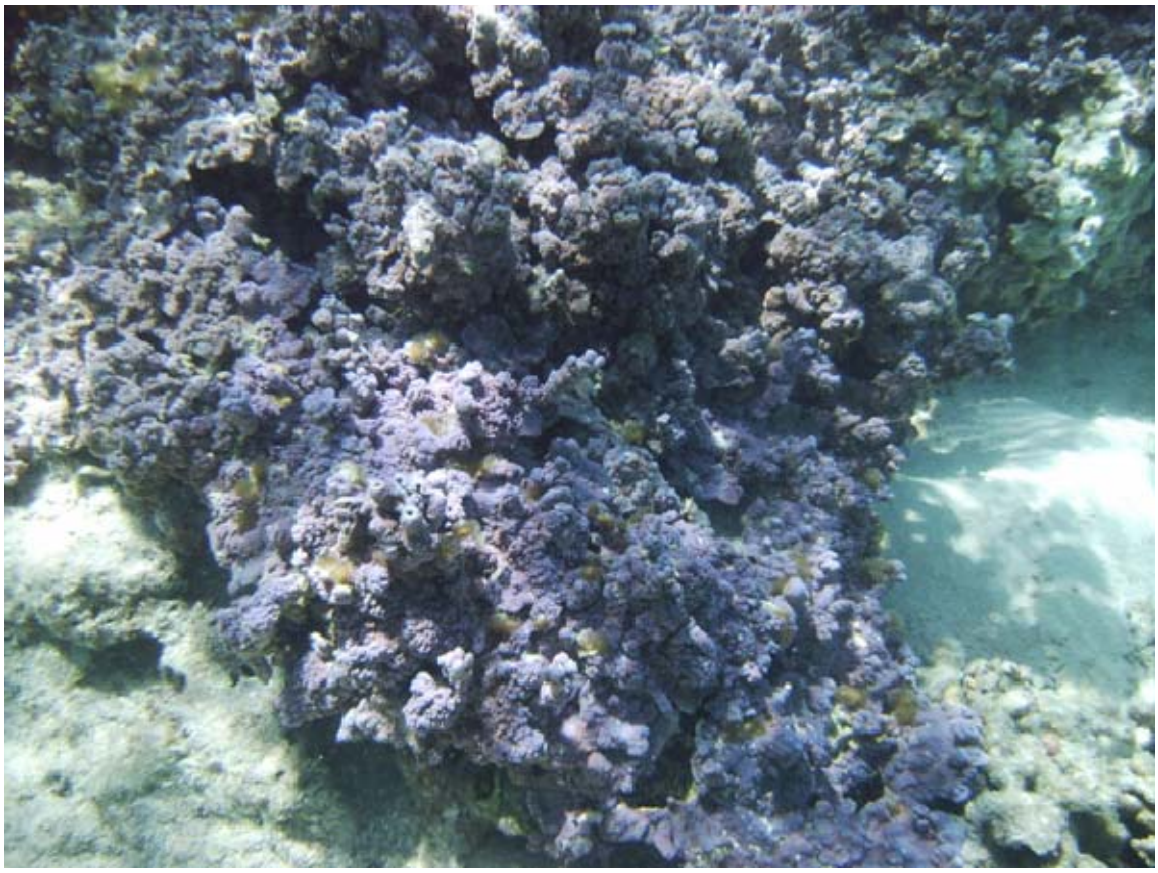

Img_0010.jpg

Img_0011.jpg

Img_0012.jpg

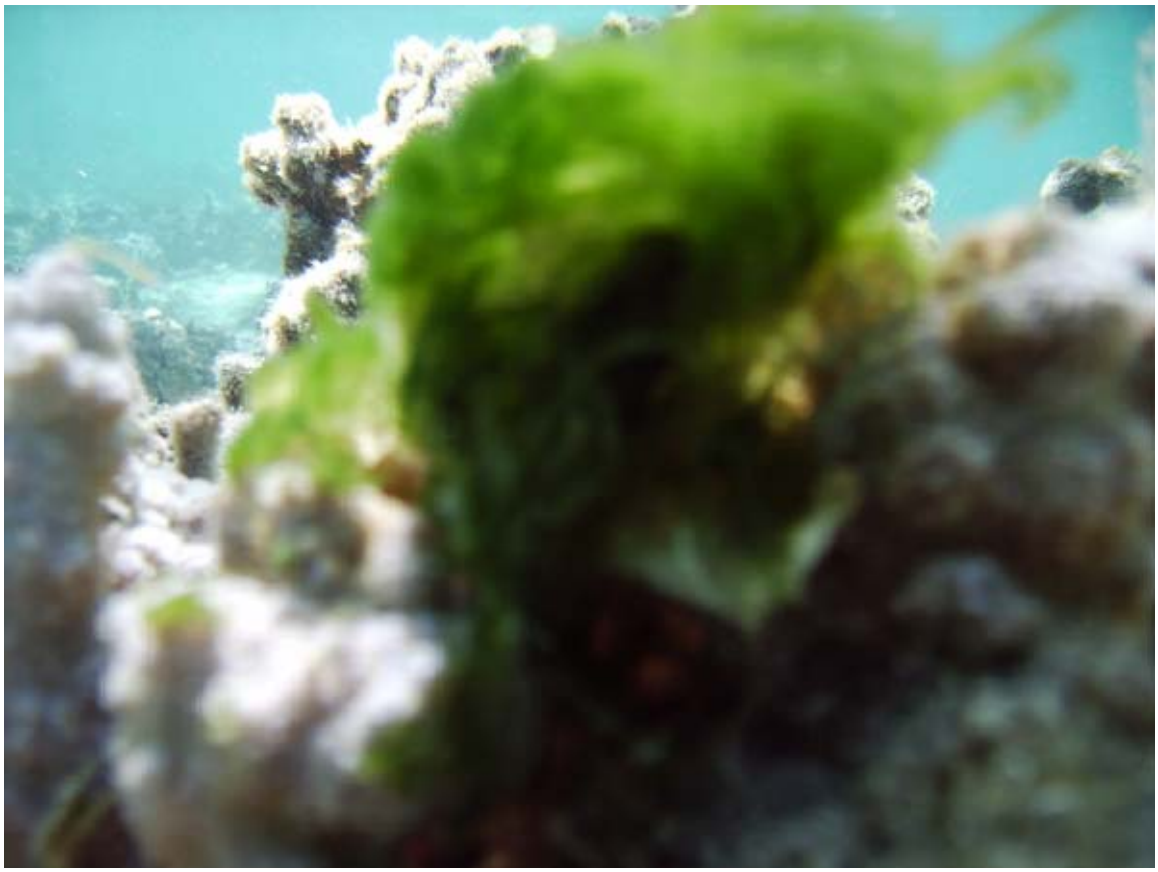

Img_0013.jpg

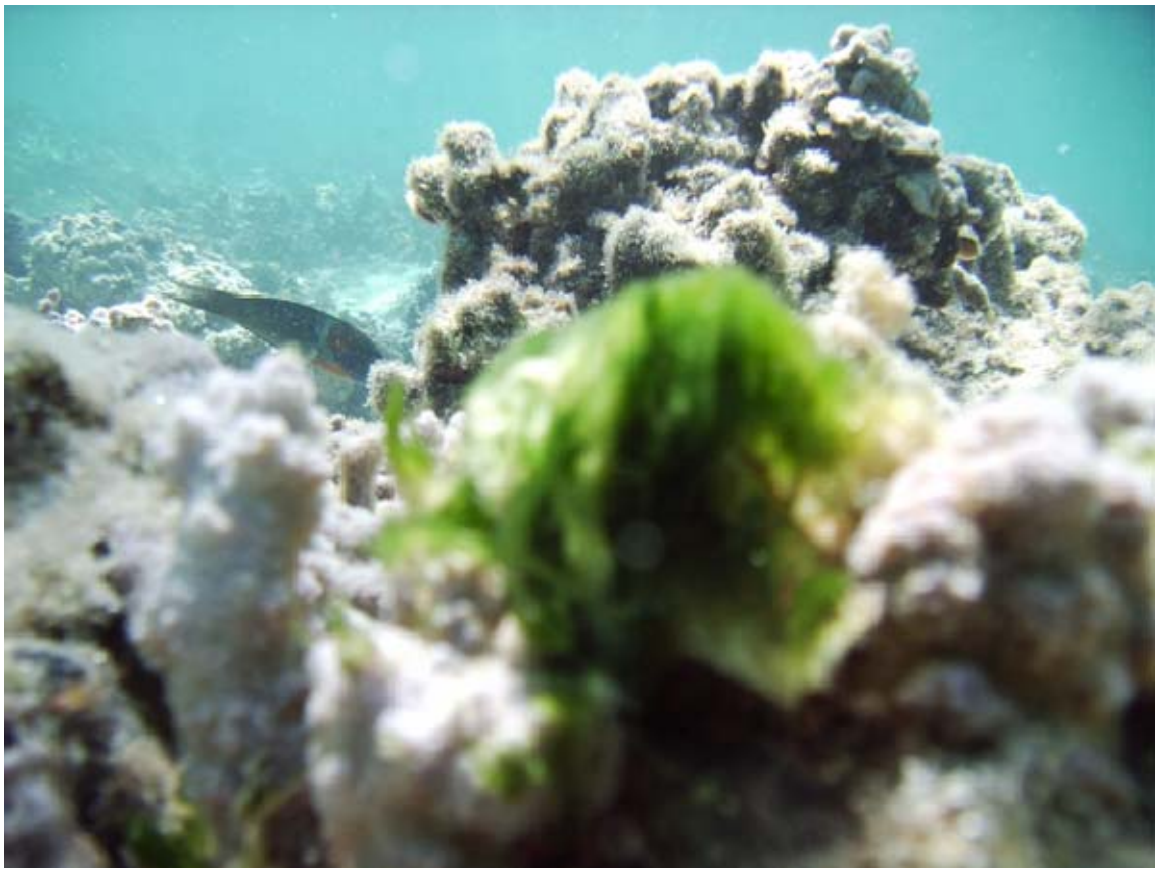

Img_0014.jpg

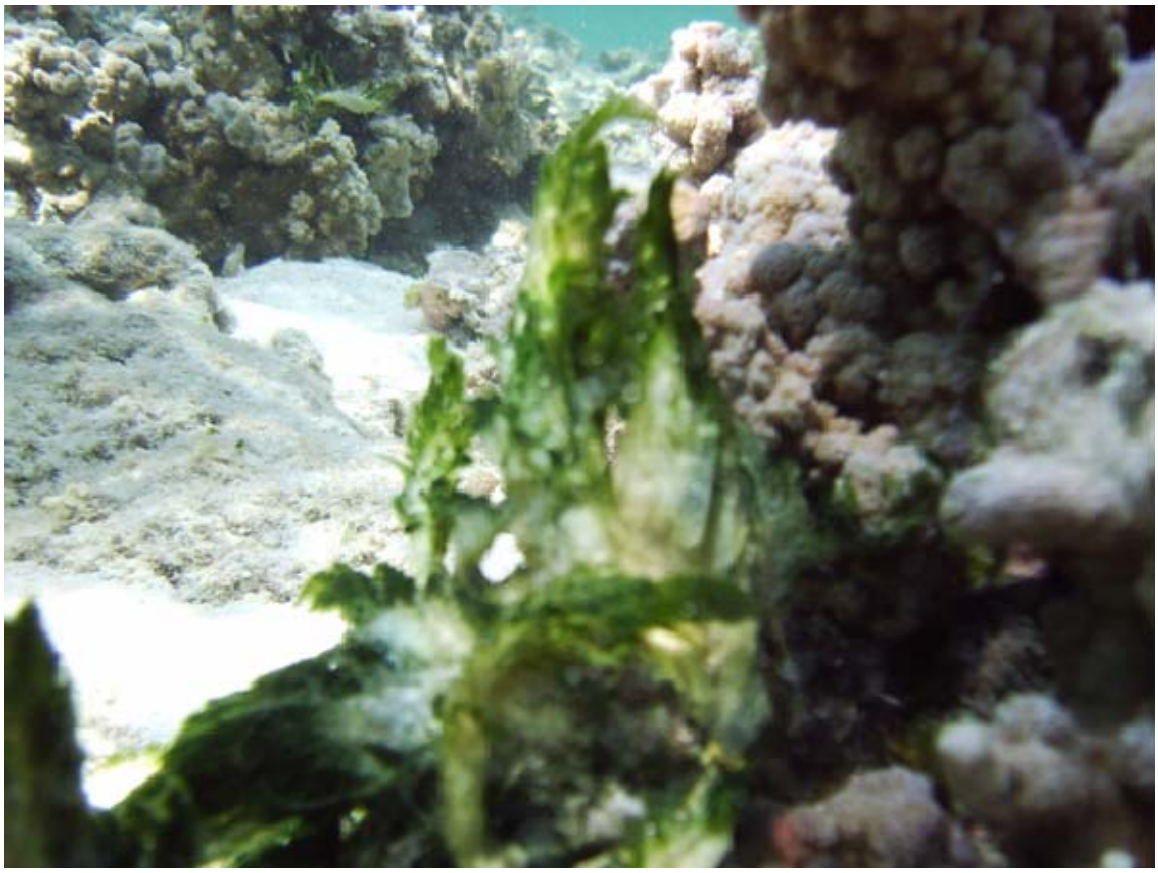

Img_0015.jpg

Img_0016.jpg

Img_0017.jpg

Img_0018.jpg

Img_0019.jpg

Img_0020.jpg

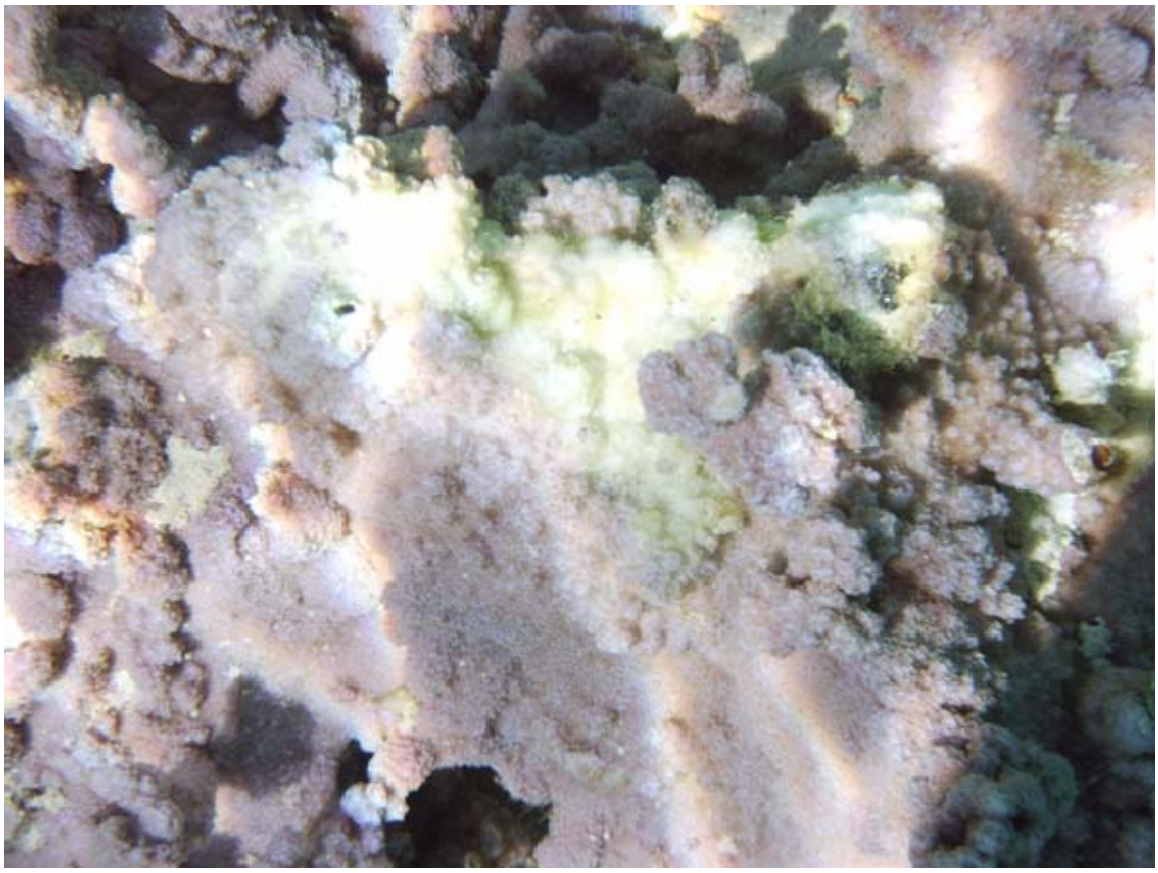

Img_0022.jpg

Img_0021.jpg

Img_0026.jpg

Img_0027.jpg

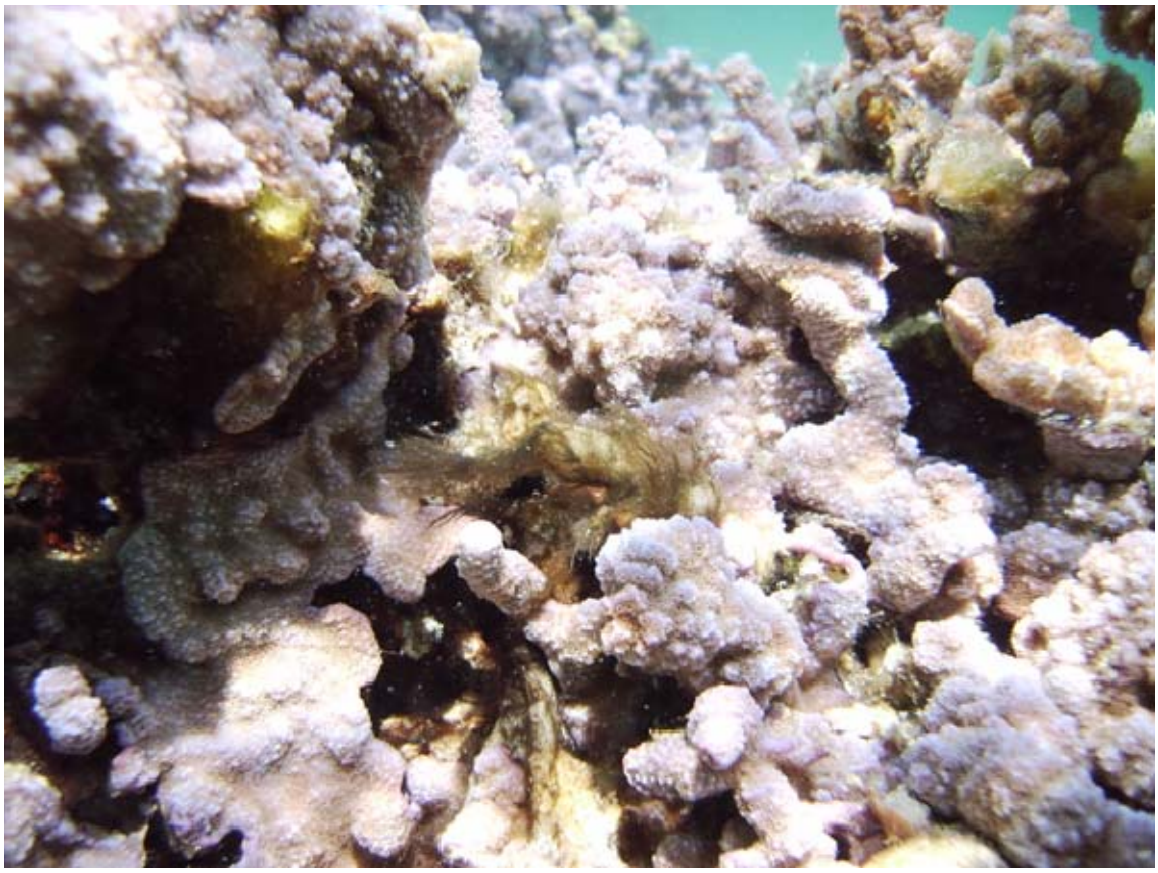

Img_0028.jpg

Img_0029.jpg

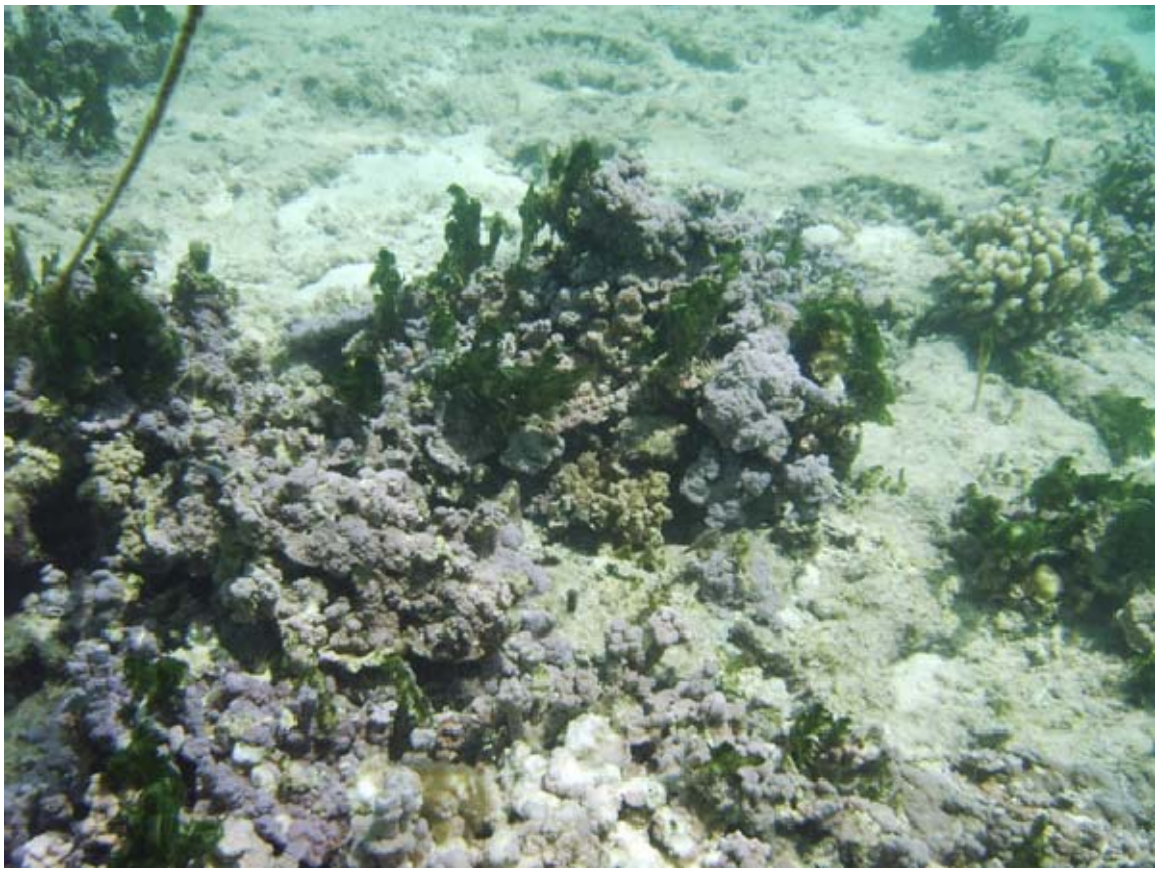

Img_0030.jpg

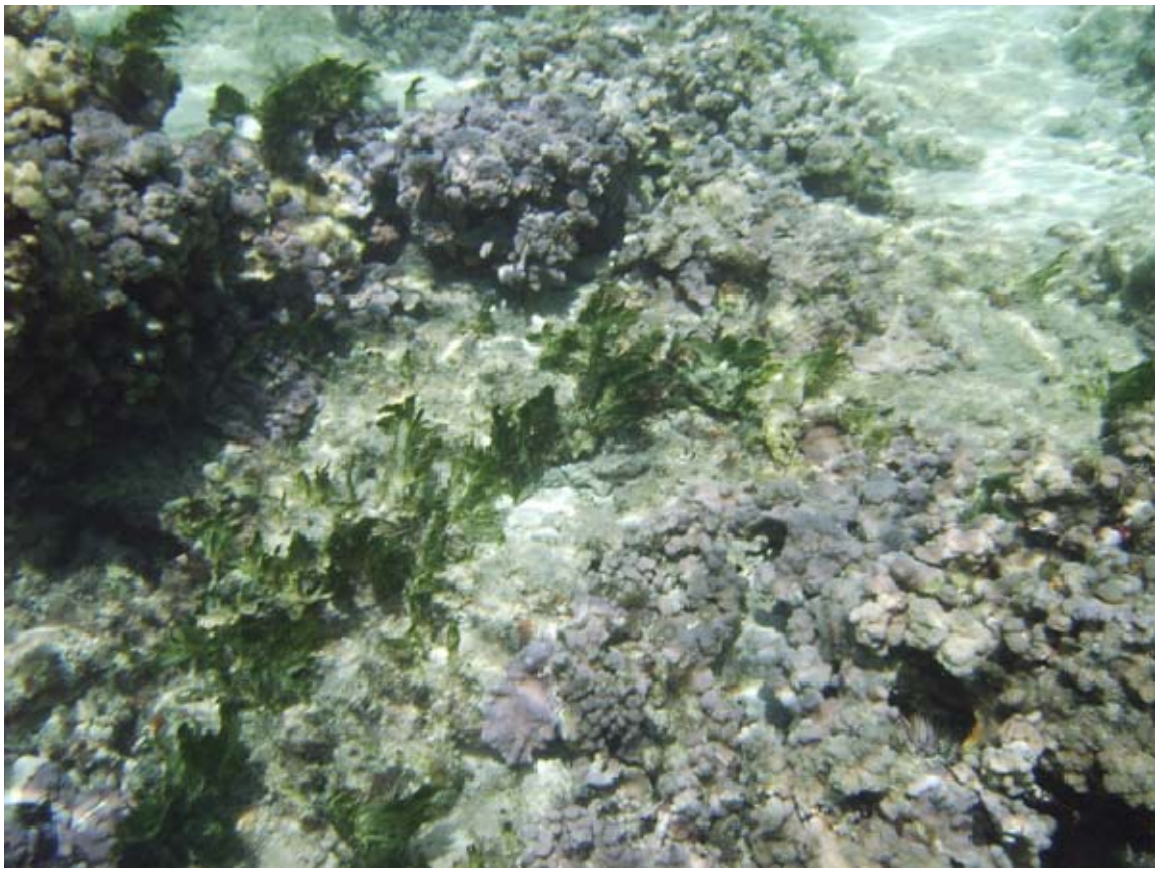

Img_0031.jpg

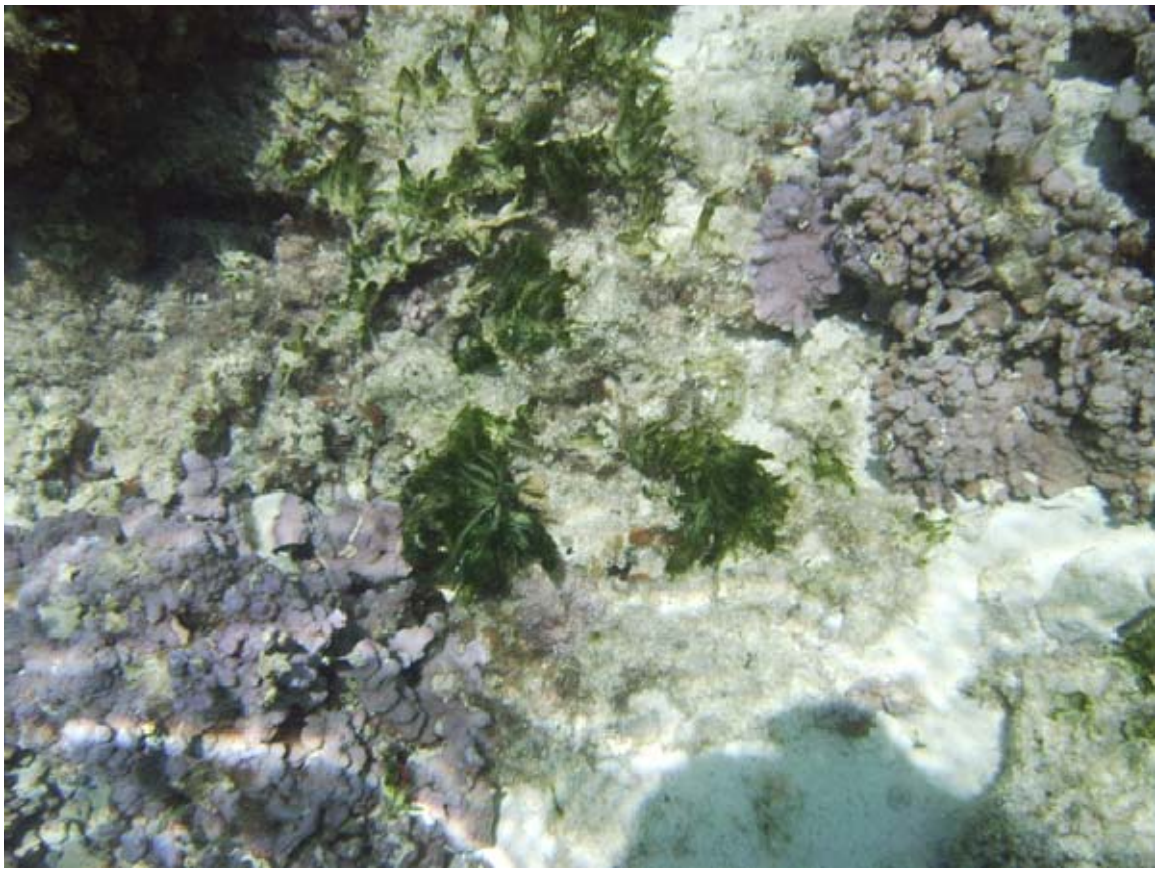

Img_0032.jpg

Img_0033.jpg

Img_0034.jpg

Img_0035.jpg

Img_0036.jpg

Img_0037.jpg

Img_0038.jpg

Img_0039.jpg

Img_0040.jpg

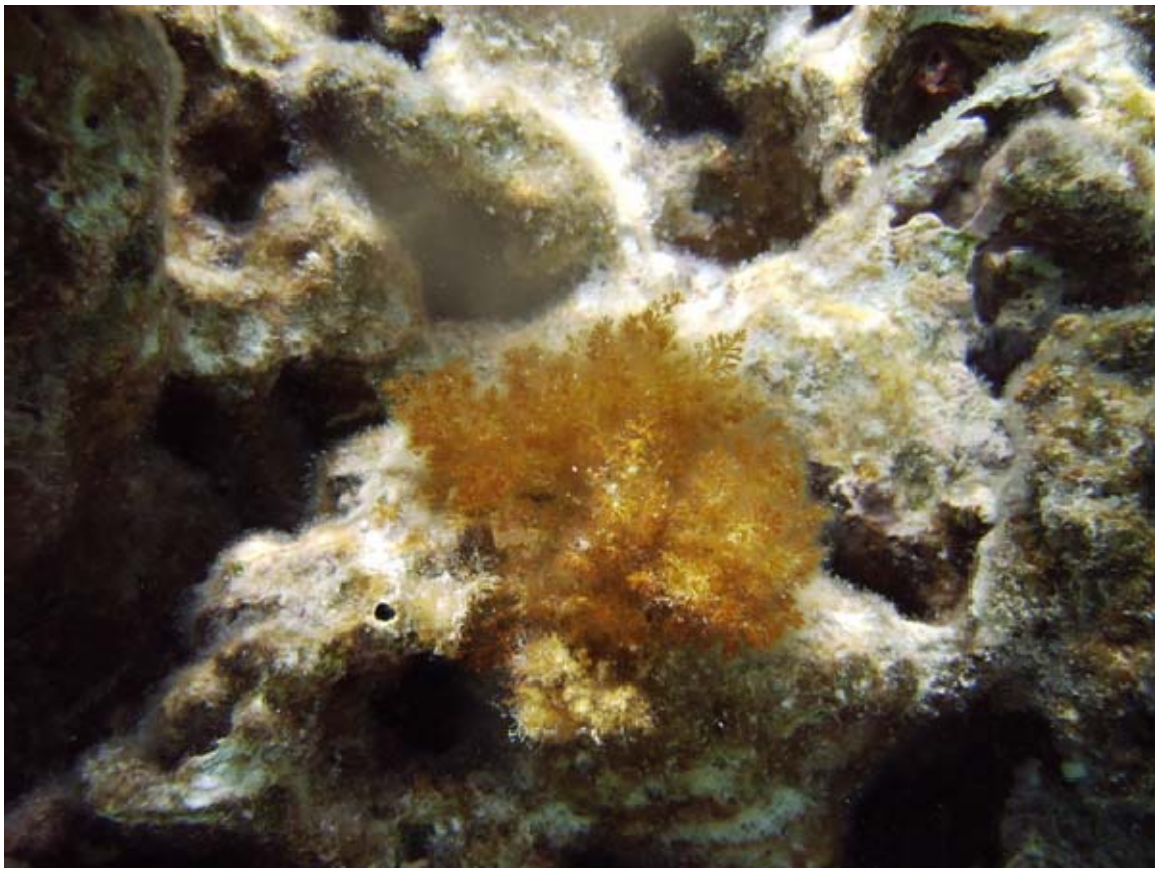

Img_0041.jpg

Img_0042.jpg

Img_0043.jpg

Img_0044.jpg

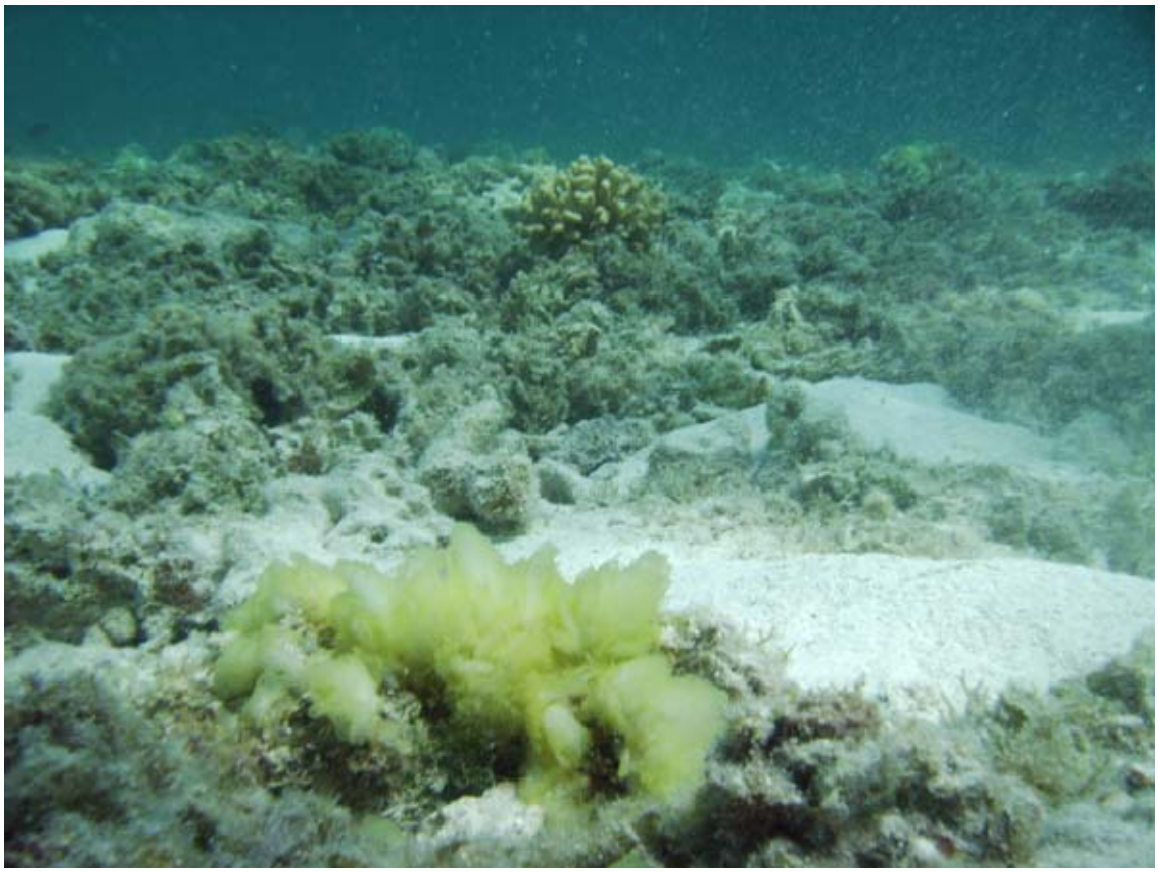

Img_0045.jpg

# APPENDIX C. AVERAGED SPECTRA

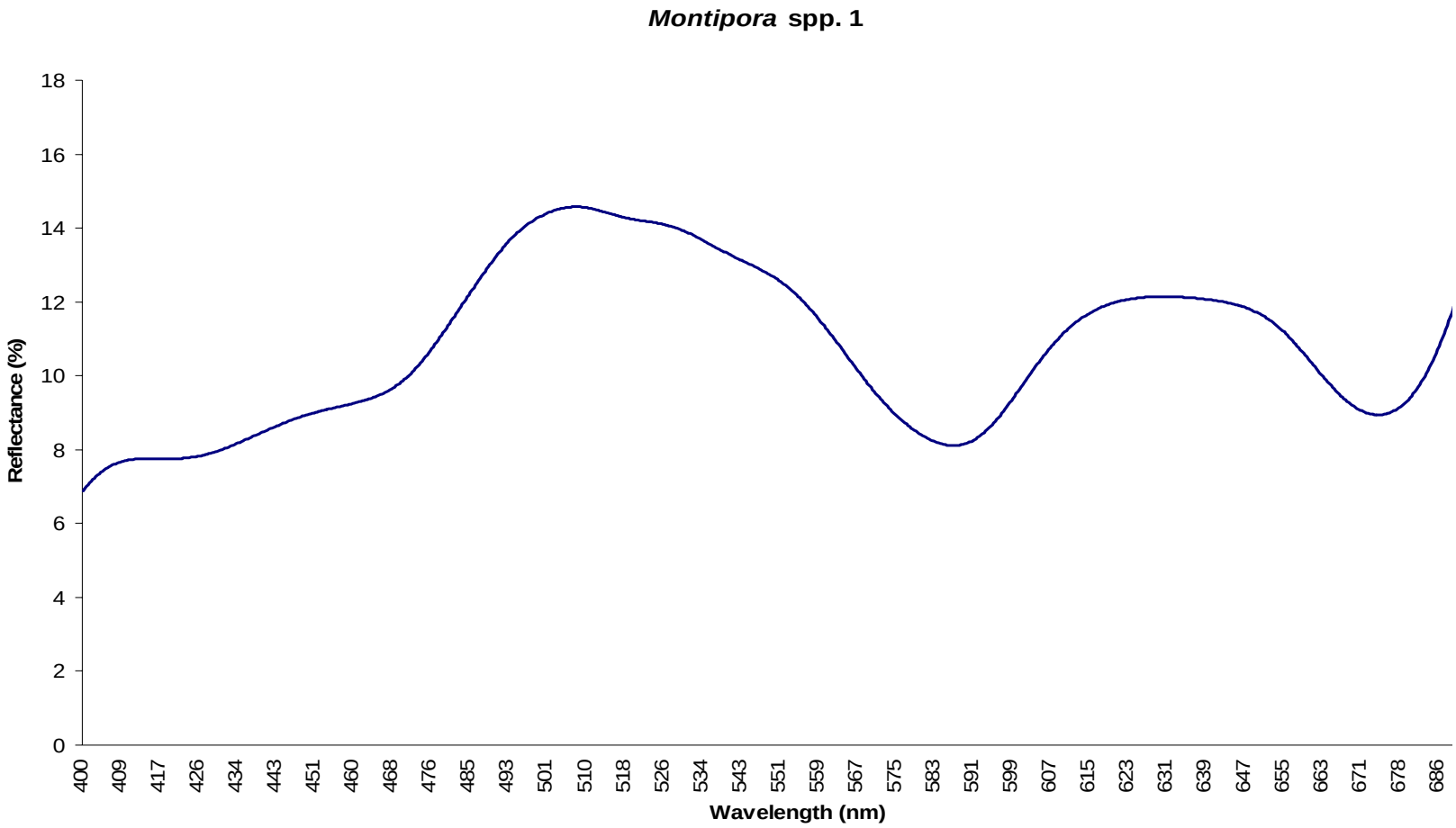

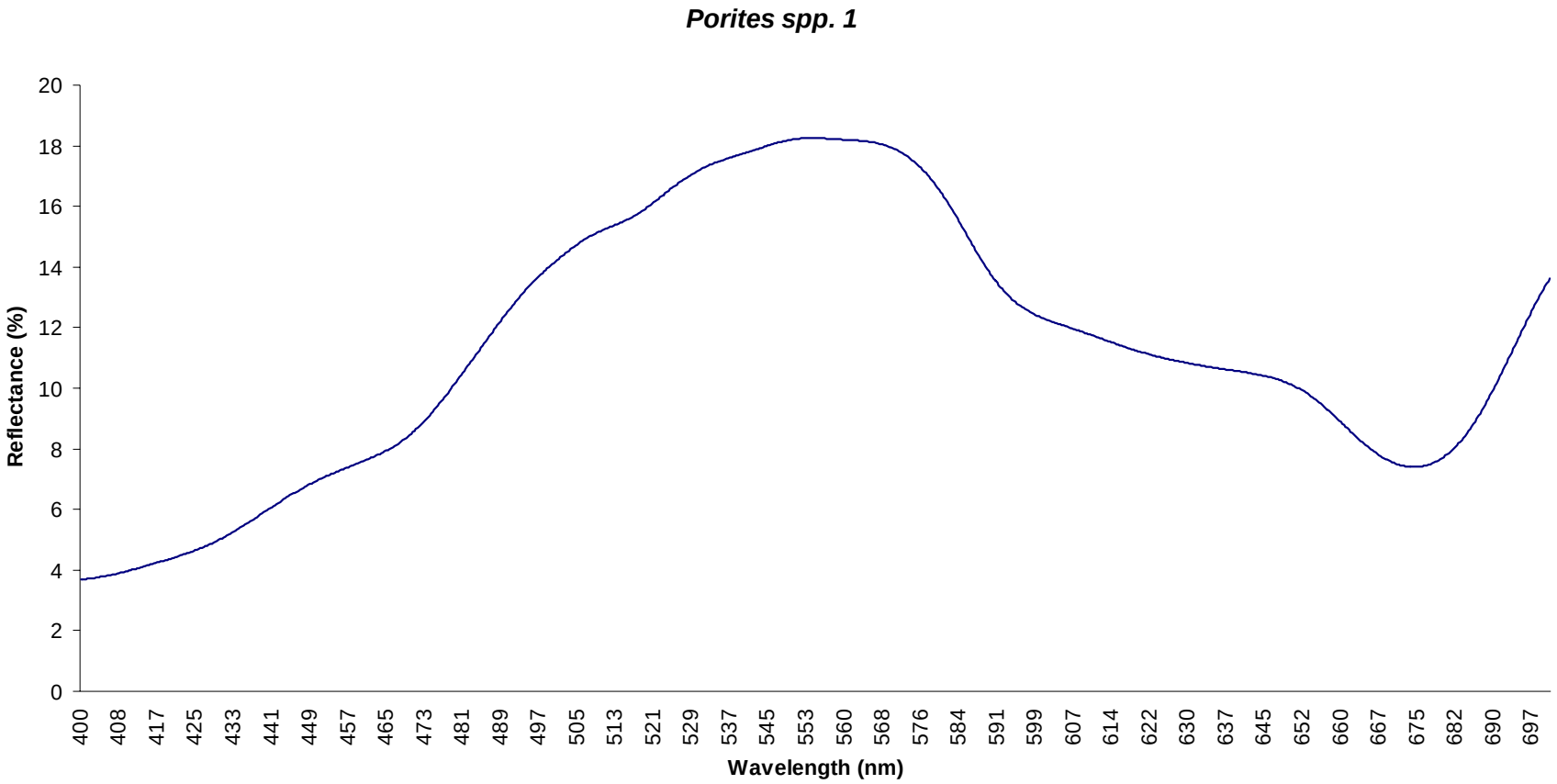
Porites spp. 1
Reflectance (%)
0
2
4
6
8
10
12
14
16
18
20
400
408
417
425
433
441
449
457
465
473
481
489
497
505
513
521
529
537
545
553
560
568
576
584
591
599
607
614
622
630
637
645
652
660
667
675
682
690
697
Wavelength (nm)

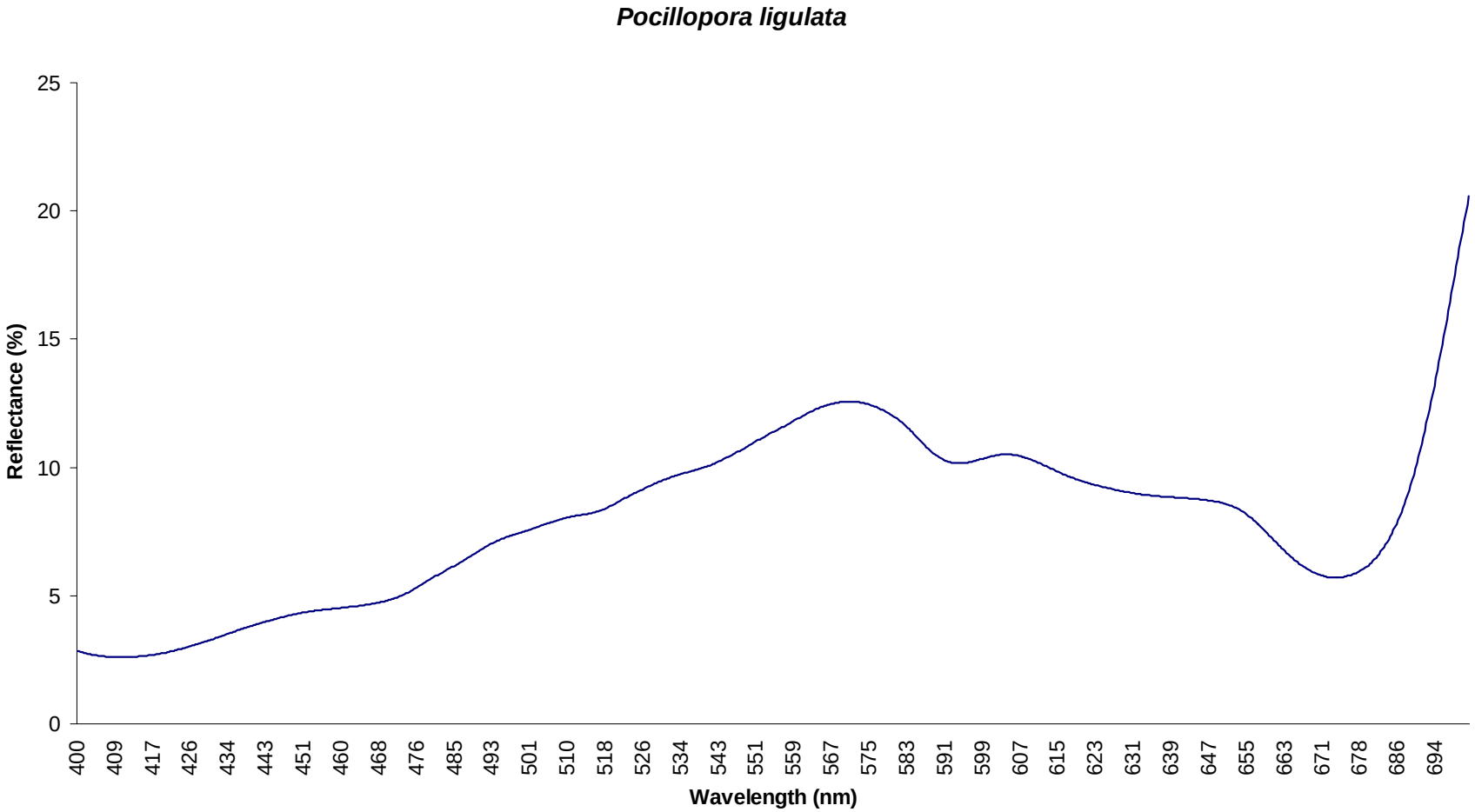
Pocillopora ligulata
Reflectance (%)
25
20
15
10
5
0
400
409
417
426
434
443
451
460
468
476
485
493
501
510
518
526
534
543
551
559
567
575
583
591
599
607
615
623
631
639
647
655
663
671
678
686
694
Wavelength (nm)

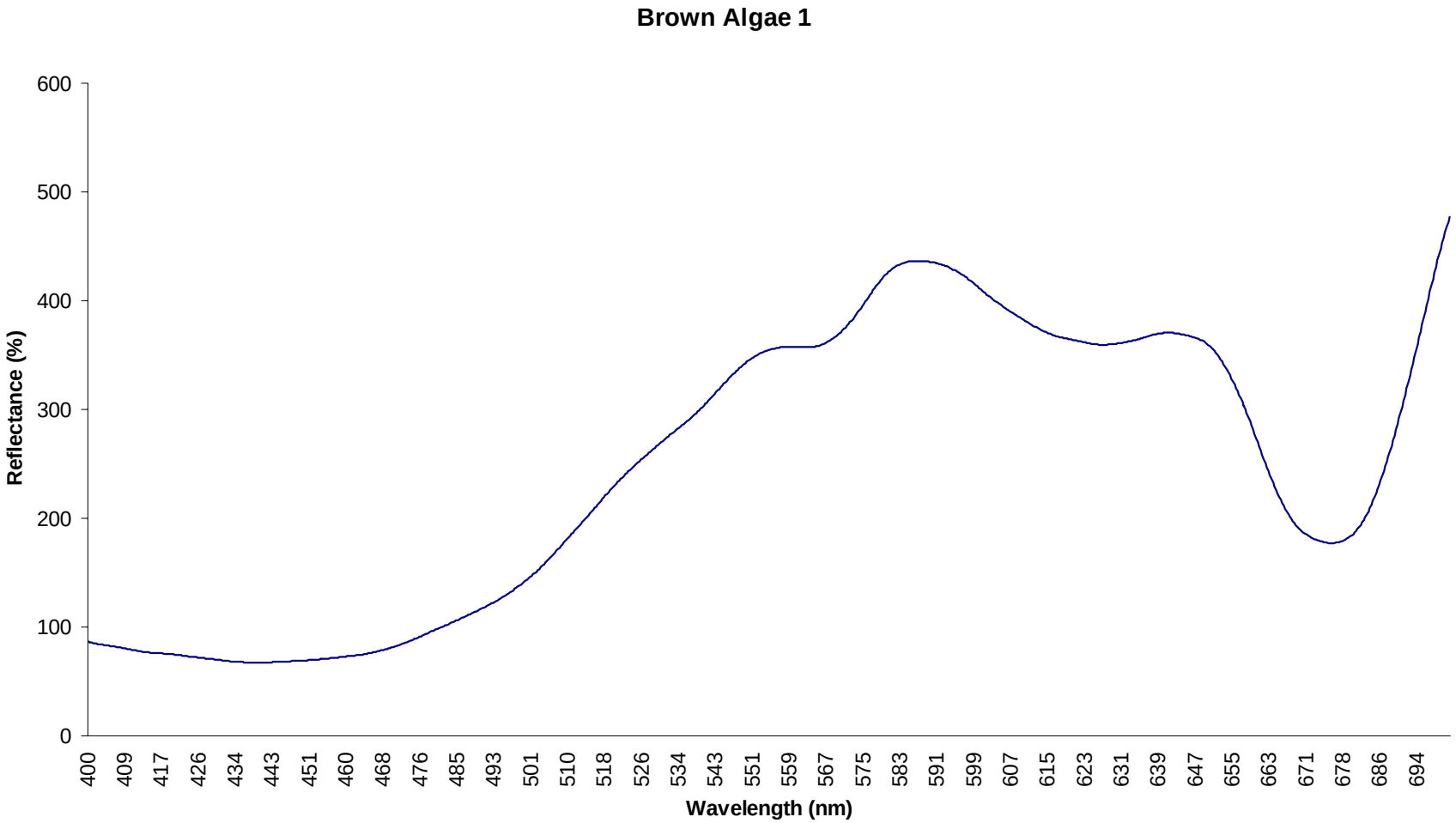
Brown Algae 1
Reflectance (%)
600
500
400
300
200
100
0
400
409
417
426
434
443
451
460
468
476
485
493
501
510
518
526
534
543
551
559
567
575
583
591
599
607
615
623
631
639
647
655
663
671
678
686
694
Wavelength (nm)

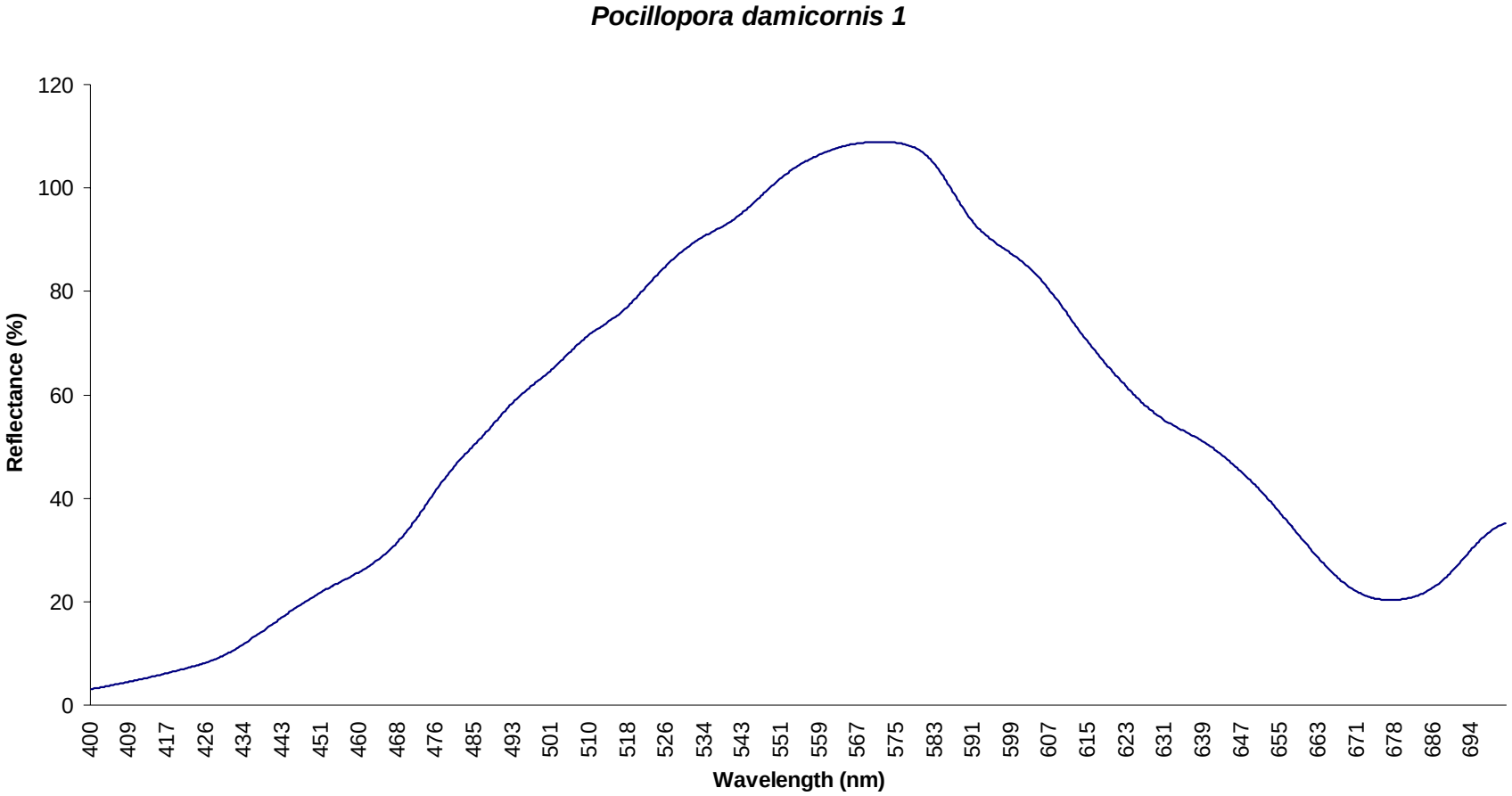
Pocillopora damicornis 1
Reflectance (%)
120
100
80
60
40
20
0
400
409
417
426
434
443
451
460
468
476
485
493
501
510
518
526
534
543
551
559
567
575
583
591
599
607
615
623
631
639
647
655
663
671
678
686
694
Wavelength (nm)

***Montipora spp. 2***

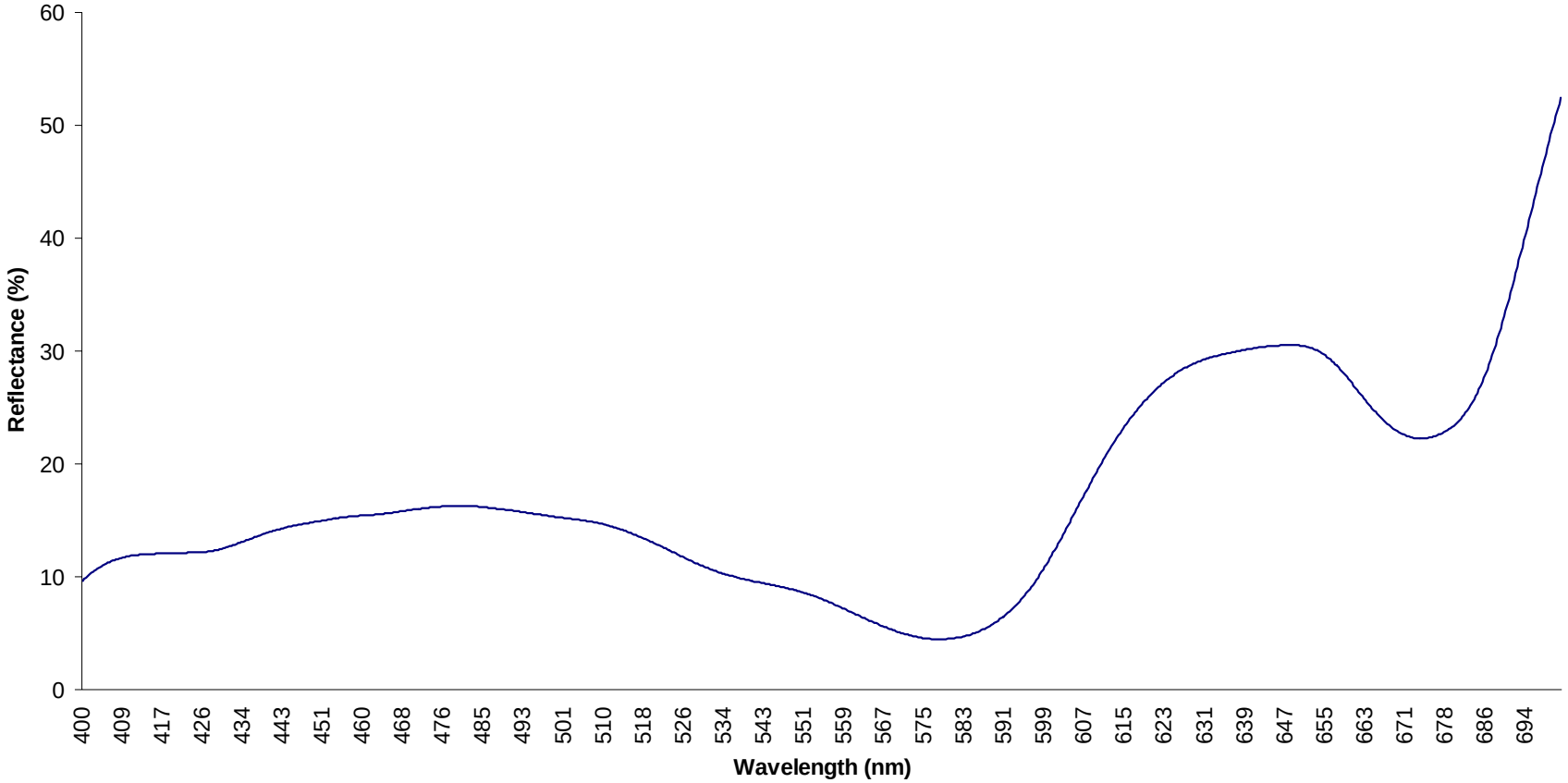

***Montipora spp. 3***

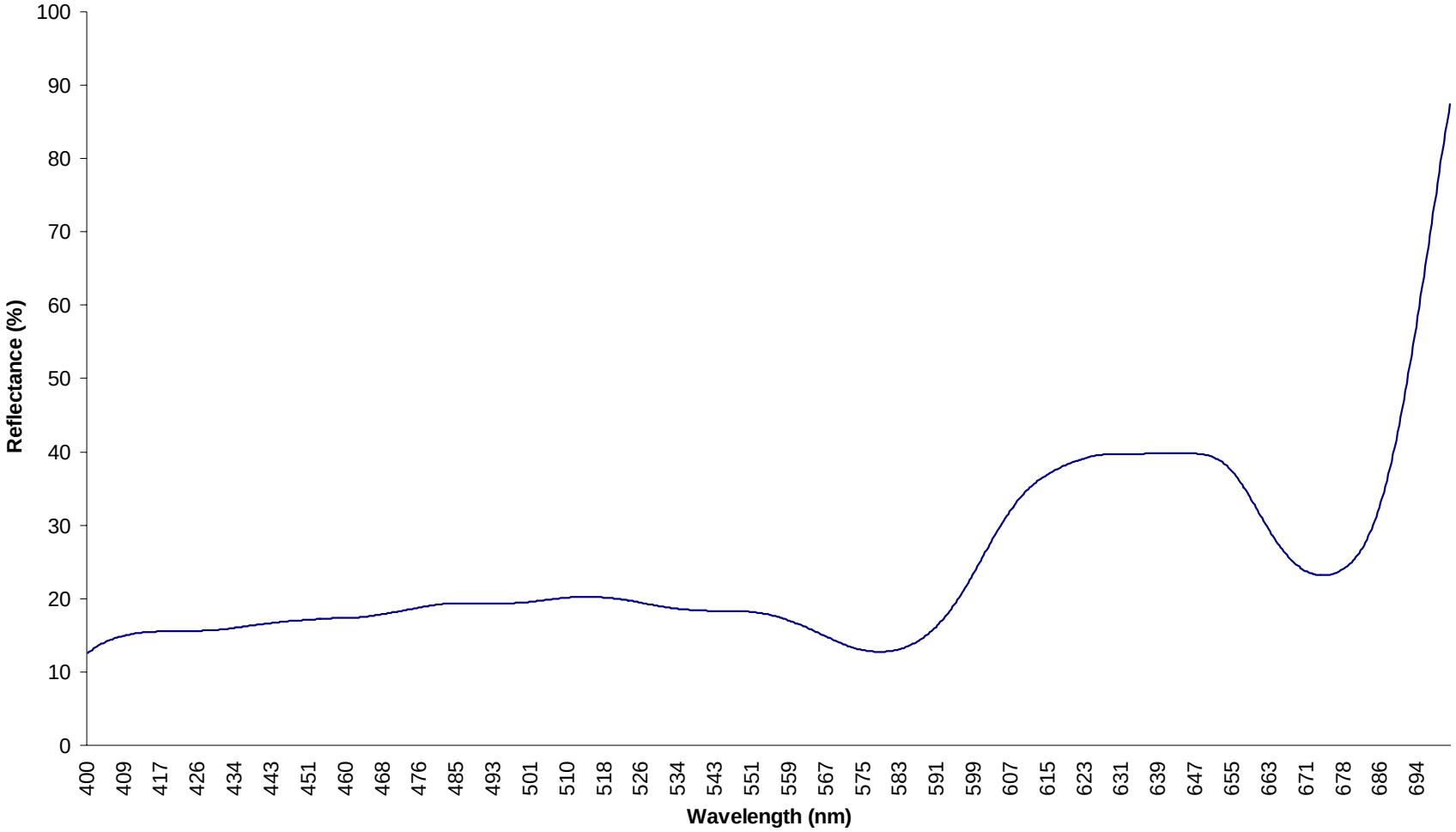

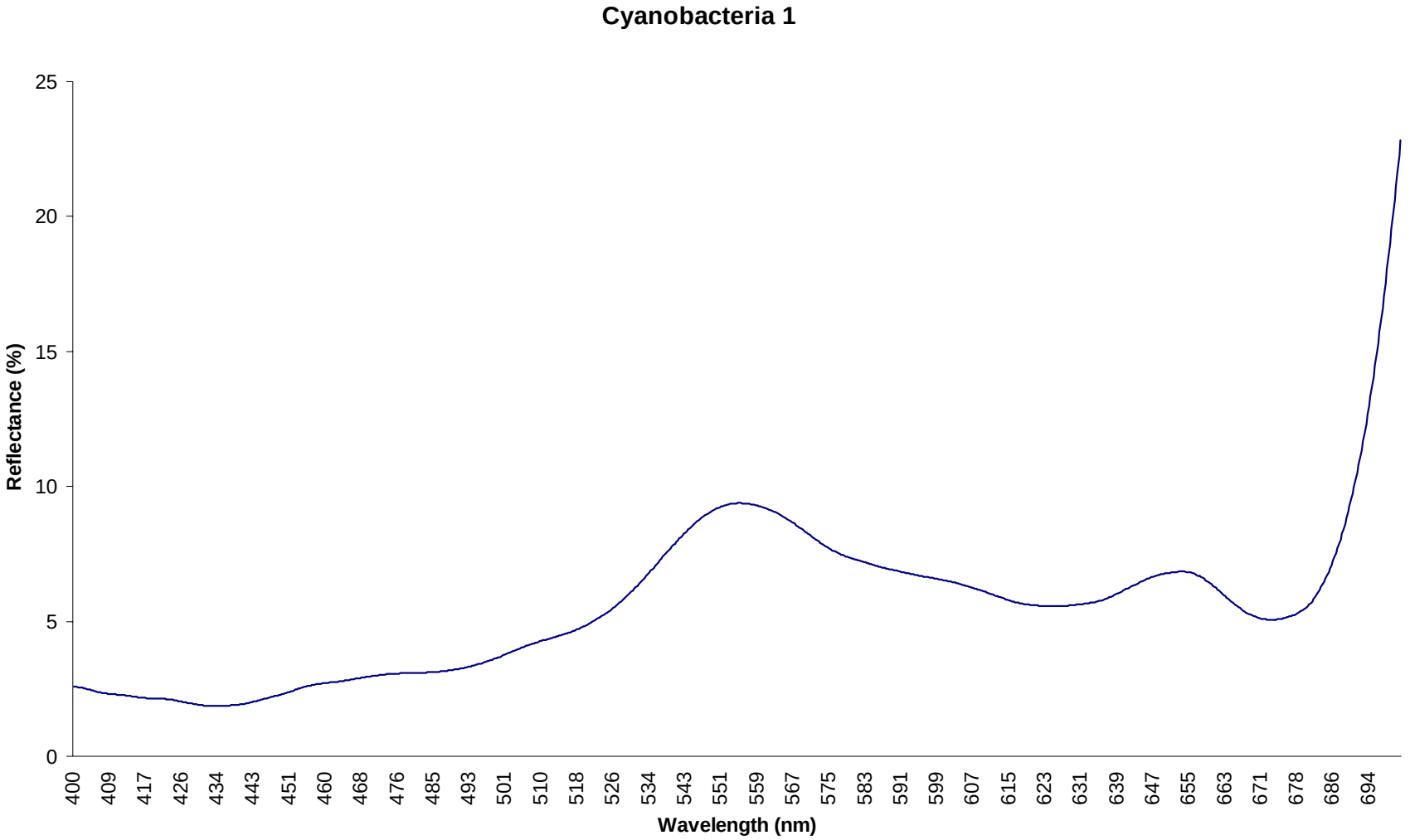
Cyanobacteria 1
Reflectance (%)
25
20
15
10
5
0
400
409
417
426
434
443
451
460
468
476
485
493
501
510
518
526
534
543
551
559
567
575
583
591
599
607
615
623
631
639
647
655
663
671
678
686
694
Wavelength (nm)

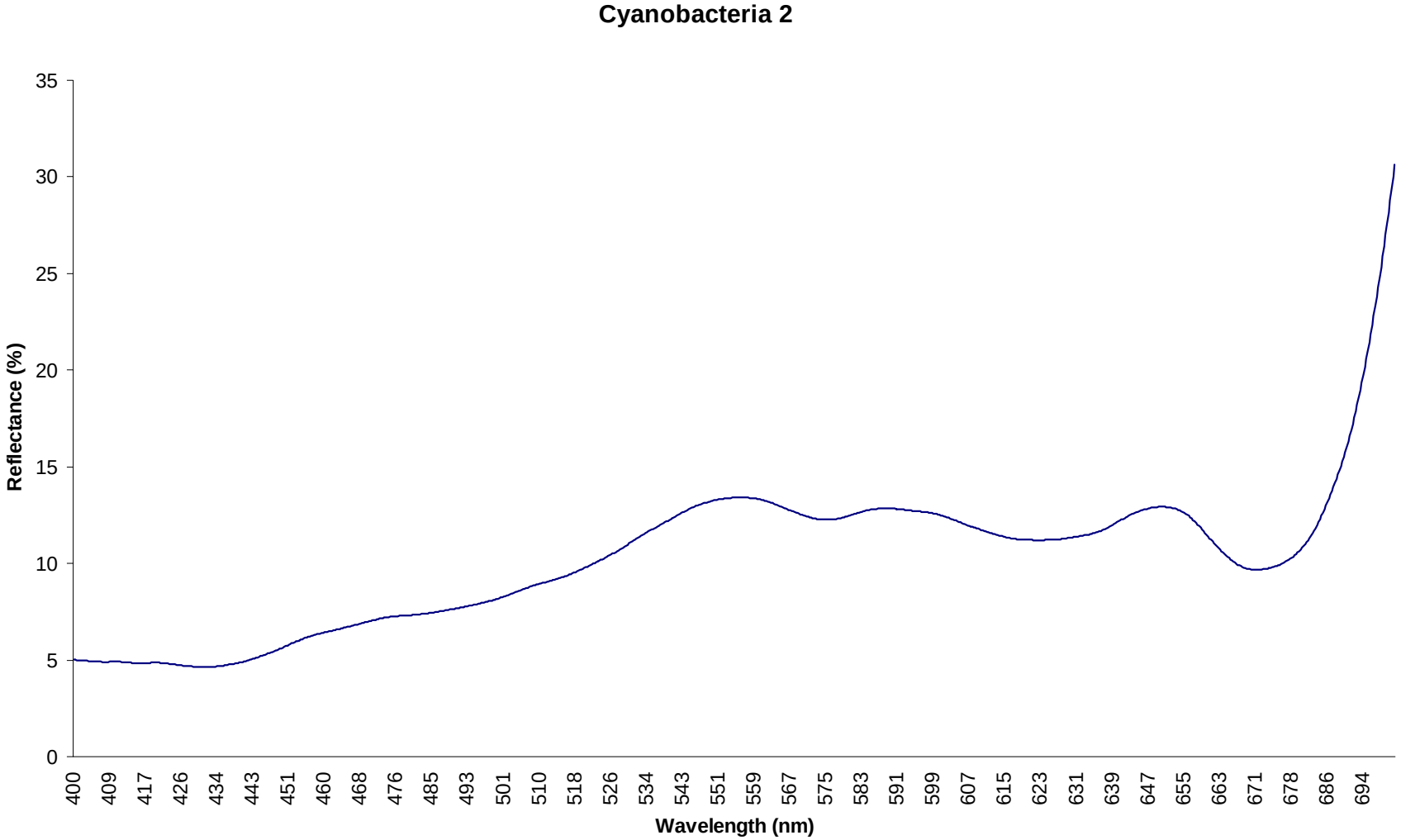
Cyanobacteria 2
Reflectance (%)
35
30
25
20
15
10
5
0
400
409
417
426
434
443
451
460
468
476
485
493
501
510
518
526
534
543
551
559
567
575
583
591
599
607
615
623
631
639
647
655
663
671
678
686
694
Wavelength (nm)

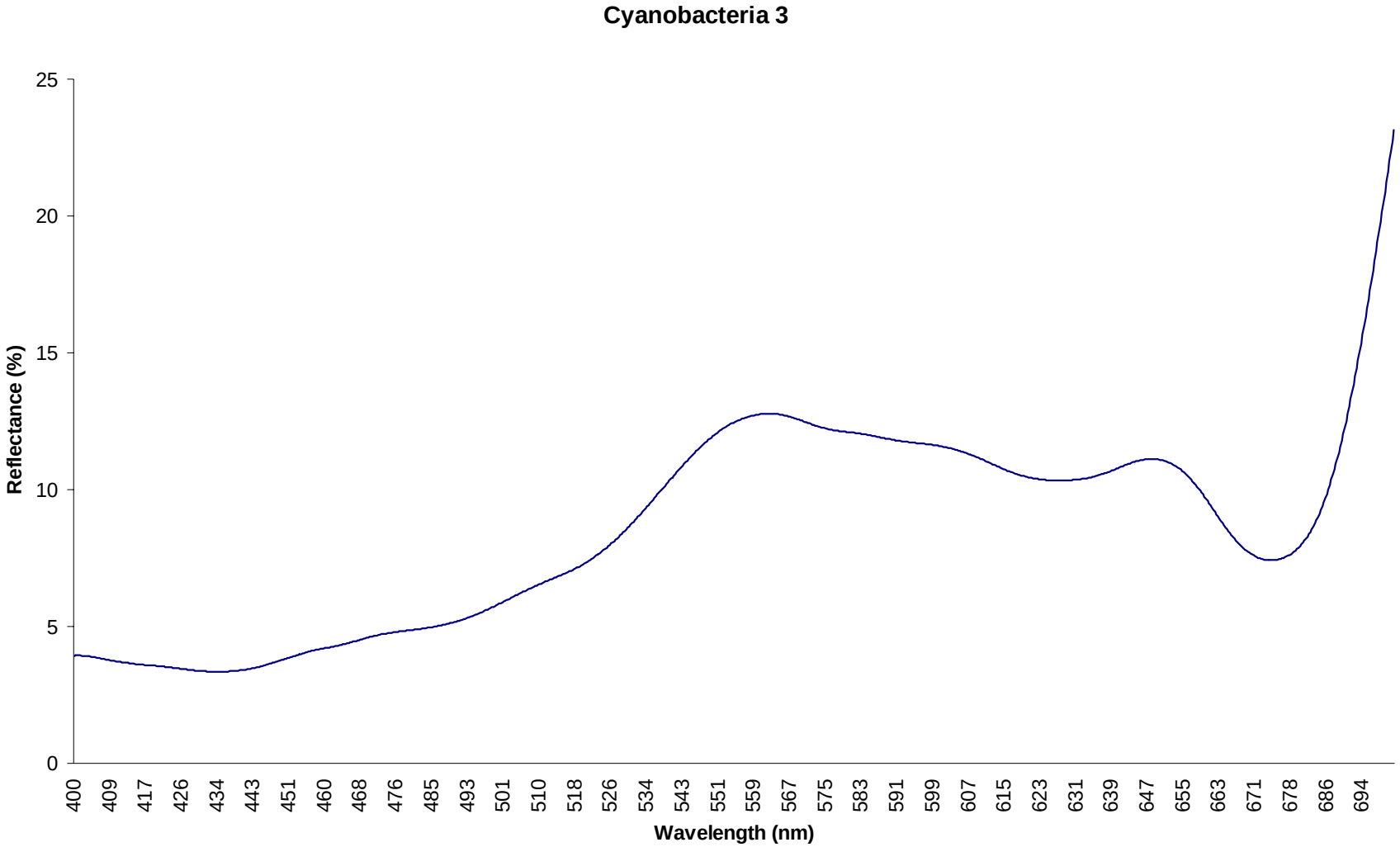
Cyanobacteria 3
Reflectance (%)
25
20
15
10
5
0
400
409
417
426
434
443
451
460
468
476
485
493
501
510
518
526
534
543
551
559
567
575
583
591
599
607
615
623
631
639
647
655
663
671
678
686
694
Wavelength (nm)

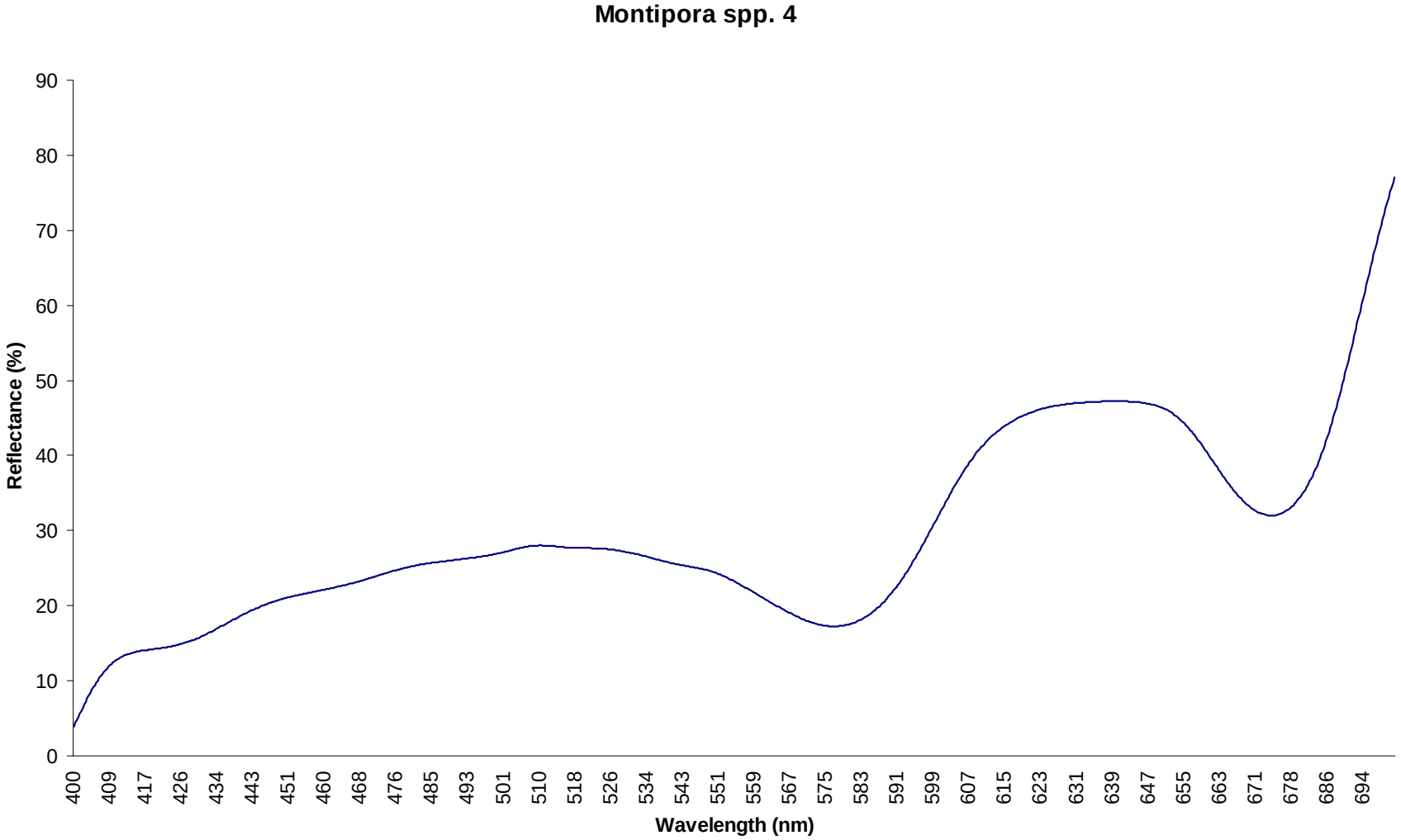
Montipora spp. 4
Reflectance (%)
90
80
70
60
50
40
30
20
10
0
400
409
417
426
434
443
451
460
468
476
485
493
501
510
518
526
534
543
551
559
567
575
583
591
599
607
615
623
631
639
647
655
663
671
678
686
694
Wavelength (nm)

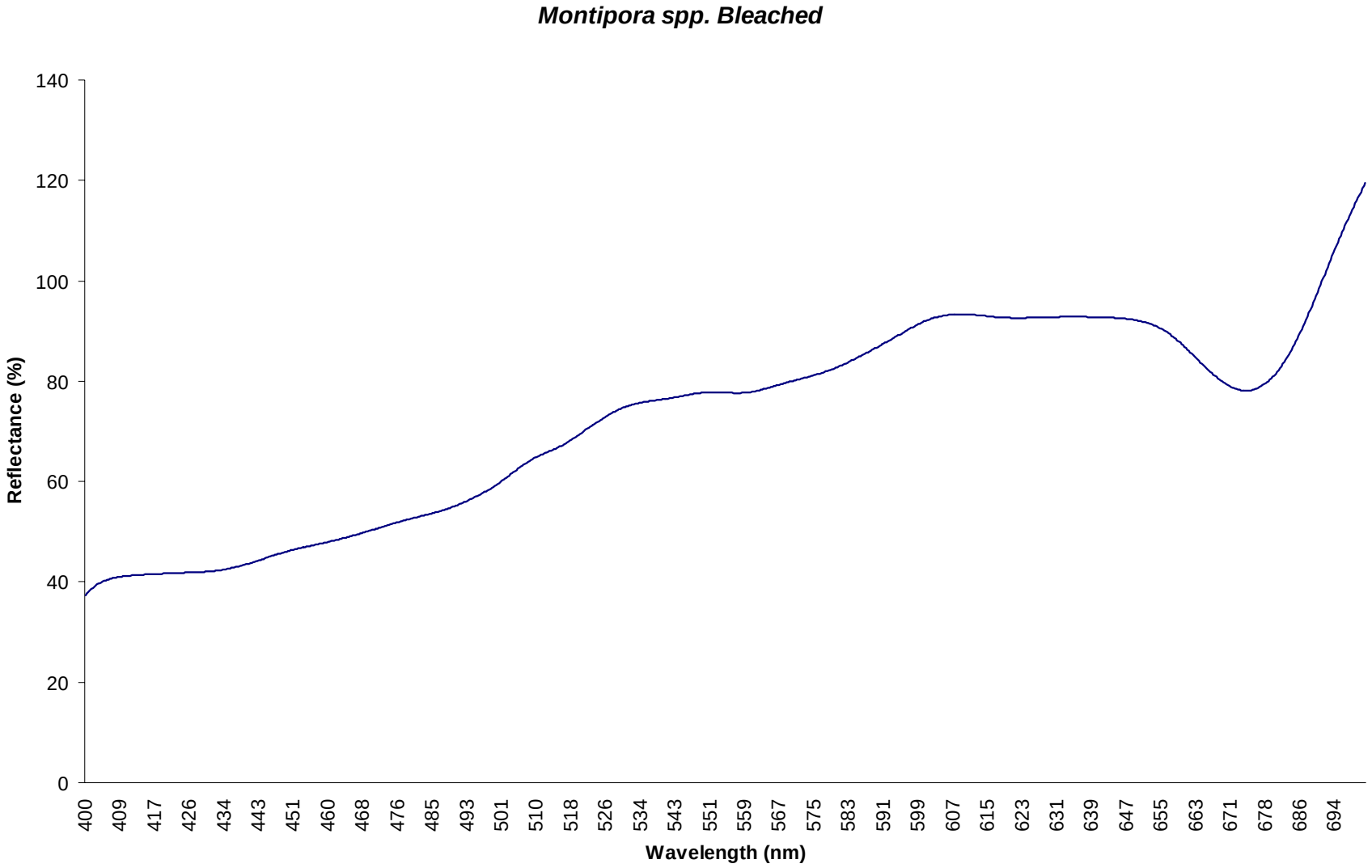
Montipora spp. Bleached
Reflectance (%)
140
120
100
80
60
40
20
0
400
409
417
426
434
443
451
460
468
476
485
493
501
510
518
526
534
543
551
559
567
575
583
591
599
607
615
623
631
639
647
655
663
671
678
686
694
Wavelength (nm)

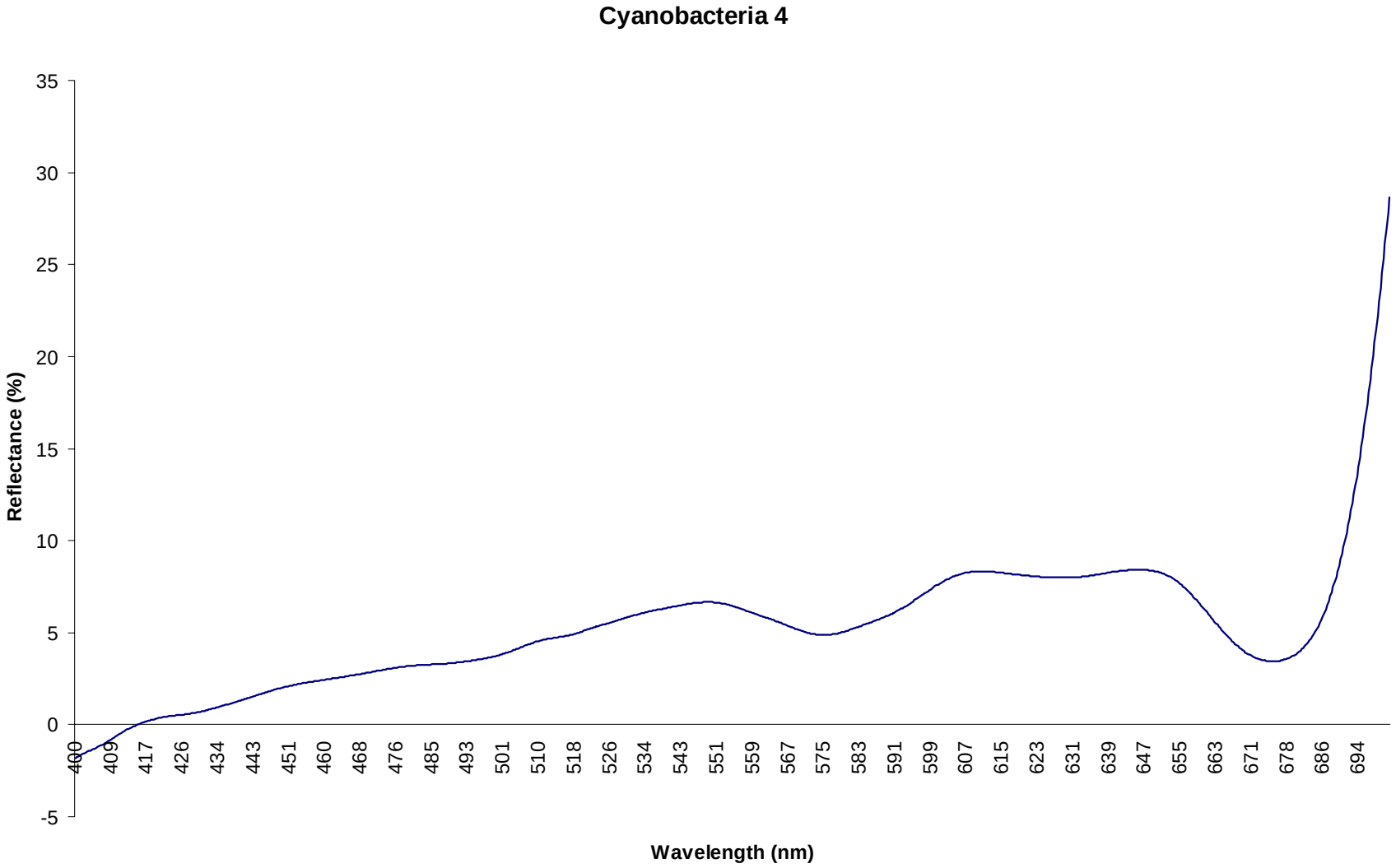
Cyanobacteria 4
Reflectance (%)
35
30
25
20
15
10
5
0
-5
400
409
417
426
434
443
451
460
468
476
485
493
501
510
518
526
534
543
551
559
567
575
583
591
599
607
615
623
631
639
647
655
663
671
678
686
694
Wavelength (nm)

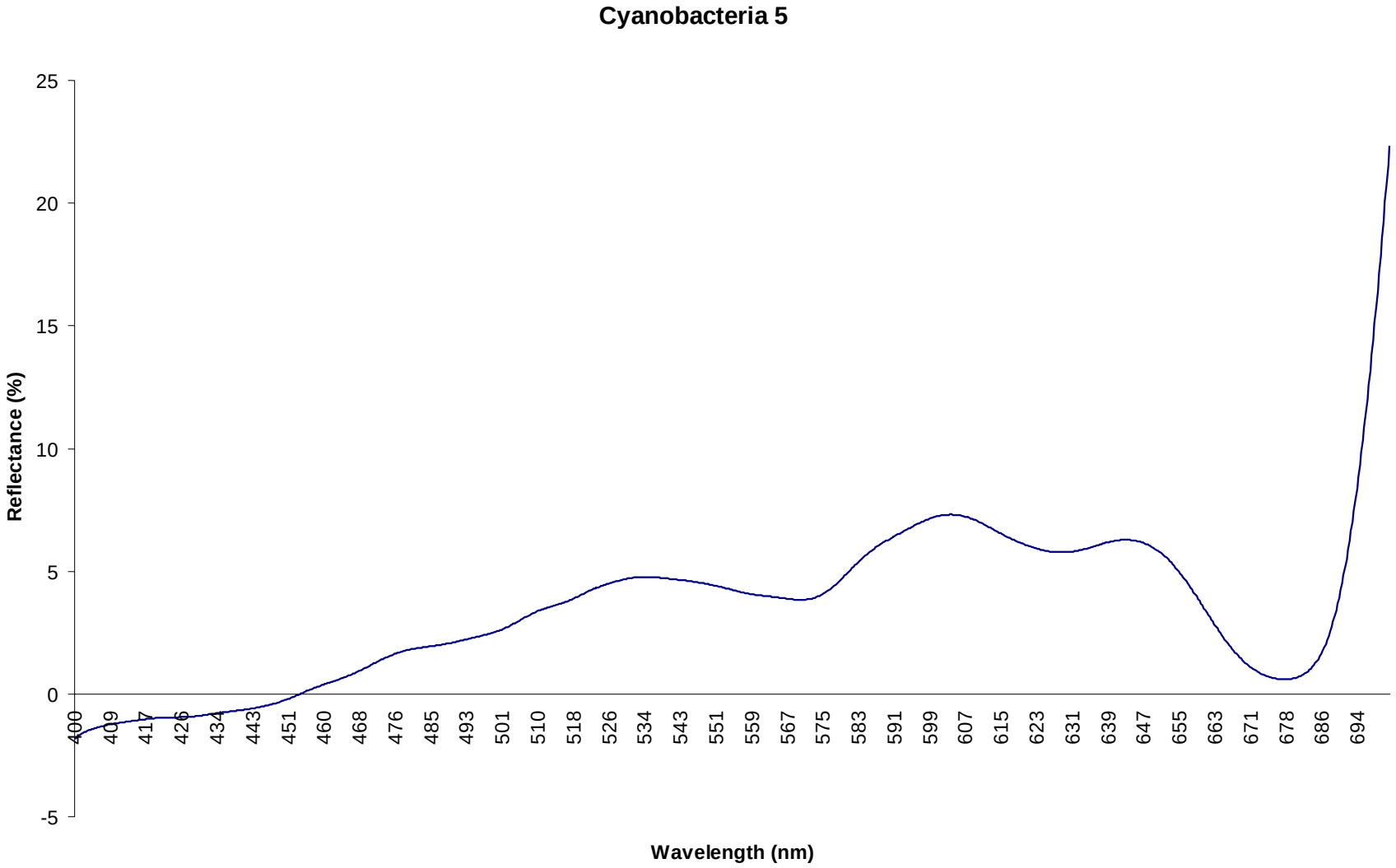
Cyanobacteria 5
Reflectance (%)
25
20
15
10
5
0
-5
400
409
417
426
434
443
451
460
468
476
485
493
501
510
518
526
534
543
551
559
567
575
583
591
599
607
615
623
631
639
647
655
663
671
678
686
694
Wavelength (nm)

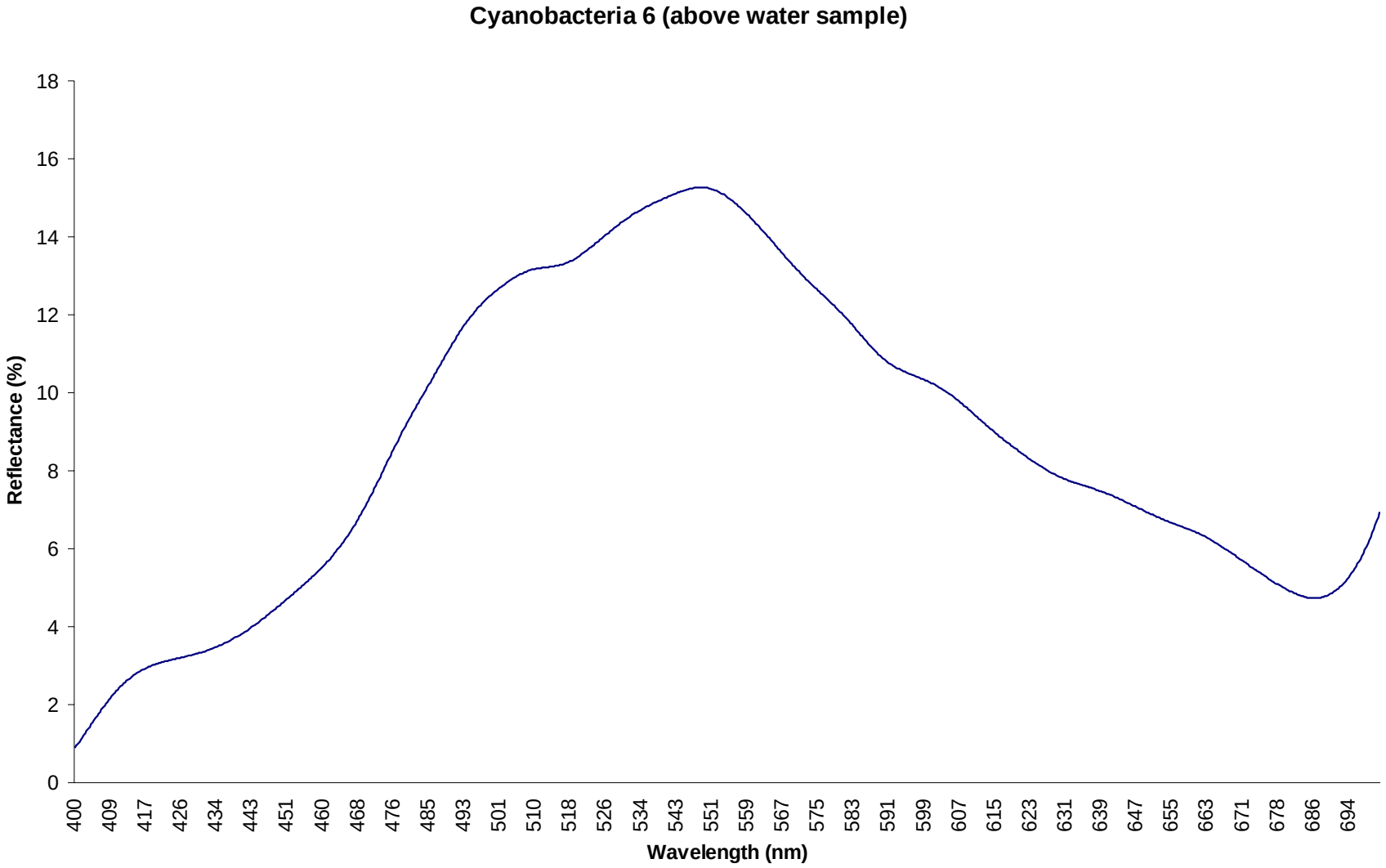
Cyanobacteria 6 (above water sample)
Reflectance (%)
0
2
4
6
8
10
12
14
16
18
400
409
417
426
434
443
451
460
468
476
485
493
501
510
518
526
534
543
551
559
567
575
583
591
599
607
615
623
631
639
647
655
663
671
678
686
694
Wavelength (nm)

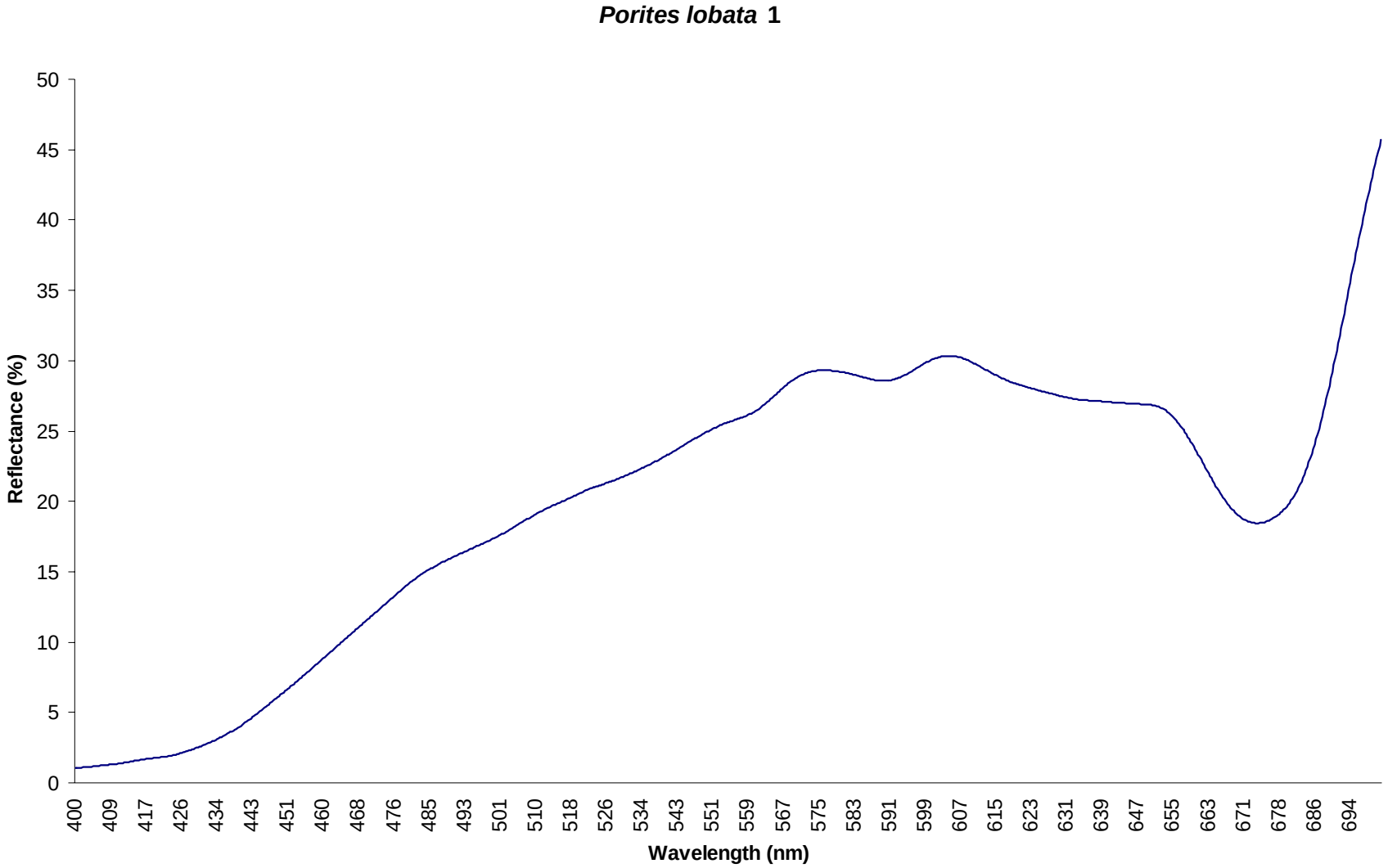
*Porites lobata* 1
Reflectance (%)
0
5
10
15
20
25
30
35
40
45
50
400
409
417
426
434
443
451
460
468
476
485
493
501
510
518
526
534
543
551
559
567
575
583
591
599
607
615
623
631
639
647
655
663
671
678
686
694
Wavelength (nm)

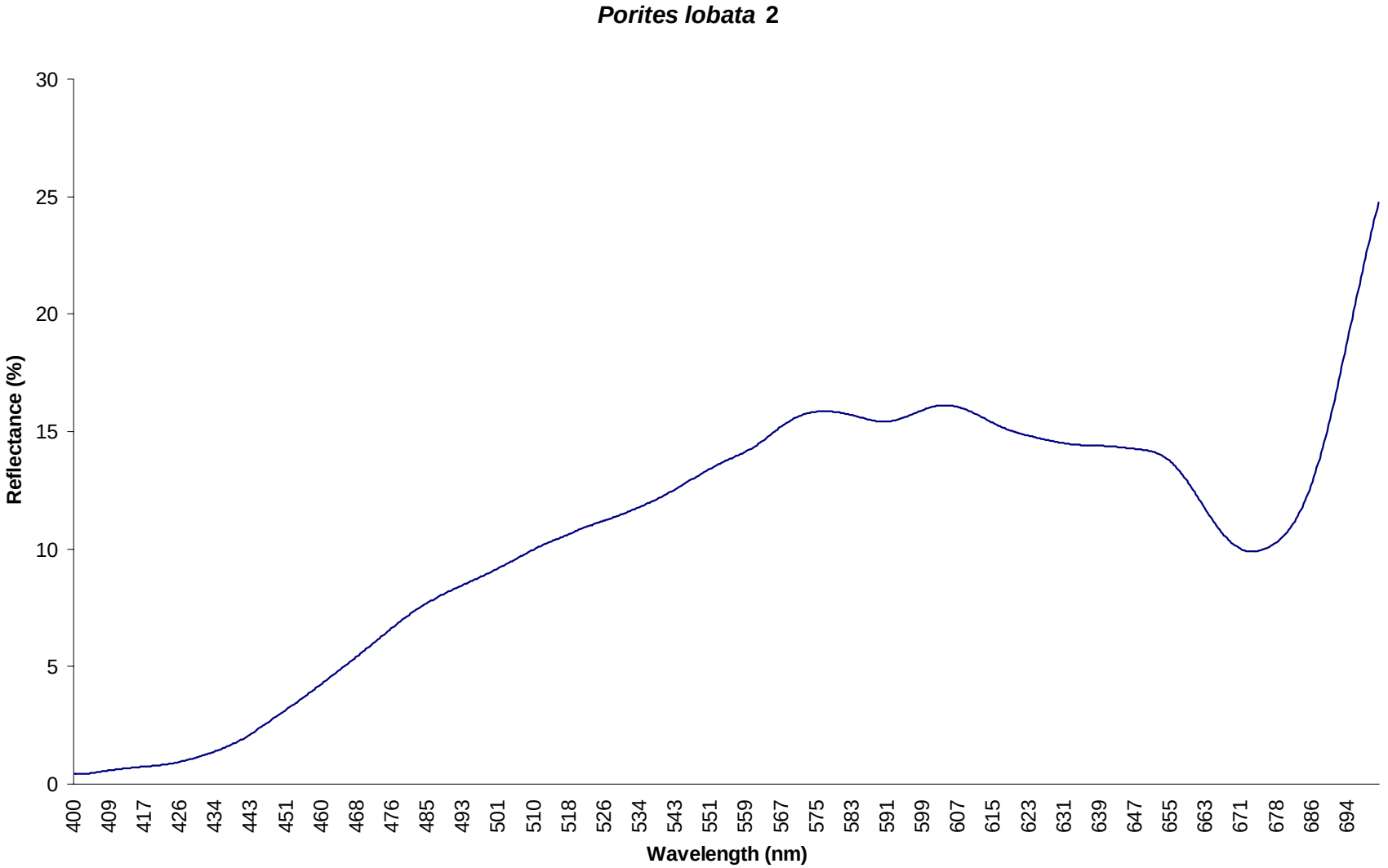
Porites lobata 2
Reflectance (%)
30
25
20
15
10
5
0
400
409
417
426
434
443
451
460
468
476
485
493
501
510
518
526
534
543
551
559
567
575
583
591
599
607
615
623
631
639
647
655
663
671
678
686
694
Wavelength (nm)

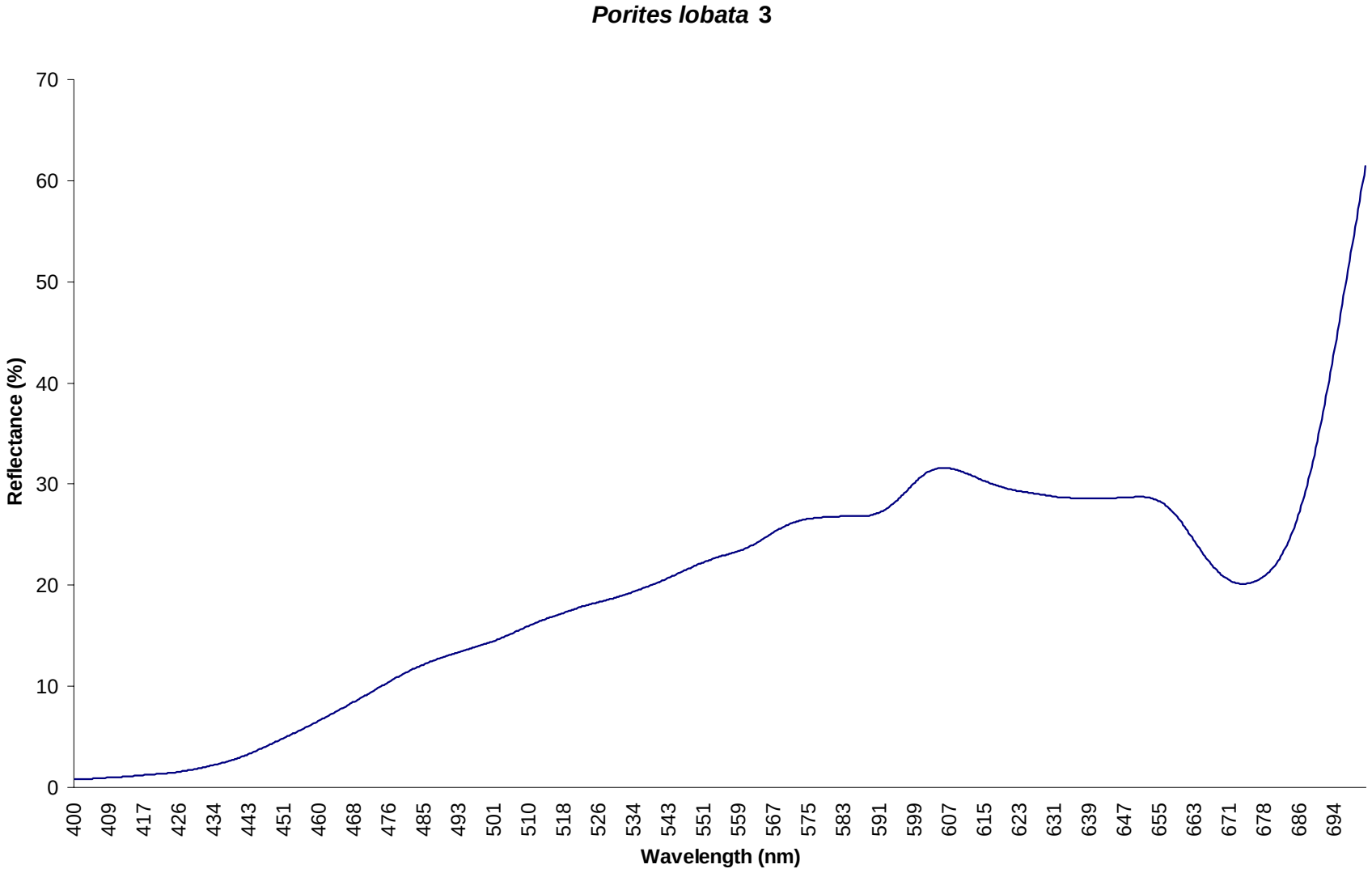
Porites lobata 3
Reflectance (%)
70
60
50
40
30
20
10
0
400
409
417
426
434
443
451
460
468
476
485
493
501
510
518
526
534
543
551
559
567
575
583
591
599
607
615
623
631
639
647
655
663
671
678
686
694
Wavelength (nm)

**Algae: *Laurentia* spp.**

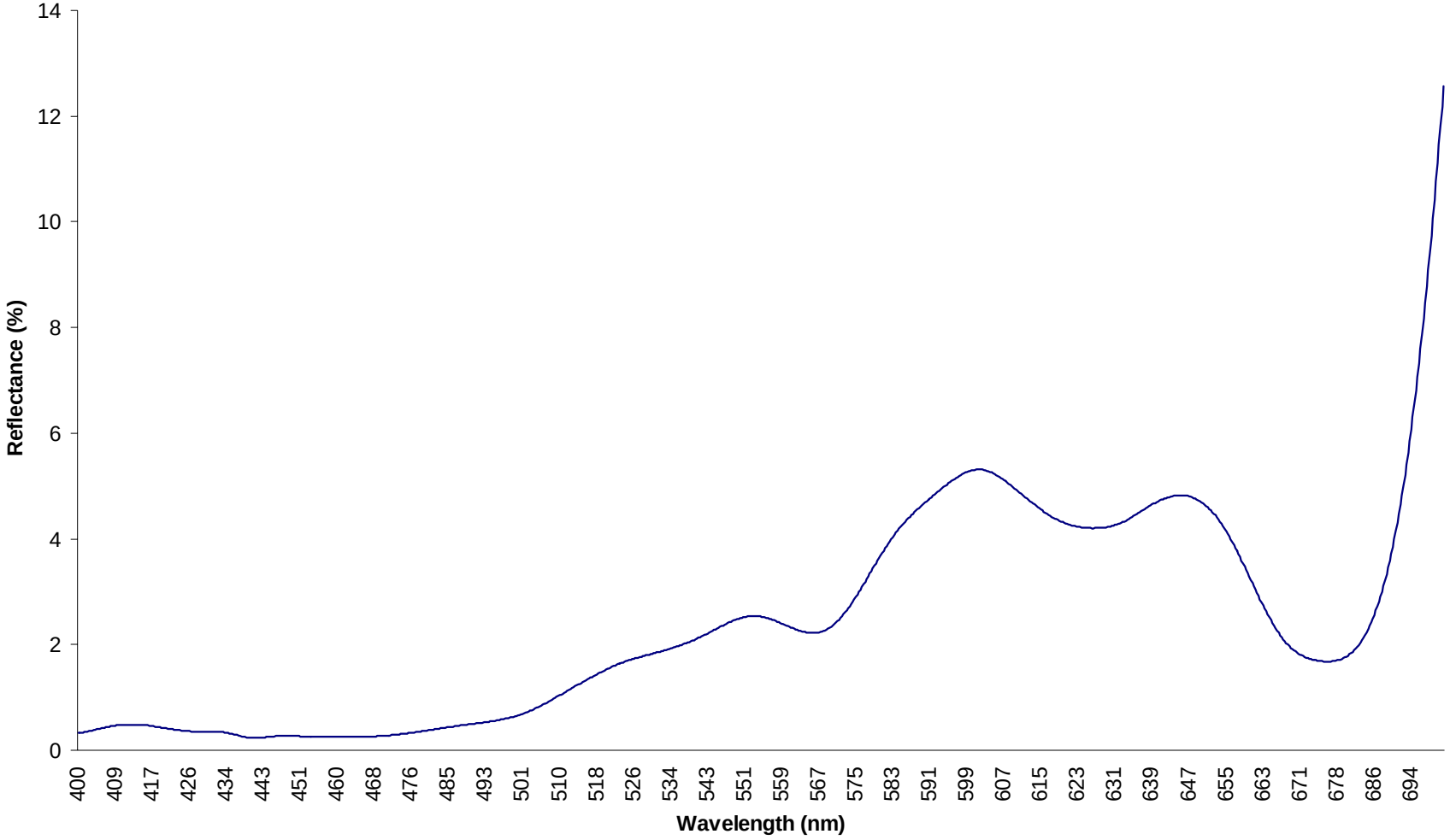

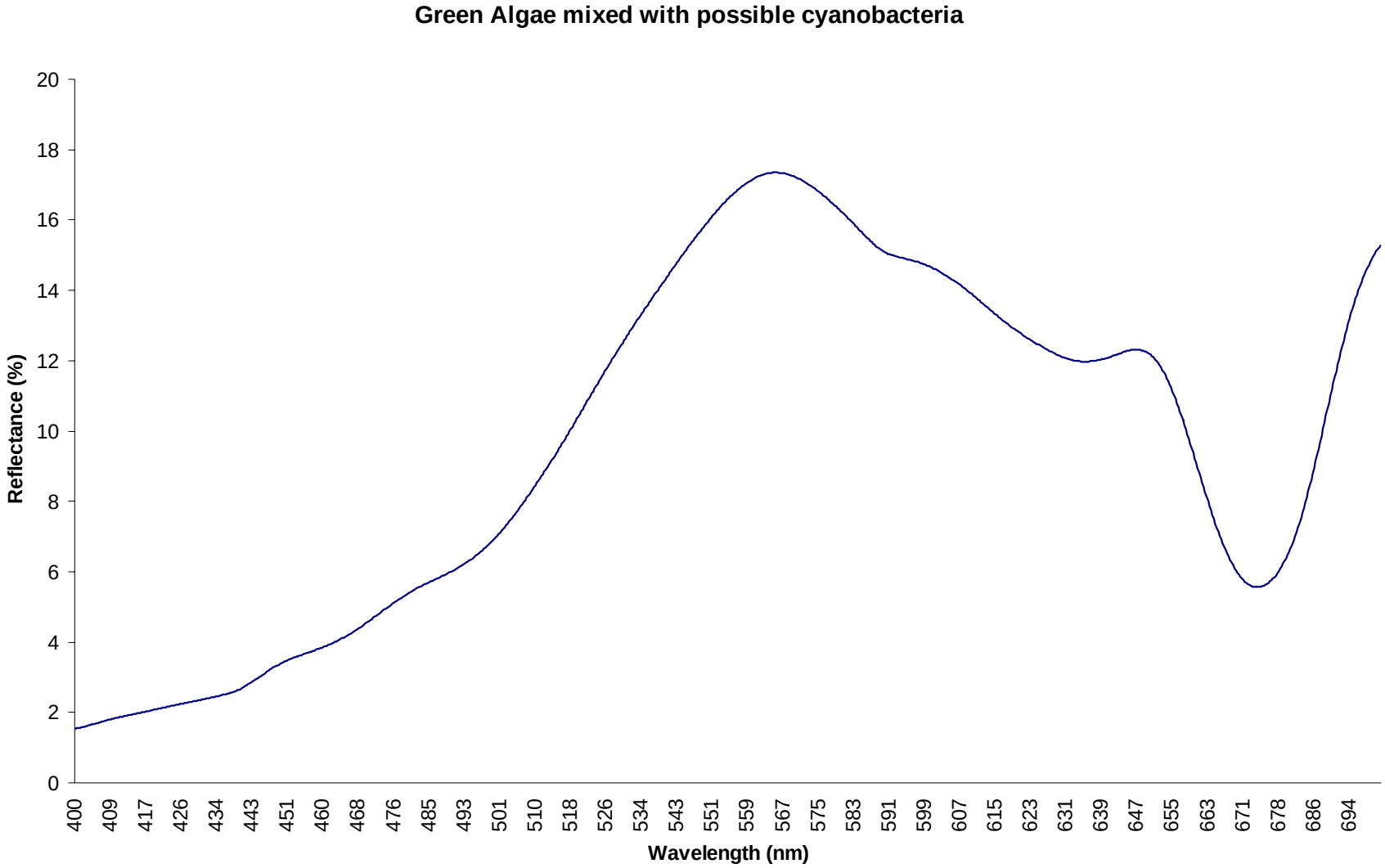
Green Algae mixed with possible cyanobacteria
Reflectance (%)
0
2
4
6
8
10
12
14
16
18
20
400
409
417
426
434
443
451
460
468
476
485
493
501
510
518
526
534
543
551
559
567
575
583
591
599
607
615
623
631
639
647
655
663
671
678
686
694
Wavelength (nm)

# APPENDIX D. FIRST DERIVATIVE CHARTS

**Montipora spp. 1**
**1st Derivative**

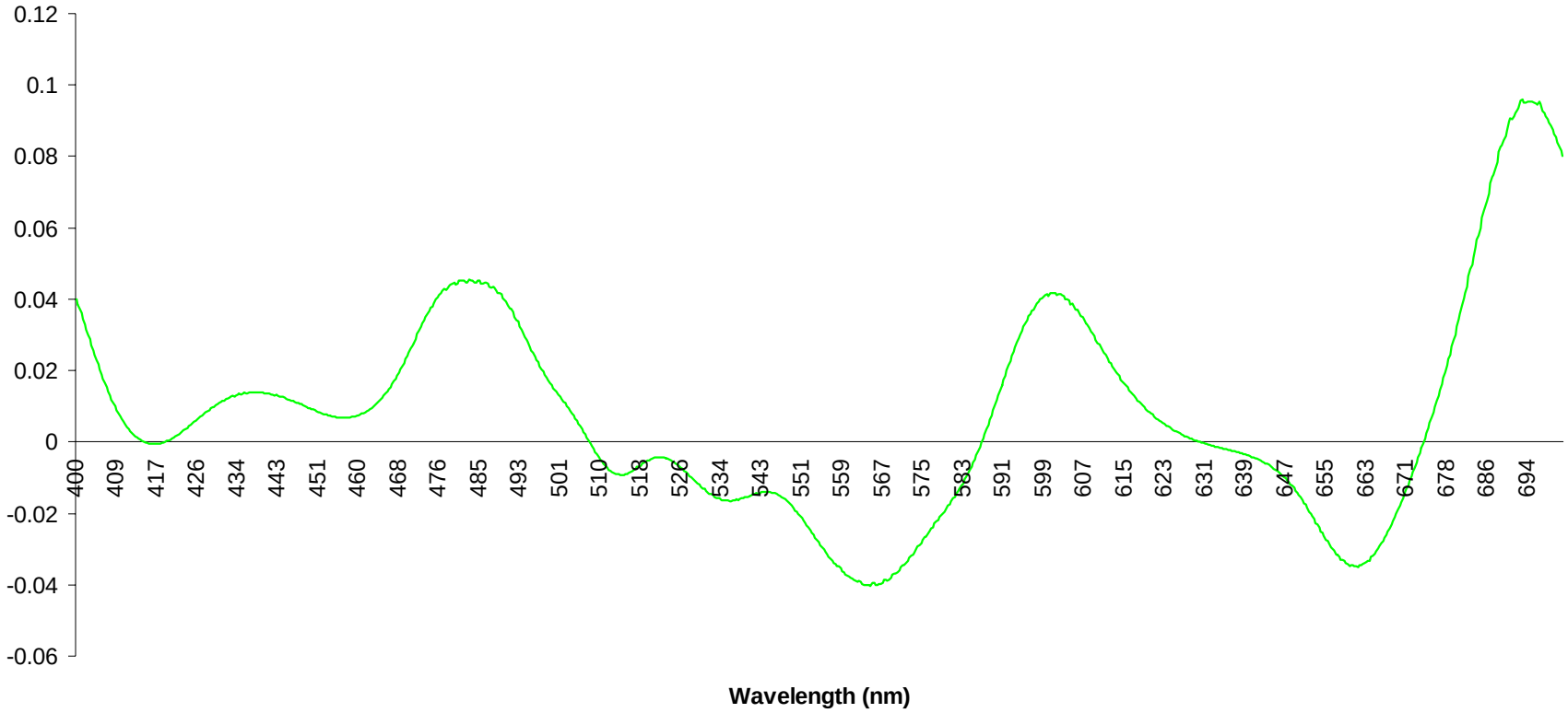

**Porites spp. 1**
**1st Derivative**

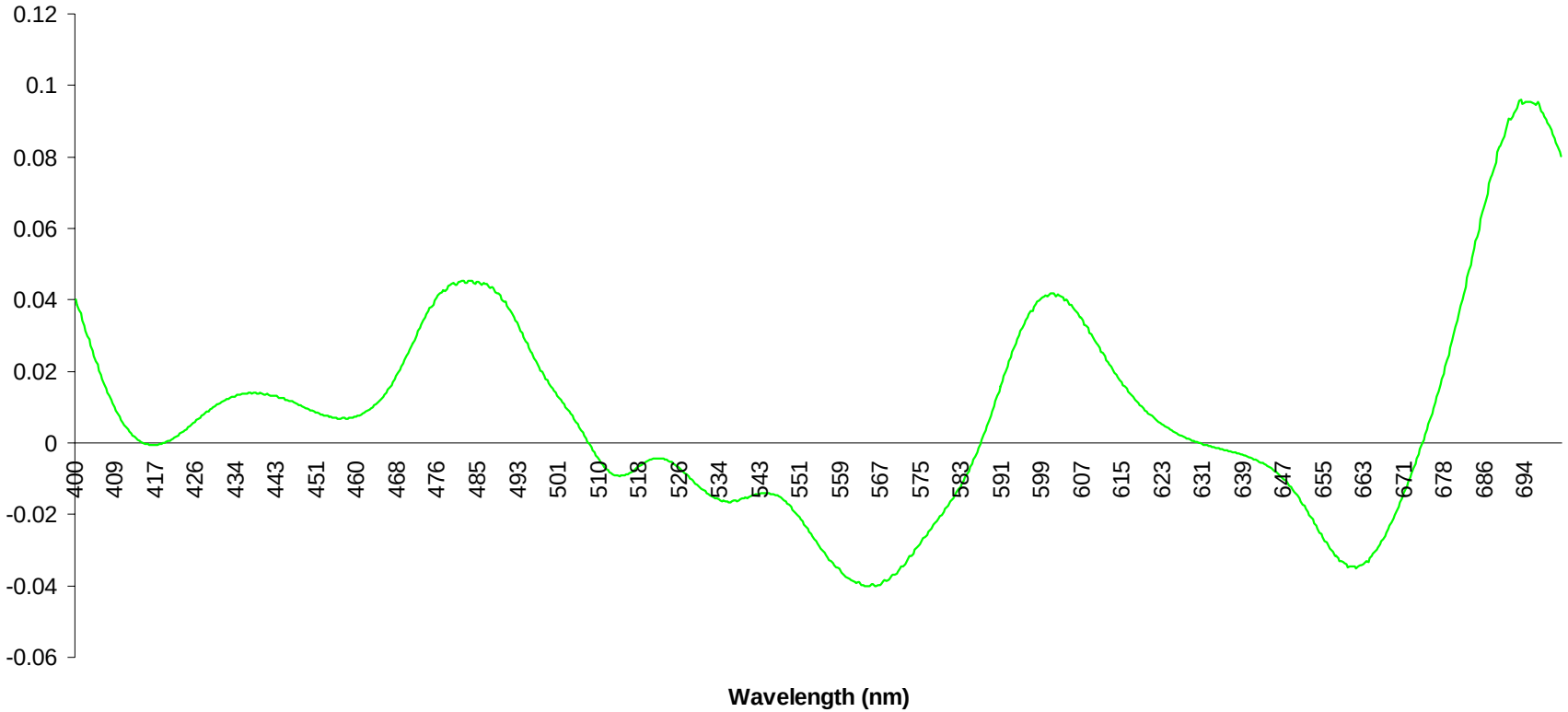

**Pocillopora ligulata**
**1st Derivative**

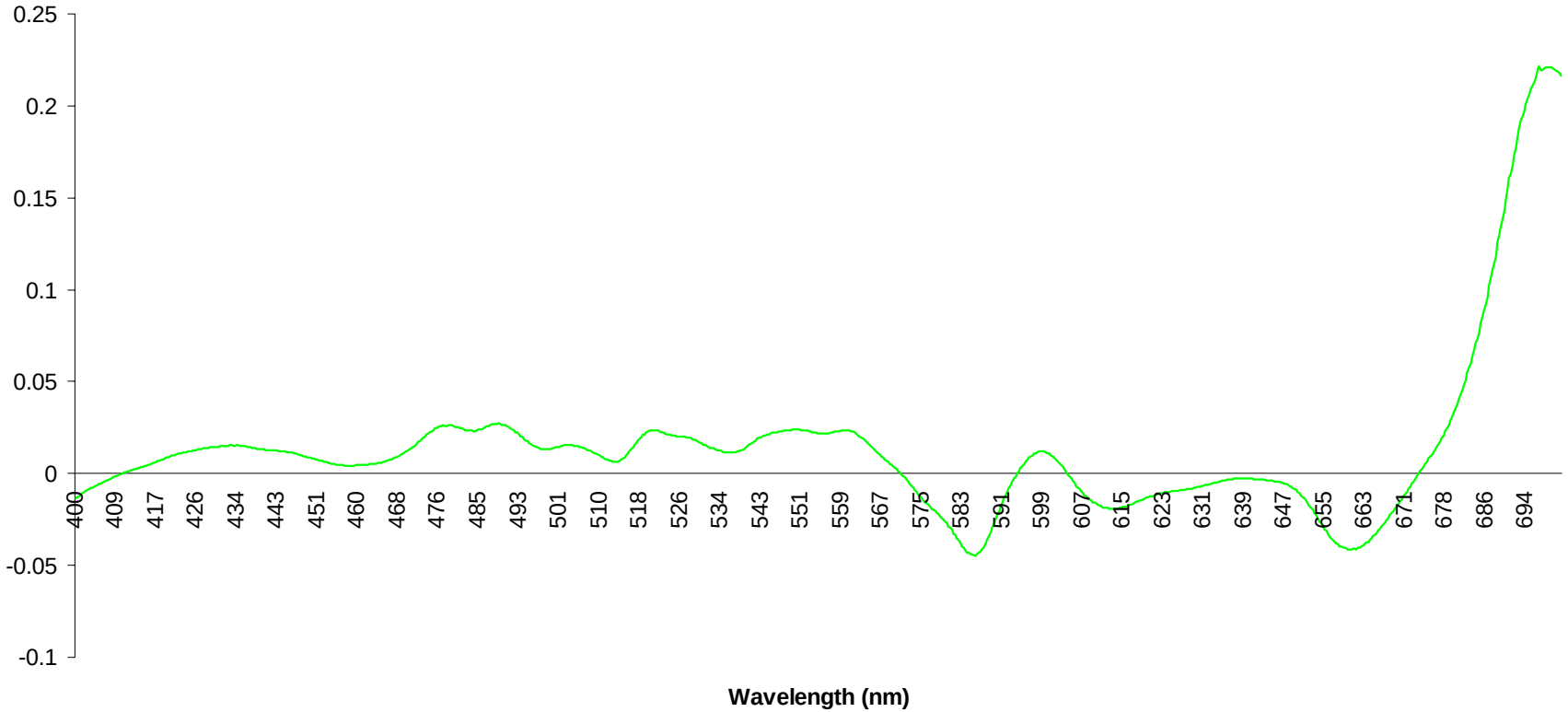

**Brown Algae 1**
**1st Derivative**

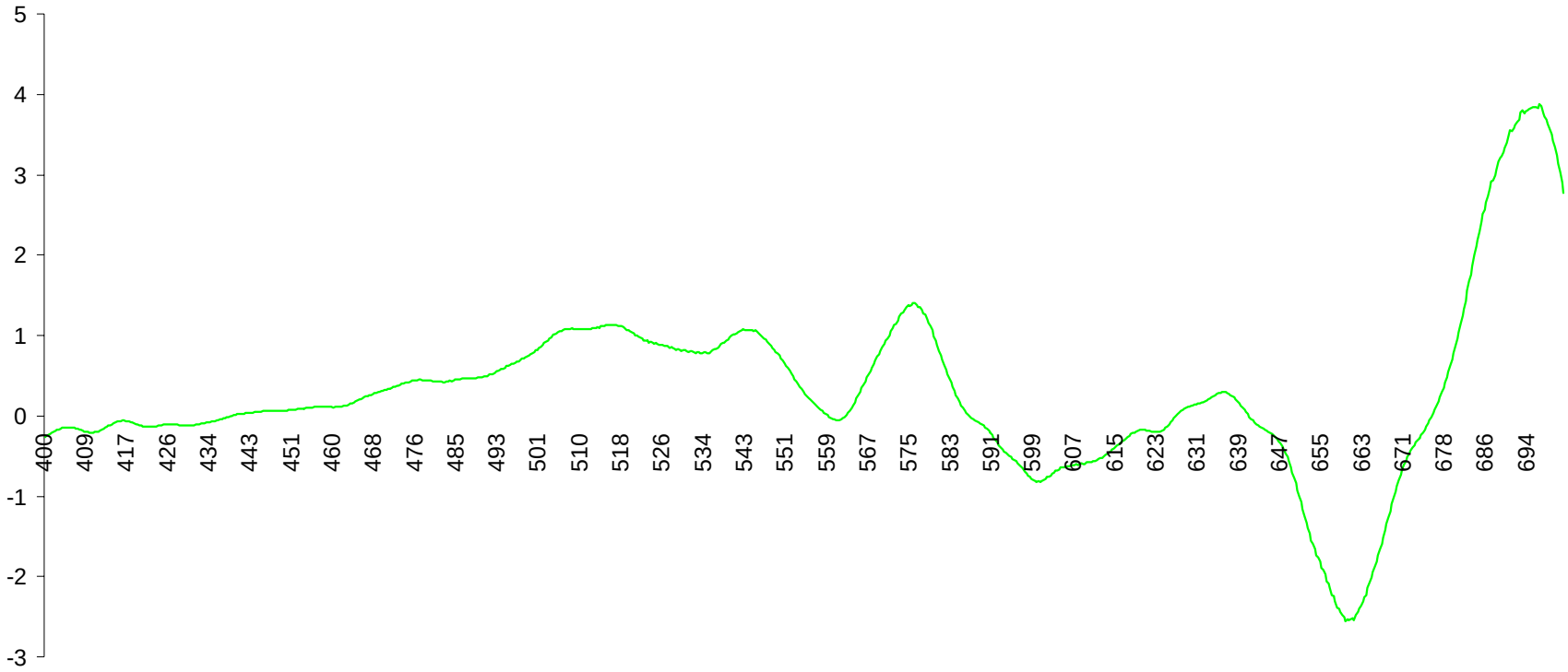

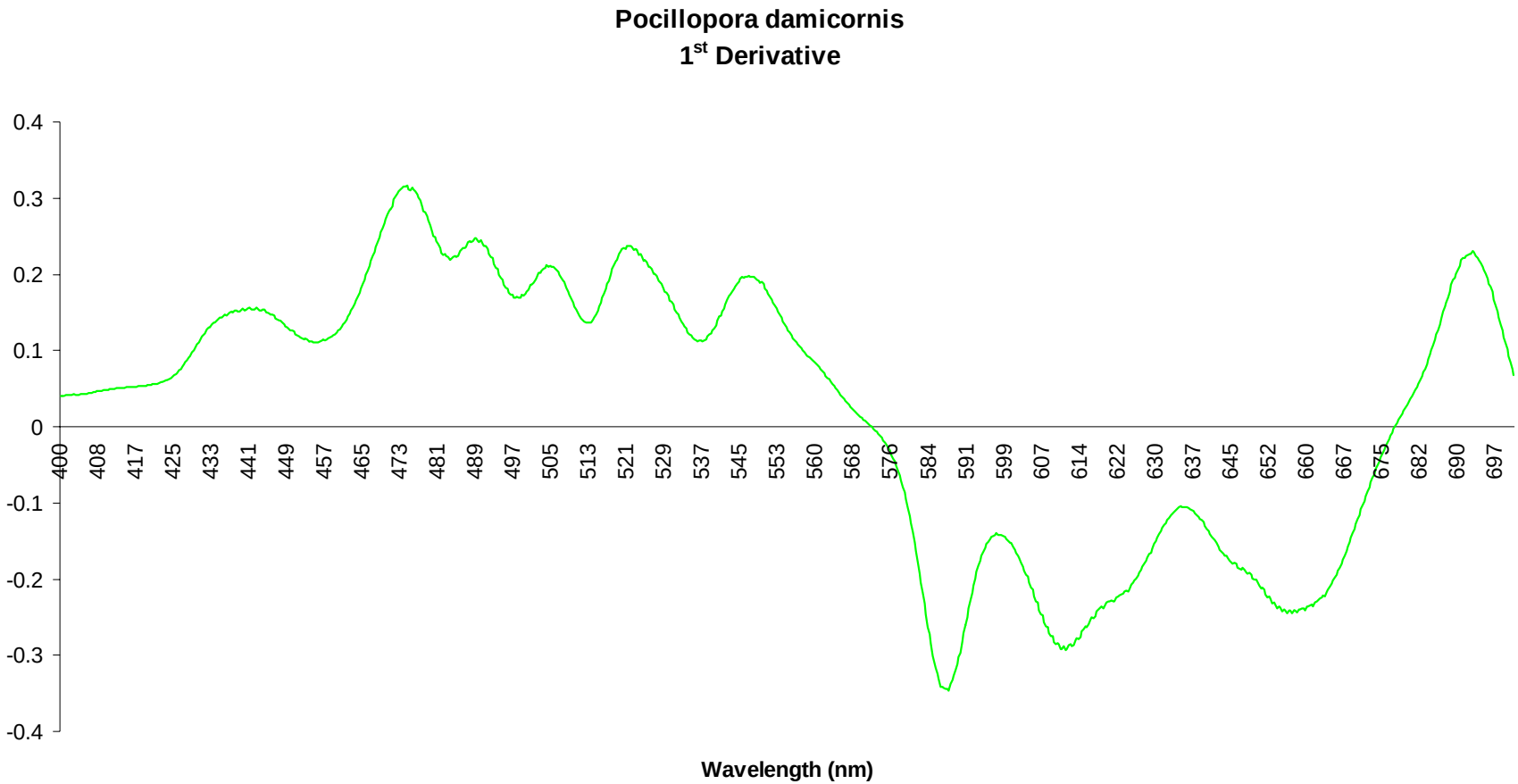
Pocillopora damicornis
1st Derivative
0.4
0.3
0.2
0.1
0
-0.1
-0.2
-0.3
-0.4
400
408
417
425
433
441
449
457
465
473
481
489
497
505
513
521
529
537
545
553
560
568
576
584
591
599
607
614
622
630
637
645
652
660
667
675
682
690
697
Wavelength (nm)

**_Montipora_ spp. 2**
**1st Derivative**

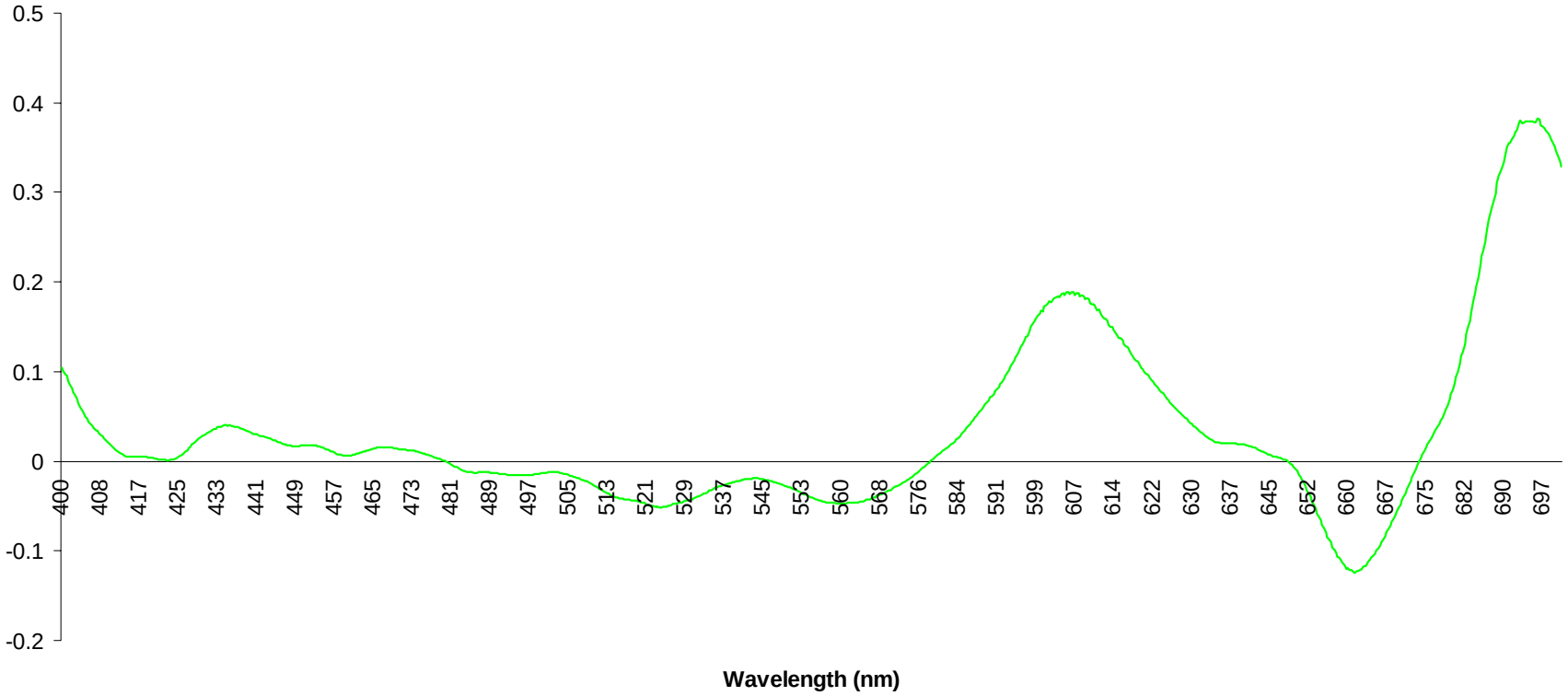

**_Montipora_ spp. 3**
**1st Derivative**

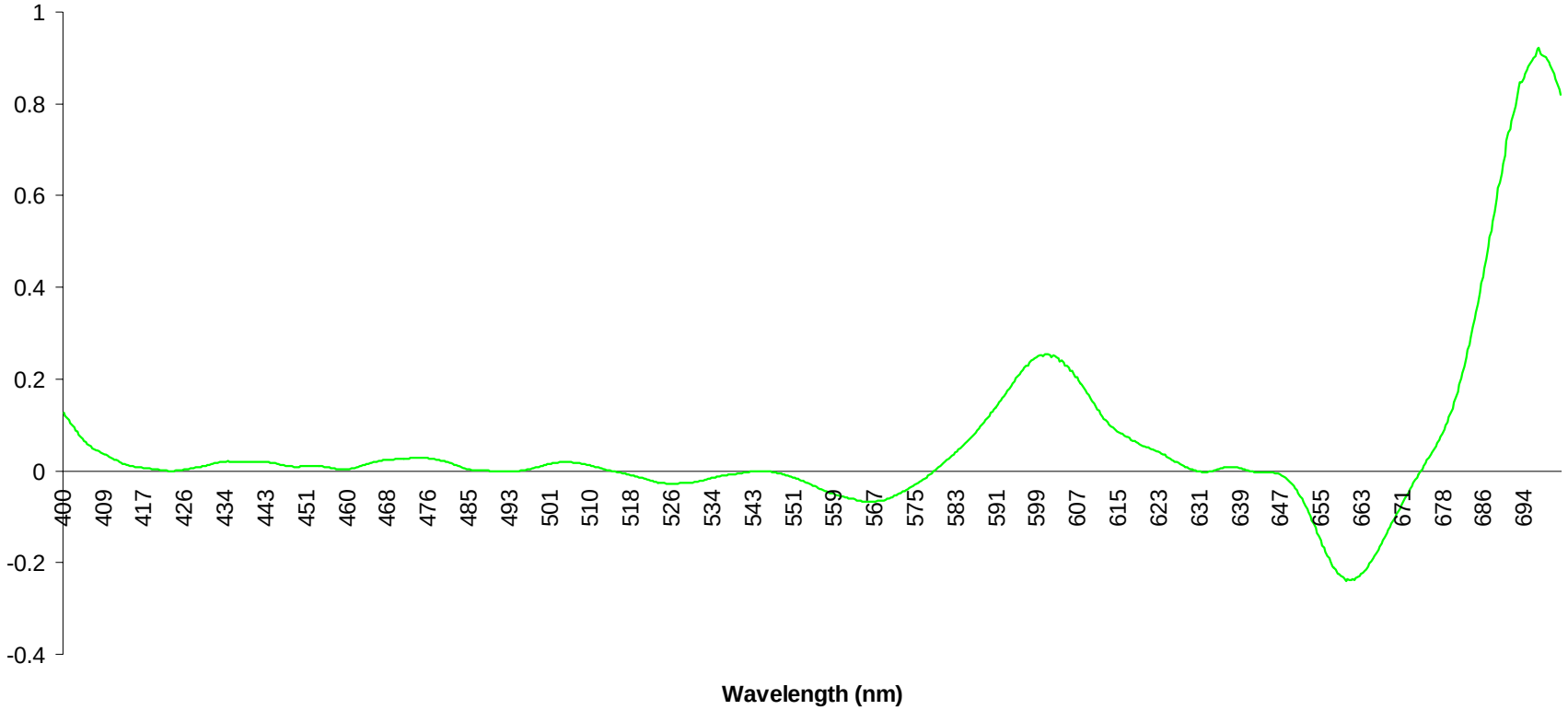

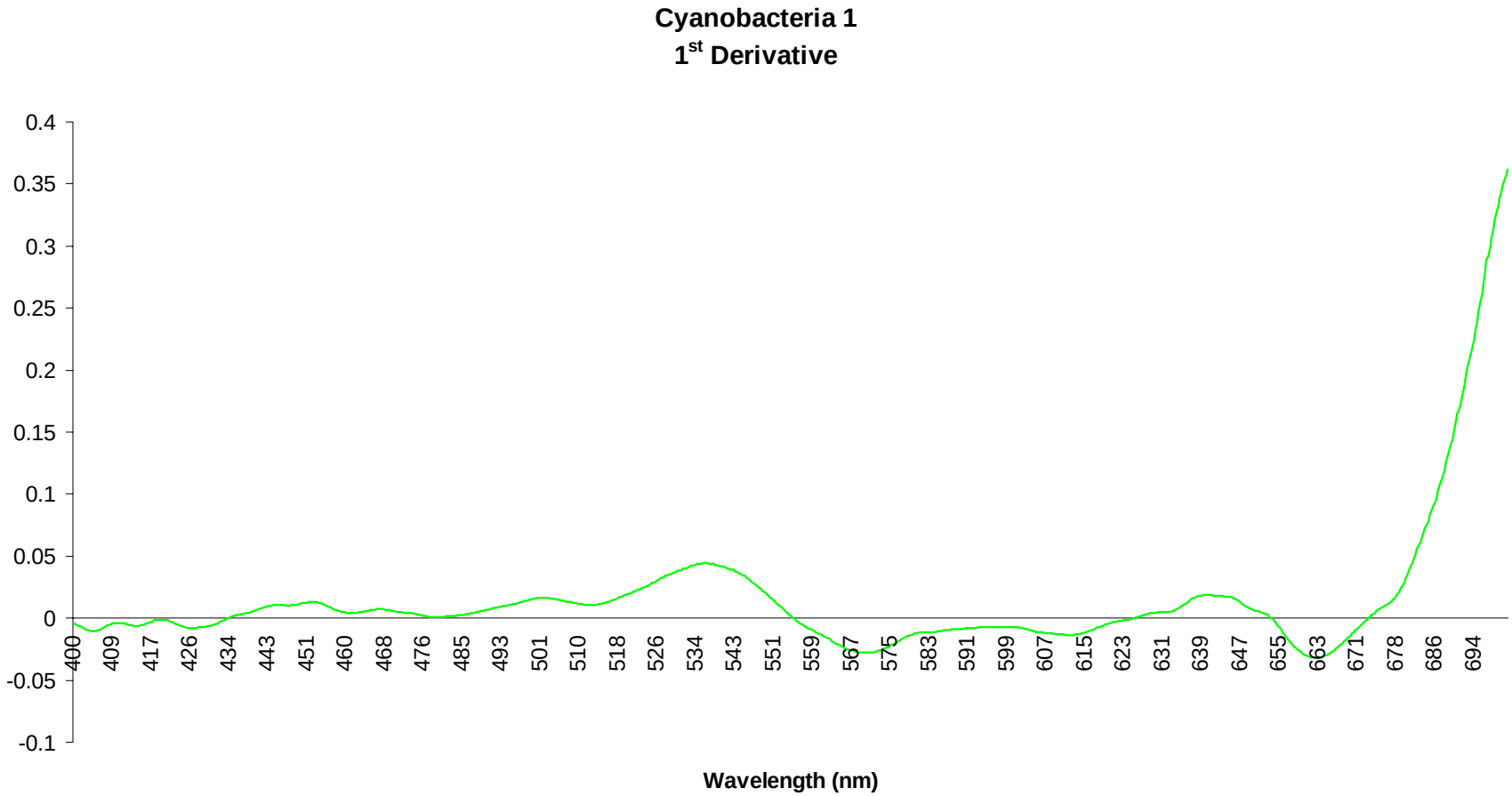
Cyanobacteria 1
1st Derivative
0.4
0.35
0.3
0.25
0.2
0.15
0.1
0.05
0
-0.05
-0.1
400
409
417
426
434
443
451
460
468
476
485
493
501
510
518
526
534
543
551
559
567
575
583
591
599
607
615
623
631
639
647
655
663
671
678
686
694
Wavelength (nm)

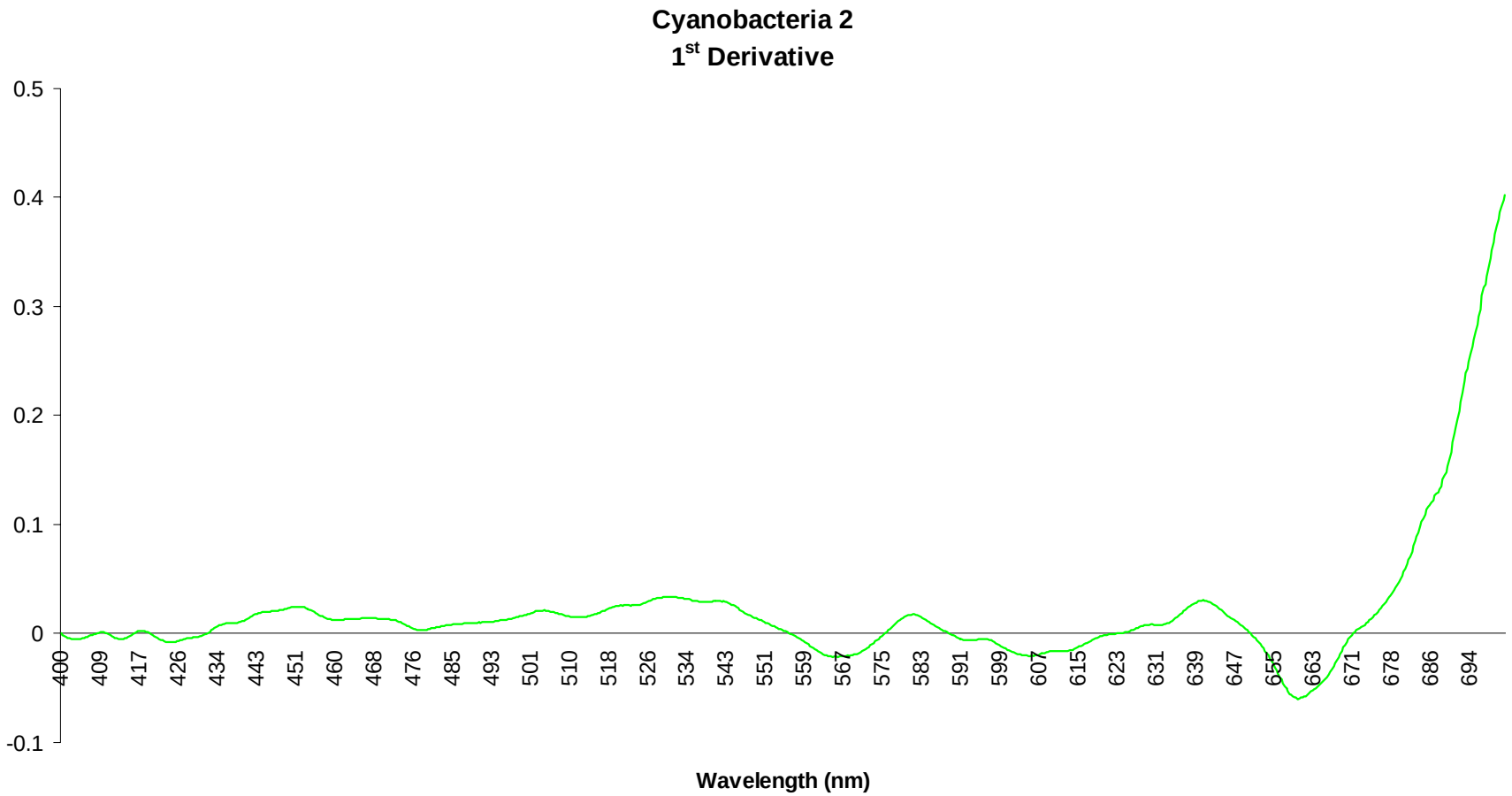
Cyanobacteria 2
1st Derivative
0.5
0.4
0.3
0.2
0.1
0
-0.1
400
409
417
426
434
443
451
460
468
476
485
493
501
510
518
526
534
543
551
559
567
575
583
591
599
607
615
623
631
639
647
655
663
671
678
686
694
Wavelength (nm)

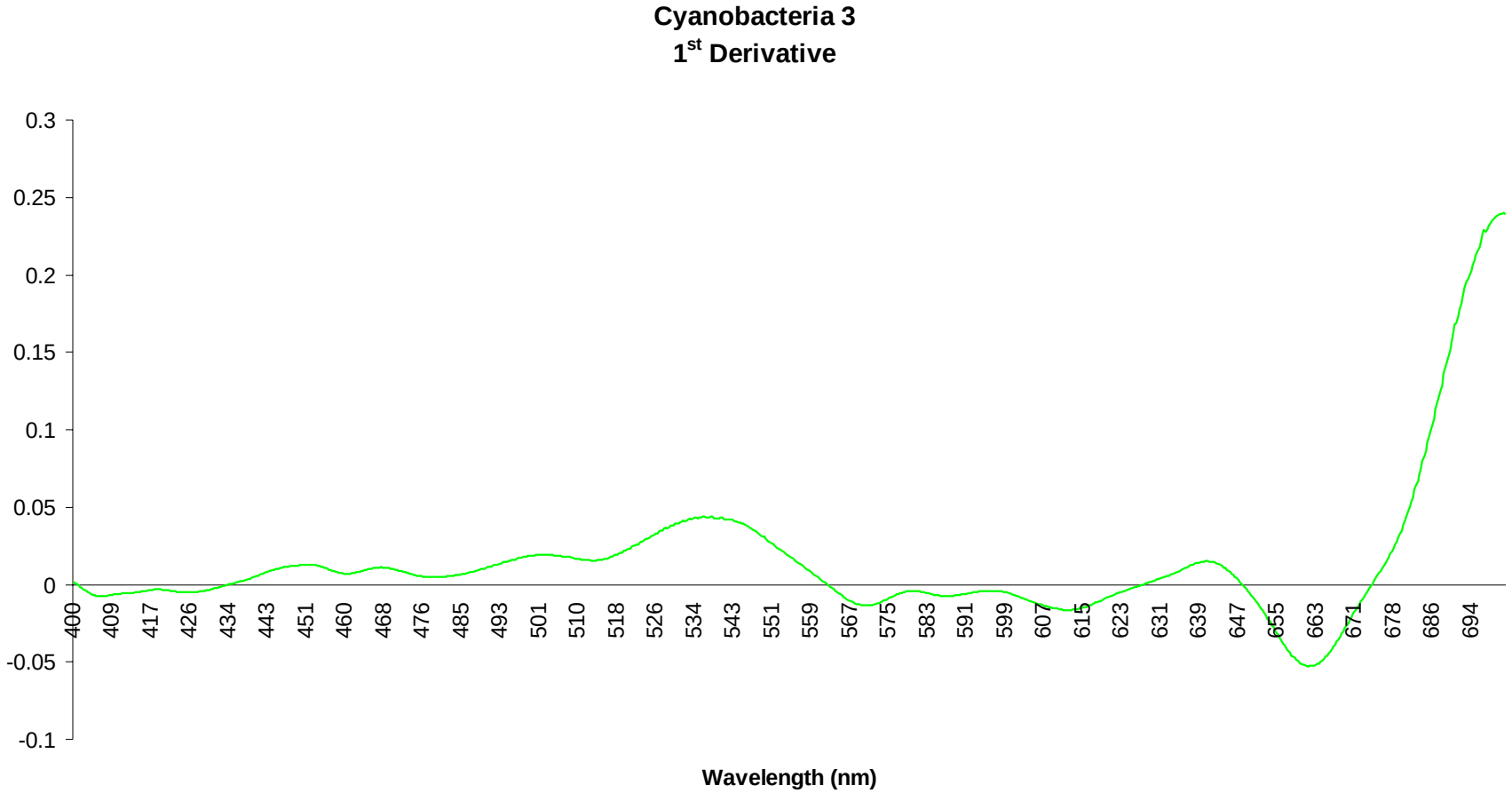
Cyanobacteria 3
1st Derivative
0.3
0.25
0.2
0.15
0.1
0.05
0
-0.05
-0.1
400
409
417
426
434
443
451
460
468
476
485
493
501
510
518
526
534
543
551
559
567
575
583
591
599
607
615
623
631
639
647
655
663
671
678
686
694
Wavelength (nm)

**Montipora spp. 4**
**1st Derivative**

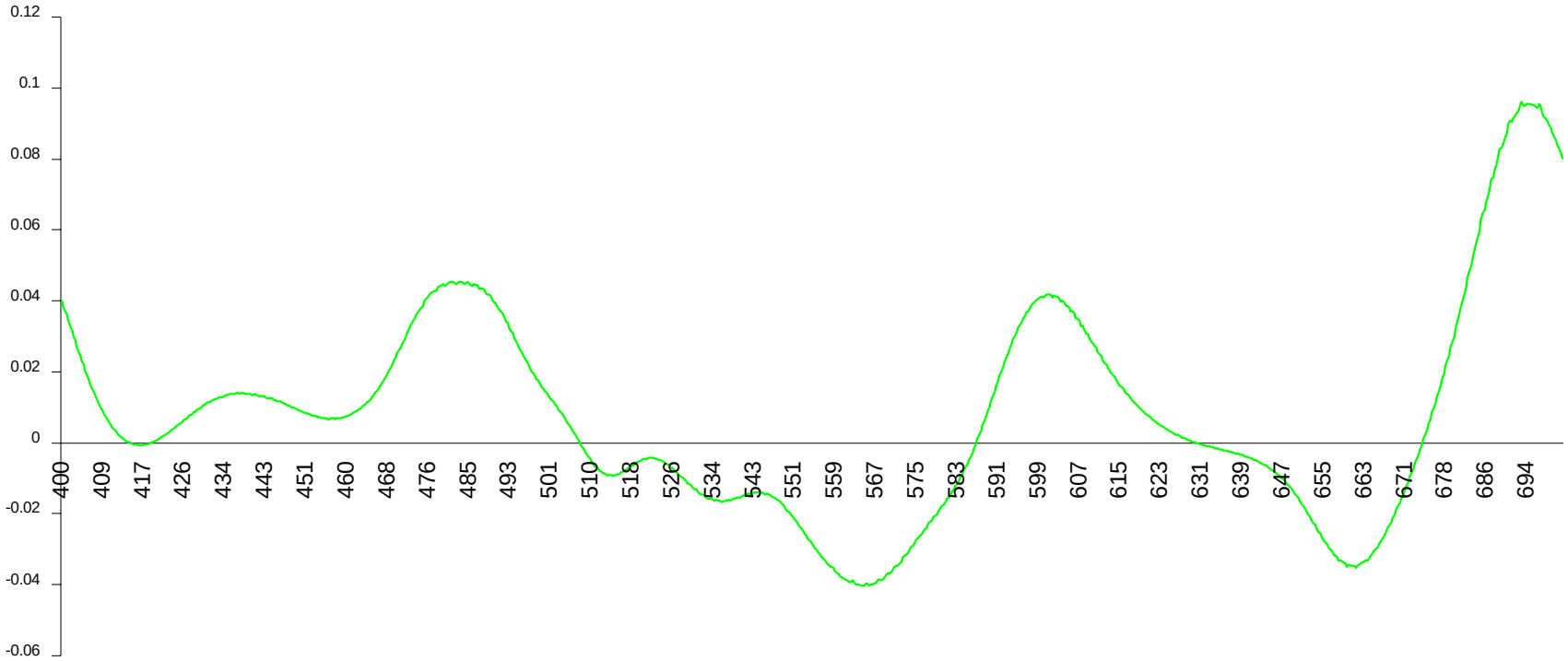

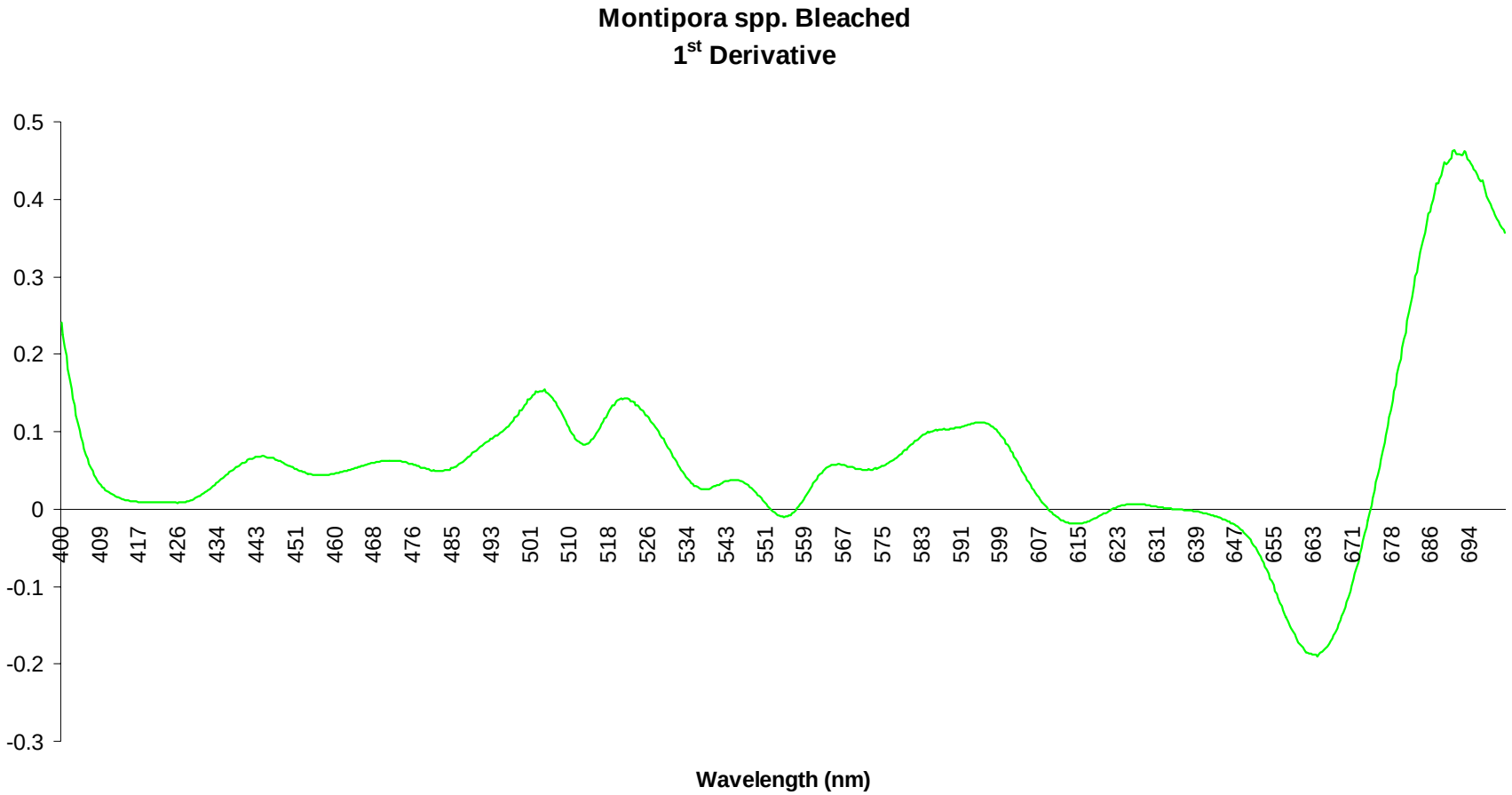
Montipora spp. Bleached
1st Derivative
0.5
0.4
0.3
0.2
0.1
0
-0.1
-0.2
-0.3
400
409
417
426
434
443
451
460
468
476
485
493
501
510
518
526
534
543
551
559
567
575
583
591
599
607
615
623
631
639
647
655
663
671
678
686
694
Wavelength (nm)

**Cyanobacteria 4**
**1st Derivative**

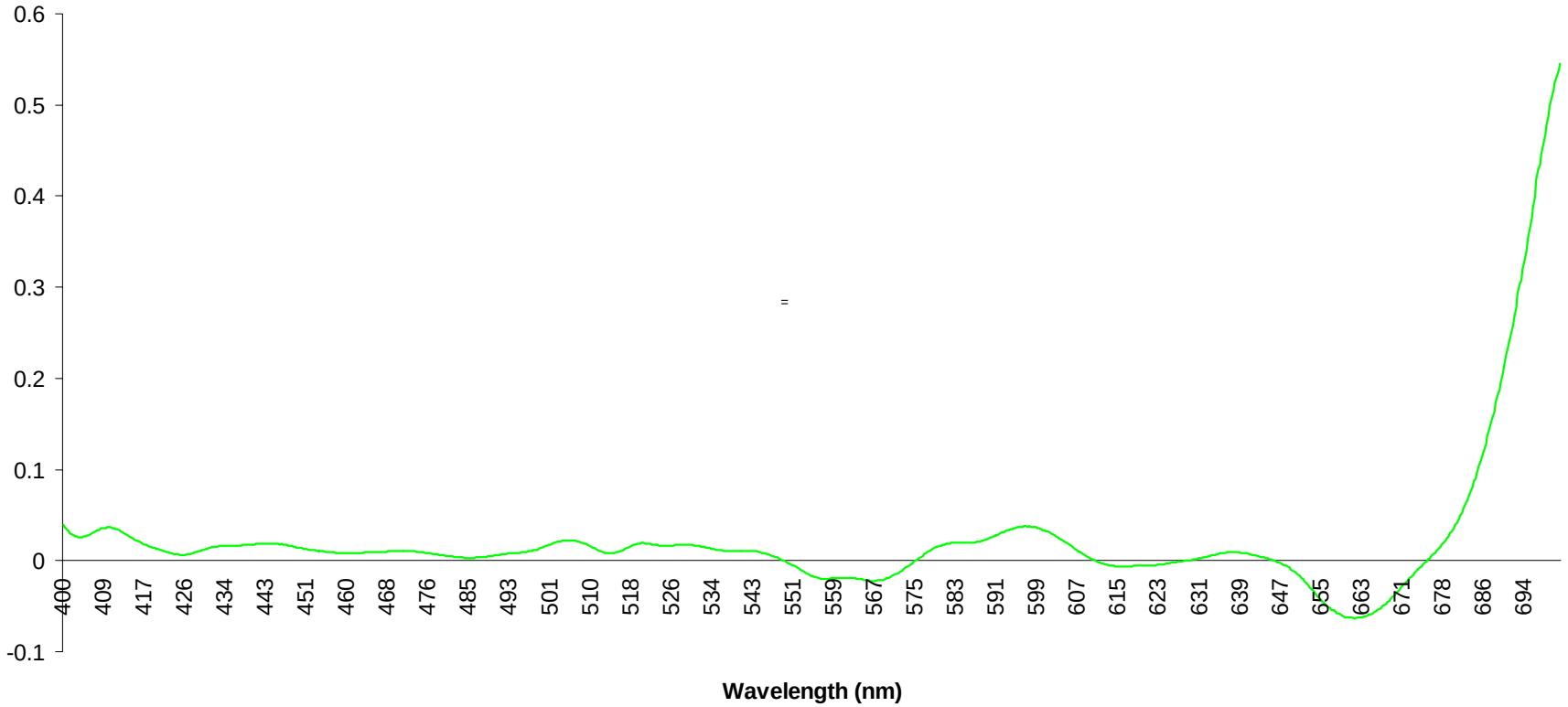

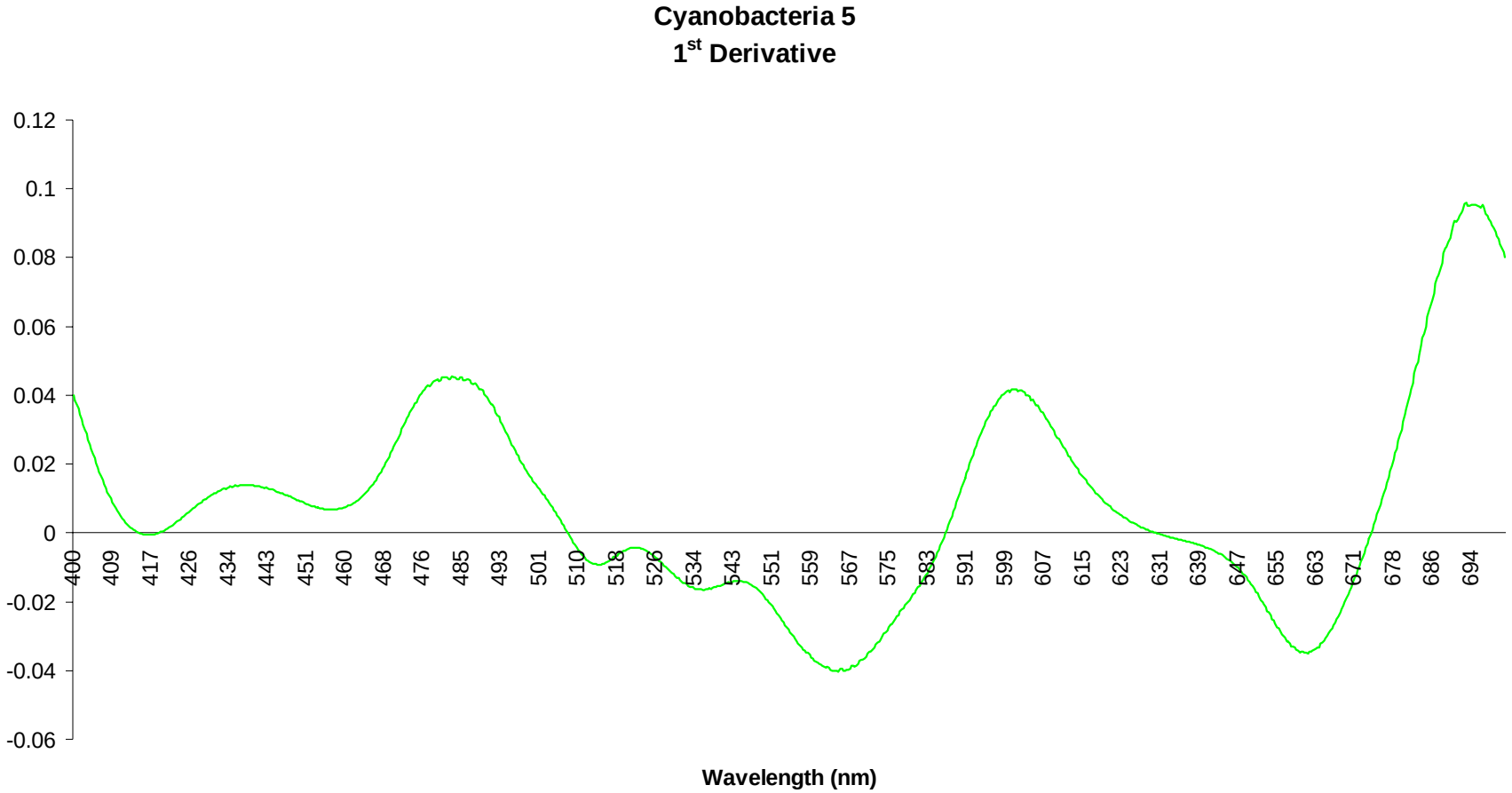
Cyanobacteria 5
1st Derivative
0.12
0.1
0.08
0.06
0.04
0.02
0
-0.02
-0.04
-0.06
400
409
417
426
434
443
451
460
468
476
485
493
501
510
518
526
534
543
551
559
567
575
583
591
599
607
615
623
631
639
647
655
663
671
678
686
694
Wavelength (nm)

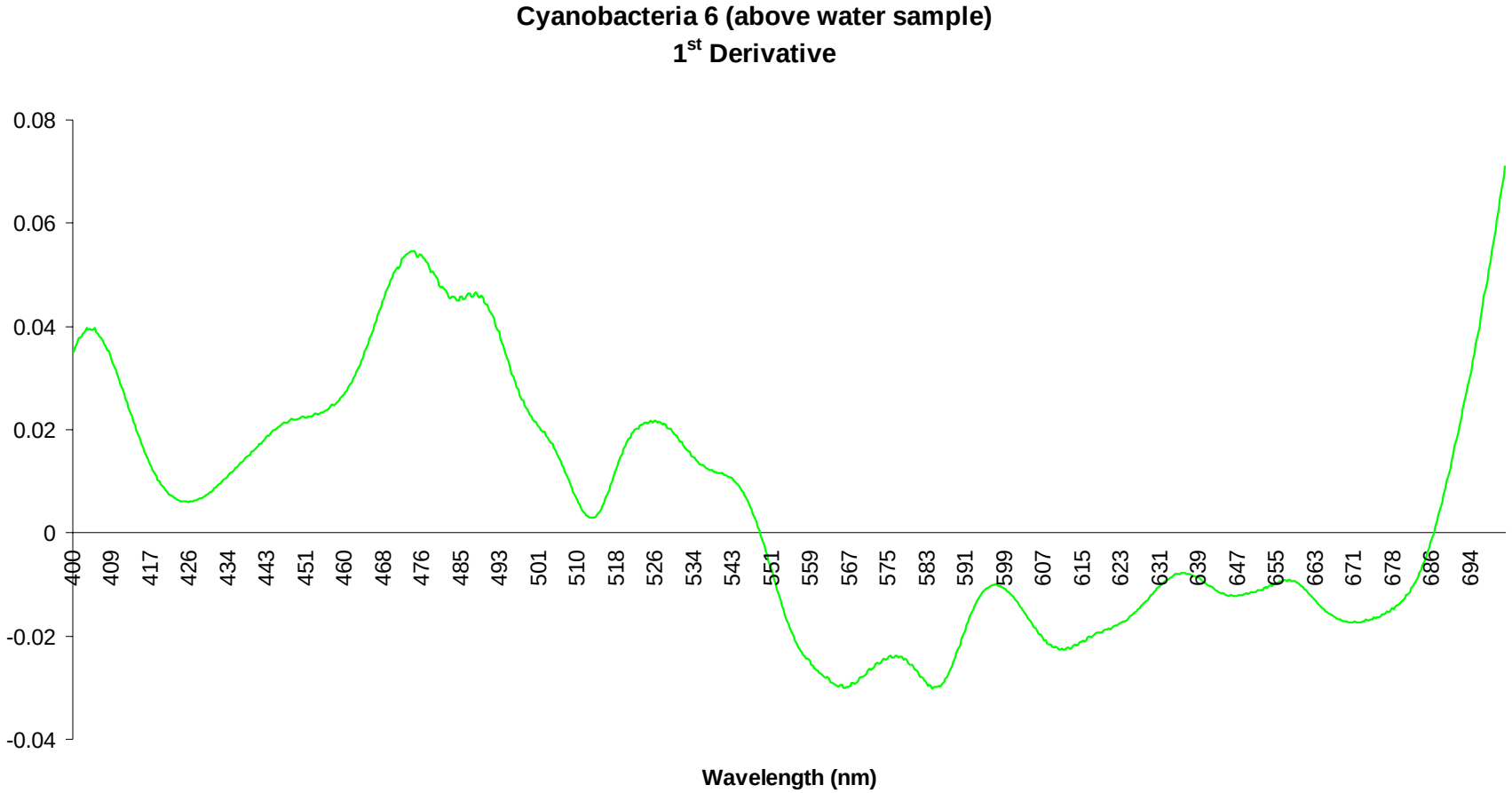
Cyanobacteria 6 (above water sample)
1st Derivative
0.08
0.06
0.04
0.02
0
-0.02
-0.04
400
409
417
426
434
443
451
460
468
476
485
493
501
510
518
526
534
543
551
559
567
575
583
591
599
607
615
623
631
639
647
655
663
671
678
686
694
Wavelength (nm)

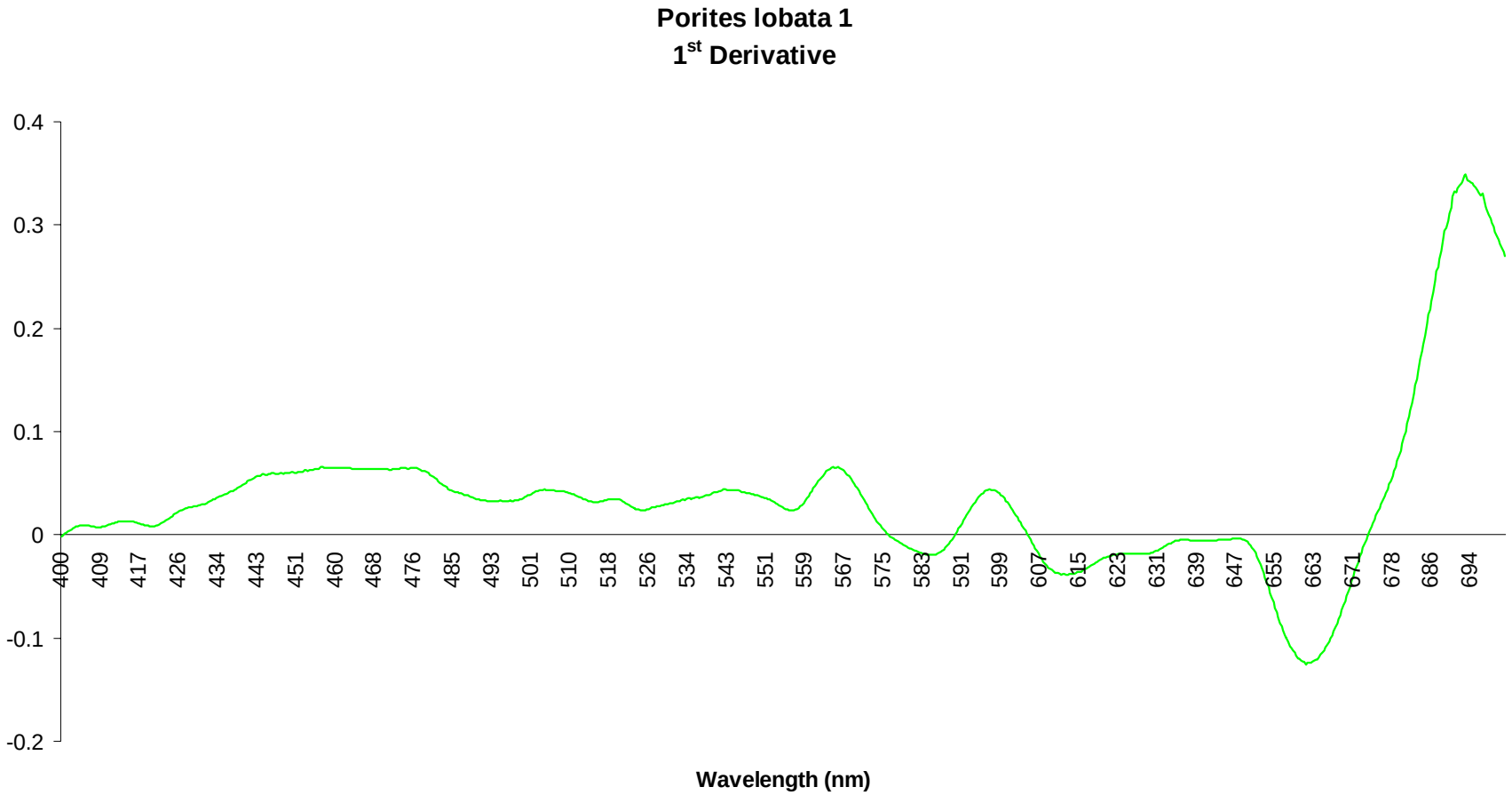
Porites lobata 1
1st Derivative
0.4
0.3
0.2
0.1
0
-0.1
-0.2
400
409
417
426
434
443
451
460
468
476
485
493
501
510
518
526
534
543
551
559
567
575
583
591
599
607
615
623
631
639
647
655
663
671
678
686
694
Wavelength (nm)

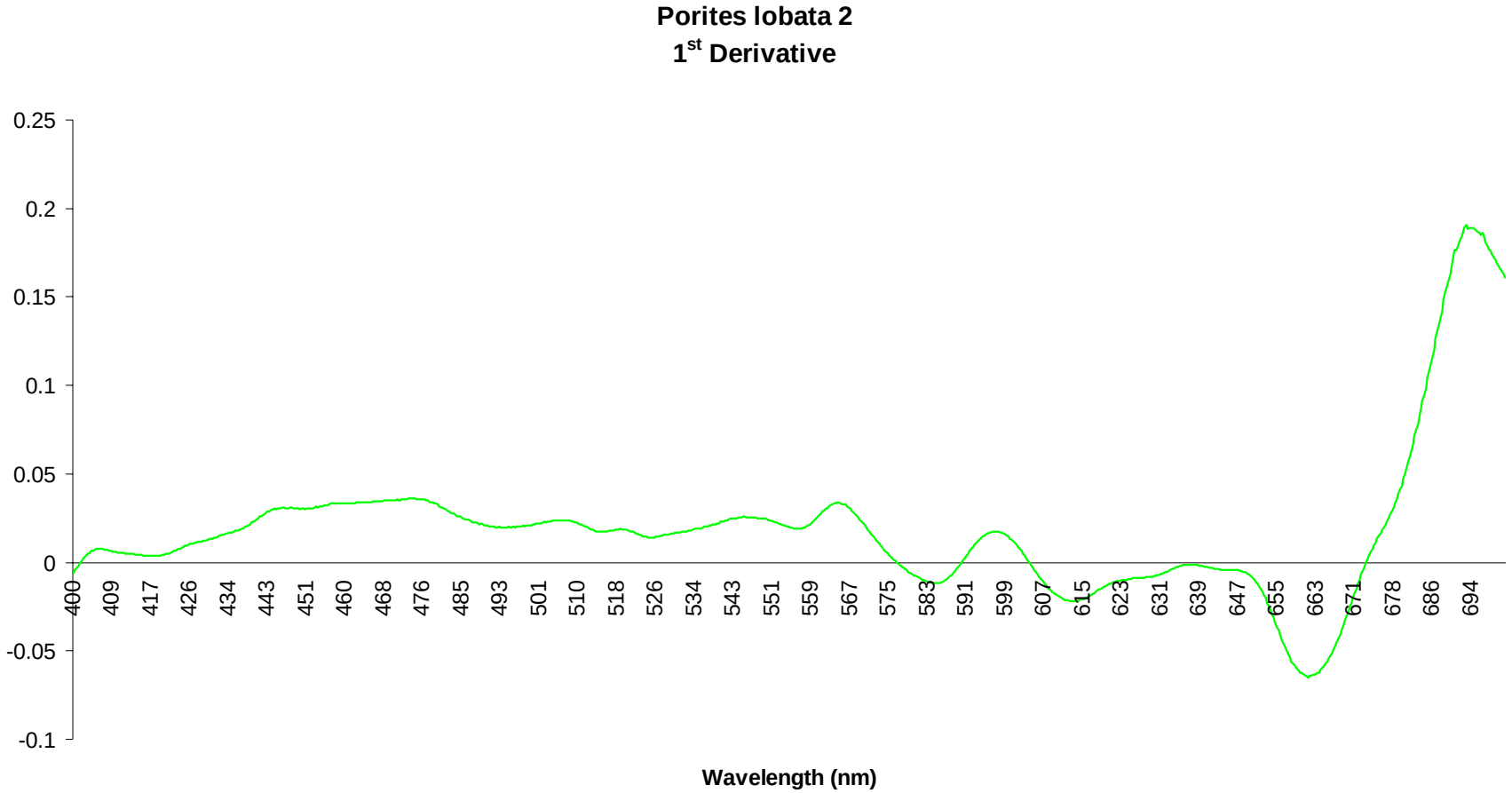
Porites lobata 2
1st Derivative
0.25
0.2
0.15
0.1
0.05
0
-0.05
-0.1
400
409
417
426
434
443
451
460
468
476
485
493
501
510
518
526
534
543
551
559
567
575
583
591
599
607
615
623
631
639
647
655
663
671
678
686
694
Wavelength (nm)

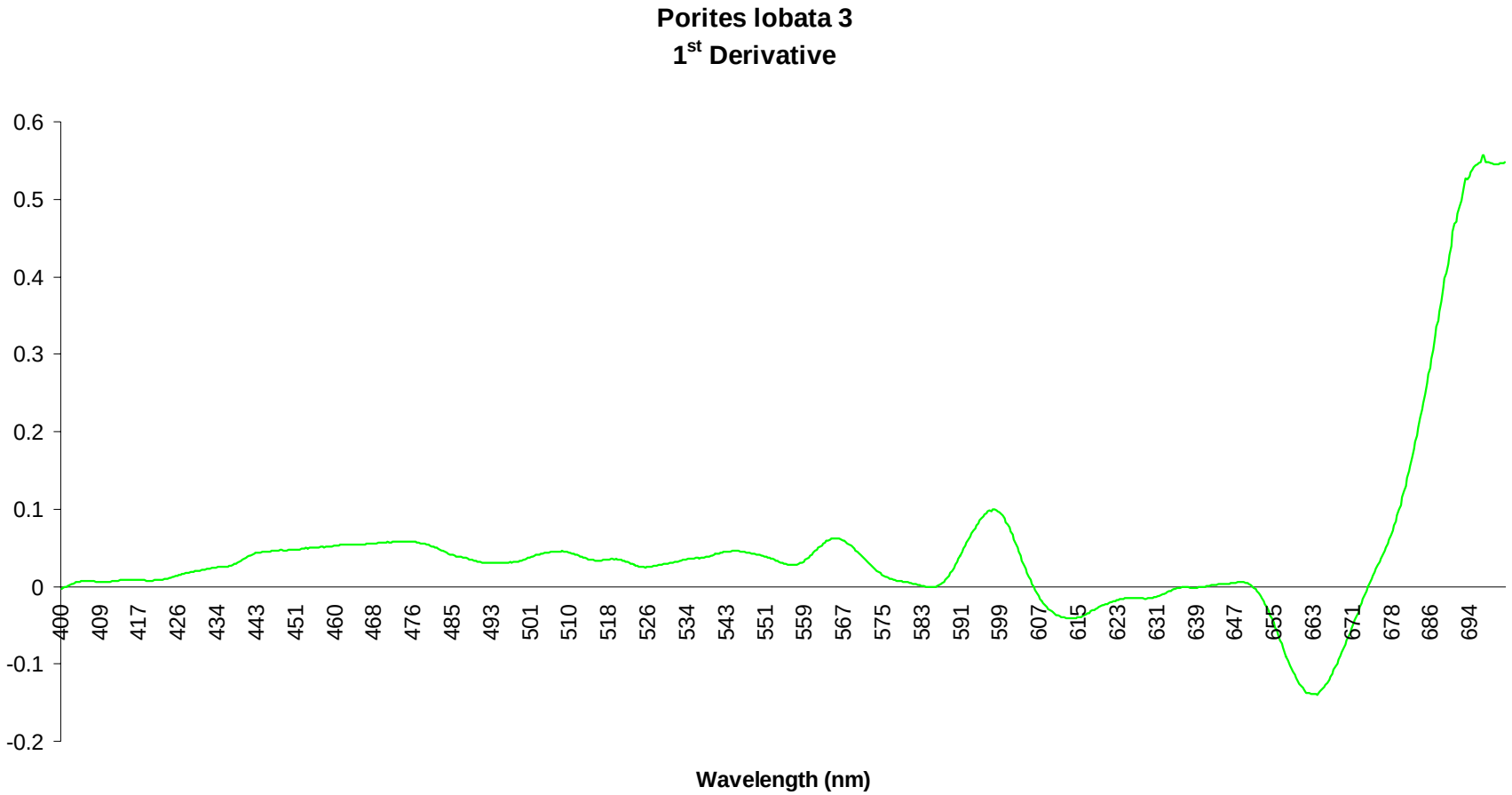
Porites lobata 3
1st Derivative
0.6
0.5
0.4
0.3
0.2
0.1
0
-0.1
-0.2
400
409
417
426
434
443
451
460
468
476
485
493
501
510
518
526
534
543
551
559
567
575
583
591
599
607
615
623
631
639
647
655
663
671
678
686
694
Wavelength (nm)

**Algae: Laurentia spp.**
**1st Derivative**

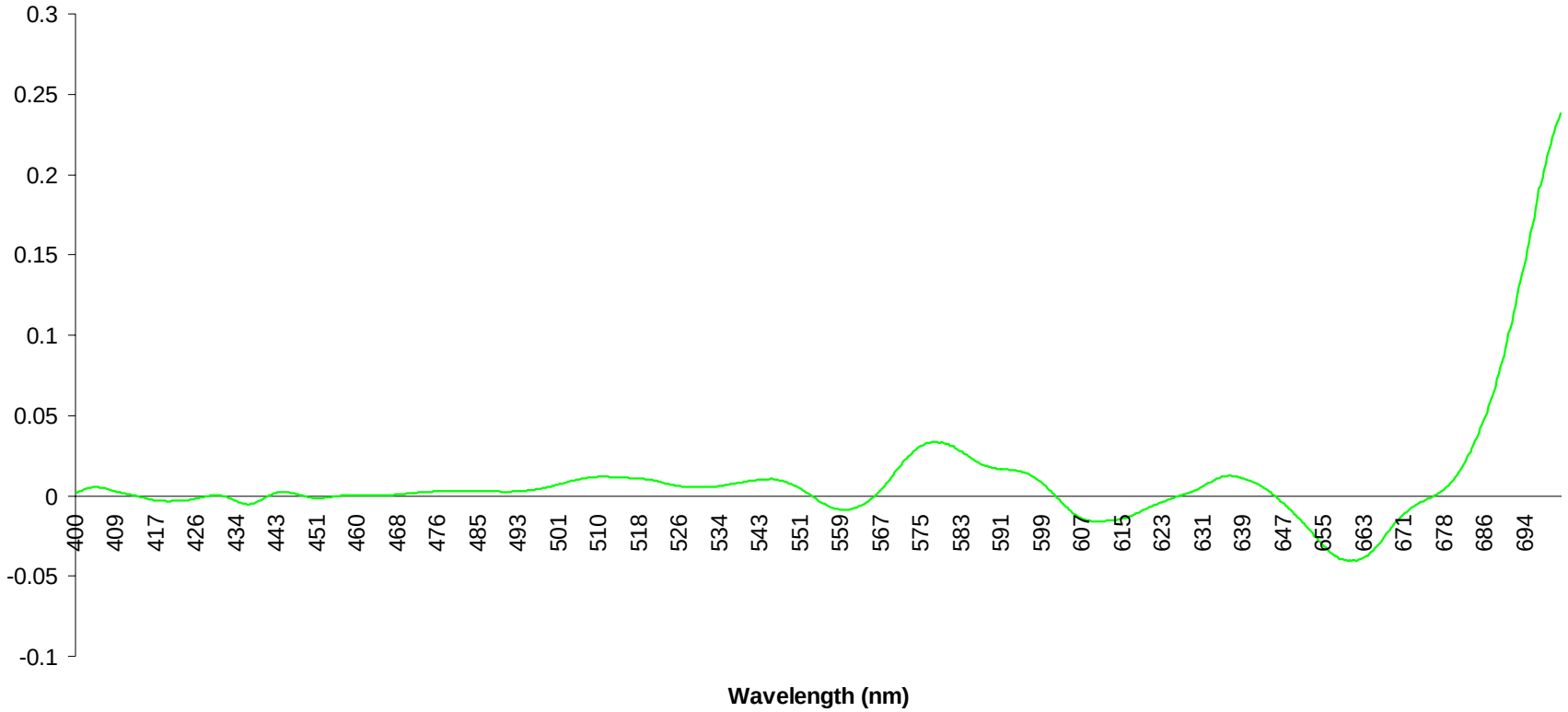

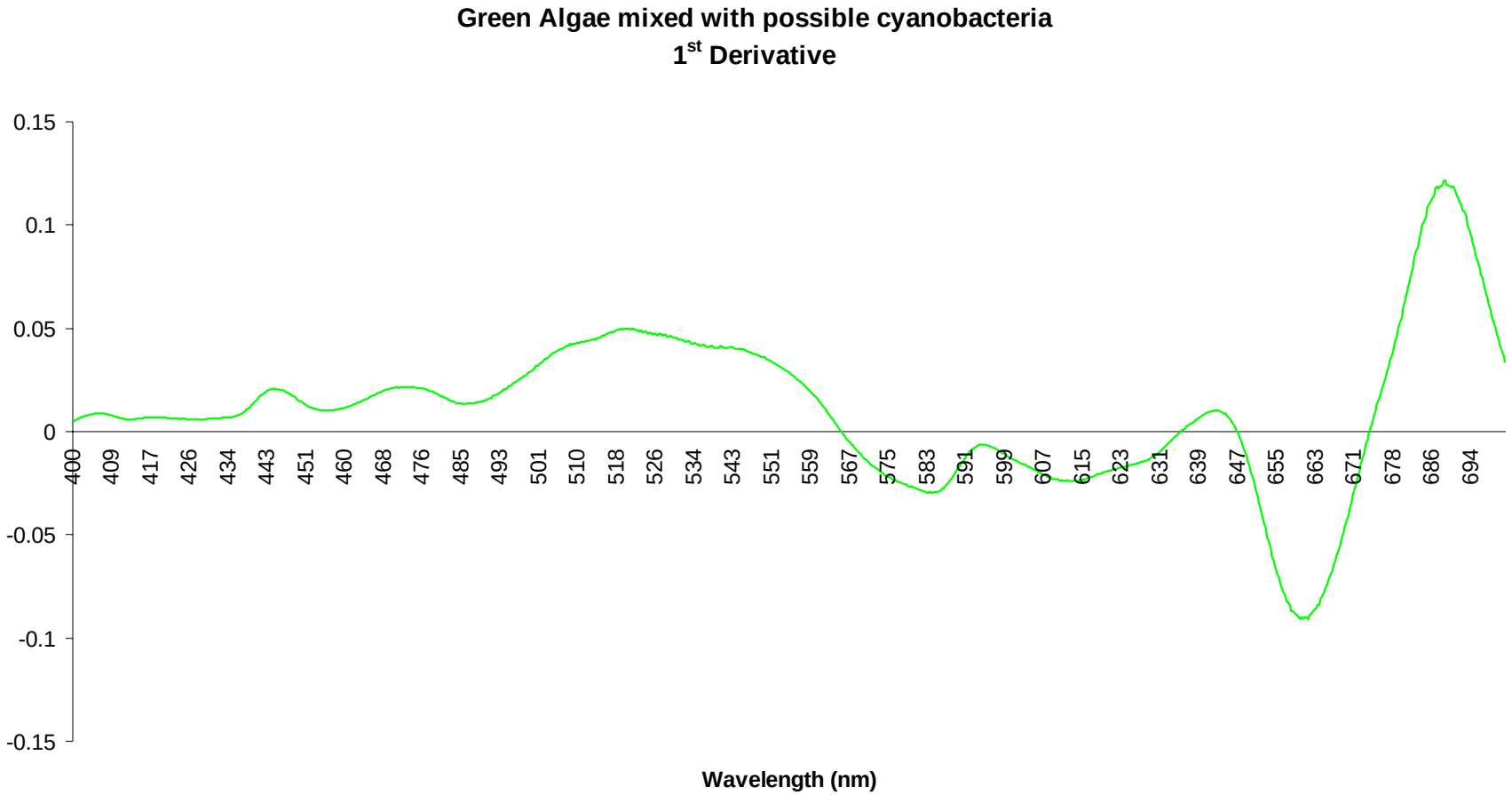
Green Algae mixed with possible cyanobacteria
1st Derivative
0.15
0.1
0.05
0
-0.05
-0.1
-0.15
400
409
417
426
434
443
451
460
468
476
485
493
501
510
518
526
534
543
551
559
567
575
583
591
599
607
615
623
631
639
647
655
663
671
678
686
694
Wavelength (nm)

# APPENDIX E. SECOND DERIVATIVE CHARTS

**Montipora spp. 1**
**2nd Derivative**

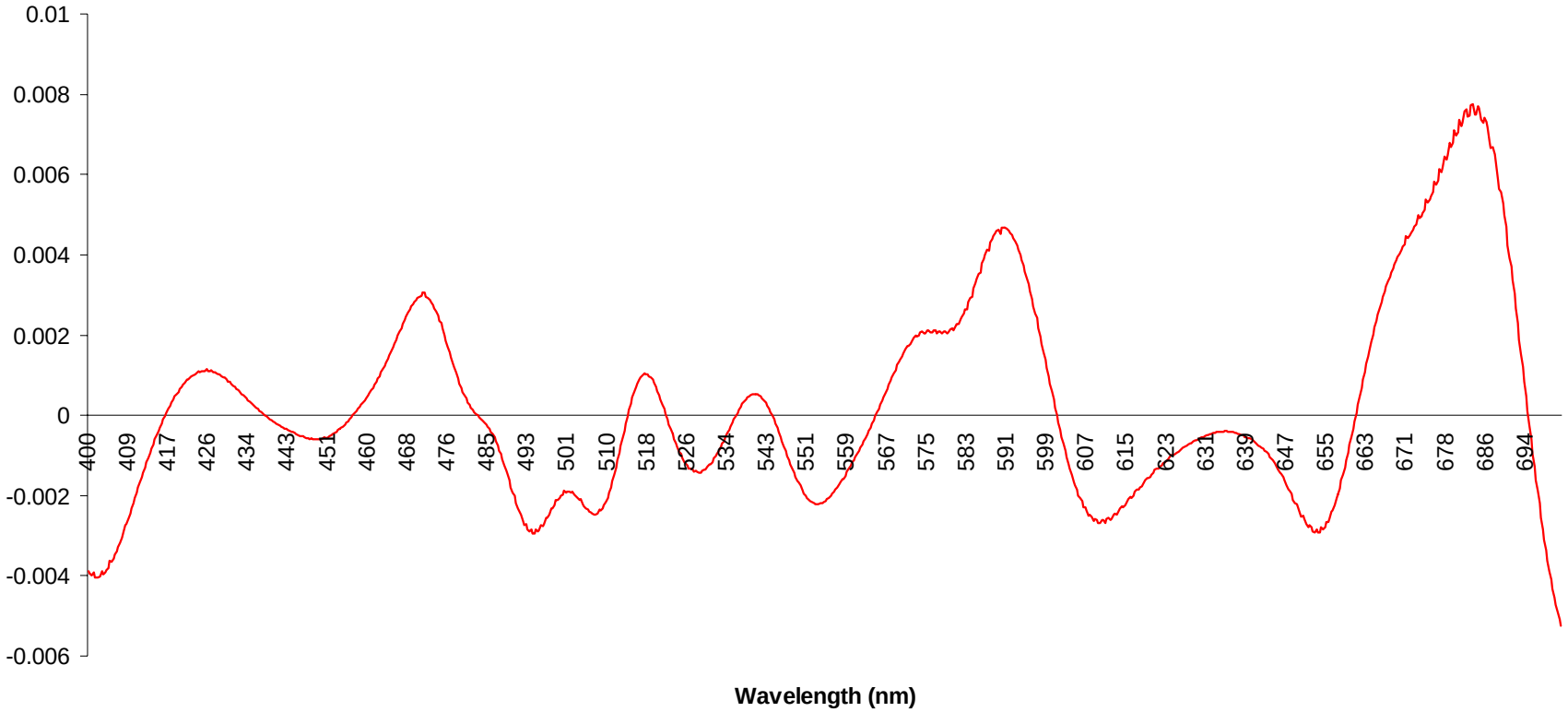

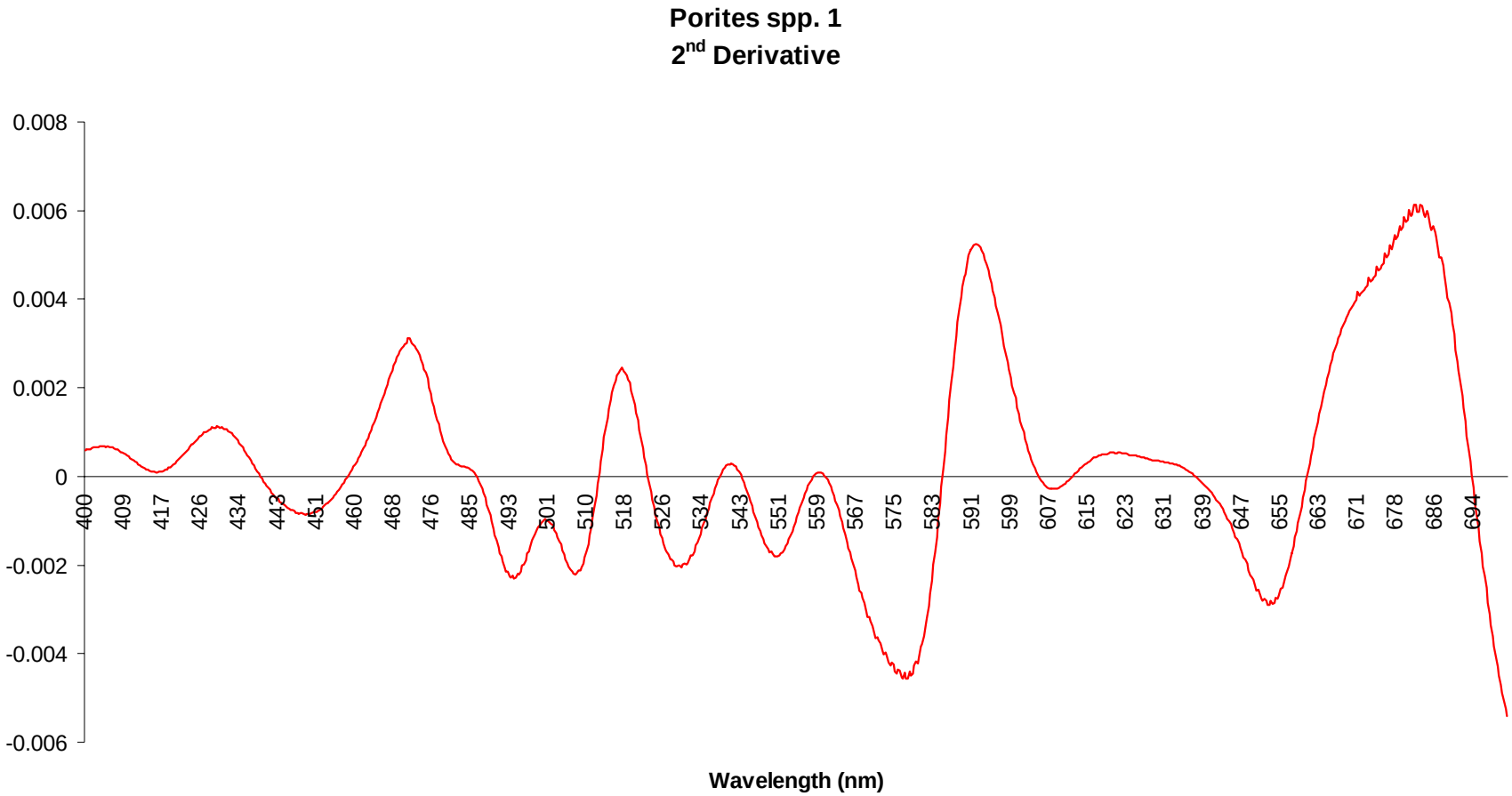
Porites spp. 1
2nd Derivative
0.008
0.006
0.004
0.002
0
-0.002
-0.004
-0.006
400
409
417
426
434
443
451
460
468
476
485
493
501
510
518
526
534
543
551
559
567
575
583
591
599
607
615
623
631
639
647
655
663
671
678
686
694
Wavelength (nm)

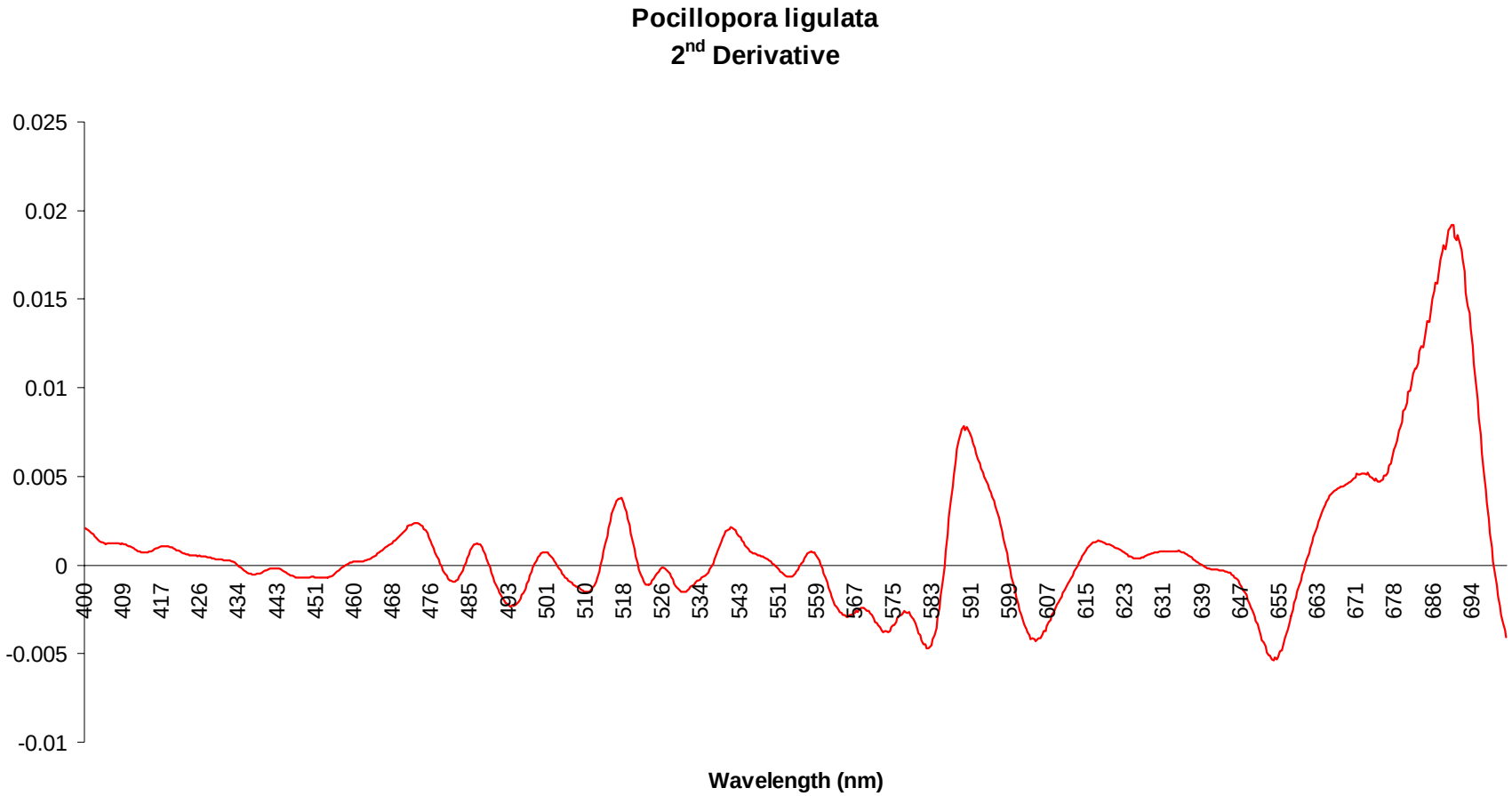
Pocillopora ligulata
2nd Derivative
0.025
0.02
0.015
0.01
0.005
0
-0.005
-0.01
400
409
417
426
434
443
451
460
468
476
485
493
501
510
518
526
534
543
551
559
567
575
583
591
599
607
615
623
631
639
647
655
663
671
678
686
694
Wavelength (nm)

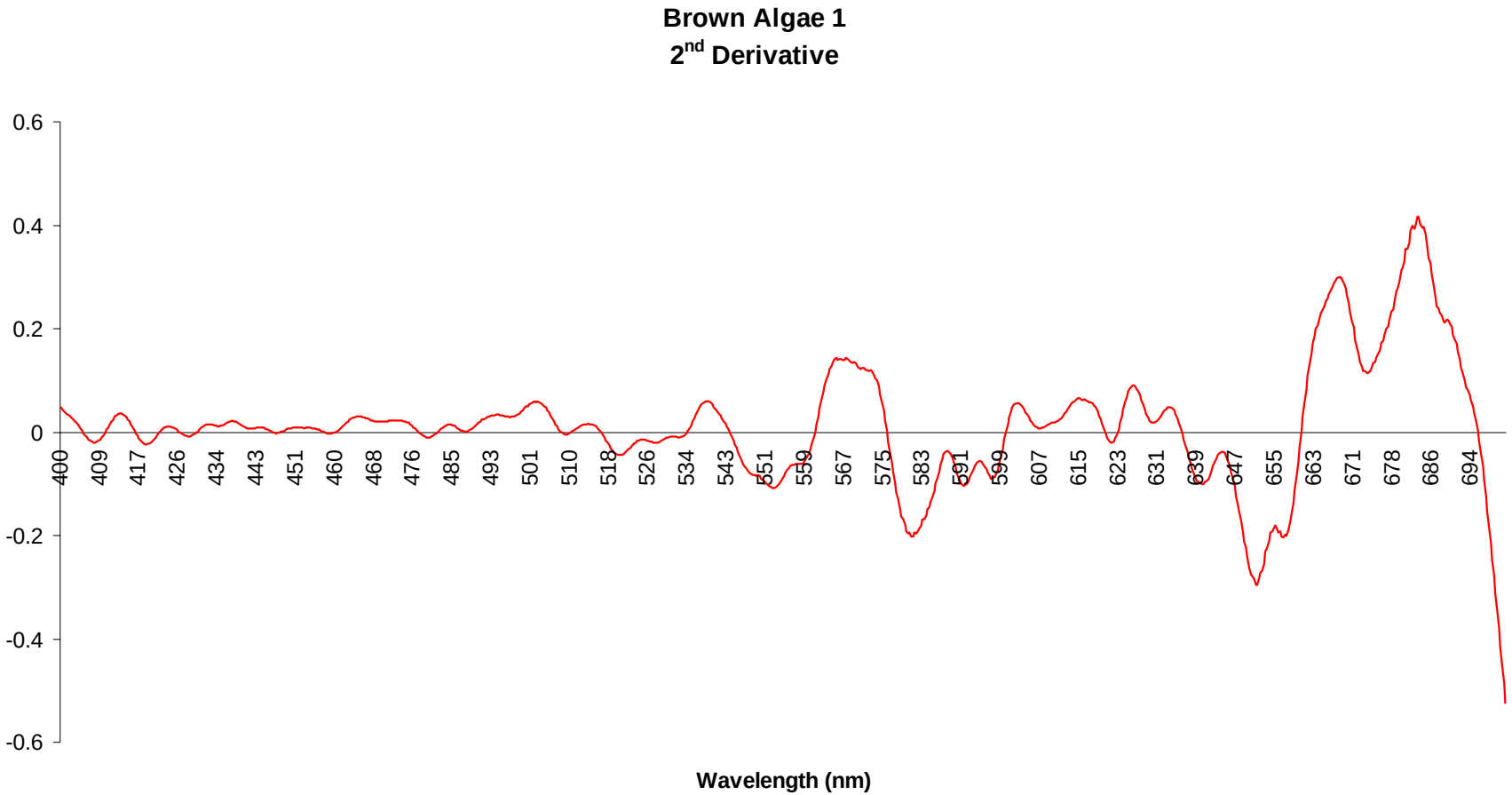
Brown Algae 1
2nd Derivative
0.6
0.4
0.2
0
-0.2
-0.4
-0.6
400
409
417
426
434
443
451
460
468
476
485
493
501
510
518
526
534
543
551
559
567
575
583
591
599
607
615
623
631
639
647
655
663
671
678
686
694
Wavelength (nm)

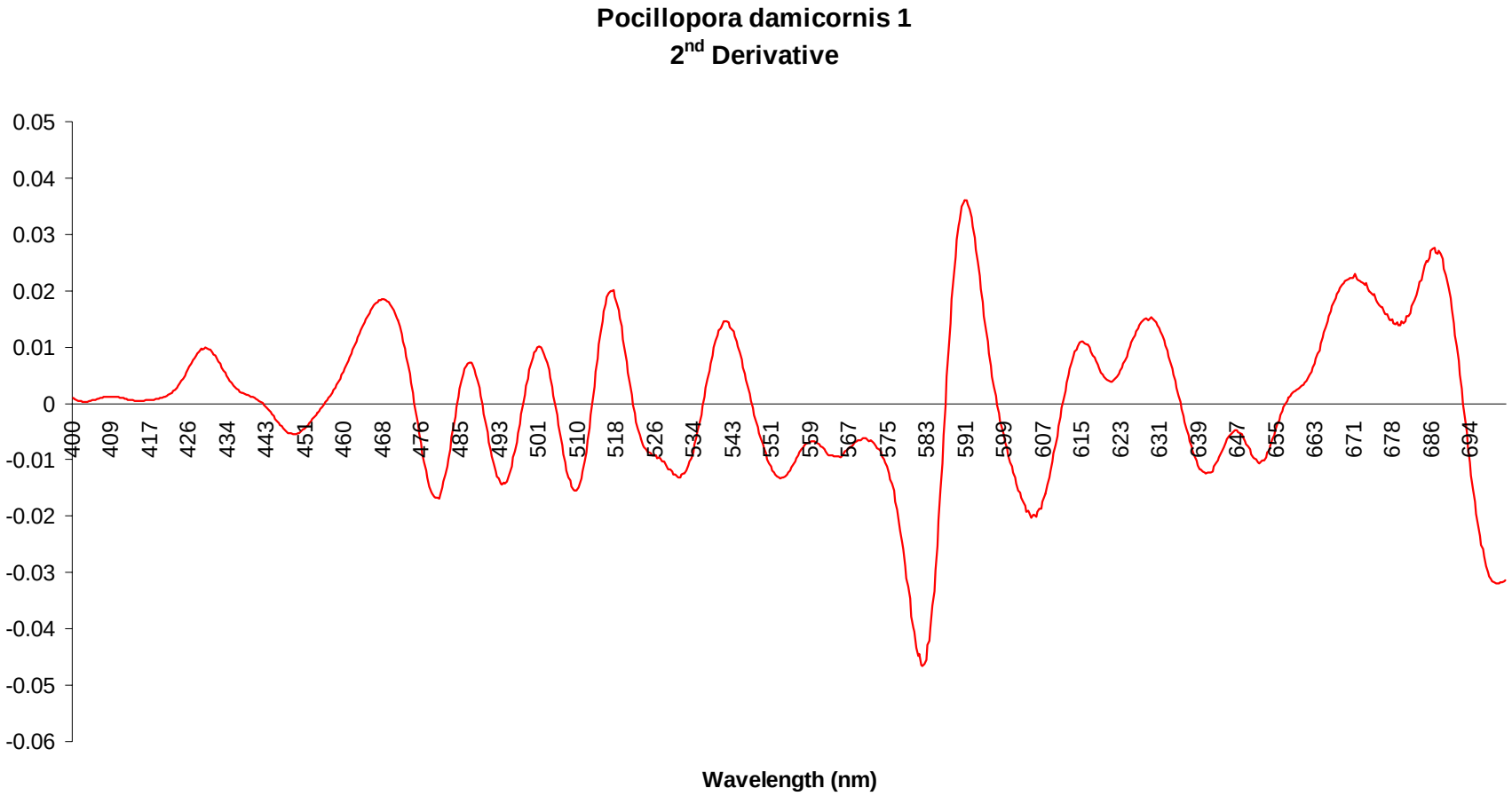
Pocillopora damicornis 1
2nd Derivative
0.05
0.04
0.03
0.02
0.01
0
-0.01
-0.02
-0.03
-0.04
-0.05
-0.06
400
409
417
426
434
443
451
460
468
476
485
493
501
510
518
526
534
543
551
559
567
575
583
591
599
607
615
623
631
639
647
655
663
671
678
686
694
Wavelength (nm)

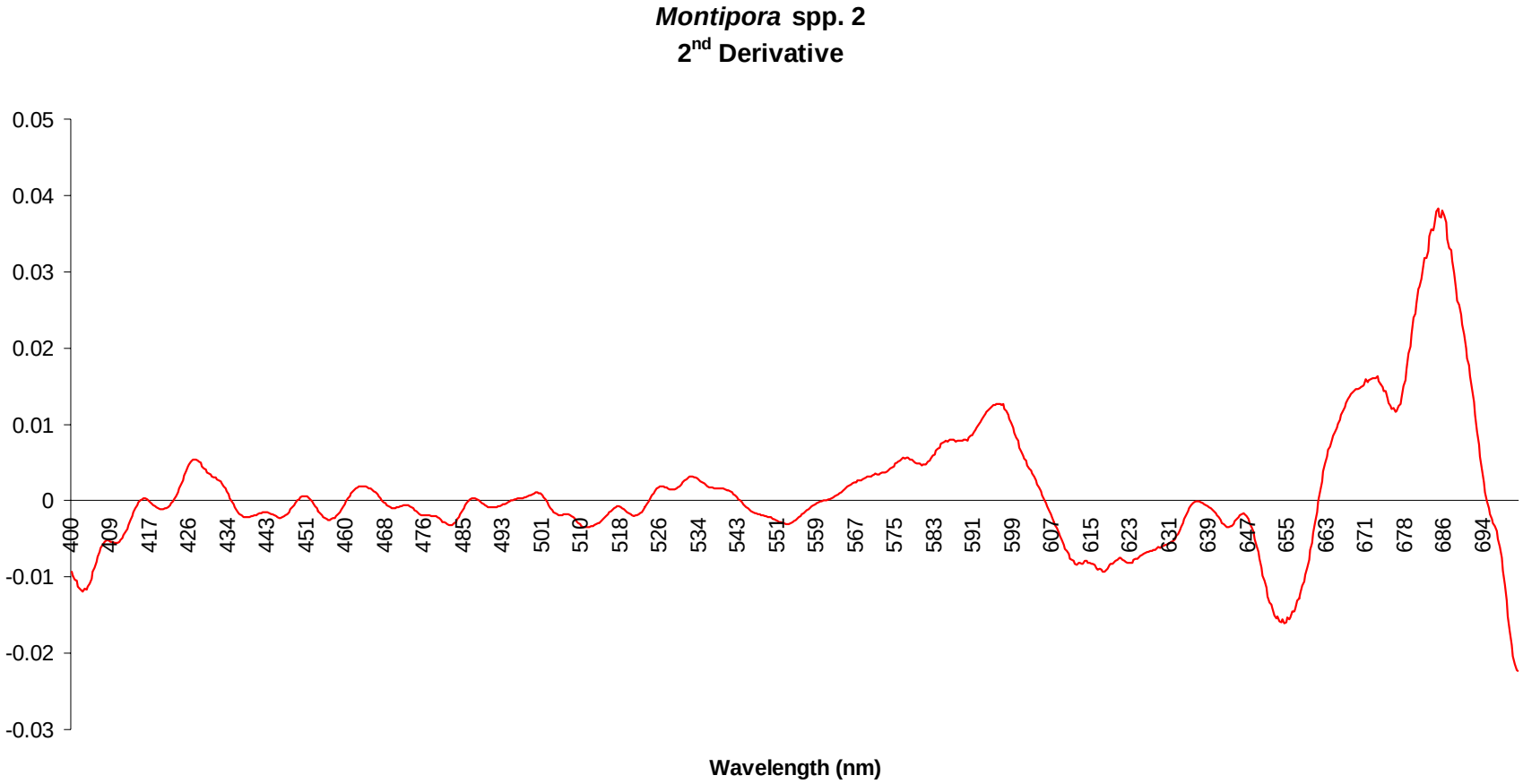
*Montipora* spp. 2
2nd Derivative
0.05
0.04
0.03
0.02
0.01
0
-0.01
-0.02
-0.03
400
409
417
426
434
443
451
460
468
476
485
493
501
510
518
526
534
543
551
559
567
575
583
591
599
607
615
623
631
639
647
655
663
671
678
686
694
Wavelength (nm)

**_Montipora_ spp. 3**
**2nd Derivative**

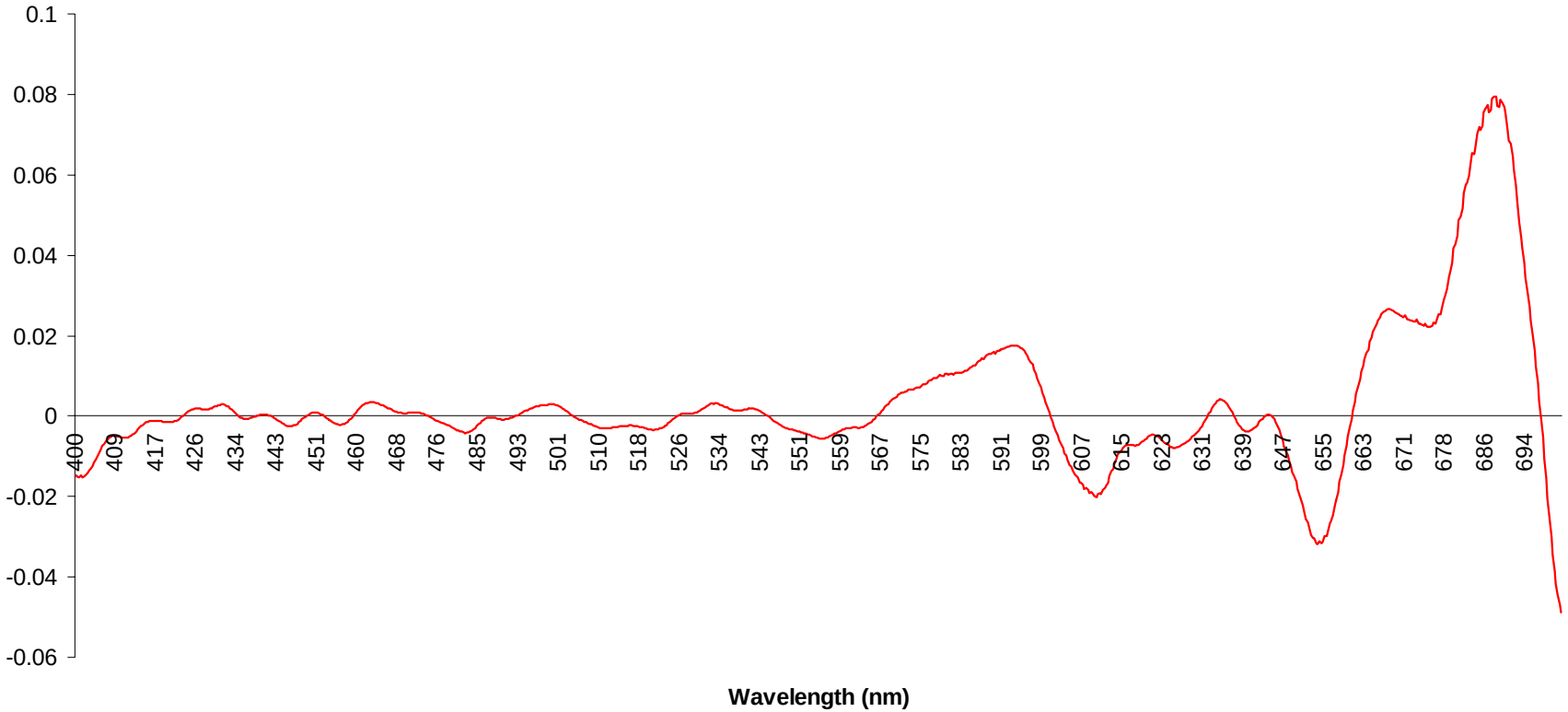

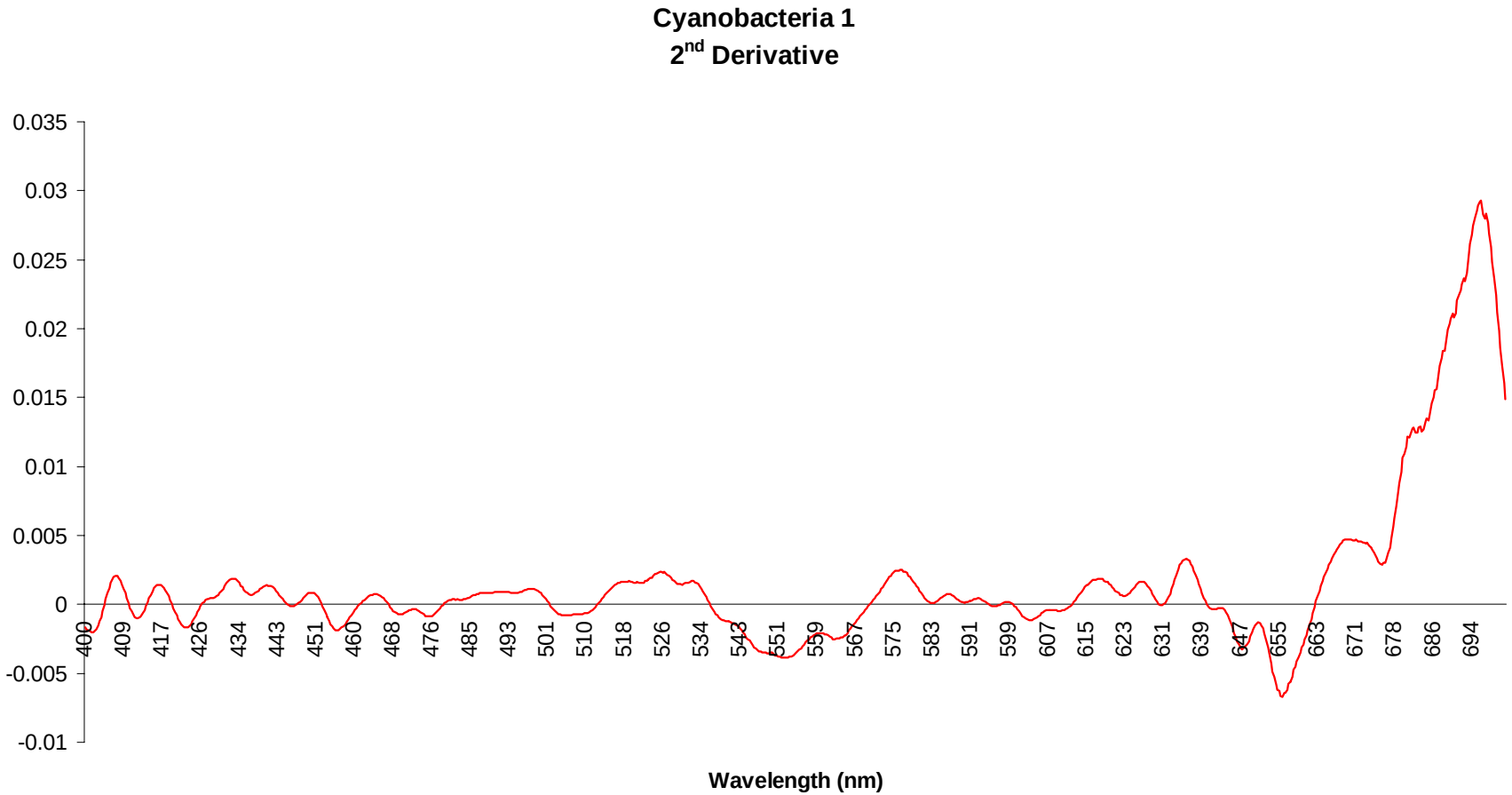
Cyanobacteria 1
2nd Derivative
0.035
0.03
0.025
0.02
0.015
0.01
0.005
0
-0.005
-0.01
400
409
417
426
434
443
451
460
468
476
485
493
501
510
518
526
534
543
551
559
567
575
583
591
599
607
615
623
631
639
647
655
663
671
678
686
694
Wavelength (nm)

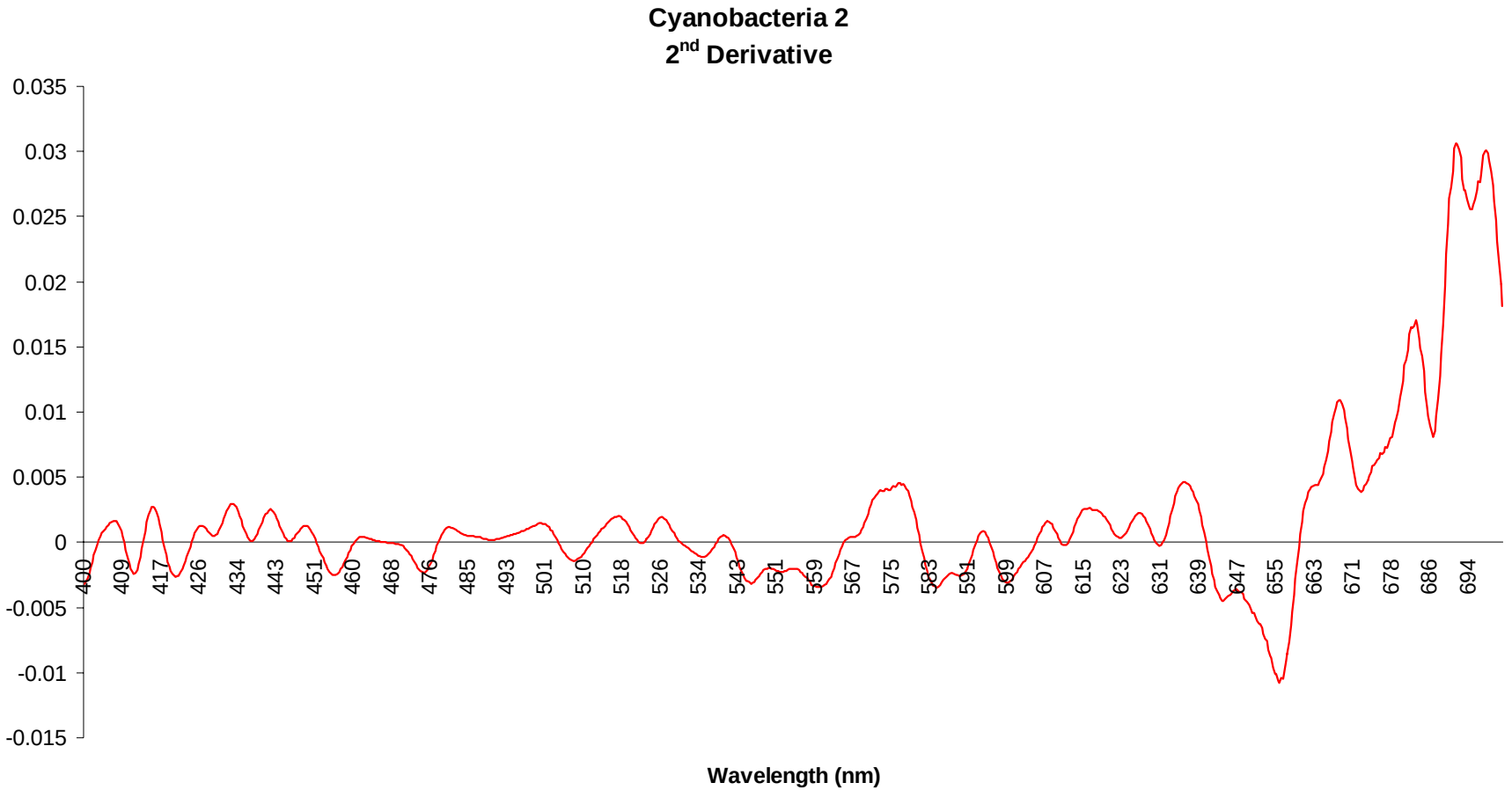
Cyanobacteria 2
2nd Derivative
0.035
0.03
0.025
0.02
0.015
0.01
0.005
0
-0.005
-0.01
-0.015
400
409
417
426
434
443
451
460
468
476
485
493
501
510
518
526
534
543
551
559
567
575
583
591
599
607
615
623
631
639
647
655
663
671
678
686
694
Wavelength (nm)

**Cyanobacteria spp. 3**
**2nd Derivative**

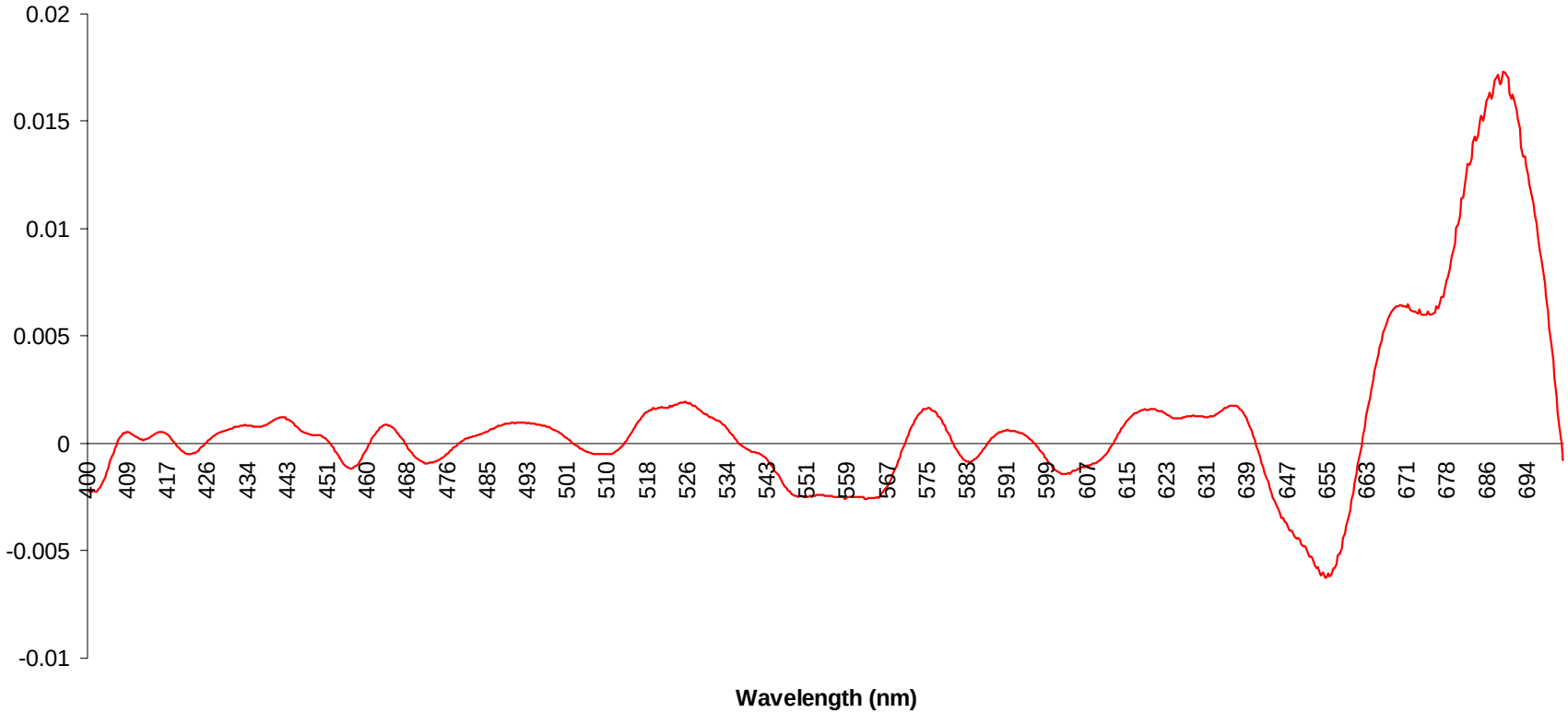

**_Montipora_ spp. 4**
**2nd Derivative**

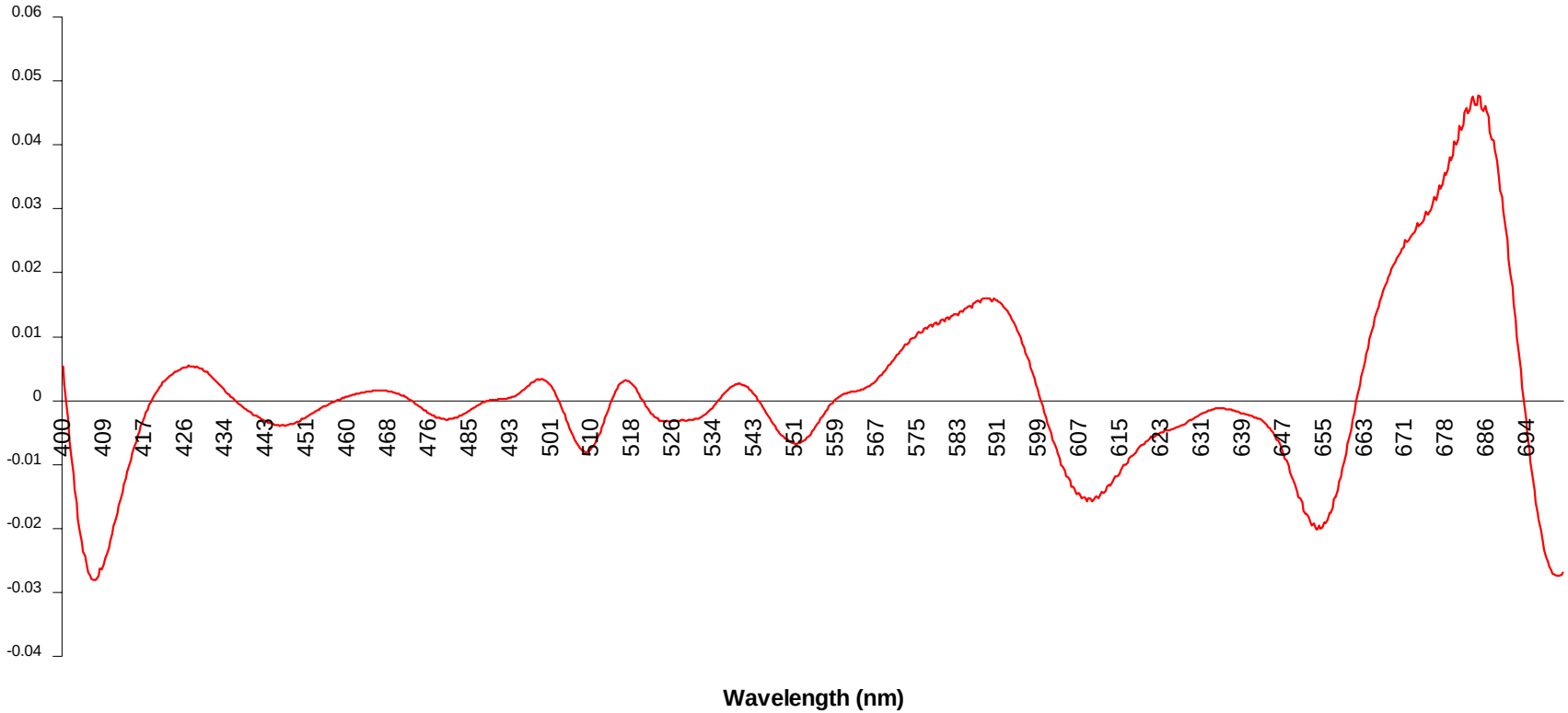

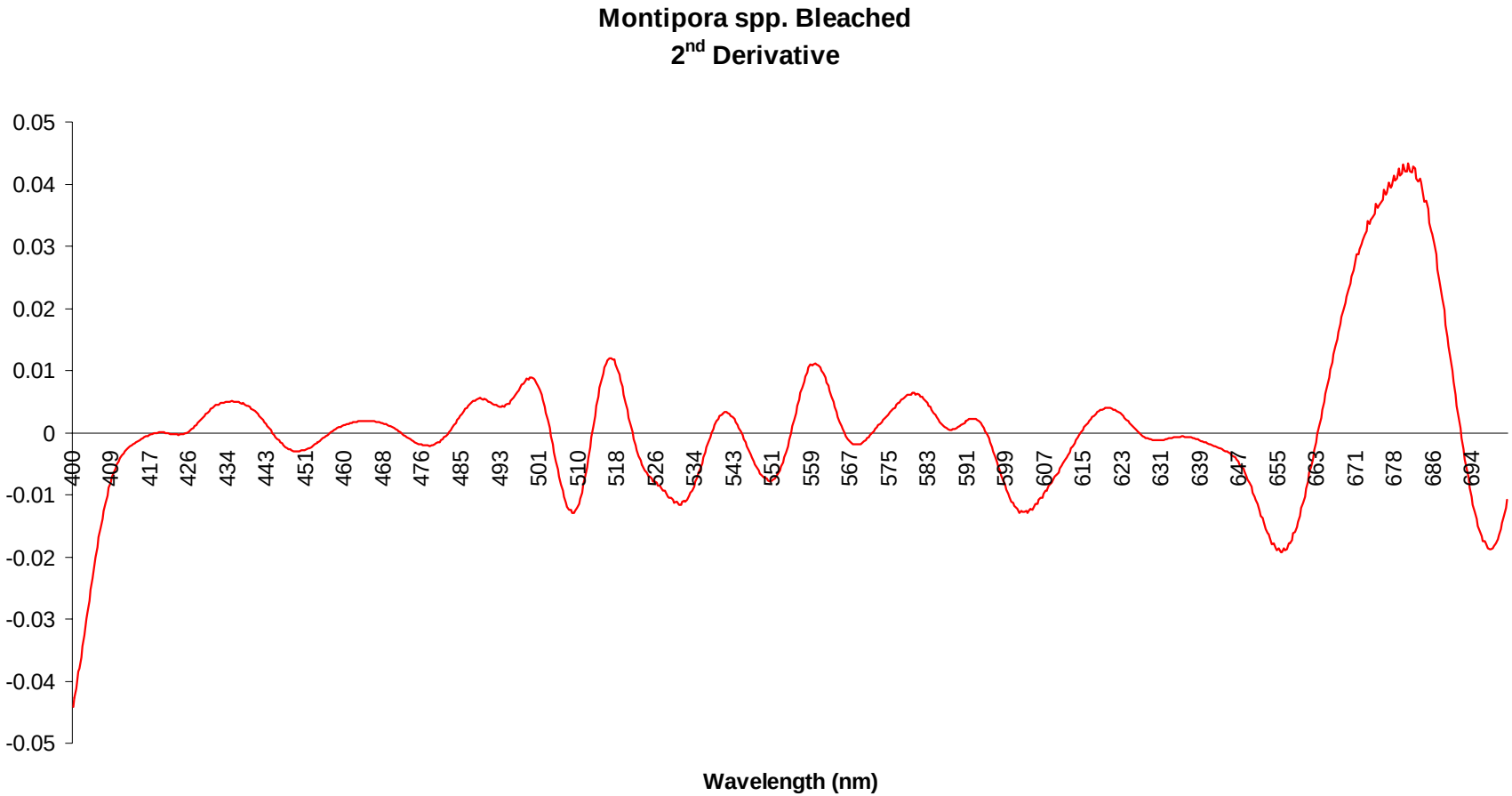
Montipora spp. Bleached
2nd Derivative
0.05
0.04
0.03
0.02
0.01
0
-0.01
-0.02
-0.03
-0.04
-0.05
400
409
417
426
434
443
451
460
468
476
485
493
501
510
518
526
534
543
551
559
567
575
583
591
599
607
615
623
631
639
647
655
663
671
678
686
694
Wavelength (nm)

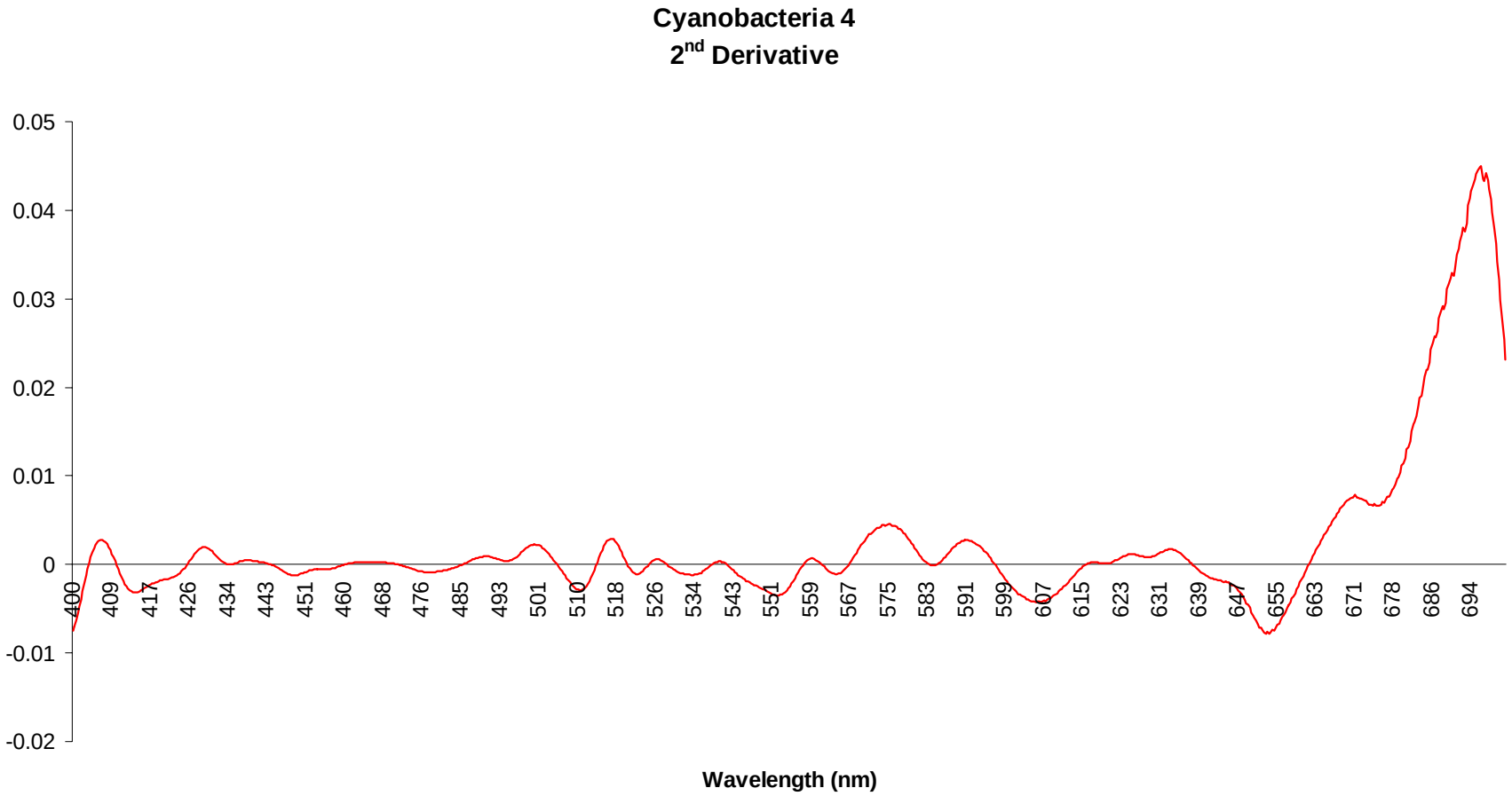
Cyanobacteria 4
2nd Derivative
0.05
0.04
0.03
0.02
0.01
0
-0.01
-0.02
400
409
417
426
434
443
451
460
468
476
485
493
501
510
518
526
534
543
551
559
567
575
583
591
599
607
615
623
631
639
647
655
663
671
678
686
694
Wavelength (nm)

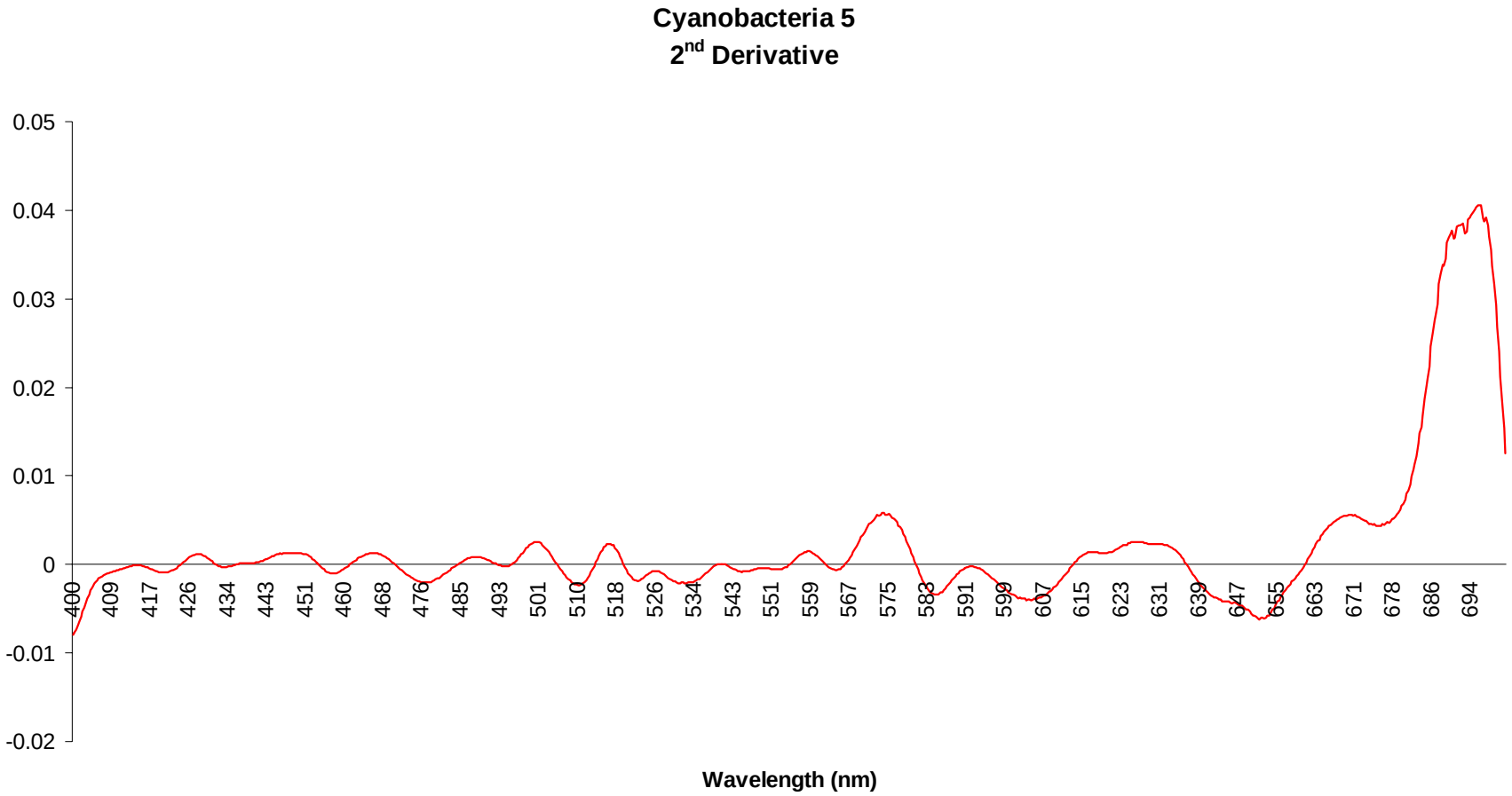
Cyanobacteria 5
2nd Derivative
0.05
0.04
0.03
0.02
0.01
0
-0.01
-0.02
400
409
417
426
434
443
451
460
468
476
485
493
501
510
518
526
534
543
551
559
567
575
583
591
599
607
615
623
631
639
647
655
663
671
678
686
694
Wavelength (nm)

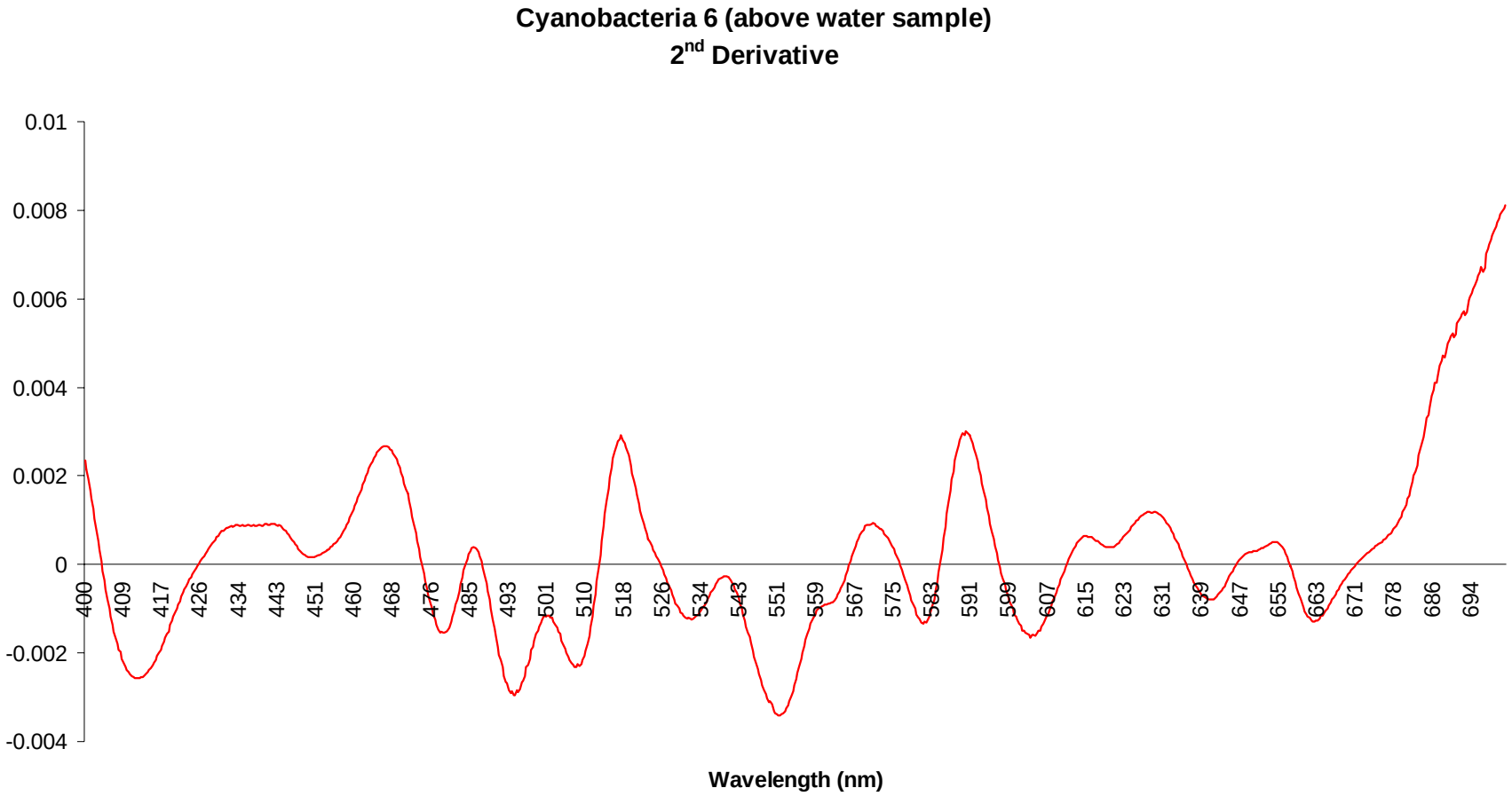
Cyanobacteria 6 (above water sample)
2nd Derivative
0.01
0.008
0.006
0.004
0.002
0
-0.002
-0.004
400
409
417
426
434
443
451
460
468
476
485
493
501
510
518
526
534
543
551
559
567
575
583
591
599
607
615
623
631
639
647
655
663
671
678
686
694
Wavelength (nm)

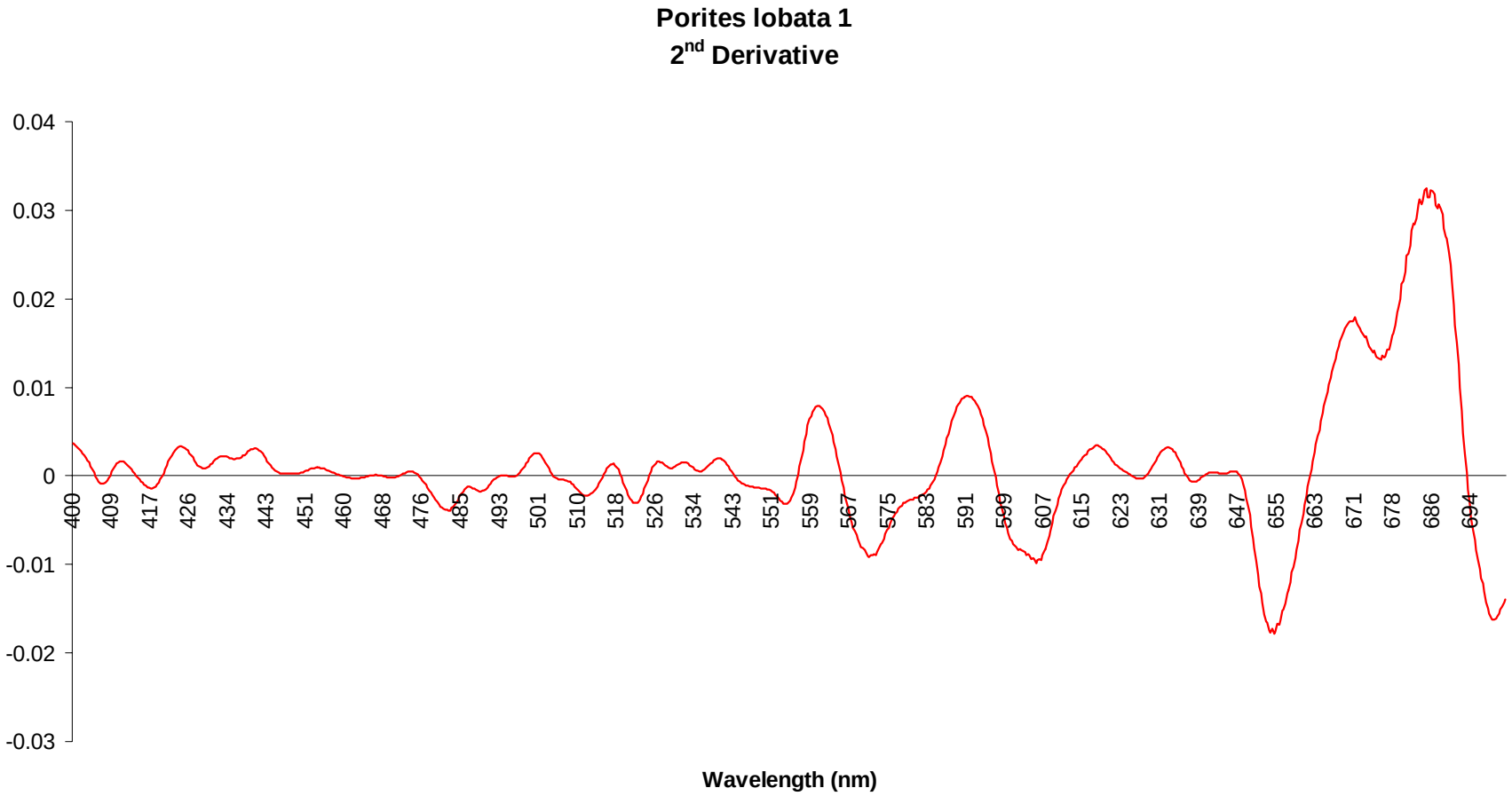
Porites lobata 1
2nd Derivative
0.04
0.03
0.02
0.01
0
-0.01
-0.02
-0.03
400
409
417
426
434
443
451
460
468
476
485
493
501
510
518
526
534
543
551
559
567
575
583
591
599
607
615
623
631
639
647
655
663
671
678
686
694
Wavelength (nm)

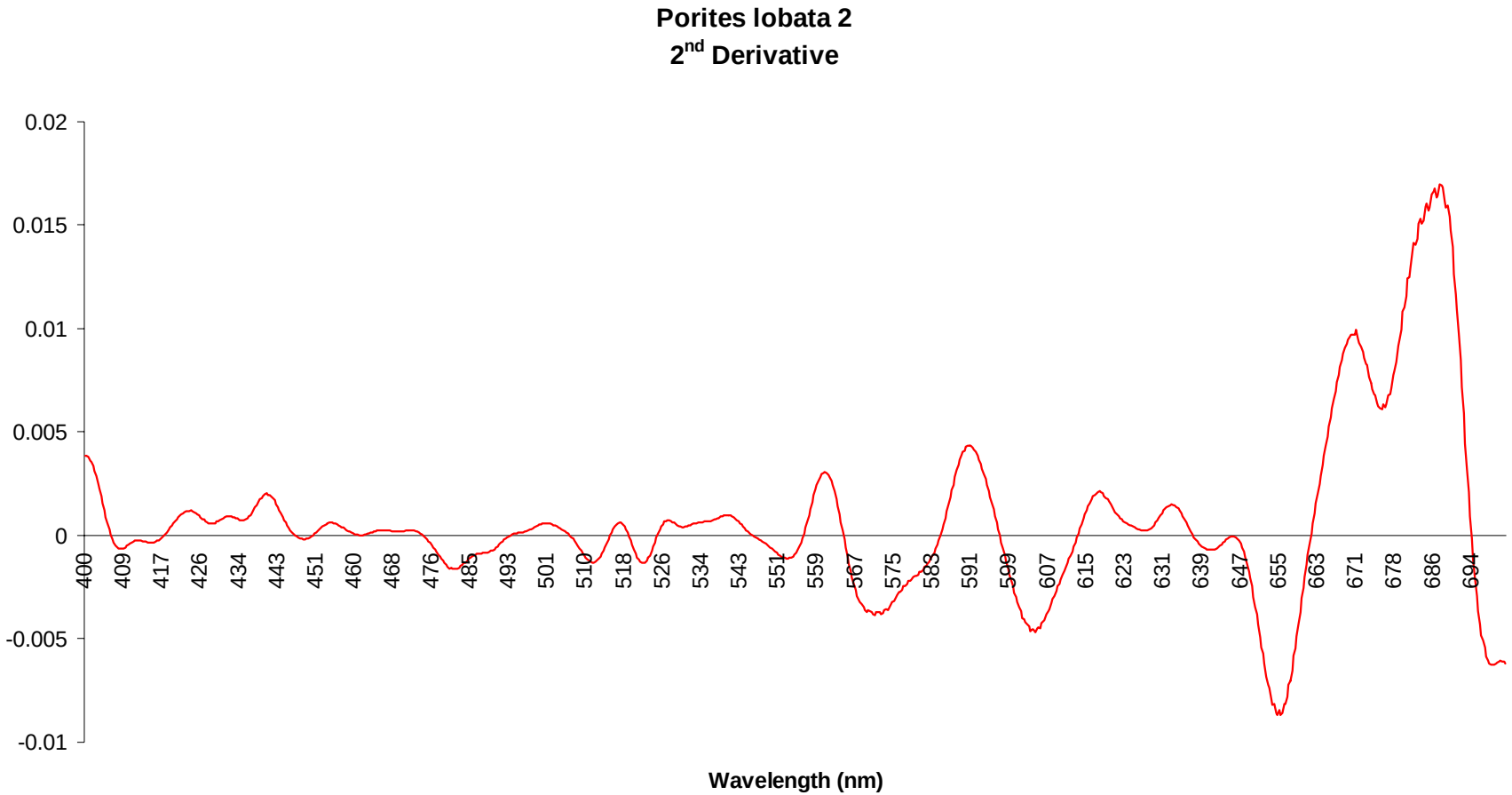
Porites lobata 2
2nd Derivative
0.02
0.015
0.01
0.005
0
-0.005
-0.01
400
409
417
426
434
443
451
460
468
476
485
493
501
510
518
526
534
543
551
559
567
575
583
591
599
607
615
623
631
639
647
655
663
671
678
686
694
Wavelength (nm)

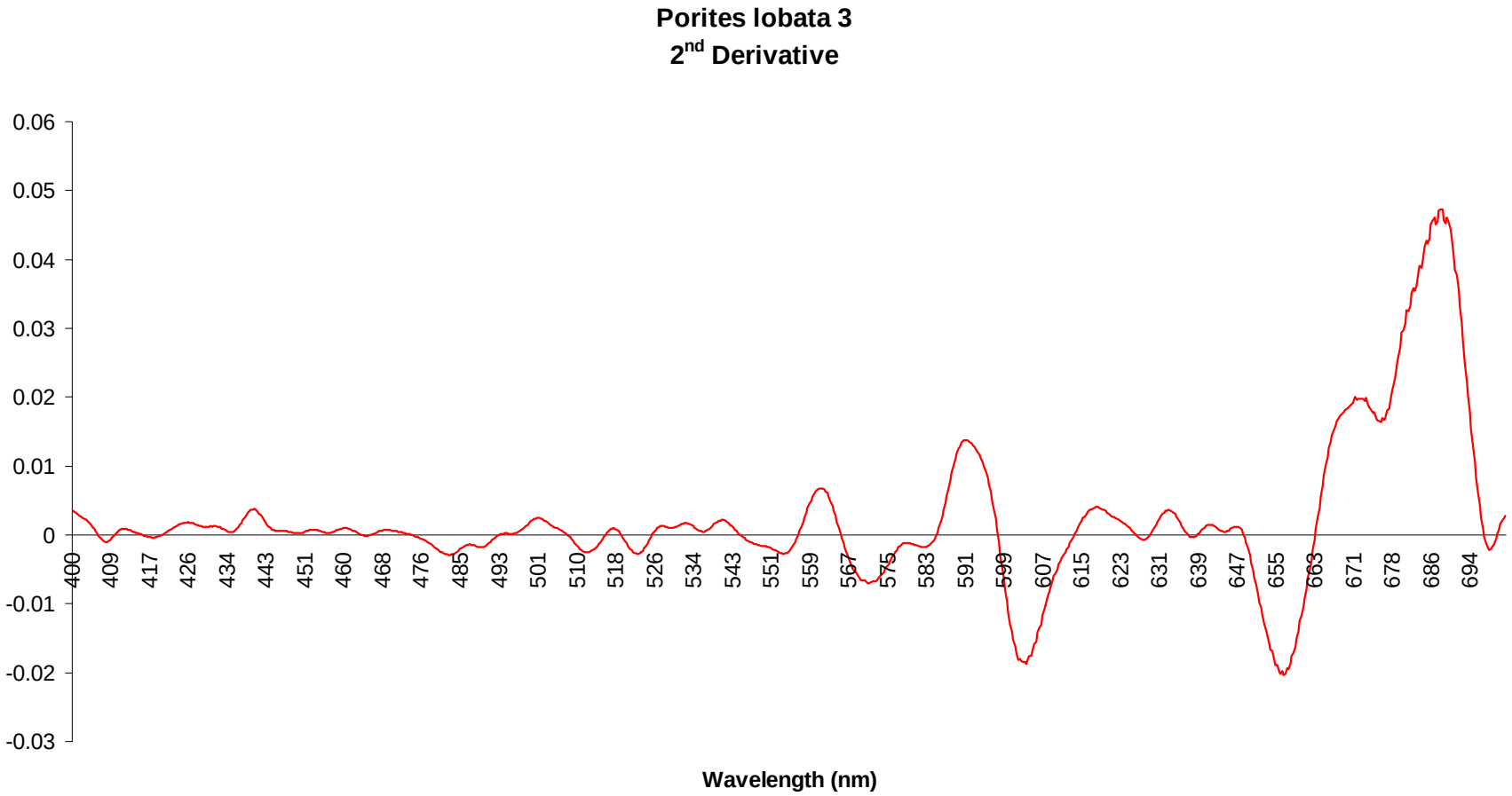
Porites lobata 3
2nd Derivative
0.06
0.05
0.04
0.03
0.02
0.01
0
-0.01
-0.02
-0.03
400
409
417
426
434
443
451
460
468
476
485
493
501
510
518
526
534
543
551
559
567
575
583
591
599
607
615
623
631
639
647
655
663
671
678
686
694
Wavelength (nm)

**Algae: Laurentia spp.**
**2nd Derivative**

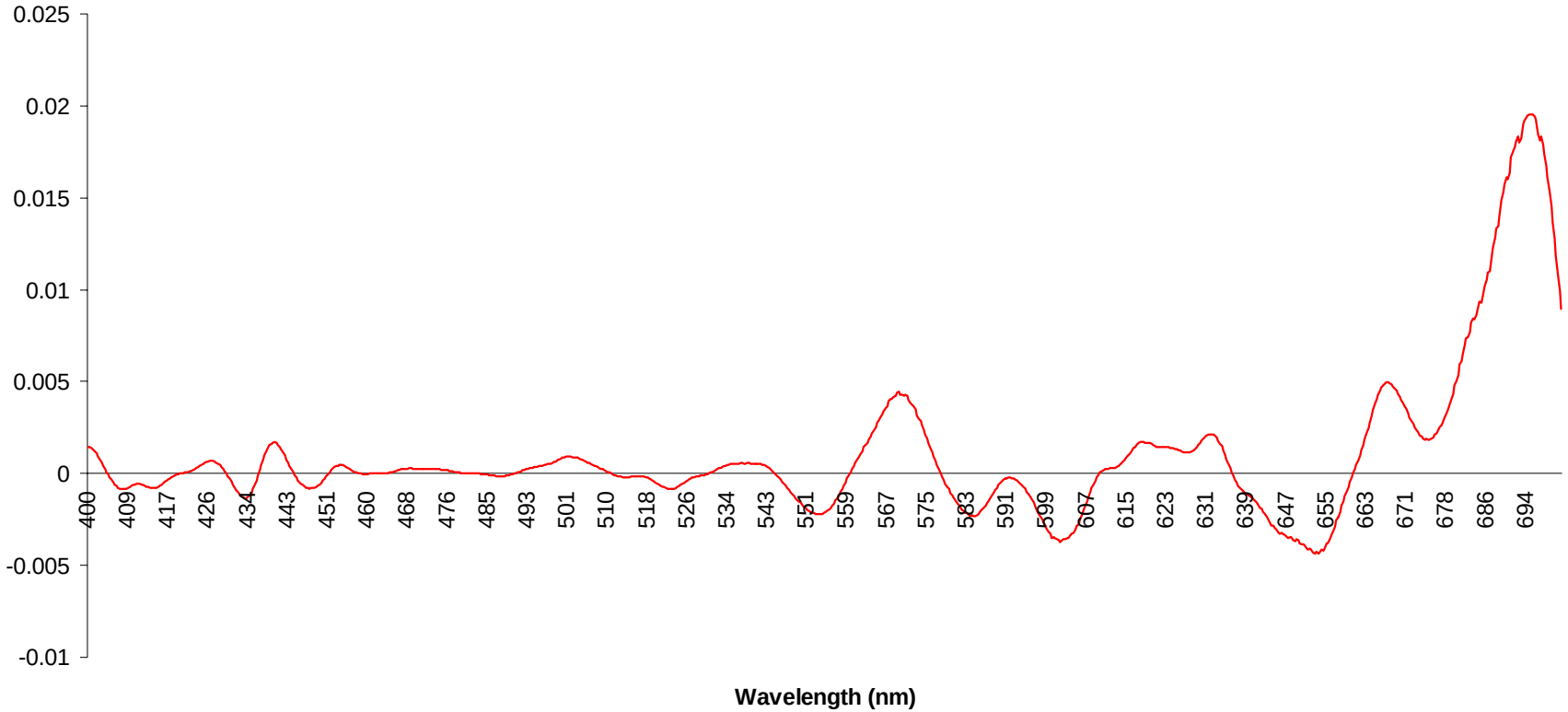

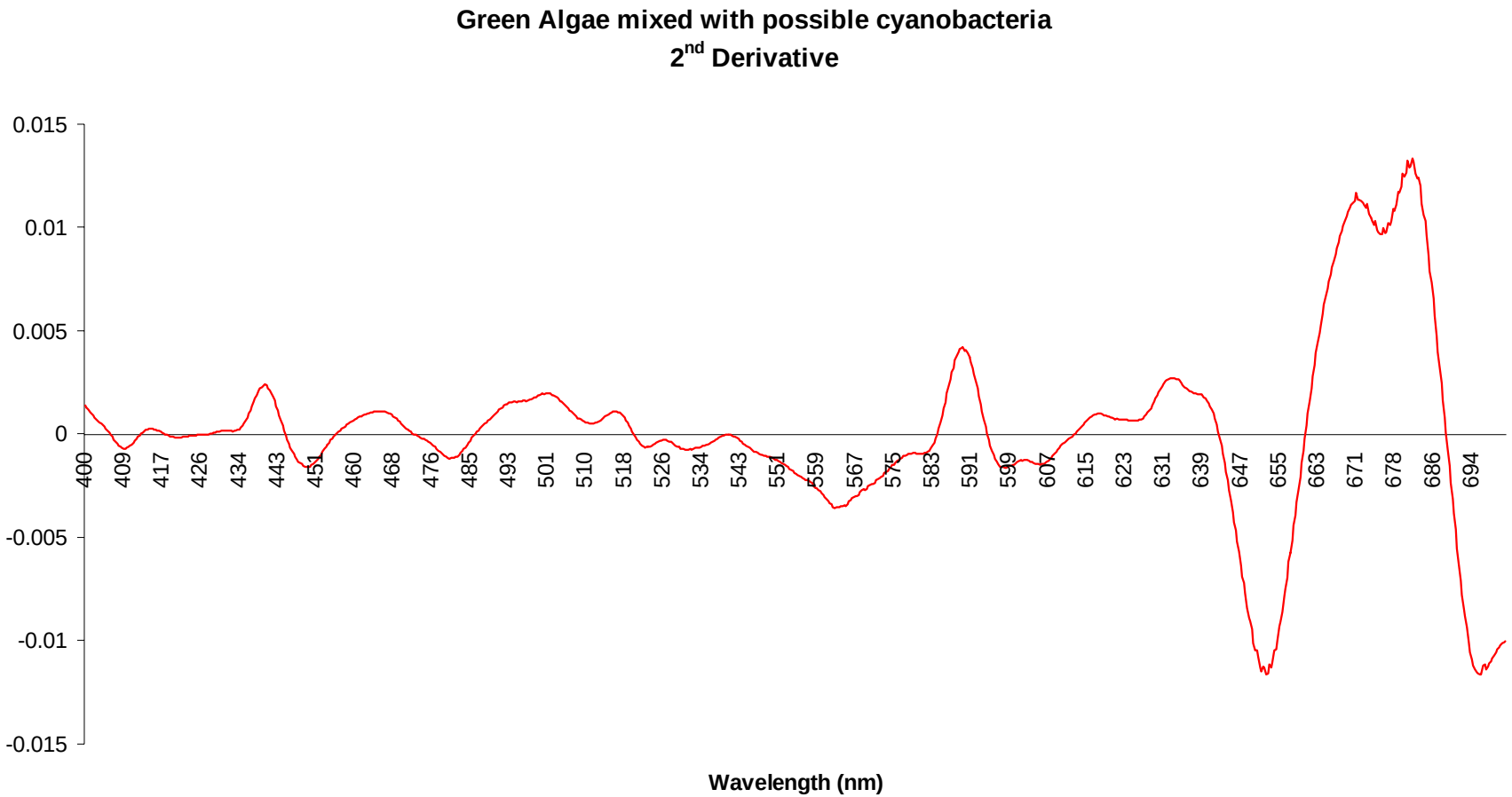
Green Algae mixed with possible cyanobacteria
2nd Derivative
0.015
0.01
0.005
0
-0.005
-0.01
-0.015
400
409
417
426
434
443
451
460
468
476
485
493
501
510
518
526
534
543
551
559
567
575
583
591
599
607
615
623
631
639
647
655
663
671
678
686
694
Wavelength (nm)

# APPENDIX F. TABLE OF SECOND DERIVATIVE MAX VALUES

| | Montipora spp.. 1 | Porites Lobata/Lutea/Compressa? | Pocillopora Ligulata | Brown Algae -1 | Pocillopora damicorus | Montipora Flabellata/Capitata | Montipora Flabellata | **Green Cyanobacteria spp. 1** | **Green Cyanobacteria (unconfirmed)** | **Cyanobacteria Lyngbya/Semiplena** | Montipora spp. 2 | Montipora spp. (Bleached) | **Green Cyanobacteria (unconfirmed) 2** | **Cyanobacteria Lynbya majuscula** | **Green Cyanobacteria (unconfirmed) 3** | Porites Lobata | Porites Lobata 2 | Porites Lobata 3 | Algae Laurentia spp. | Algae mix w/ trace Cyanobacteria | Number of occurrences |
|---|---|---|---|---|---|---|---|---|---|---|---|---|---|---|---|---|---|---|---|---|---|
| | 1 | 2 | 3 | 4 | 5 | 6 | 7 | **8** | **9** | 10 | 11 | 12 | 13 | 14 | 15 | 16 | **17** | **18** | 19 | 20 | |
| 405 | | 405 | | | | | | | | | | | | | | | | | | | 1 |
| 406 | | | | | | | | | | | | | **406** | | | | | | | | 1 |
| 407 | | | | | | | | **407** | **407** | | | | | | | | | | | | 2 |
| 408 | | | | | | | | | | **408** | | | | | | | | | | | 1 |
| 409 | | | | | | | | | | | | | | | | 411 | | | 411 | | 2 |
| 410 | | | | | | | | | | | | | | | | | 412 | 412 | | | 2 |
| 414 | | | | | 414 | | | | | | | | | **414** | | | | | | | 2 |
| 415 | | | | | | | | | **415** | | | | | | | | | | | 415 | 2 |
| 416 | | | | | | 416 | | **416** | | **416** | | | | | | | | | | | 3 |
| 420 | | | | | | | | | | | | 420 | | | | | | | | | 1 |
| 424 | | | | 424 | | | | | | | | | | | | 424 | 424 | | | | 3 |
| 425 | 425 | | | | | | | | | | | | | | | | | | | | 1 |
| 426 | | | | | | | | | | | | | | | | | | 426 | | | 1 |
| 427 | | | | | | | | | | | 427 | | | | | | | | 427 | | 2 |
| 428 | | | | | | 428 | | | | | | | | **428** | | | | | | | 2 |
| 429 | | | | | | | | | | | | | **429** | | | | | | | | 1 |
| 430 | | 430 | | | 430 | | | | | | | | | | | | | | | | 2 |
| 431 | | | | | | | 431 | | | | | | | | | | | | | 431 | 2 |
| 432 | | | | | | | | | | | | | | | | | | 432 | | | 1 |
| 433 | | | | | | | | **433** | **433** | | | | | | | 433 | 433 | | | | 4 |
| 434 | | | | | | | | | | | | | | | **434** | | | | | | 1 |
| 435 | | | | | | | | | | | | 435 | | | | | | | | | 1 |
| 439 | | | | | | | | | | | | | **439** | | | | | 439 | | | 2 |
| 440 | | | | | | | 440 | | | | | | | | | 440 | | | 440 | 440 | 4 |
| 441 | | | | | | | | **441** | **441** | | | | | | | | 441 | | | | 3 |
| 442 | | | | | | 442 | | | | **442** | | | | | **442** | | | | | | 3 |
| 449 | | | | | | | | | | | | | | **449** | | | | | | | 1 |
| 450 | | | | | | | | **450** | **450** | | | | | | | | | | | | 2 |
| 451 | | | | | | 451 | 451 | | | | | | | | | | | | | | 2 |

| | Montipora spp.. 1 | Porites Lobata/Lutea/Compressa? | Pocillopora Ligulata | Brown Algae -1 | Pocillopora damicorus | Montipora Flabellata/Capitata | Montipora Flabellata | **Green Cyanobacteria spp. 1** | **Green Cyanobacteria (unconfirmed)** | **Cyanobacteria Lyngbya/Semiplena** | Montipora spp. 2 | Montipora spp. (Bleached) | **Green Cyanobacteria (unconfirmed) 2** | **Cyanobacteria Lynbya majuscula** | **Green Cyanobacteria (unconfirmed) 3** | Porites Lobata | Porites Lobata 2 | Porites Lobata 3 | Algae Laurentia spp. | Algae mix w/ trace Cyanobacteria | Number of occurrences |
|---|---|---|---|---|---|---|---|---|---|---|---|---|---|---|---|---|---|---|---|---|---|
| 454 | | | | | | | 463 | | | | | | | | | 454 | | 454 | 454 | | 3 |
| 455 | | | | | | | | | | | | | | | | | 455 | | | | 1 |
| 460 | | | | | | | | | | | | | | | | | | 460 | | | 1 |
| 463 | | | | | | | | | | | | | | | | | | | | | 1 |
| 464 | | | | | | 464 | | **464** | **464** | **464** | | | | | | | | | | | 4 |
| 465 | | | | | | | | | | | | 465 | **465** | | | | | | | 465 | 3 |
| 466 | | | | | | | | | | | | | | **466** | **466** | | 466 | | | | 3 |
| 467 | | | | | | | | | | | | | | | | 467 | | | | | 1 |
| 468 | | | | | 468 | | | | | | | | | | | | | | | | 1 |
| 469 | | | | | | | | | | | 469 | | | | | | | 469 | | | 2 |
| 470 | | | | | | | | | | | | | | | | | | | 470 | | 1 |
| 471 | 471 | 471 | | | | | | | | | | | | | | | | | | | 2 |
| 472 | | | | | | | | | | | | | | | | | 472 | | | | 1 |
| 473 | | | 473 | | | 473 | | | | | | | | | | | | | | | 2 |
| 474 | | | | | | | | | | | | | | | | 474 | | | | | 1 |
| 480 | | | | | | | | **480** | **480** | | | | | | | | | | | | 2 |
| 484 | | | | 484 | | | | | | | | | | | | | | | | | 1 |
| 486 | | | 486 | | 486 | | | | | | | | | | **486** | 486 | | 486 | | | 5 |
| 488 | | | | | | | 488 | | | | | 488 | | | | | | | | | 2 |
| 489 | 489 | | | | | | | | | | | | | **489** | | | | | | | 2 |
| 490 | | | | | | | | | | | | | **490** | | | | | | | | 1 |
| 492 | | | | | | | | | | **492** | | | | | | | | | | | 1 |
| 494 | | | | | | | | | | | | | | | | 494 | | 494 | | | 2 |
| 495 | | | | | | | | | | | | | | | | | | | | 495 | 1 |
| 498 | | | | | | | | **498** | | | | | | | | | | | | | 1 |
| 499 | | | | | | | 499 | | | | | 499 | | | | | | | | | 2 |
| 500 | | | | | | 500 | | | **500** | | 500 | | | | | | | | | | 3 |
| 501 | | 501 | 501 | | | | | | | | | | **501** | **501** | **501** | 501 | | 501 | | 501 | 8 |
| 502 | 502 | | | 502 | 502 | | | | | | | | | | | | 502 | | 502 | | 5 |
| 514 | | | | 514 | | | | | | | | | | | | | | | | | 1 |
| 516 | | | | | | | | | | | | 516 | | **516** | | | | | | 516 | 3 |
| 517 | | 517 | 517 | | 517 | | | | **517** | | 517 | | **517** | | **517** | 517 | 517 | | 517 | | 10 |
| 518 | 518 | | | | | | | | | | | | | | | | | 518 | | | 2 |
| 519 | | | | | | 519 | | | | | | | | | | | | | | | 1 |

| | Montipora spp.. 1 | Porites Lobata/Lutea/Compressa? | Pocillopora Ligulata | Brown Algae -1 | Pocillopora damicorus | Montipora Flabellata/Capitata | Montipora Flabellata | **Green Cyanobacteria spp. 1** | **Green Cyanobacteria (unconfirmed)** | **Cyanobacteria Lyngbya/Semiplena** | Montipora spp. 2 | Montipora spp. (Bleached) | **Green Cyanobacteria (unconfirmed) 2** | **Cyanobacteria Lynbya majuscula** | **Green Cyanobacteria (unconfirmed) 3** | Porites Lobata | Porites Lobata 2 | Porites Lobata 3 | Algae Laurentia spp. | Algae mix w/ trace Cyanobacteria | Number of occurrences |
|---|---|---|---|---|---|---|---|---|---|---|---|---|---|---|---|---|---|---|---|---|---|
| 526 | | | 526 | | | | | **526** | **526** | **526** | | | | **526** | | | | | | 526 | 6 |
| 527 | | | | | | | | | | | | | **527** | | | 527 | 527 | 527 | | | 4 |
| 532 | | | | | | 532 | | | | | | | | | | | | | | | 1 |
| 533 | | | | | | | | | | | | | | | | 533 | | 533 | | | 2 |
| 534 | | | | | | | 534 | | | | | | | | | | | | | | 1 |
| 538 | | | | 538 | | | | | | | | | | | | | | | | | 1 |
| 539 | | | | | | | | | | | | | | | **539** | 539 | | | 539 | | 3 |
| 540 | 540 | 540 | | | | | | | | | 540 | | **540** | **540** | | | | 540 | | 540 | 7 |
| 541 | | | 541 | | 541 | | | | | | | 541 | | | | | 541 | | | | 4 |
| 549 | | | | | | | | | | | | | | **549** | | | | | | | 1 |
| 558 | | | 558 | | | | | | | | | | | | | | | | | | 1 |
| 559 | | | | | | | | | | | | | **559** | **559** | | | | | | | 2 |
| 560 | | 560 | | | 560 | | | **560** | | | | 560 | | | | | | | | | 4 |
| 561 | | | | | | | | | | | | | | | | 561 | 561 | 561 | | | 3 |
| 566 | | | | 566 | | | | | | | | | | | | | | | | | 1 |
| 569 | | | 569 | | | | | | | | | | | | | | | | | | 1 |
| 570 | | | | | 570 | | | | | | | | | | | | | | 570 | | 2 |
| 571 | | | | | | | | | | | | | | | **571** | | | | | | 1 |
| 574 | | | | | | | | | | | | | | **574** | | | | | | | 1 |
| 575 | 575 | | | | | | | | | **575** | | | **575** | | | | | | | | 3 |
| 576 | | | | | | | | **576** | | | | | | | | | | | | | 1 |
| 577 | | | | | | 577 | | | **577** | | | | | | | | | | | | 2 |
| 578 | | | 578 | | | | | | | | | | | | | | | | | 578 | 2 |
| 579 | | | | | | | | | | | | | | | | | | 579 | | | 1 |
| 580 | | | | | | | | | | | | 580 | | | | | | | | | 1 |
| 587 | | | | | | 587 | | **587** | | | | | | | | | | | | | 2 |
| 588 | | | | 588 | | | | | | | | | | | | | | | | | 1 |
| 589 | | | | | | | | | | | 589 | | | | | | | | | | 1 |
| 590 | | | | | | | | | | | | | | | **590** | | | | | 590 | 2 |
| 591 | 591 | | 591 | | 591 | | | | | **591** | | | | | | | 591 | 591 | | | 6 |
| 592 | | 592 | | | | | | | | | | | **592** | | | 592 | | | 592 | | 4 |
| 593 | | | | | | | | **593** | | | | 593 | | **593** | | | | | | | 3 |
| 594 | | | | | | | 594 | | | | | | | | | | | | | | 1 |
| 595 | | | | 595 | | | | | **595** | | | | | | | | | | | | 2 |

| | Montipora spp.. 1 | Porites Lobata/Lutea/Compressa? | Pocillopora Ligulata | Brown Algae -1 | Pocillopora damicorus | Montipora Flabellata/Capitata | Montipora Flabellata | **Green Cyanobacteria spp. 1** | **Green Cyanobacteria (unconfirmed)** | **Cyanobacteria Lyngbya/Semiplena** | Montipora spp. 2 | Montipora spp. (Bleached) | **Green Cyanobacteria (unconfirmed) 2** | **Cyanobacteria Lynbya majuscula** | **Green Cyanobacteria (unconfirmed) 3** | Porites Lobata | Porites Lobata 2 | Porites Lobata 3 | Algae Laurentia spp. | Algae mix w/ trace Cyanobacteria | Number of occurrences |
|---|---|---|---|---|---|---|---|---|---|---|---|---|---|---|---|---|---|---|---|---|---|
| 596 | | | | | | 596 | | | | | | | | | | | | | | | 1 |
| 599 | | | | | | | | **599** | | | | | | | | | | | | | 1 |
| 603 | | | | 603 | | | | | | | | | | | | | | | | 603 | 2 |
| 608 | | | | | | | | | **608** | | | | | | | | | | | | 1 |
| 612 | | | | | | | | | | | | | | | | | | | 612 | | 1 |
| 615 | | | | 615 | 615 | | | | | | | | | | | | | | | | 2 |
| 616 | | | | | | | | | | | | | | | **616** | | | | | | 1 |
| 617 | | | | | | | | | | | | | | **617** | | | | | | | 1 |
| 618 | | | 618 | | | | | **618** | **618** | | | | **618** | | | | 618 | 618 | | 618 | 7 |
| 619 | | | | | | | | | | | | | | | | 619 | | | 619 | | 2 |
| 620 | | | | | | | | | | **620** | | | | | | | | | | | 1 |
| 621 | | 621 | | | | | 621 | | | | | 621 | | | | | | | | | 3 |
| 625 | | | | | | | | | | | | | **625** | | | | | | | | 1 |
| 627 | | | | 627 | | | | **627** | **627** | | | | | **627** | | | | | | | 4 |
| 629 | | | | | 629 | 629 | | | | | | | | | **629** | | | | | | 3 |
| 632 | | | | | | | | | | | | | | | | | | 632 | 632 | | 2 |
| 633 | | | | | | | | | | | | | **633** | | | 633 | 633 | | | 633 | 4 |
| 634 | | | | 634 | | | 634 | | | | | | | | | | | | | | 2 |
| 635 | 635 | | | | | | | | | | 635 | | | | | | | | | | 2 |
| 636 | | | | | | | | **636** | | **636** | | 636 | | | | | | | | | 3 |
| 637 | | | | | | | | | **637** | | | | | | | | | | | | 1 |
| 638 | | | | | | 638 | | | | | | | | | | | | | | | 1 |
| 641 | | | | | | | | | | | | | | | | 641 | | 641 | | | 2 |
| 644 | | | | 644 | | | 644 | | | | | | | | | | | | | | 2 |
| 645 | | | | | | 645 | | | | | | | | | | | 645 | | | | 2 |
| 646 | | | | | | | | | | | | | | | | 646 | | | | | 1 |
| 647 | | | | | 647 | | | | | | | | | | | | | 647 | | | 2 |
| 652 | | | | | | | | **652** | | | | | | | | | | | | | 1 |
| 654 | | | | | | | | | | | | | | | **654** | | | | | | 1 |
| 667 | | | | | | | 667 | | | | | | | | | | | | 667 | | 2 |
| 668 | | | | 668 | | | | | **668** | **668** | | | | | | | | | | | 3 |
| 669 | | | | | | | | **669** | | | | | | **669** | | | | | | | 2 |
| 670 | | | | | 670 | 670 | | | | | | | | | | 670 | 670 | | | 670 | 5 |
| 671 | | | | | | | | | | | | | **671** | | | | | 671 | | | 2 |

| | Montipora spp.. 1 | Porites Lobata/Lutea/Compressa? | Pocillopora Ligulata | Brown Algae -1 | Pocillopora damicorus | Montipora Flabellata/Capitata | Montipora Flabellata | **Green Cyanobacteria spp. 1** | **Green Cyanobacteria (unconfirmed)** | **Cyanobacteria Lyngbya/Semiplena** | Montipora spp. 2 | Montipora spp. (Bleached) | **Green Cyanobacteria (unconfirmed) 2** | **Cyanobacteria Lynbya majuscula** | **Green Cyanobacteria (unconfirmed) 3** | Porites Lobata | Porites Lobata 2 | Porites Lobata 3 | Algae Laurentia spp. | Algae mix w/ trace Cyanobacteria | Number of occurrences |
|---|---|---|---|---|---|---|---|---|---|---|---|---|---|---|---|---|---|---|---|---|---|
| 680 | | | | | | | | | | | | 680 | | | | | | | | | 1 |
| 682 | | | | | | | | | | | | | | | | | | | | 682 | 1 |
| 683 | 683 | 683 | | 683 | | | | | **683** | | | | | | | | | | | | 4 |
| 684 | | | | | | | | | | | 684 | | | | | | | | | | 1 |
| 686 | | | | | 686 | 686 | | | | | | | | | | 686 | | | | | 3 |
| 687 | | | | | | | | | | | | | | | | | 687 | | | | 1 |
| 688 | | | | | | | 688 | | | | | | | | | | | 688 | | | 2 |
| 689 | | | 689 | | | | | | | **689** | | | | | | | | | | | 2 |
| 692 | | | | | | | | | **692** | | | | | | | | | | | | 1 |
| 695 | | | | | | | | **695** | | | | | **695** | **695** | | | | | 695 | | 4 |
| 697 | | | | | | | | | **697** | | | | | | | | | | | | 1 |
| 700 | | | | | | | | | | | | | | | **700** | | | | | | 1 |

THIS PAGE INTENTIONALLY LEFT BLANK

# APPENDIX G. FOURTH DERIVATIVE CHARTS

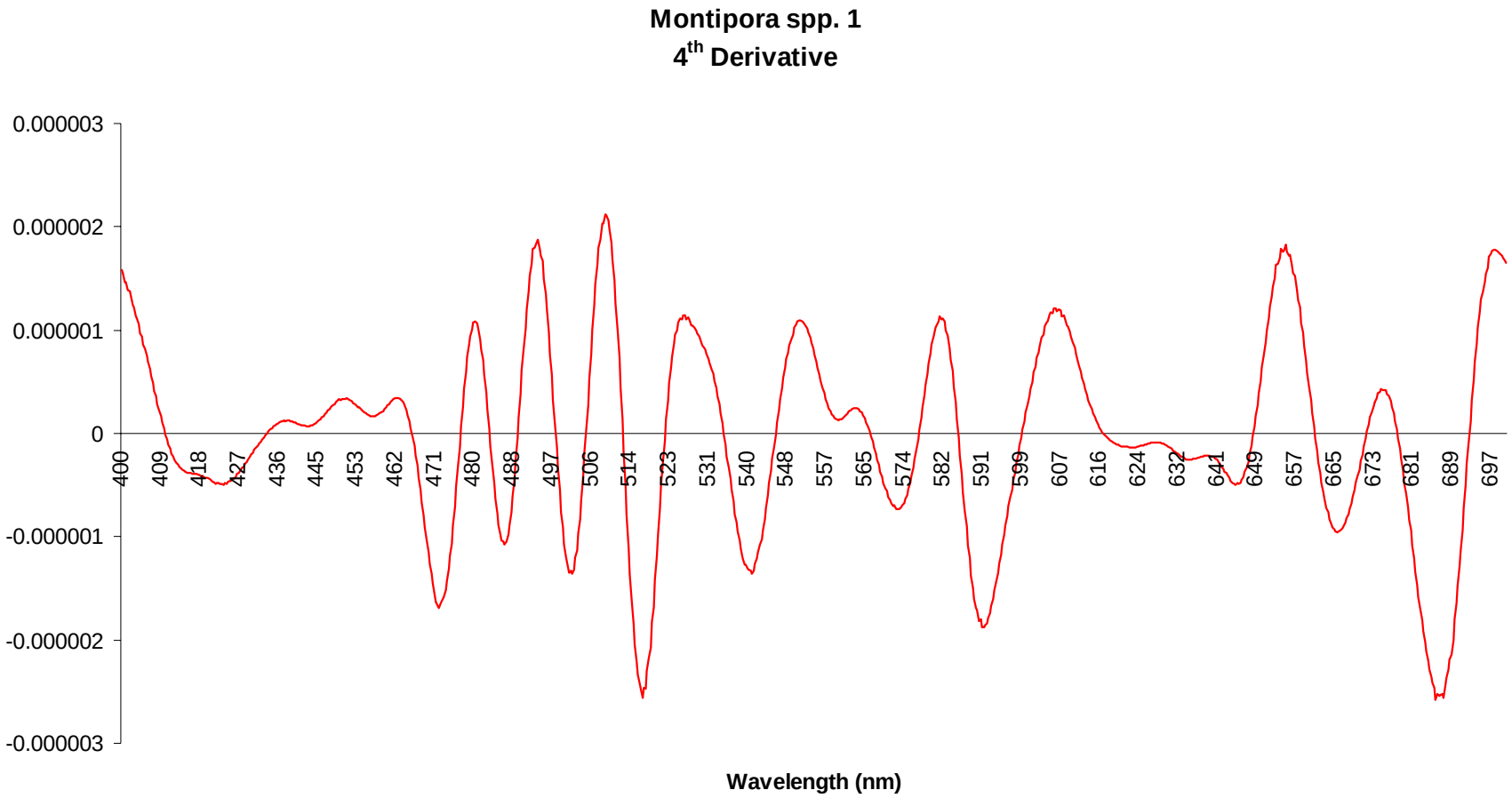

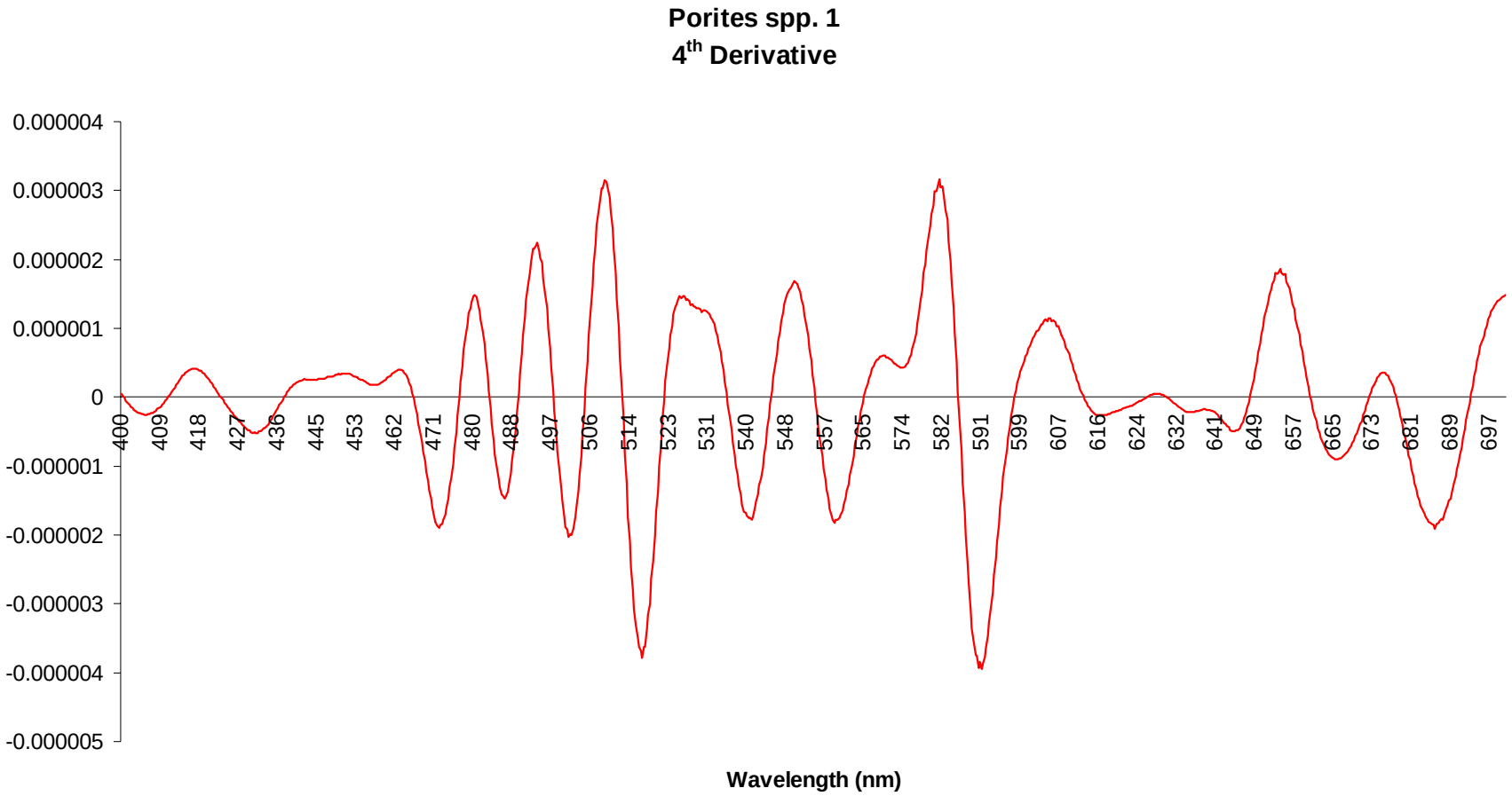
Porites spp. 1
4th Derivative
0.000004
0.000003
0.000002
0.000001
0
-0.000001
-0.000002
-0.000003
-0.000004
-0.000005
400
409
418
427
436
445
453
462
471
480
488
497
506
514
523
531
540
548
557
565
574
582
591
599
607
616
624
632
641
649
657
665
673
681
689
697
Wavelength (nm)

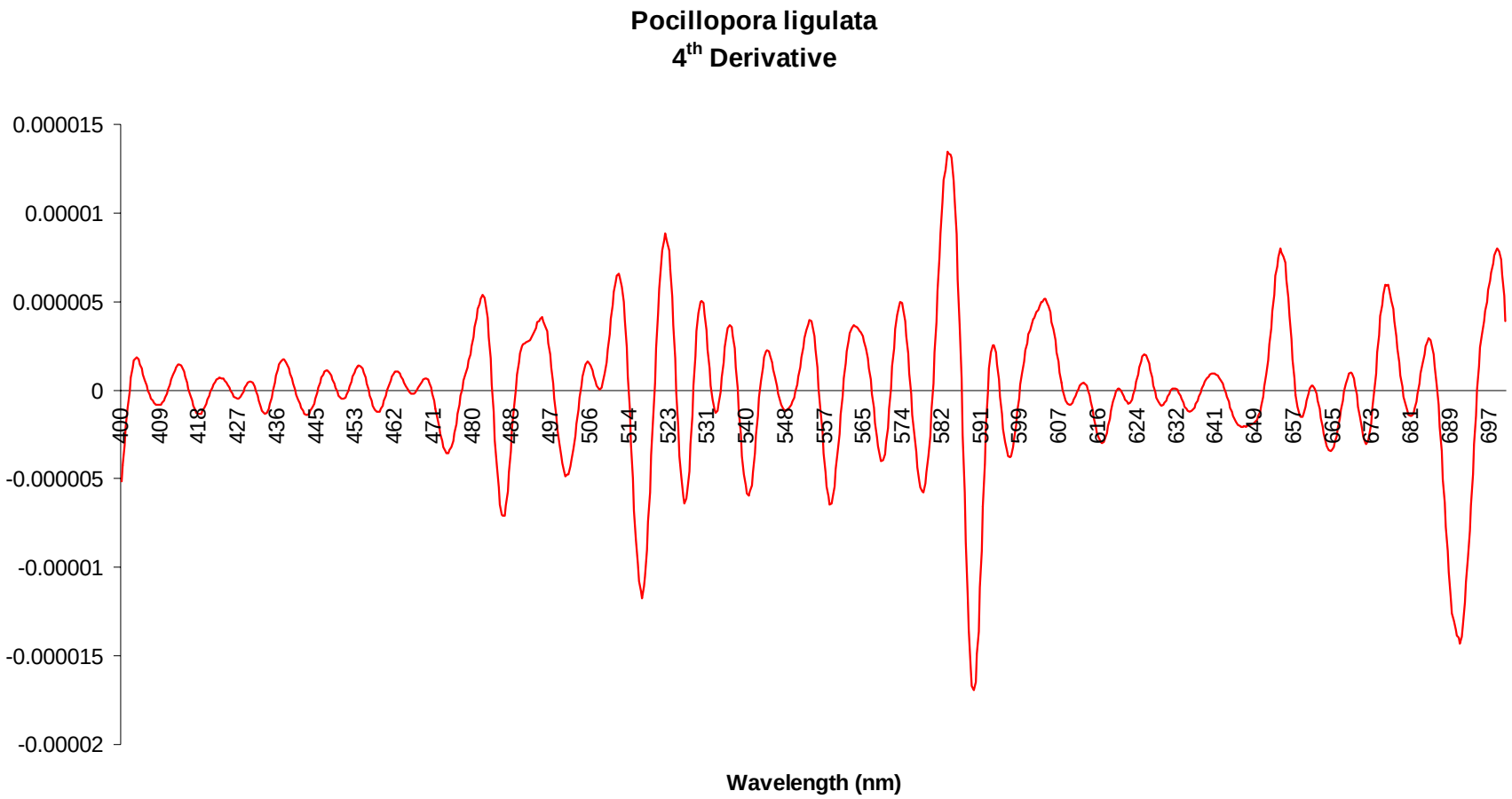
Pocillopora ligulata
4th Derivative
0.000015
0.00001
0.000005
0
-0.000005
-0.00001
-0.000015
-0.00002
400
409
418
427
436
445
453
462
471
480
488
497
506
514
523
531
540
548
557
565
574
582
591
599
607
616
624
632
641
649
657
665
673
681
689
697
Wavelength (nm)

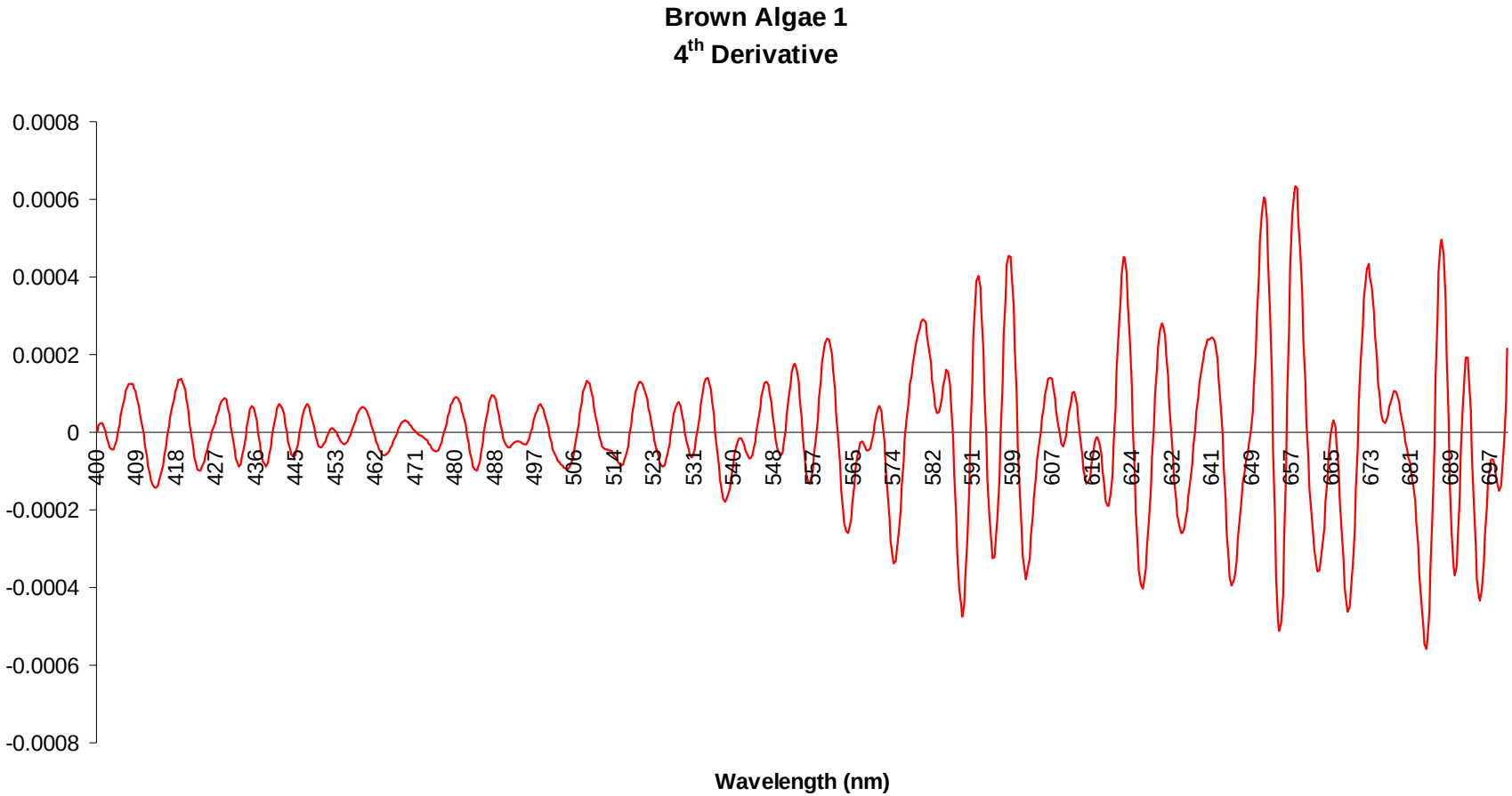
Brown Algae 1
4th Derivative
0.0008
0.0006
0.0004
0.0002
0
-0.0002
-0.0004
-0.0006
-0.0008
400
409
418
427
436
445
453
462
471
480
488
497
506
514
523
531
540
548
557
565
574
582
591
599
607
616
624
632
641
649
657
665
673
681
689
697
Wavelength (nm)

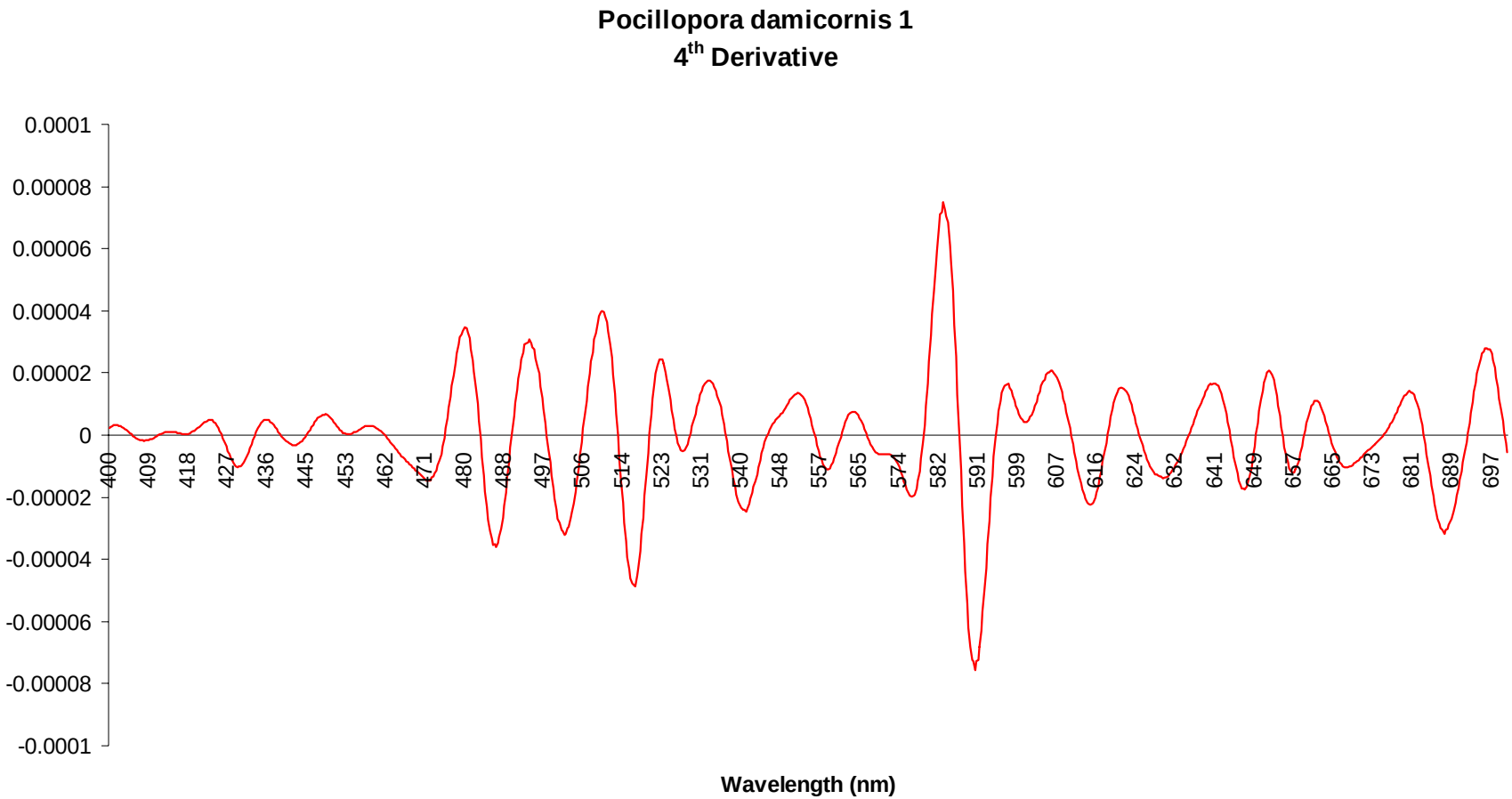
Pocillopora damicornis 1
4th Derivative
0.0001
0.00008
0.00006
0.00004
0.00002
0
-0.00002
-0.00004
-0.00006
-0.00008
-0.0001
400
409
418
427
436
445
453
462
471
480
488
497
506
514
523
531
540
548
557
565
574
582
591
599
607
616
624
632
641
649
657
665
673
681
689
697
Wavelength (nm)

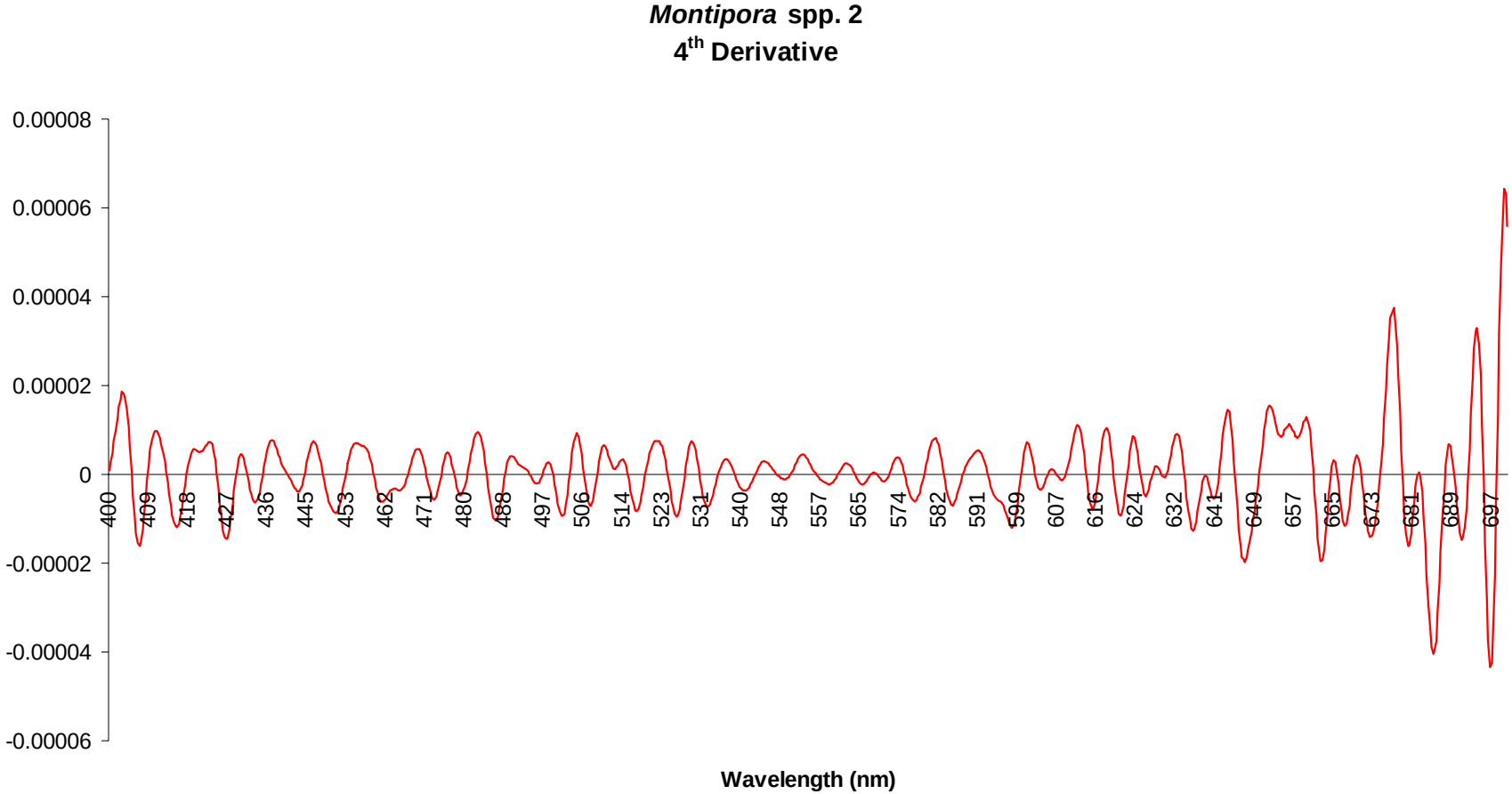
*Montipora* spp. 2
4th Derivative
0.00008
0.00006
0.00004
0.00002
0
-0.00002
-0.00004
-0.00006
400
409
418
427
436
445
453
462
471
480
488
497
506
514
523
531
540
548
557
565
574
582
591
599
607
616
624
632
641
649
657
665
673
681
689
697
Wavelength (nm)

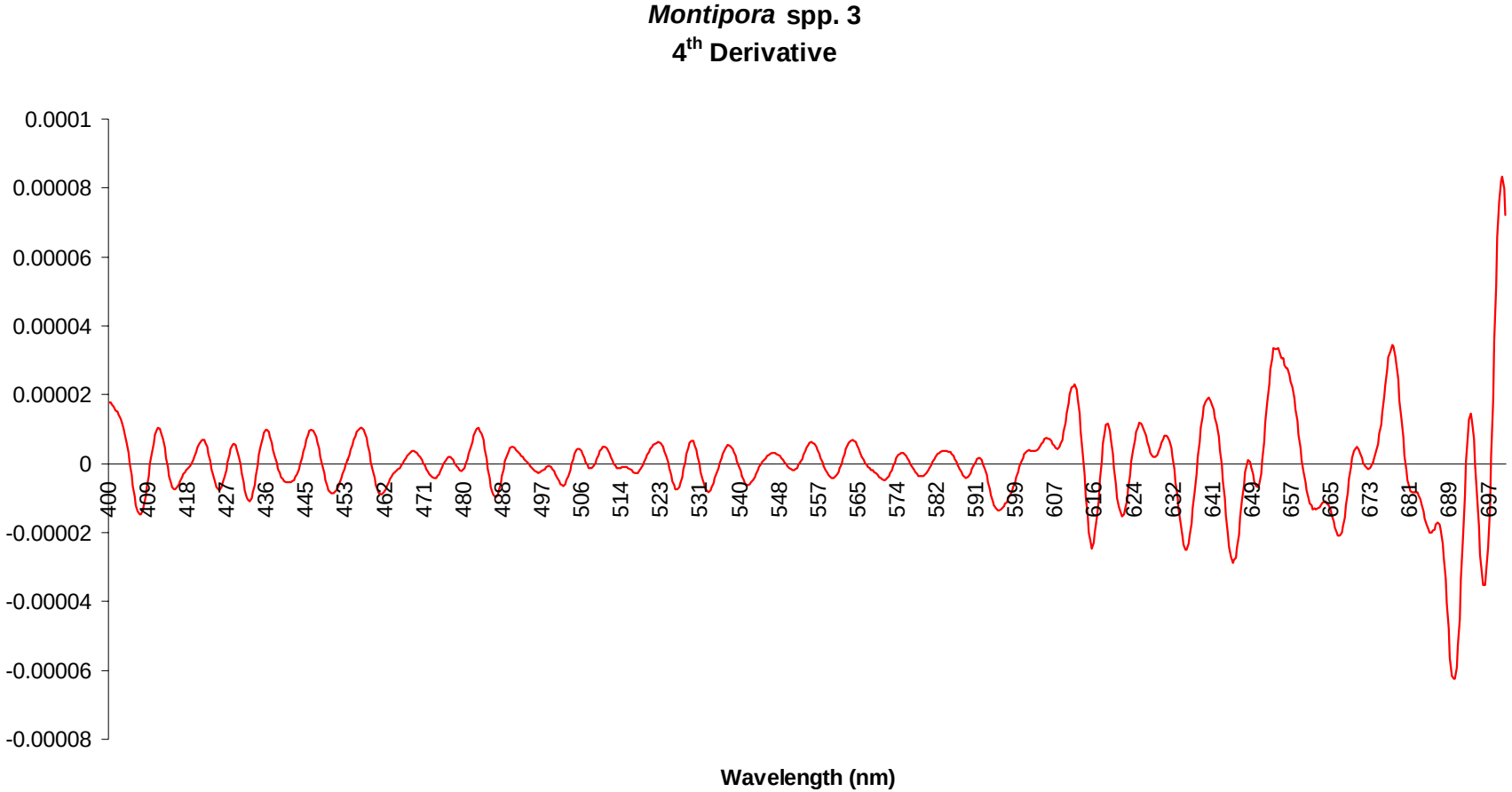
*Montipora* spp. 3
4th Derivative
0.0001
0.00008
0.00006
0.00004
0.00002
0
-0.00002
-0.00004
-0.00006
-0.00008
400
409
418
427
436
445
453
462
471
480
488
497
506
514
523
531
540
548
557
565
574
582
591
599
607
616
624
632
641
649
657
665
673
681
689
697
Wavelength (nm)

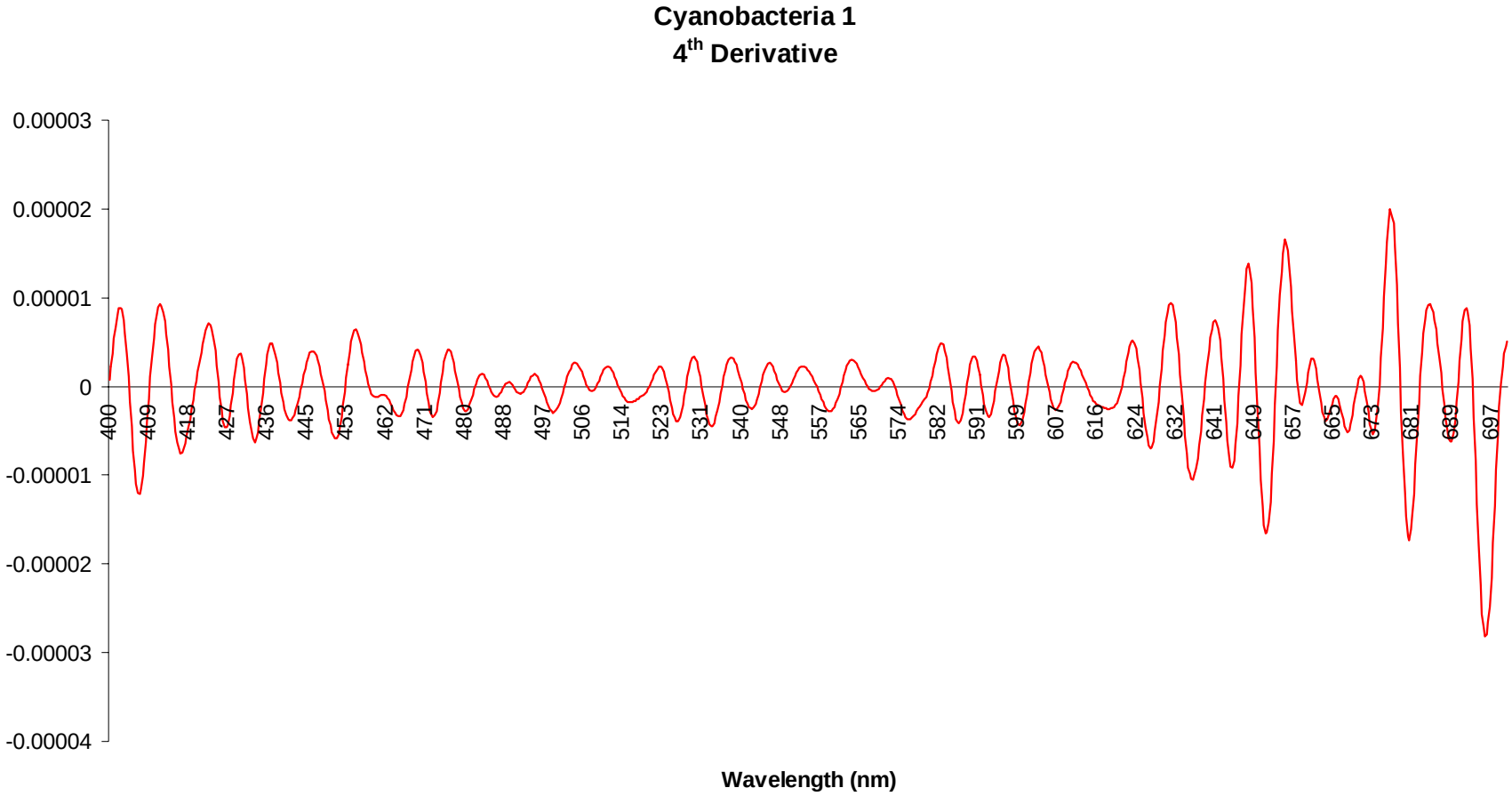
Cyanobacteria 1
4th Derivative
0.00003
0.00002
0.00001
0
-0.00001
-0.00002
-0.00003
-0.00004
400
409
418
427
436
445
453
462
471
480
488
497
506
514
523
531
540
548
557
565
574
582
591
599
607
616
624
632
641
649
657
665
673
681
689
697
Wavelength (nm)

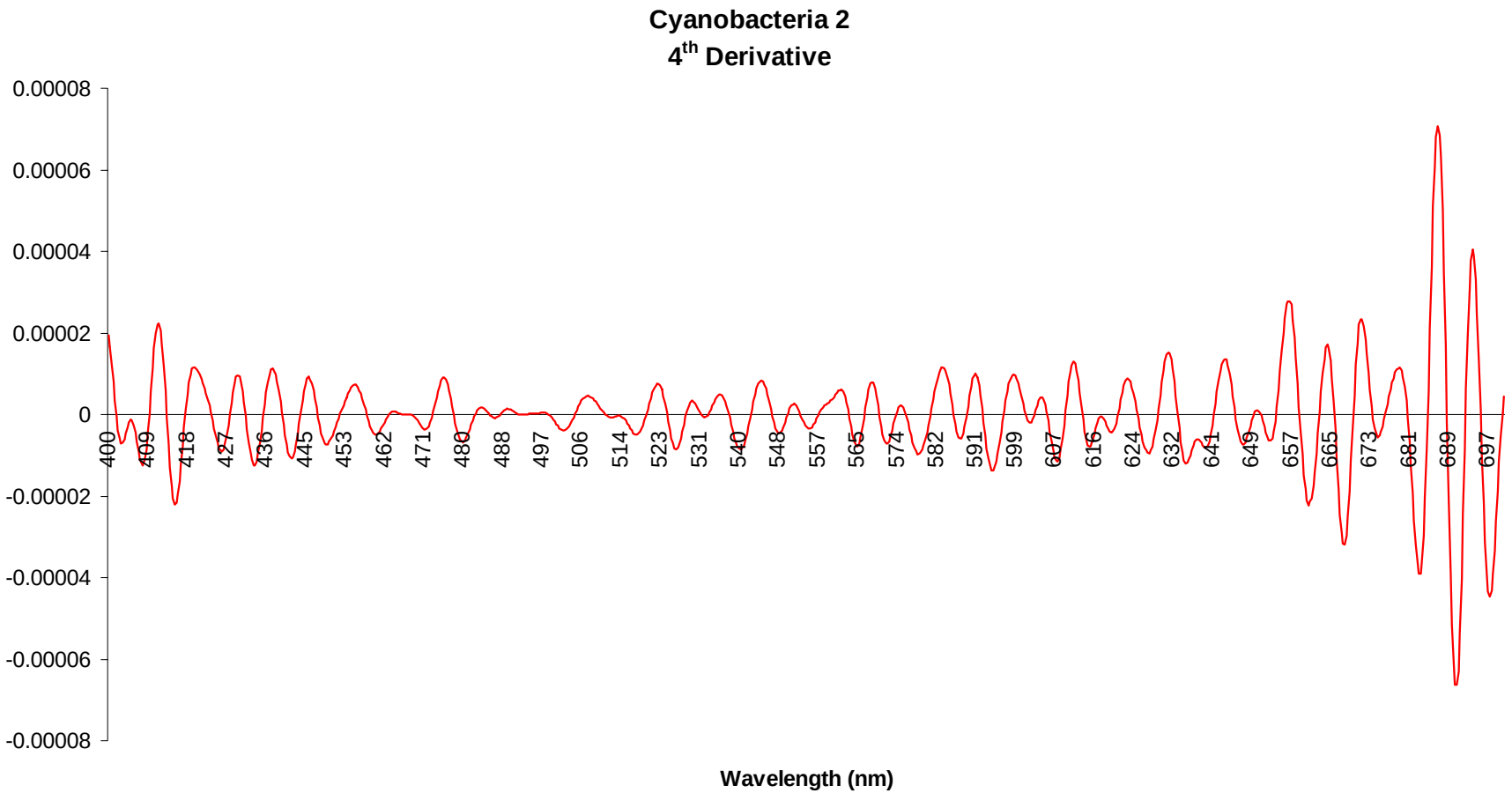
Cyanobacteria 2
4th Derivative
0.00008
0.00006
0.00004
0.00002
0
-0.00002
-0.00004
-0.00006
-0.00008
400
409
418
427
436
445
453
462
471
480
488
497
506
514
523
531
540
548
557
565
574
582
591
599
607
616
624
632
641
649
657
665
673
681
689
697
Wavelength (nm)

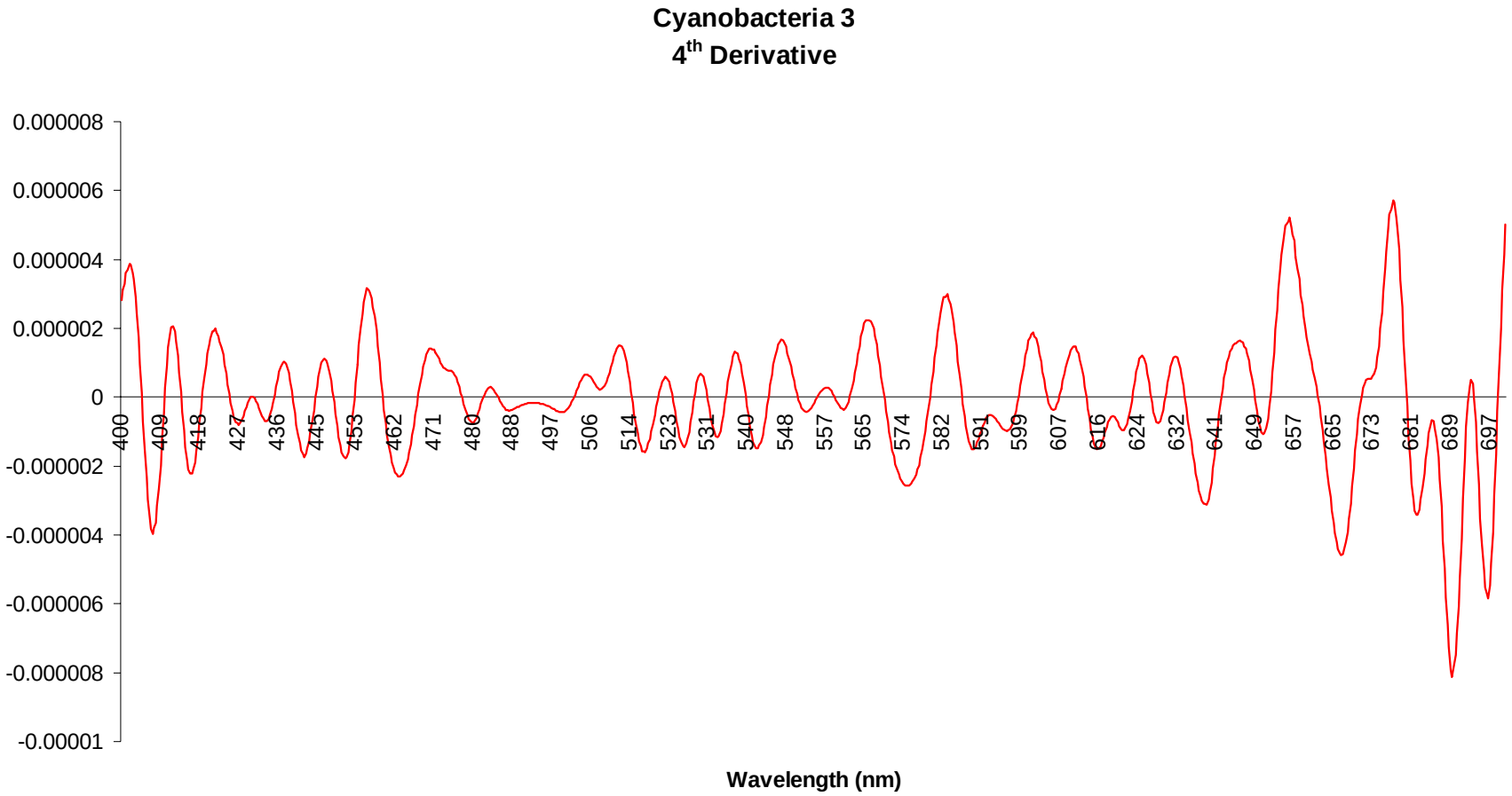
Cyanobacteria 3
4th Derivative
0.000008
0.000006
0.000004
0.000002
0
-0.000002
-0.000004
-0.000006
-0.000008
-0.00001
400
409
418
427
436
445
453
462
471
480
488
497
506
514
523
531
540
548
557
565
574
582
591
599
607
616
624
632
641
649
657
665
673
681
689
697
Wavelength (nm)

**Montipora spp. 4**
**4th Derivative**

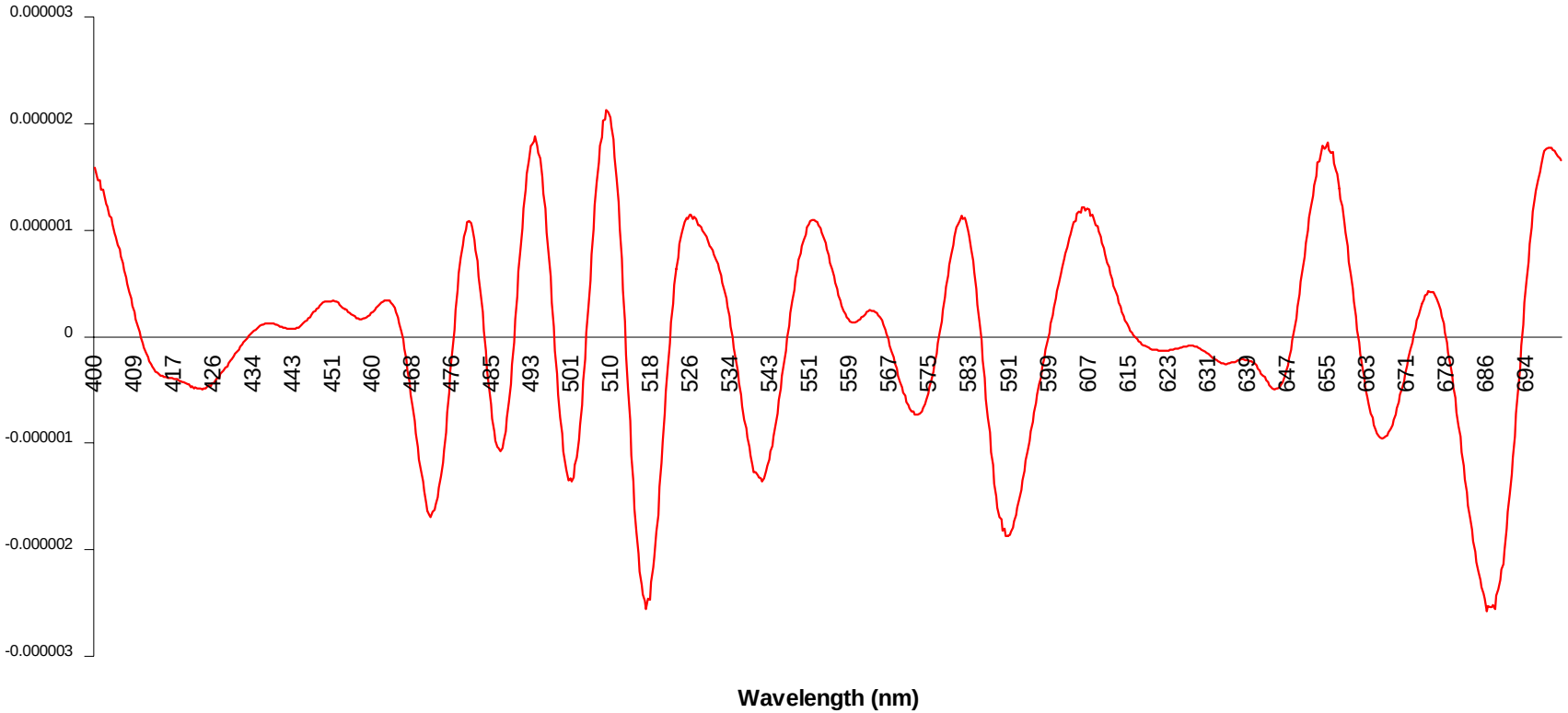

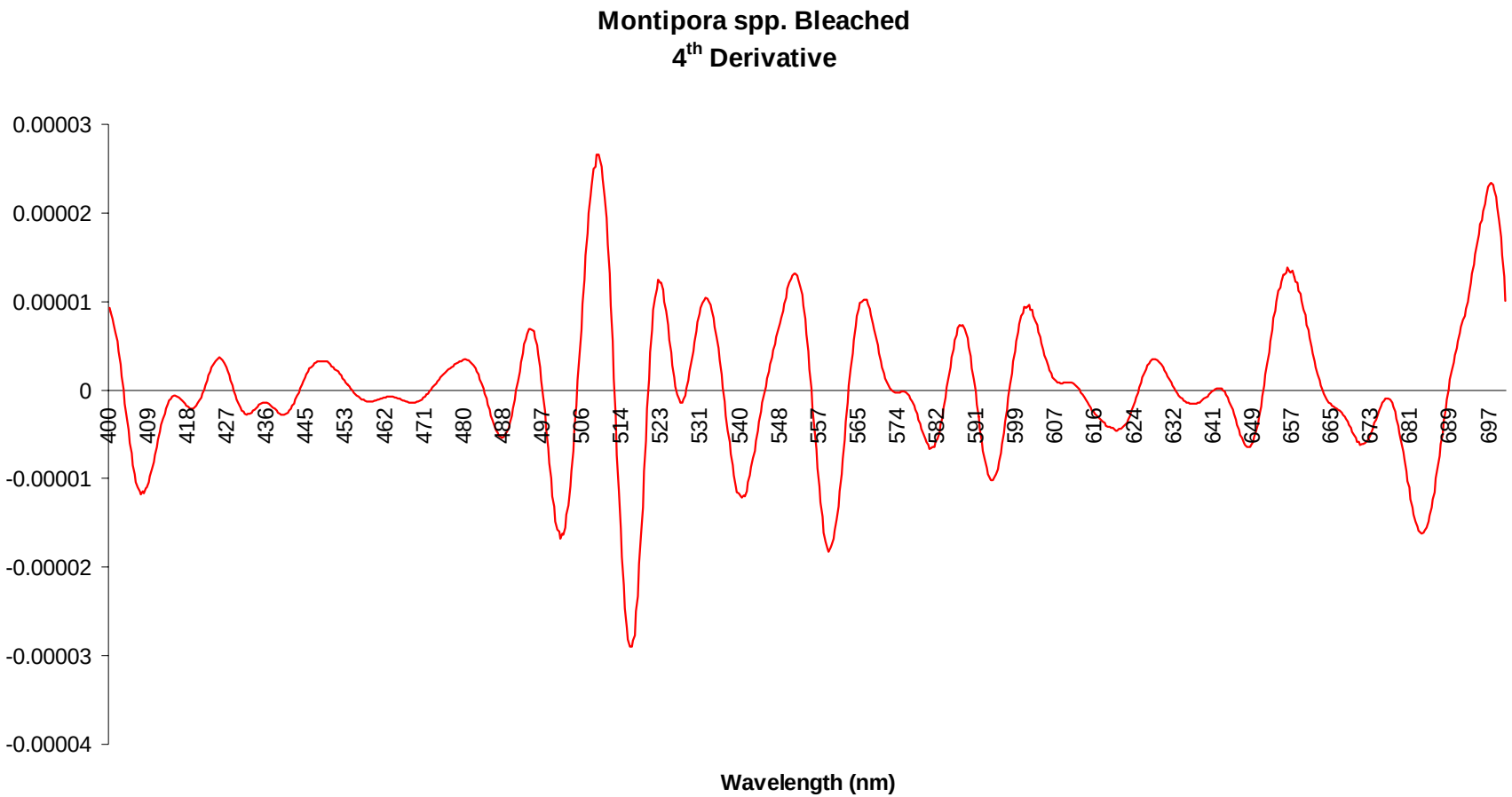
Montipora spp. Bleached
4th Derivative
0.00003
0.00002
0.00001
0
-0.00001
-0.00002
-0.00003
-0.00004
400
409
418
427
436
445
453
462
471
480
488
497
506
514
523
531
540
548
557
565
574
582
591
599
607
616
624
632
641
649
657
665
673
681
689
697
Wavelength (nm)

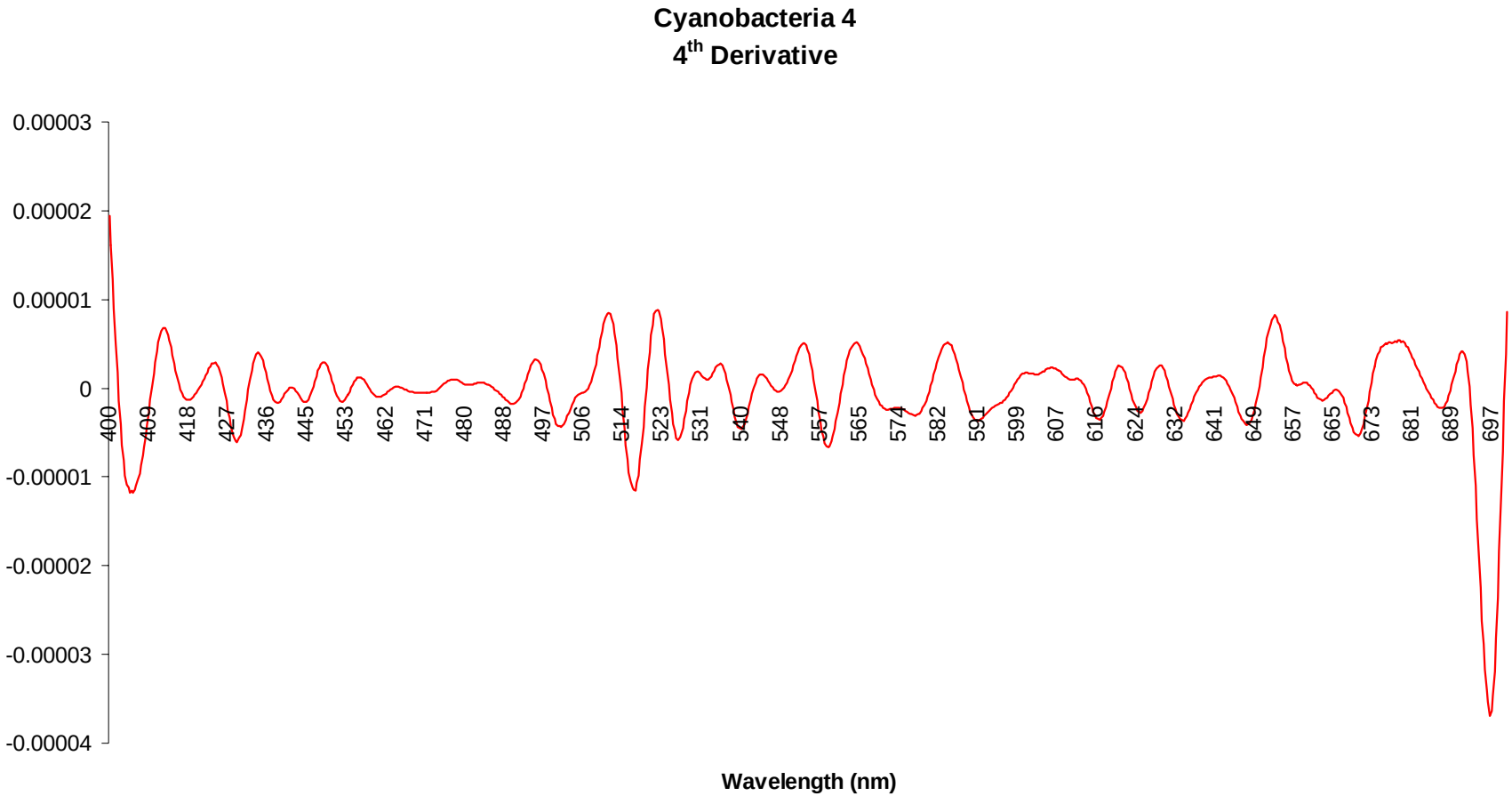
Cyanobacteria 4
4th Derivative
0.00003
0.00002
0.00001
0
-0.00001
-0.00002
-0.00003
-0.00004
400
409
418
427
436
445
453
462
471
480
488
497
506
514
523
531
540
548
557
565
574
582
591
599
607
616
624
632
641
649
657
665
673
681
689
697
Wavelength (nm)

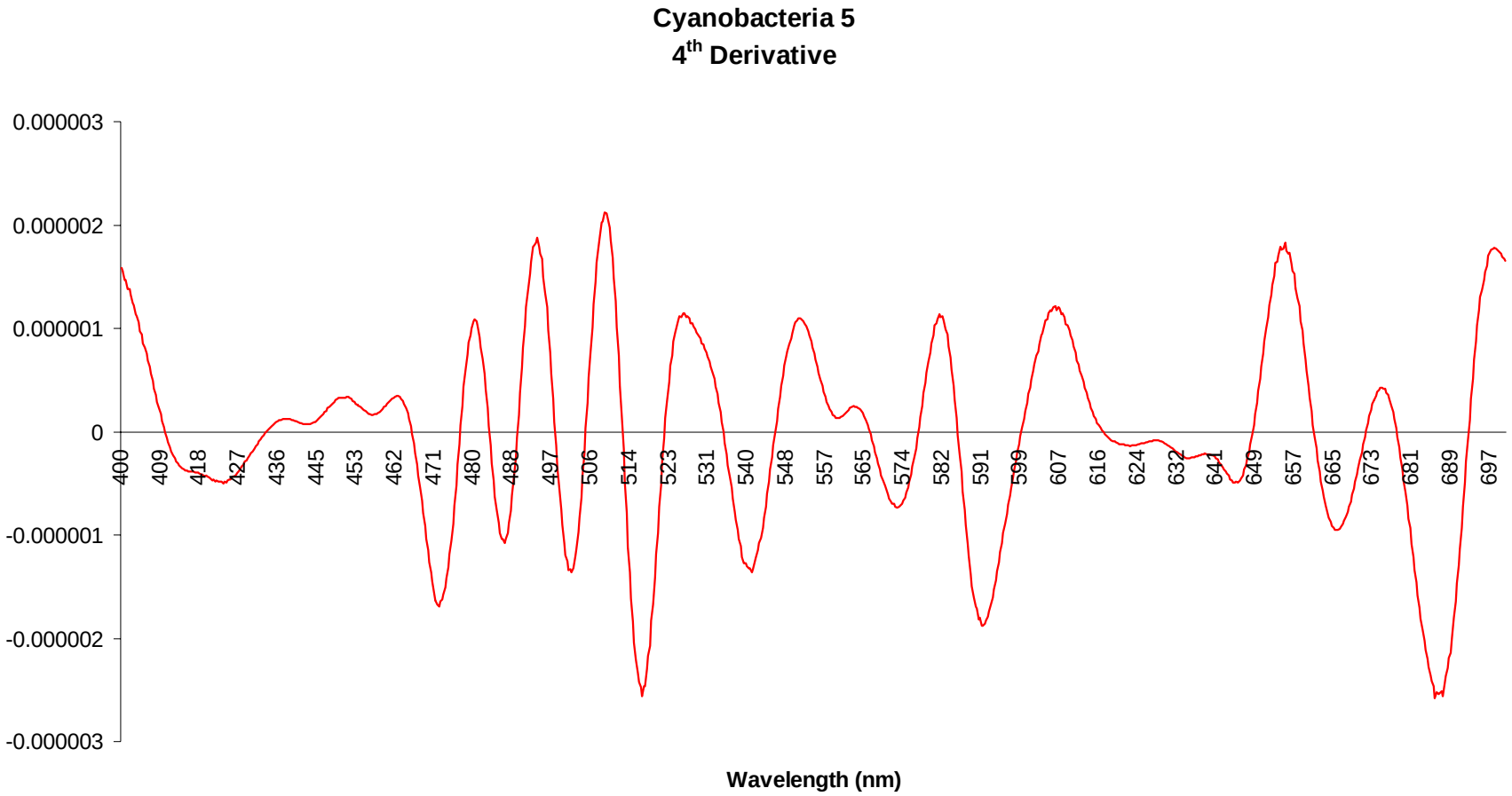
Cyanobacteria 5
4th Derivative
0.000003
0.000002
0.000001
0
-0.000001
-0.000002
-0.000003
400
409
418
427
436
445
453
462
471
480
488
497
506
514
523
531
540
548
557
565
574
582
591
599
607
616
624
632
641
649
657
665
673
681
689
697
Wavelength (nm)

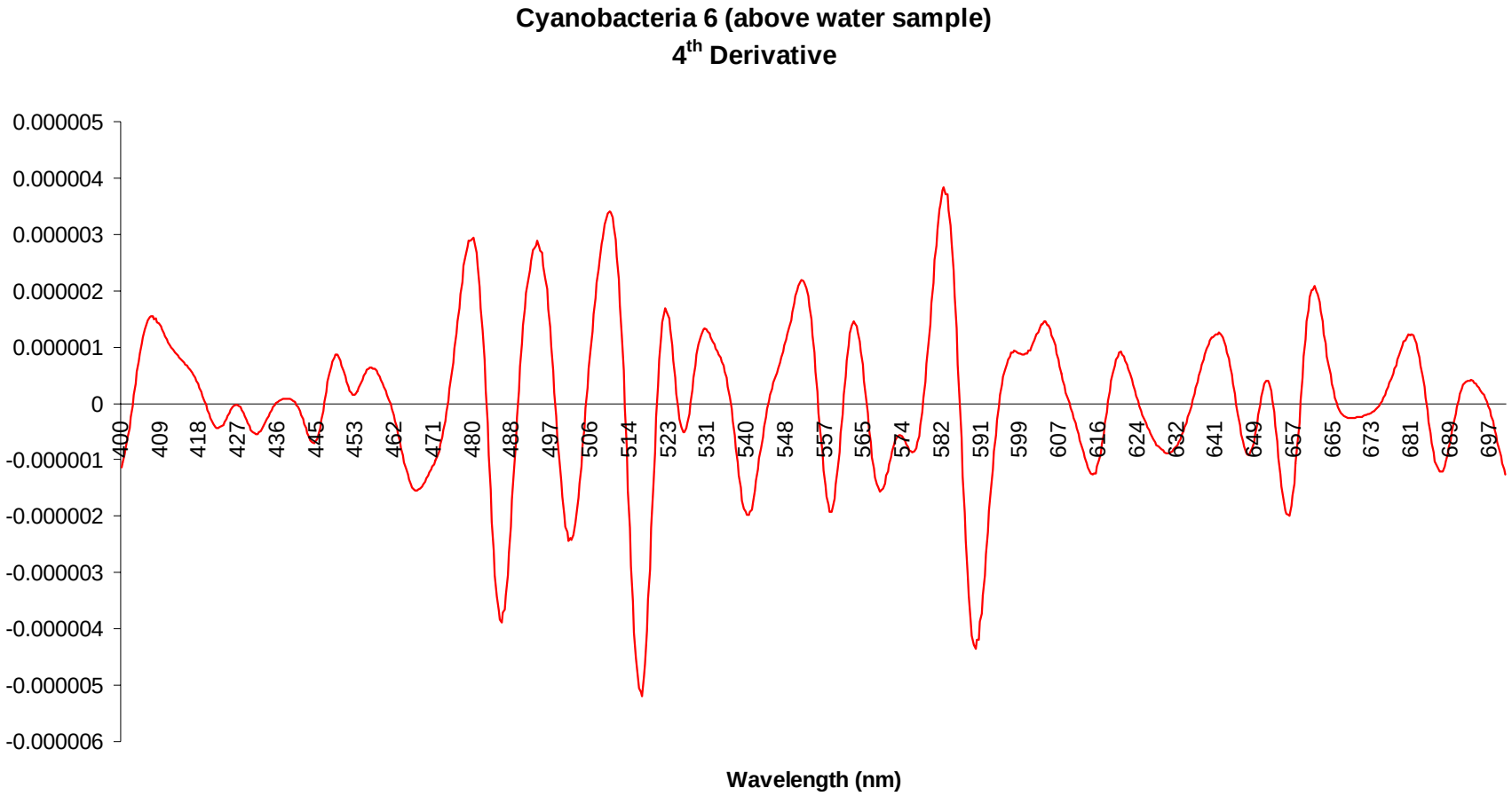
Cyanobacteria 6 (above water sample)
4th Derivative
0.000005
0.000004
0.000003
0.000002
0.000001
0
-0.000001
-0.000002
-0.000003
-0.000004
-0.000005
-0.000006
400
409
418
427
436
445
453
462
471
480
488
497
506
514
523
531
540
548
557
565
574
582
591
599
607
616
624
632
641
649
657
665
673
681
689
697
Wavelength (nm)

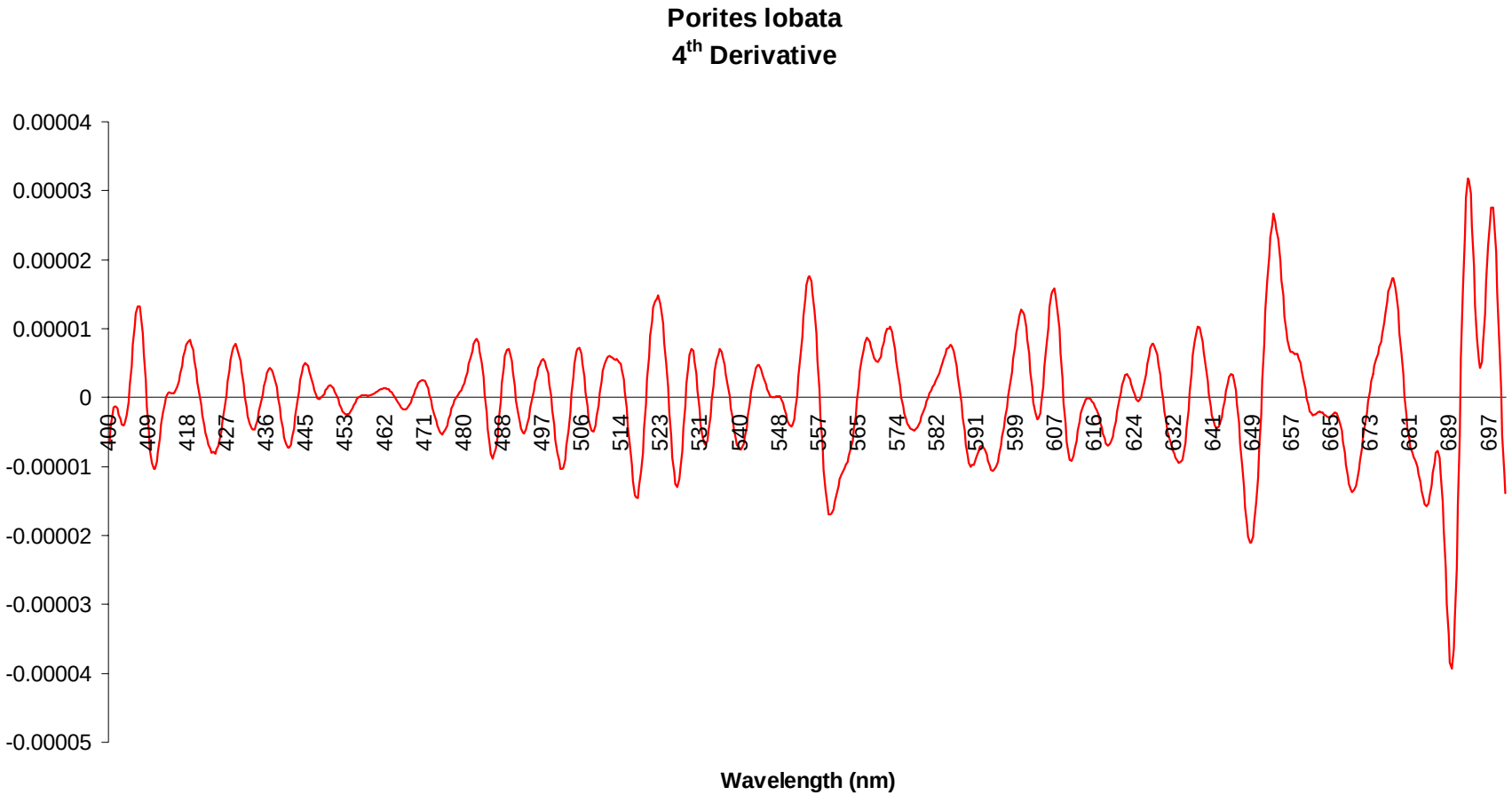
Porites lobata
4th Derivative
0.00004
0.00003
0.00002
0.00001
0
-0.00001
-0.00002
-0.00003
-0.00004
-0.00005
400
409
418
427
436
445
453
462
471
480
488
497
506
514
523
531
540
548
557
565
574
582
591
599
607
616
624
632
641
649
657
665
673
681
689
697
Wavelength (nm)

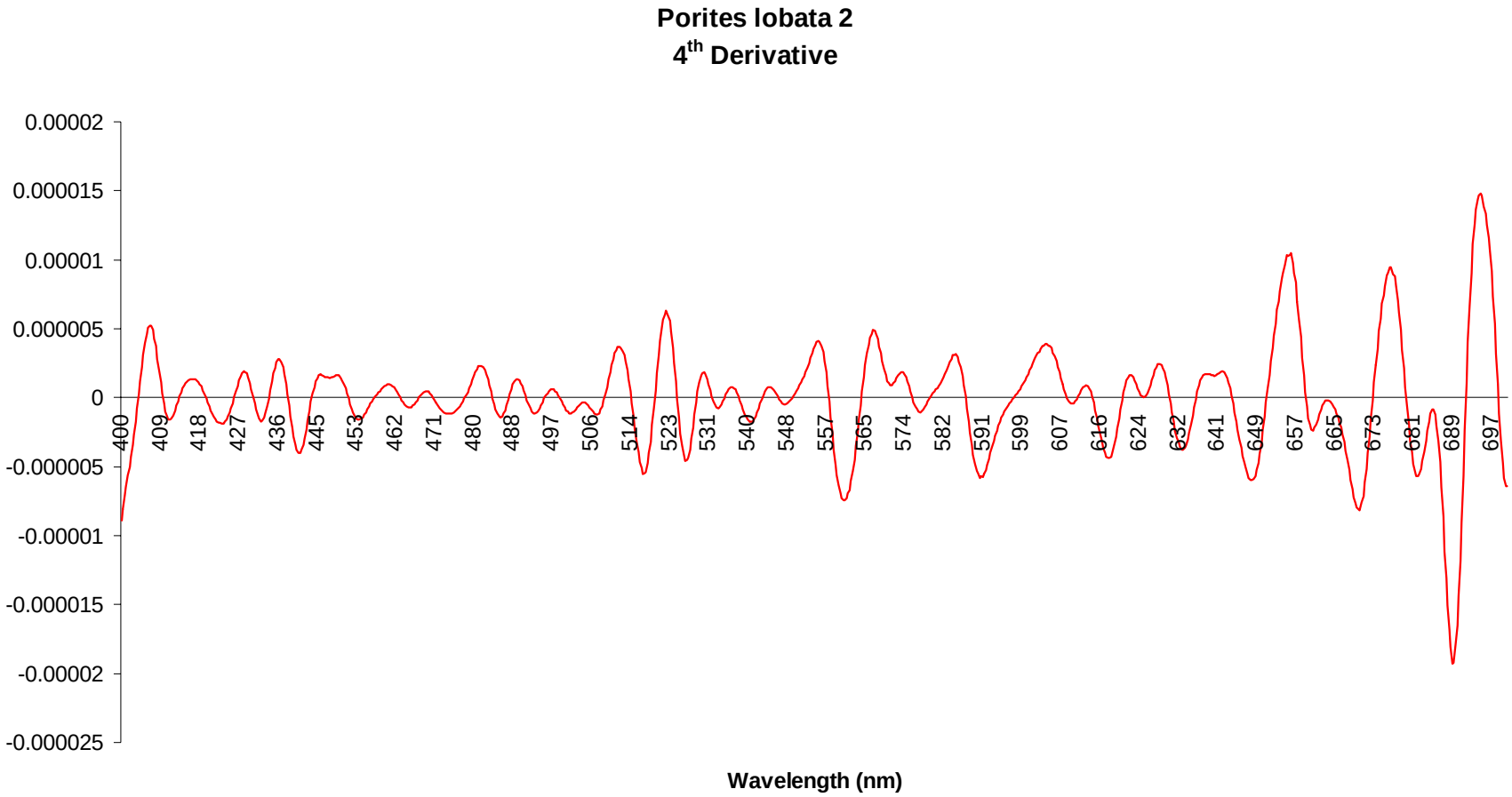
Porites lobata 2
4th Derivative
0.00002
0.000015
0.00001
0.000005
0
-0.000005
-0.00001
-0.000015
-0.00002
-0.000025
400
409
418
427
436
445
453
462
471
480
488
497
506
514
523
531
540
548
557
565
574
582
591
599
607
616
624
632
641
649
657
665
673
681
689
697
Wavelength (nm)

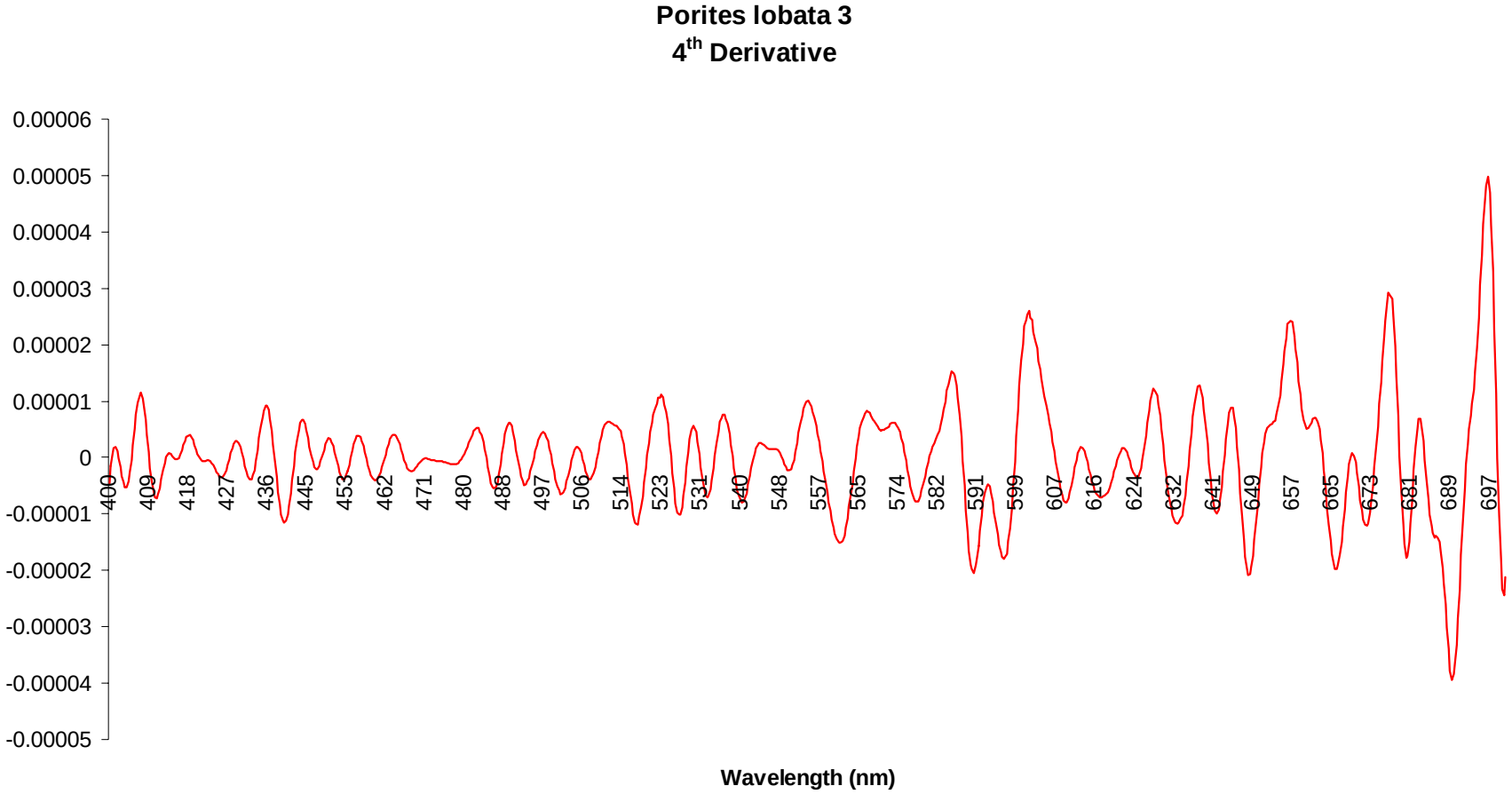
Porites lobata 3
4th Derivative
0.00006
0.00005
0.00004
0.00003
0.00002
0.00001
0
-0.00001
-0.00002
-0.00003
-0.00004
-0.00005
400
409
418
427
436
445
453
462
471
480
488
497
506
514
523
531
540
548
557
565
574
582
591
599
607
616
624
632
641
649
657
665
673
681
689
697
Wavelength (nm)

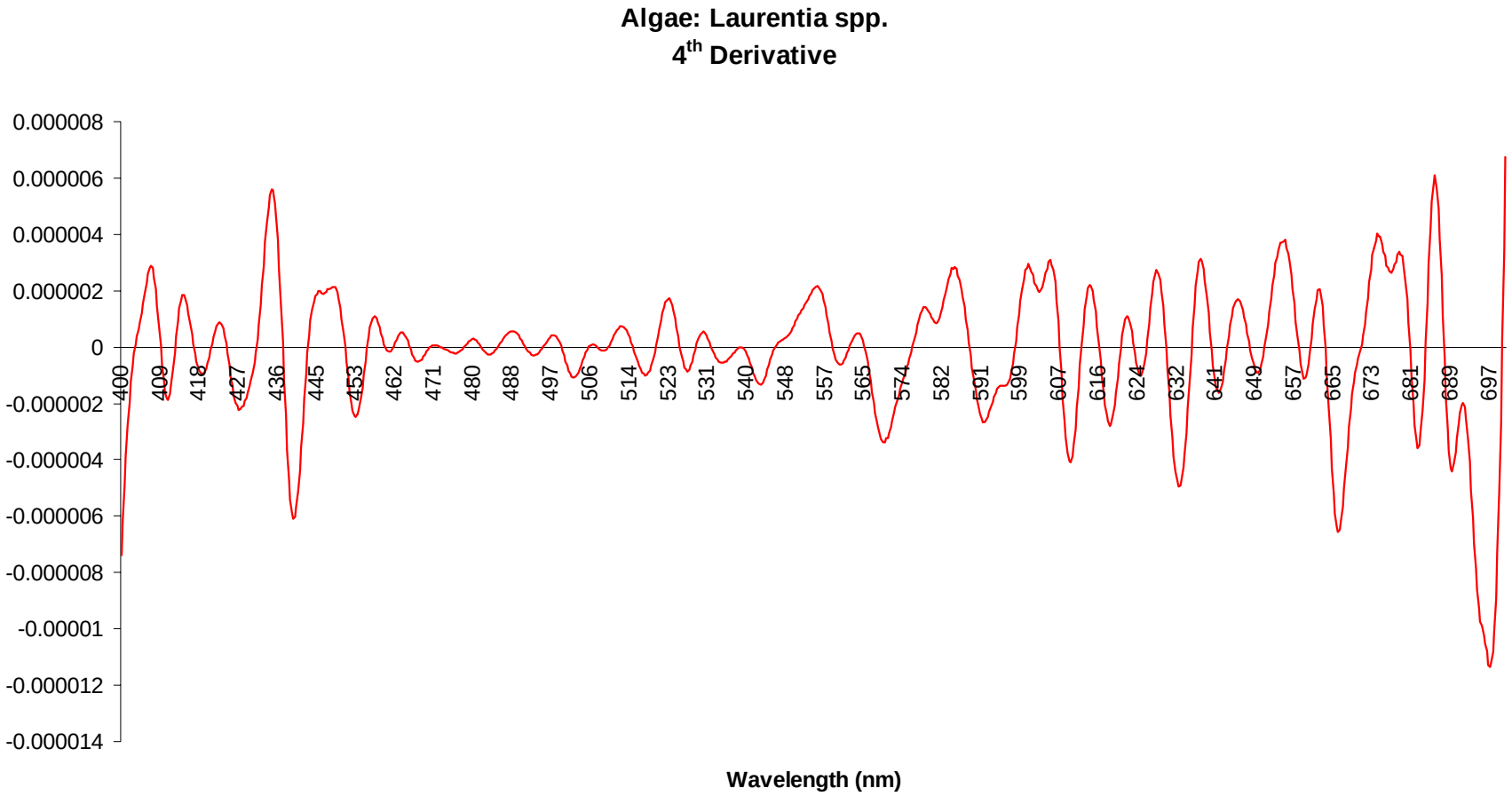
Algae: Laurentia spp.
4th Derivative
0.000008
0.000006
0.000004
0.000002
0
-0.000002
-0.000004
-0.000006
-0.000008
-0.00001
-0.000012
-0.000014
400
409
418
427
436
445
453
462
471
480
488
497
506
514
523
531
540
548
557
565
574
582
591
599
607
616
624
632
641
649
657
665
673
681
689
697
Wavelength (nm)

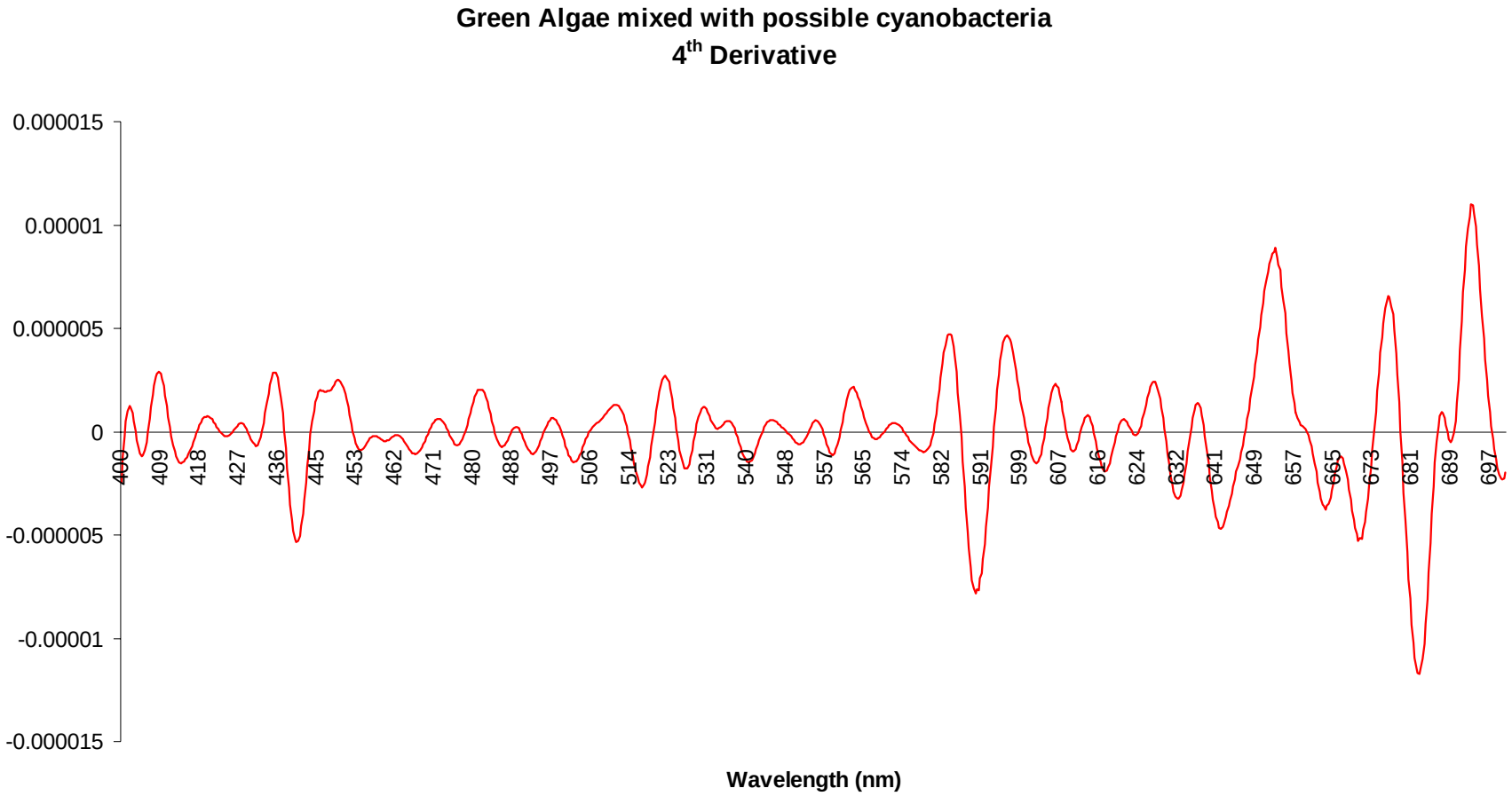
Green Algae mixed with possible cyanobacteria
4th Derivative
0.000015
0.00001
0.000005
0
-0.000005
-0.00001
-0.000015
400
409
418
427
436
445
453
462
471
480
488
497
506
514
523
531
540
548
557
565
574
582
591
599
607
616
624
632
641
649
657
665
673
681
689
697
Wavelength (nm)

# LIST OF REFERENCES


Apte, S. K., and N. Prabhavathi (1994). Rearrangements of Nitrogen Fixation (nif) Genes in the Heterocystous Cyanobacteria. *Journal of Biosciences*, vol. 19(5): 579-602.

Andréfouët, S., Payri, C., Hochberg, E. J., Che, L. M., and M. J. Atkinson (2003). Airborne hyperspectral detection of microbial mat pigmentation in Rangiroa Atoll (French Polynesia). *Limnology and Oceanography*, vol. 48 (1, part 2): 426-430.

Barnes, R. A., Holmes, A. W., Barnes, W. L., Esaias, W. E., McClain, C. R., and T. Svitek (1994). Sea WiFS Prelaunch Radiometric Calibration and Spectral Characterization, *NASA Technical Memorandum 104566,* vol. 23.

Beach, K. S., Borgeas, H. B., Nishimura, N. J., and C. M. Smith (1997). *In vivo* absorbance spectra and the ecophysiology of reef macroalgae. *Coral Reefs*, vol. 16: 21-28.

Behrenfeld, M. J., and Z. S. Kolber (1999). Widespread iron limitation of phytoplankton in the South Pacific Ocean, *Science,* vol. 283: 840-843.

Berk, A., Anderson, G. P., Bernstein, L. S., Acharya, P. K., Dothe, H., Matthew, M. W., Alder-Golden, S. M., Chetwynd, J. H., Richtsmeier, S. C., Pukall, B., Allred, C. L., Jeong, L. S., and M. L. Hoke (1999). MODTRAN4 Radiative Transfer Modeling for Atmospheric Correction. *SPIE Proceeding, Optical Spectroscopic Techniques and Instrumentation for Atmospheric and Space Research III*, vol. 3756.

Berman-Frank, I., Lundgren, P., and P. Falkowski (2003). Nitrogen Fixation and Photosynthetic Oxygen Evolution in Cyanobacteria. *Research in Microbiology*, vol. 154: 157-164.

Borstad, G., Brown, L., Cross, W., Nallee, M., and P. Wainwright (1997). Towards A Management Plan for a Tropical Reef-Lagoon System Using Airborne Multispectral Imaging and GIS. *ERIM Fourth International Conference on Remote Sensing for Marine and Coastal Environments,* Orlando, FL, p. 5.

Boussiba, S. and A. E. Richmond (1980). C-Phycocyanins as a storage protein in the blue-green alga *Spirulina platensis, Archives of Microbiology*, vol. 125: 143-147.

Butler, W. L., and D. W. Hopkins (1970). Higher derivatives analysis of complex absorption spectra. *Photochemistry, Photobiology*, vol. 12: 439-450.

Chang, G. C., and T. D. Dickey (1999). Partitioning *in situ* total spectral absorption by use of moored spectral absorption – attenuation meters. *Applied Optics*, vol. 38: 3876-3887.

Christian, G. D. and J. E. O'Reilly (1986). *Instrumental Analysis*, Second Edition, Allyn and Bacon, Boston, Massachusetts.

Cocks, T., Jenssen, R., Stewart, A., Wilson, I., and T. Shields (1998). The HyMap Airborne Hyperspectral Sensor: The system, calibration and performance. *Proceediings 1st EARSEL Workshop on Imaging Spectroscopy*, 6-8 October 1998, Zurich, EARSeL, Paris: 37-42.

Davis, C. O., Bowles, J., Leather, R. A., Korwan, D., Downes, T. V., Snyder, W. A., Rhea, W. J. Chen, W., Fisher, J., Bissett, P. W., R. A. Reisse (2002). Ocean PHILLS hyperspectral imager: design, characterization, and calibration. *Optics Express*, vol. 10 (4): 210-221.

EO Offers First Hyperspectral Images (2001), *Space Daily*, retrieved January 17, 2001 from http://www.spacedaily.com/news/eo-sats-01b.html

Estes, J. E. (2006). *The History of Remote Sensing*, University of California, Santa Barbara, for the Department of Geography. http://www.geog.ucsb.edu/~jeff/115a/remotesensinghistory.html retrieved 19 May 2006.

Fell, A. F., and G. Smith (1982). Higher derivative methods in ultraviolet-visible and infrared spectrophotometry. *Analytical Proceedings*, vol. 54: 28-32.

Gao, B., Montes, M. J., C. O. Davis (2001). Removal of atmospheric effects from hyperspectral imaging data for remote sensing of coastal waters, Hyperspectral Remote Sensing of the Ocean. *Proceedings of SPIE—The International Society for Optical Engineering*, vol. 4154: 31-40.

Gordon, H. R. (1994) Modeling and simulating radiative transfer in the ocean. In M. J. Perry (Ed.) *Ocean Optics*. New York: Oxford University Press: 3-39.

Green, E. P., Mumby, P. J., Edwards, A. J., C. D. Clark (Ed. Edwards, A. J.), (2000). *Remote sensing handbook for tropical coastal management*. Coastal Management Sourcebooks 3, UNESCO, Paris.

Gross, M., Ustin, S., V. Klemas (1988). Jet Propulsion Lab, California Institutes of Technology, Proceedings of the Airborne Visible/Infrared Imaging Spectrometer (AVIRIS) Performance Evaluation Workshop: 128-133.

Halliday, D., Resnick, R, J. Walker (2001). *Fundamentals of Physics, Sixth Edition*, John Wiley & Sons, Inc., Hoboken, NJ.: 817.

Haltrin, V. I. (2005). Water-leaving Radiance of Deep and Shallow Wind-Roughened Water Body Illuminate by Sun and Sky, *Proceedings of the III International Conference "Current Problems in Optics of Natural Waters,"* ONW'2005, Eds. Iosif Levin and Gary Gilbert, St. Petersburg, Russia.

Hochberg, E. J. and M. J. Atkinson (2000). Spectral discrimination of coral reef benthic communities, *Coral Reefs*, Vol. 19: 164-171.

Hochberg, E. J. and M. J. Atkinson (2003). Capabilities of remote sensors to classify coral, algae, and sand as pure and mixed spectra. *Remote Sensing of the Environment*, vol. 85: 174-189.

Hochberg, E. J., Atkinson, M. J., Apprill, A., and S. Andréfouët (2004). Spectral Reflectance of Coral. *Coral Reefs*, vol. 23: 84-95.

Hochberg, E. J., Apprill, A. M., Atkinson, M. J., and R. R. Bidigare (2006). Bio-optical modeling of photosynthetic pigments in corals. *Coral Reefs*, vol. 25: 99-109.

Hoge, F. E., Wright, C. W., Lyon, P. E., Swift, R. N., and J. K. Yungel (1999). Satellite retrieval of the absorption coefficient of phytoplankton phycoerythrin pigment: theory and feasibility status, *Applied Optics*, Vol. 38 (36): 7431-7441.

Holden, H., and E. LeDrew (2000). Accuracy assessment of hyperspectral classification of coral reef features. *Feocarta International*, vol. 15: 5-11.

Holden, H., and E. LeDrew (2001). Hyperspectral discrimination of healthy versus stressed coral using *in situ* reflectance. *Journal of Coastal Research*, vol. 17 (4): 850-858.

Hoover, J. (2004), *Diving the Darwin Point*, CoralReal.com, retrieved August 10, 2006 from http://www.coralrealm.com/fish/midwayJH.html

Jensen, J. R. (2000). *Remote Sensing of the Environment: An Earth Resource Perspective*, 2nd Edition, Upper Saddle River, NJ, Prentice-Hall, Inc.

Jerlov, N. G. (1976). *Marine Optics*, Elsevier, 1976.

Jones, G.J., Palenik, B.P., F. M. M. (1987). Molybdenum availability, nitrogen limitation and phytoplankton growth in natural waters. Science vol. 229: 653–655.

Jupiter, S. D., Potts, D. C., Siciliano, D., Joyce, K. E., and K. Wasson (2002). Habitat Variation and Health Assessment of a Dominant Saltmarsh Plant, *Salicornia virginica*, Using Hyperspectral Tools, presented at 7th Annual Conference on Remote Sensing for Marine and Coastal Environments, 20-22 May 2002 in Miami, FL.

Jupp, D. L. B., Kirk, J. T. O., and D. P. Harris (1994). Detection, identification and mapping of cyanobacteria using remote sensing to measure the optical quality of turbid inland waters. *Australian Journal of Marine and Freshwater Research*, vol. 45: 801-828.

Kirk, J. T. O. (1994). *Light and Photosynthesis in Aquatic Ecosystems*. Cambridge University Press, Cambridge.

Kruse, F. A., Boardman, J. W., Lefkoff, A. B., Young, J. M., Kierein-Young, K. S., Cocks, T. D., Jenssen, R., and P. A. Cocks (2002). HyMap: An Australian Hyperspectral Sensor Solving Global Problems – Results from USA HyMap Data Acquisitions. *Proceedings of the 10th Australasian Remote Sensing and Photogrammetry Conference*, Adelaide, Australia, 21-25 August 2000, Causal Productions (www.causalproductions.com), published on CD-ROM.

Ladd, H.S., J.I. Tracey Jr., and M. G. Gross (1967). Drilling at Midway Atoll. *Science*, vol. 156(3778): 1088–1095.

Larson, W. J., J. R. Wertz (2004). *Space Mission Analysis and Design, 3rd Edition*, Microcosm Press, El Segundo.

Lemasson, C., Tandeau de Marsac, N., and G. Cohen-Bazire (1973). Role of Allophocyanin as a Light-Harvesting Pigment in Cyanobacteria. *Proceedings of the National Academy of Sciences USA*, vol. 70 (11): 3130-3133.

Lewotsky, K. (1994). Hyperspectral imaging: evolution of imaging spectrometry, *OE Reports*.

Li, J., Shi, H. (1986). *Zhongguo Xitu Xuebao*, pp. 85-87.

Lillesand, T. M. and R. W. Kiefer (1994). *Remote Sensing and Image Interpretation*, John Wiley & Sons, Inc., New York.

Louchard, E. M., Reid, R. P., Stephens, C. F., Davis, C. O., Leathers, R. A., Downes, V., and R. Maffione (2002). Derivative Analysis of absorption features in hyperspectral remote sensing data of carbonate sediments. *Optics Express*, vol. 10 (26): 1573-1584.

Malmstadt, H. V., Enke, C. G., G. Horlick (1974). *Electronic Measurements for Scientists*, W. A. Benjamin, Menlo Park: 816-870.

Maathuis, B. H. P. and J. L. Van Genderen (2004). A review of satellite and airborne sensors for remote sensing based detection of minefields and landmines. *International Journal of Remote Sensing*, vol. 25 (23): 5201-5245.

McFee, J. E. and H. T. Ripley (1997). Detection of buried landmines using a CASI hyperspectral imager. *Proceedings SPIE*, vol. 3079: 738-749.

McFee, J. E. (1996). Preliminary study of detection of buried landmines using a programmable hyperspectral imager. *SPIE Proceedings*, vol. 2765: 476-488.

Mishra, D. R. (2005). Characterizing the vertical diffuse attenuation coefficient for downwelling irradiance in coastal waters: Implications for water penetration by high resolution satellite data. *ISPRS Journal of Photogrammetry & Remote Sensing*, vol. 60: 48-64.

Mobley, C. D. (1994). *Light and Water: Radiative Transfer in Natural Waters*, Academic Press, Inc., San Diego, CA.

Morel, A., Maritorena, S. (2001). Bio-optical Properties of Oceanic Waters: A reappraisal. *Journal of Geophysical Research*, vol. 106: 7163-7180.

Mumby, P. J., Skirving, W., Strong, A. E., Hardy, J. T., LeDrew, E. F., Hochberg, E. J., Stumpf, R. P., L. R. David (2004). Remote sensing of coral reefs and their physical environment, *Marine Pollution Bulletin 48*: 219-228.

NASA's Observatorium, *Remote Sensing in History 3*, retrieved May 22, 2006 from http://observe.arc.nasa.gov/nasa/exhibits/history/history_4.html.

Olsen, R. C. (2006). *Remote Sensing from Air and Space*, SPIE, Press Monograph PM162.

Richardson, L. L., Buisson, D., Liu, C., and V. Ambrosia (1994). The Detection of Algal Photosynthetic Accessory Pigments Using Airborne Visible-Infrared Imaging Spectrometer (AVIRIS) Spectral Data. *Marine Technology Science Journal*, vol. 28 (3): 10-21.

Richardson, L.L., and F.A. Kruse (1999). Identification and classification of mixed phytoplankton assemblages using AVIRIS image-derived spectra. *Summaries of the Eighth JPL Airborne Earth Science Workshop*, 09–11 February, Pasadena, California.

Robinson, I. S. (2004). *Measuring the Oceans from Space: The Principles and Methods of Satellite Oceanography*, Praxix Publishing Ltd, Chichester, U. K.

Saffo, M. B. (1987). New Light On Seaweeds: Recent studies have forced reassessment of the role of light-harvesting pigments in depth zonation of seaweeds, *Bioscience*, vol. 37 (9): 654-664.

Saldino, R. (1998). *Trip Report: Midway Atoll – Home of the Gooney Birds January 25 - February 1, 1998*, retrieved August 10, 2006 from http://www.camacdonal.com/birding/tripreports/Midway98.html

Schopf, J. W. (1975). The Age of Microscopic Life. *Endeavor*, vol. 34: 51-58.

Seppala, J., Ylostalo, P., and H. Kuosa (2005). Spectral absorption and fluorescence characteristics of phytoplankton in different size fractions across a salinity gradient in the Baltic Sea. *International Journal of Remote Sensing*, vol. 26 (2): 387-414.

Shifrin, K. S. (1994). *Physical Optics of Ocean Water*, American Institute of Physics, New York.

Short, N. M. Sr. (2006). *The Remote Sensing Tutorial*, retrieved May 22, 2006 from http://rst.gsfc.nasa.gov/Intro/Part2_24.html.

Siciliano, D. (2002). Remote Sensing in the Northwest Hawaiian Islands. *Coral Reef Ecosystems of the Northwestern Hawaiian Island: Interim Results Emphasizing the 2000 Surveys*. Maragos, J. and Gulko, D. (eds), U.S. Fish and Wildlife Service and the Hawai'i Department of Land and Natural Resources, Honolulu, Hawai'i, vol. 46: 20-21.

Siciliano, D. (2005). Latitudinal limits to coral reef accretion: Testing the Darwin Point Hypothesis at Kure Atoll, Northwestern Hawaiian Islands, using new evidence from high resolution remote sensing and *in situ* data. Ph.D. Dissertation, University of California, Santa Cruz.

Siciliano, D., and D.C. Potts (2001). Coral reef habitat mapping and assessment using AVIRIS: the French Frigate Shoals atoll, Northwest Hawaiian Islands. *Summaries of the Eleventh JPL Airborne Earth Science Workshop*. February 27-March 2, Pasadena, CA.

Smith, C. M. and R. S. Alberte (1994). Characterization of *in vivo* absorption features of chlorophyte, phaeophyte and rhodophyte algal species. *Marine Biology Journal*, Springer Berlin / Heidelberg, Vol. 118 (3): 511-521.

Smith, R. A., Irish, J. L., and M. Q. Smith (2006). Airborne LIDAR and Airborne Hyperspectral Imagery: A Fusion of Two Proven Sensors for Improved Hydrographic Surveying, retrieved August 12, 2006 from http://shoals.sam.usace.army.mil/downloads/Publications/27Smith_Irish_Smith_00.pdf.

Smith, R. C. and K. Baker (1981). Optical Properties of the Clearest Natural Waters. *Applied Optics*, vol. 20(2): 177-184.

Talsky, G. (1994). *Derivative Spectrophotometry: Low and Higher Order*. VCH Verlagsgesellschaft mbH, Weinheim, Germany.

Terrie, Gregory E., Applications of Hyperspectral Data in Coastal Marine Environments,Report Number AD-A302222 NRL/FR/7442--95-9630.

Tsai, F., and W. Philpot (1998). Derivative analysis of Hyperspectral Data. *Remote Sensing of the Environment*, vol. 66: 41-51.

U.S. Centennial of Flight Commission, *Balloons in the American Civil War*, retrieved May 22, 2006 from http://www.centennialofflight.gov/essay/Lighter_than_air/Civil_War_balloons/LTA5.htm.

Vince, J., Earnshaw, R. (2002). *Advances in Modeling, Animation and Rendering*. Springer-Verlag London Limited, Great Britain: 490.

Wettle, M., Ferrier, G., Lawrence, A. J., and K. Anderson (2003). Fourth derivative analysis of Red Sea coral reflectance spectra. *International Journal of Remote Sensing*, vol. 24 (19): 3867-3872.

THIS PAGE INTENTIONALLY LEFT BLANK

# INITIAL DISTRIBUTION LIST

1. Defense Technical Information Center
   Ft. Belvoir, Virginia

2. Dudley Knox Library
   Naval Postgraduate School
   Monterey, California